

Chemical modifications of embelin, a benzoquinone from *Embelia schimperi* Vatke and optimized application in selected textile fibers

MARGARET CHEPKEMOI KOSKE

BSc., MSc

A Thesis Submitted in Partial Fulfillment of the Requirements for the Degree of Doctor of Philosophy in Analytical Chemistry of the Department of Chemistry and Biochemistry,

Moi University

2022

DECLARATION

This research thesis is my original work and has not been submitted wholly or in part for an award in any institution.

Signature  _____ Date: 18/11/2022 _____

Margaret Chepkemai Koske
PHD/ACH/4320/20

This research thesis has been prepared under our supervision and has our approval to be presented for examination as per the University regulations.

Signature  _____ Date: 18/11/2022 _____

Sir. Prof. Ambrose Kiprop
Department of Chemistry and Biochemistry,
School of Sciences and Aerospace Studies,
Moi University,
P.O. BOX 3900-30100
Eldoret, Kenya.

Signature  _____ Date: 18/11/2022 _____

Dr. Sarah Chepkwony (PhD)
Department of Chemistry and Biochemistry,
School of Sciences and Aerospace Studies,
Moi University
P.O. BOX 3900-30100
Eldoret, Kenya.

Signature  _____ Date: 18/11/2022 _____

Dr. Isaac O. K'Owino (PhD),
Adjunct Senior Lecturer, Department of Chemistry and Biochemistry,
Moi University
Senior Lecturer, Department of Chemistry,
Department of Chemistry,
Masinde Muliro University of Science and Technology,
P.O. BOX 190-50100
Kakamega, Kenya.

DEDICATION

To my husband Jonah and my children, Collins, Faith, Allan and Ephraim for their love and patience during my studies.

ABSTRACT

Globally there is resurgence in the use of natural dyes such as embelin as a suitable replacement for synthetic dyes, which have caused a negative impact to the ecosystem. However, natural dyes have poor colour quality and low solubility. Additionally, they have limited shades and inadequate fastness properties. There is, therefore, need to improve the dyeing properties of some of the natural dyes. The aim of this study was to isolate and derivatize embelin compound and assess the dyeing properties of the embelin derivatives on various textile fibers. The specific objectives were to: isolate and characterize embelin from *E. schimperi* berries; chemically modify and characterize embelin derivatives; evaluate and optimize their dyeing properties on cotton, silk and wool fibers. *E. schimperi* stem barks were collected from Kericho, Nandi and Narok Counties, however the yield was low. *E. schimperi* berries were collected from Kericho County, dried, ground and extracted by maceration method using acetone. Isolation of embelin (**1**) was done using column chromatography and chemical modification was done by condensation reactions of embelin with different aldehydes in the presence of acetic acid. Optimization of dyeing conditions was achieved using Response Surface Methodology (RSM) and mordanting was executed via simultaneous, pre-and post-mordanting techniques. The dyeing properties were evaluated using colour fastness and colour strengths. Characterization of all the compounds was done using; elemental analyses, UV/VIS spectroscopy, Fourier Transform Infra-Red spectroscopy (FTIR), Gas Chromatography-Tandem Mass Spectroscopy, Liquid Chromatography-Electron Spray Ionization - Mass Spectroscopy (LC-ESI/MS), Nuclear Magnetic Resonance (NMR), Scanning electron microscopy (SEM) and Thermal Gravimetric Analysis. Embelin of high purity isolated from berries (yield 40.0 ± 0.01%) was modified to; vilangin (**3**); methyl vilangin (**4**); embelin -2, 4-dihydroxybenzaldehyde (**5**), and embelin ninhydrin (**6**). UV/Vis spectroscopy revealed λ max at 292 nm for all the compounds, due to $\pi \rightarrow \pi^*$ transitions. The FTIR revealed 3301.84 cm^{-1} (-OH), 1610.49 cm^{-1} (-C=O) (**1**), 3313.63 cm^{-1} (-OH), 1610.49 cm^{-1} (-C=O) (**3**), 3316.57 cm^{-1} (-OH), 1616.39 cm^{-1} (-C=O) (**4**), 3298 cm^{-1} (-OH), 1610.49 cm^{-1} (-C=O) (**5**) 3307.73 cm^{-1} (-OH), 1716.57 cm^{-1} (-C=O) (1610.49 cm^{-1} (- α , β -unsaturated C=O) (**6**). GC-MS revealed the presence of embelin, with a m/z 294 in the crude extract. LC-ESI/MS analysis showed the [M-H]⁻ for embelin at m/z 292.9 (**1**), m/z 599.4 for vilangin (**3**), m/z 613.2 (C₃₆H₅₄O₈), (**4**), m/z 292.9 for (C₁₇H₂₆O₄), (**5**) and m/z 452.9 for (C₂₆H₃₀O₇) (**6**). Elemental analyses confirmed theoretical C, H, and O values. NMR spectroscopy confirmed the structures of the derivatives synthesized by the disappearance of ¹H NMR peak at 5.59 ppm and ¹³C NMR peak at δ 104.45 and the formation of new peaks between 172-200 ppm. Vilangin and embelin ninhydrin (ENn) were soluble in water because of added functional (-OH) groups upon modification which made them soluble at alkaline pH and were therefore used for dyeing. The ENn dyed wool fiber gave the best colour strengths of 15.8 at optimum conditions of pH 9, 90 minutes and 90 °C. The colour fastness was in the range of 4-5 in all the dyed fibers and different shades were achieved using different metallic mordants. SEM images showed the formation of aggregated dye on the surface of dyed fibers. Thermal stability of 400 - 500 °C was established in dyed fibers. The good colour strengths and dyeing properties show that embelin is a suitable precursor for the semi-synthesis of efficient and eco-friendly dyes. For maximum exploits on the derivatized dyes, this study recommends adoption of optimum dyeing conditions and use of mordants to obtain green, violet and brown shades.

TABLE OF CONTENTS

DECLARATION	ii
DEDICATION	iii
ABSTRACT.....	iv
TABLE OF CONTENTS	v
LIST OF TABLES.....	xii
LIST OF FIGURES.....	xiv
LIST OF EQUATIONS.....	xviii
LIST OF SCHEMES	xix
LIST OF ABBREVIATIONS AND ACRONYMS.....	xx
ACKNOWLEDGEMENT.....	xxiii
CHAPTER ONE	1
INTRODUCTION	1
1.1. Background Information	1
1.2. Statement of the problem	4
1.3. General objective	5
1.3.1. Specific objectives.....	5
1.4. Hypotheses	5
1.5. Justification	5
CHAPTER TWO	7
LITERATURE REVIEW	7
2.1. History of natural dyes	7
2.2. Application of dyes	8
2.3. Plants as natural sources of dyes.....	11
2.4. Techniques for extracting natural dyes	11
2.5. Qualities of a good dye	12
2.6. Chemical modification of natural dyes	12

2.7. Limitations of natural dyes.....	13
2.8. Cellulosic fibers: Cotton	13
2.9. Protein fibers (silk and wool).....	14
2.10. Mordants	15
2.11. Improving natural dyes' quality.....	16
2.11.1. Light fastness.....	16
2.11.2. Wash Fastness	17
2.12. Evaluation of fastness properties	17
2.13. Evaluation of colour strength.....	18
2.14. Factors controlling the dyeing process.....	19
2.15. Semi-synthetic dyes	20
2.16. Benzoquinone dyes from Myrsinaceae plants.....	20
2.17. Extraction of embelin.....	21
2.18. Embelin derivatives.....	25
2.19. Reactions of embelin.....	26
2.20. Uses of embelin and its derivatives.....	31
2.21. Response surface methodology (RSM).....	32
2.22. Physical and spectroscopic techniques.....	32
2.22.1. Melting point determinations	32
2.22.2. UV-VIS Spectroscopy	33
2.22.3. Attenuated Total Reflectance-Fourier Transform Infra-Red Spectroscopy	33
2.22.4. Nuclear Magnetic Resonance	34
2.22.5. Scanning Electron Microscopy.....	35
2.22.6. Elemental analyzer	35
2.22.7. Thermal Gravimetric Analysis	35
CHAPTER THREE.....	36

MATERIALS AND METHODS	36
3.1. Study area.....	36
3.2. Preparation of plants for extraction.....	37
3.3. Materials and reagents.....	37
3.3.1. Instruments	37
3.4. Extraction of <i>Embelia schimperi</i> stem bark.....	38
3.4.1. Extraction using maceration method.....	38
3.4.2. Stem bark extraction using ultrasonication technique.....	38
3.4.3. Soxhlet extraction.....	39
3.5. Preparation of crude extracts from <i>Embelia schimperi</i> berries.....	39
3.6. Qualitative phytochemical screening of <i>Embelia schimperi</i> crude extract.....	40
3.6.1. The Wagner's reagent Test for Alkaloids.....	40
3.6.2. Detection of phenol (Ferric Chloride determination).....	40
3.6.3. Terpenoid testing (Salkowski test).....	40
3.6.4. Salkowski test for steroid detection.....	40
3.6.5. Test for Flavonoids.....	41
3.6.6. Test for Tannins.....	41
3.6.7. Detection for Saponins:.....	41
3.6.8. Test for Glycosides (Cardiac glycoside Keller-Killani Test).....	41
3.7. Quantification of embelin from crude extracts using LC/UV/PDA.....	41
3.8. Thin-layer chromatography.....	42
3.9. Isolation and purification of embelin.....	43
3.10. Characterization of embelin.....	43
3.11. Chemical modifications of embelin.....	43
3.11.1. Synthesis of vilangin (3).....	45

3.11.2. Synthesis of methyl vilangin (4).....	45
3.11.3. Synthesis of embelin-2,4-dihydroxy benzaldehyde derivative (5).....	45
3.11.4. Synthesis of embelin ninhydrin derivative (6)	46
3.12. Chemical and physical characterization of embelin derivatives	47
3.12.1. Melting point determination.....	48
3.12.2. UV-Visible spectrophotometric spectroscopy.....	48
3.12.3. Fourier Transform Infra-Red spectroscopy	48
3.12.4. Liquid chromatography-Mass Spectrometry	49
3.12.5. Gas chromatography-Mass spectrometry (GC-MS).....	50
3.12.6. Nuclear Magnetic Resonance spectroscopy	50
3.12.7. Elemental analysis	51
3.13. Application of embelin and derivatives on textile fibers	51
3.13.1. Dyeing processes	51
3.13.2. Mordanting	52
3.14. Method optimization for dyeing procedures	52
3.14.1. Model validation.....	53
3.15. Testing of Colour Fastness.....	54
3.15.1. Colour fastness to rubbing.....	54
3.15.2. Colour fastness to washing.....	54
3.15.3. Colour fastness to Light.....	55
3.15.4. Evaluation of colour strength using CIELAB	55
3.16. Thermal stability and surface characterization of dyed textile fibers	56
3.16.1. Thermogravimetric analysis	56
3.16.2. Scanning electron microscopy.....	56

3.17. Statistical analysis	57
3.18. Model validation	57
CHAPTER FOUR.....	58
RESULTS AND DISCUSSION	58
4.1. Extraction Yields.....	58
4.2. Phytochemical screening results	62
4.3. UV/Vis spectra of Kericho sample crude extract.....	67
4.4. GC-MS spectra from Kericho County berries crude samples.....	68
4.4.1. Quantification of embelin from Kericho berries sample extract	69
4.5. FT-IR Spectroscopic characterization of crude extracts	70
4.6. Isolation and purification of embelin	71
4.6.1. Column chromatography	72
4.7. Structure elucidation of characterized embelin.....	73
4.7.1. Melting point determination	73
4.7.2. UV-Visible spectroscopy of Embelin.....	73
4.7.3. FTIR spectroscopy of embelin and embelin standard	74
4.7.4. ESI-MS spectrum of embelin in the negative mode.....	75
4.7.5. ¹ H and ¹³ C NMR spectroscopy	77
4.7.6. Elemental analysis of embelin.....	80
4.8. Derivatives of embelin	80
4.8.1. Characterization of vilangin	81
4.8.2. Characterization of methyl vilangin (4)	87
4.8.3. Characterization of Embelin-2,4 -dihydroxybenzaldehyde derivative.....	93
4.8.4. Characterization of embelin with ninhydrin derivative(6)	98
4.9. Effect of semi-synthetic derivatives on textile fibers.....	105

4.10. Dyeing of textile fibers.....	105
4.10.1. Dyeing of textile fibers with embelin dyes (1).....	105
4.10.2. Dyeing of textile fibers with vilangin dyes (3).....	105
4.10.3. Dyeing of cotton fabric with embelin ninhydrin dye optimization	114
4.10.4. Dyeing of silk with embelin ninhydrin.....	127
4.10.5. Dyeing of wool with ENn.....	139
4.11. Thermal stability and surface characterization of dyed cotton fibers	152
4.11.1. Thermo Gravimetric Analysis (TGA) /Differential Scanning Calorimetry (DSC)cotton blank fabric	152
4.11.2. TGA/DSC of vilangin dyed cotton fabric	153
4.11.3. TGA/DSC of embelin-ninhydrin dye	157
4.12. FTIR spectroscopy and scanning electron microscopy of vilangin dyed cotton fiber	159
4.12.1. Surface characterization of embelin ninhydrin dyed cotton fiber	161
4.12.2. Surface characterization of dyed silk with embelin ninhydrin	163
4.12.3. Surface characterization of wool dyed fabric with ENn dye.....	166
CHAPTER FIVE	169
CONCLUSION AND RECOMMENDATIONS.....	169
5.1. Conclusion.....	169
5.2. Recommendations	170
REFERENCES.....	171
APPENDICES	203
APPENDIX 1: Semi-synthetic experimental set up.....	203
APPENDIX 2: ATR-FTIR equipment.....	203
APPENDIX 3: LC/MS equipment	204
APPENDIX 4: Embelin Ninhydrin Dyes.....	204

APPENDIX 5: TGA/DSC Embelin	205
APPENDIX 6: TGA/DSC Emv -alum.....	205
APPENDIX 7: TGA/DSC Emv -cu	206
APPENDIX 8: TGA/DSC Emv -Fe.....	207
APPENDIX 9 :TGA/DSC Emv -Ni.....	207
APPENDIX 10: TGA/DSC Emv –no mordant.....	208
APPENDIX 11: TGA/DSC ENn –Alum	208
APPENDIX 12: TGA/DSC ENn –Cu.....	209
APPENDIX 14: TGA/DSC ENn –Ni	209
APPENDIX 15: TGA/DSC ENn –unmordant.....	210

LIST OF TABLES

Table 2.1: List of natural dyes, their application and sources.....	9
Table 3.1: Actual levels of independent variables (Design Experts software)	53
Table 4.1: Percentage yield of stem bark crude extracts by maceration method	60
Table 4.2: Kericho County Samples extraction based on different techniques	61
Table 4.3: Percentage yield of acetonic extracts from berries crude extraction by maceration method.....	62
Table 4.4: Phytochemical Screening Test Results of <i>Embelia schimperi</i> stem bark crude extracts by maceration method	64
Table 4.5: Phytochemical Screening Test Results of <i>Embelia schimperi</i> stem bark (Kericho county) crude extracts by ultrasonic and soxhlet method.....	65
Table 4.6: Phytochemical Screening Test Results of <i>Embelia schimperi</i> Kericho County berries acetonic crude extracts.....	65
Table 4.7: Elemental analysis of vilangin compound	87
Table 4.8: Elemental analysis of methyl vilangin compound	93
Table 4.9: Elemental analysis of compound embelin-2,4 -dihydroxybenzaldehyde (5) compound.....	98
Table 4.10: Elemental analysis of compound ENn compound	105
Table 4.11: Experimental design and results for the colour strength of cotton fibers dyed with vilangin (3).....	109
Table 4.12: Analysis of Variance.....	110
Table 4.13: Model Summary	110
Table 4.14: Colour strength and shades of modified vilangin dye cotton fabrics.....	113
Table 4.15: Colour fastness of the vilangin dyed fabric using different methods of mordanting.....	114
Table 4.16: Effect of dyeing variables on dye exhaustion of ENn on cotton fabric	118
Table 4.17: Model Summary.....	118
Table 4.18: ANOVA of cotton dyed embelin ninhydrin	119
Table 4.19: Evaluated colour measurements of the ENn cotton dyed fabric with mordants	125

Table 4.20: The Colourfastness of dyed fabric with different methods of mordant used..	126
Table 4.21: Experimental design and results for dye exhaustion of silk fibers dyed with Embelin ninhydrin dye.....	131
Table 4.22: Model summary of ENn silk dye	132
Table 4.23: Analysis of variance.....	132
Table 4.24: Colour measurements of the silk dyed fabric using different methods of mordanting.....	134
Table 4.25: Colour fastness of the dyed fabric using different methods of mordanting....	139
Table 4.26: Experimental design and results for dye exhaustion of wool fibers dyed with Embelin ninhydrin dye.....	143
Table 4.27: ANOVA for wool dyeing with ENn	145
Table 4.28: Model Summary of wool	145
Table 4.29: Colour measurements of the wool dyed fabric using different methods of mordanting.....	151
Table 4.30: Colour fastness of the dyed fabric using different methods of mordanting....	152
Table 4.31: Different cotton dyed and mordanted fabrics weights.....	153

LIST OF FIGURES

Figure 1.1: Embelin structure	4
Figure 2.1: Application of natural dyes	8
Figure 2.2 Illustrates the structure of cotton with intermolecular and intramolecular hydrogen bonds.....	14
Figure 2.3: (a) CIELAB coordinates (b) Grey scale for colour change	19
Figure 2.4: Examples of isolated benzoquinones (1-4)	22
Figure 2.5: Pentacyclic triterpenoids from <i>Embelia schimperi</i>	23
Figure 2.6: Structure of Methyl vilangin	24
Figure 2.7: Structure of biembelin	24
Figure 2.8: Electron density in 2,5-dihydroxy-3-undecyl-1,4-benzoquinone.....	26
Figure 2.9: Embelin derivative with lipophilic chain	27
Figure 2.10: embelin analogs as inhibitors of —X-Linked inhibitor of apoptosis protein (XIAP) derivatives.....	28
Figure 3.1: Sampling area Map; Kericho, Narok and Nandi Counties	37
Figure 4.1: UV-VIS spectrum of acetonic crude extract from Kericho County	67
Figure 4.2: GC-MS chromatogram from Kericho County <i>Embelia schimperi</i> acetonic extract.....	68
Figure 4.3: GC-MS Spectrum of embelin.....	69
Figure 4.4: Squalene	69
Figure 4.5: (a) Embelin standard chromatogram (b) Embelin standard 3D chromatogram	70
Figure 4.6: (a) LC-UV-MS chromatogram and (b) 3D at 280 nm of crude <i>Embelia schimperi</i> fruit acetonic extract, Kericho County sample.....	70
Figure 4.7: The FTIR spectra of Kericho crude acetonic extract	71
Figure 4.8: various TLC profiles of <i>Embelia schimperi</i> crude extract	72
Figure 4.9: Removal of the excess solvent from embelin crude sample	72
Figure 4.10: TLC of isolated embelin compound (a) and embelin standard (b).....	73
Figure 4.11: UV-VIS spectra of embelin and embelin standard in dichloromethane, scan 200-800 nm	74

Figure 4.12: FTIR of isolated embelin and embelin standard	75
Figure 4.13: ESI-MS spectrum of embelin in the negative mode	76
Figure 4.14: ESI-MS spectrum of embelin standard in the negative mode.....	76
Figure 4.15: ¹ H NMR of embelin (1) (400 MHz, DMSO, ppm)	78
Figure 4.16: Dept NMR of embelin (1) (400 MHz, DMSO, ppm)	78
Figure 4.17: ¹ H NMR of embelin standard (2) (400 MHz, DMSO, ppm)	79
Figure 4.18: Dept NMR of embelin standard (2) (400 MHz, DMSO, ppm).....	80
Figure 4.19: Synthesized vilangin dyes	81
Figure 4.20: UV-VIS spectra of embelin and embelin standard and vilangin in Dichloromethane,scan 200-800 nm	82
Figure 4.21: FTIR of vilangin (3)	83
Figure 4.22: LC-ESI-MS spectrum of vilangin (3) in the negative mode	84
Figure 4.23: ¹ H NMR of vilangin (3) (400 MHz, DMSO, ppm)	85
Figure 4.24: ¹³ C NMR of vilangin (3) (400 MHz, DMSO, ppm).....	86
Figure 4.25: UV-VIS spectra of embelin and embelin standard and methyl vilangin in dichloromethane, scan 200-800 nm	88
Figure 4.26: FTIR of embelin and embelin standard and methyl vilangin	89
Figure 4.27: LC-ESI/MS spectrum of methyl vilangin (4) in the negative mode	90
Figure 4.28: ¹ H NMR of methyl vilangin (4) (400 MHz, DMSO, ppm)	92
Figure 4.29: ¹³ C NMR of methyl vilangin (4) (400 MHz, DMSO, ppm).....	92
Figure 4.30: UV-VIS spectra of embelin and embelin standard and compound 5 in dichloromethane,scan 200-800 nm	94
Figure 4.31: FTIR of embelin and embelin standard and embelin-2,4 - dihydroxybenzaldehyde (5)	94
Figure 4.32: LC-ESI/MS spectrum of embelin 2,4-dihydroxybenzaldehyde derivative	95
Figure 4.33: ¹ H NMR of embelin-2,4 -dihydroxybenzaldehyde (5) (400 MHz, DMSO, ppm)	97
Figure 4.34: ¹³ C NMR of embelin-2,4 -dihydroxybenzaldehyde (5) (400 MHz, DMSO, ppm)	97
Figure 4.35: The UV-Vis absorbance spectra for embelin, embelin standard and embelin ninhydrin	99

Figure 4.36: The ATR- FT-IR spectra of embelin, embelin standard and embelin ninhydrin in the range 4000-500 cm^{-1}	100
Figure 4.37: LC-ESI/MS spectrum of embelin ninhydrin in the negative mode.....	102
Figure 4.38: ^1H NMR spectra of embelin ninhydrin (6) (400 MHz, d-DMSO, ppm).....	104
Figure 4.39 : ^{13}C NMR spectra of embelin ninhydrin (6) (400 MHz, DMSO, ppm).....	104
Figure 4.40: Effect of pH on colour strength of cotton dyeing with vilangin	106
Figure 4.41: Effect of time on colour strength of cotton dyeing with vilangin	107
Figure 4.42: Effect of temperature on dye exhaustion of cotton dyeing with vilangin	108
Figure 4.43: Plot of 3-D (a) Temperature vs pH (b) Temperature vs time (c) Time vs pH	111
Figure 4.44: Effect of pH on dye exhaustion with ENn cotton dyeing.....	115
Figure 4.45: Effect of time on colour strength of cotton dyeing with ENn	116
Figure 4.46: Effect of temperature on dye exhaustion of cotton dyeing with ENn	117
Figure 4.47: Plot of 3-D (a)- Temperature vs pH (b) time versus pH (c) temperature versus time	120
Figure 4.48: Plot of unmordanted and mordanted ENn cotton dyed fabric.....	122
Figure 4.49: Plot of unmordanted and simultaneous mordanted ENn cotton dyed fabric	122
Figure 4.50: Plot of unmordanted and post mordanted ENn cotton dyed fabric	123
Figure 4.51: Plot of unmordanted and pre- mordanted ENn cotton dyed fabric	124
Figure 4.52: Effect of temperature on dye exhaustion silk dyeing with ENn.....	128
Figure 4.53: Effect of time on dye exhaustion with ENn silk dyeing.....	129
Figure 4.54: Effect of pH on dye exhaustion with ENn silk dyeing.....	129
Figure 4.55: Plot of 3-D (a)- pH vs Temperature (b) pH vs time (c) Time vs temperature	133
Figure 4.56: Plot of colour coordinates for simultaneous mordanted silk fibers.....	135
Figure 4.57: Plot of colour coordinates for post-mordanted silk fibers.....	135
Figure 4.58: Plot of colour coordinates for Pre-mordanted samples	138
Figure 4.59: Effect of pH on dye exhaustion wool dyeing with ENn.....	140
Figure 4.60: Effect of time on dye exhaustion of wool dyeing with ENn	141

Figure 4.61: Effect of temperature on dye exhaustion of wool dyeing with ENn	142
Figure 4.62: 3 D plots of wool ENn dyeing(a)- temp vs pH (b) temp vs time (c) time vs pH strength (K/S), at a temperature of between 65-70 °C Figure 4.79 (a). At a time of 60 min.	146
Figure 4.63: Plot of colour coordinates for simultaneous mordanted wool fibers.....	148
Figure 4.64: Plot of colour coordinates for post-mordanted silk fibers.....	148
Figure 4.65: Plot of colour coordinates for Pre-mordanted samples	150
Figure 4.66: TGA/DSC Curve for blank cotton.....	154
Figure 4.67: TGA /DSC curve of vilangin dye.....	155
Figure 4.68: Overlay of Vilangin dyed cotton fabrics	156
Figure 4.69: TGA/DSC of embelin ninhydrin dye	157
Figure 4.70: Overlay of embelin ninhydrin dyed cotton fabrics	158
Figure 4.71: FTIR analysis of cotton fabric dyed with vilangin.....	160
Figure 4.72 (a): SEM of undyed cotton and (b) vilangin dyed cotton fiber	161
Figure 4.73: ATR-FTIR Spectra of embelin ninhydrin dyed cotton fabric	162
Figure 4.74: (a) SEM of undyed cotton and (b) embelin ninhydrin dyed cotton fiber	163
Figure 4.75: Structure of embelin ninhydrin dye and cellulosic structure interaction.....	163
Figure 4.76: FTIR of dyed silk with embelin ninhydrin and undyed silk	164
Figure 4.77: (a) SEM Blank silk fiber (b) SEM ENn silk dyed fiber	164
Figure 4.78: Structure of embelin ninhydrin dye and metal mordant on silk.....	165
Figure 4.79: FTIR spectrum of wool undyed fiber.....	166
Figure 4.80: Wool ENn dyed without mordants.....	167
Figure 4.81: Possible mechanism between ENn dye molecule and wool fiber	167
Figure 4.82: (a) SEM Blank wool fiber (b) SEM ENn wool dyed fiber.....	168

LIST OF EQUATIONS

Equation 3.1: Chroma equation.....	55
Equation 3.2: Hue angle equation	55
Equation 3.3: Kubelka–Munk equation.....	55
Equation 3.4: General model equation for dyeing using RSM	57
Equation 4.1: Equation for RSM optimization vilangin cotton dyeing.....	110
Equation 4.2: Cotton ENn dyeing model equation using RSM methodology	118
Equation 4.3: S Silk ENn dyeing model equation using RSM methodology using RSM methodology	132
Equation 4.4: Wool ENn dyeing model equation using RSM methodology	144

LIST OF SCHEMES

Scheme 2.1: Scheme for the formation of embelin derivative (10)	28
Scheme 2.2: Synthetic scheme of 2-hydroxy-5-substituted-3-undecylcyclohexa-2,5-diene-1,4-diones (embelin derivative)	29
Scheme 2.3: Embelin ninhydrin adduct synthesis.....	30
Scheme 3.1: Mechanistic formation of embelin derivatives from different substituted aldehydes	44
Scheme 3.2: Mechanistic formation of embelin ninhydrin derivative	47

LIST OF ABBREVIATIONS AND ACRONYMS

a*	Red/Green value
ANOVA	Analysis of Variance
API-ES	Atmospheric pressure electrospray ionization
ATR-FTIR	Attenuated Total Reflectance-Fourier Transform Infra-Red spectrometer
b*	Blue/Yellow value
BC	Before Christ
C*	Chroma
¹³ C-NMR	carbon-13 Nuclear Magnetic Spectroscopy
CCM	Central composite design
CHO	Carbon,hydrogen,oxygen
CID	Collision Induced Dissociation
CETELOR	Centre D'Essais Textile Lorraine,France
CHNS	Carbon, Hydrogen, Nitrogen ,Sulphur
CIELAB	CIE-Commision on Illumination,L-luminosity,a*,b*-represent unique colouts;red,green,blue,yellow
DEPT	Distortionless Enhancement by Polarization Transfer
DSC	Differential scanning calorimetry
DW	dry weight
D65	CIELAB illuminant-North Sky Daylight
DKHDA	domino Knoevenagel hetero Diels–Alder reaction
DPPH	2,2-Diphenyl-1-picrylhydrazyl
DSC	Differential scanning microscopy
ENn	Embelin Ninhydrin
ESI	Electrospray ionization
ESI/MS/MS	Electro spray Ionization Tandem Mass spectrometry
FAA	Free Amino Acids
GAE	gallic acid equivalent

GC-MS	Gas Chromatography-Mass Spectrometry
GPS	Geographical positioning system
H.E.A: A	Hexane/ethyl acetate/acetic acid
H:E.A	Hexane/ethyl acetate
¹ H NMR	Proton Nuclear Magnetic Spectroscopy
HOMO	highest occupied molecular orbital
Hp-AIs-SL	High performance autosampler
HPTLC	High-performance thin-layer chromatography
h ⁰	hue angle
ISO	International Standard Organization
K/S	K (absorption coefficient and S -light scattering coefficient (S)
L*	Lightness
LC/ESI/MS	Liquid chromatography-Electro spray ionization-mass spectrometry
LC-MS	Liquid chromatography-mass spectrometry
LC/MSD	Lab liquid Chromatograph/Mass selective detector
LC/UV/PDA	Liquid chromatography-ultra violet-photo diode Array detector
LUMO	lowest unoccupied molecular orbital
M/Z	Mass-to-charge ratio
¹ H NMR and ¹³ C-	Proton and carbon-13 Nuclear Magnetic Spectroscopy
NMR	
PDA	Photo Diode Array
pH	Potential of hydrogen
Q-TOF-MS	Quadrupole time- of- flight micro mass spectrometer
Rf	retardation factor
RSM	Response surface methodology
SD	Standard deviation
SEM	Scanning Electron Microscopy
TCC	Thermostated column compartment
TGA	Thermogravimetric analysis
TLC	Thin layer chromatography
TMCS	Trimethylchlorosilane

TPC	total phenolic content
UHPLC	Ultra-High Performance Liquid Chromatography
UV	Ultra-Violet
UV-VIS	Ultra-Violet Visible spectrophotometry
VWD	Variable wavelength detector
XIAP	X-linked inhibitor of apoptosis protein

ACKNOWLEDGEMENT

First and foremost, I am grateful to GOD Almighty, for the grace and favour in this life to be where I am today. Special thanks goes to my supervisors, Sir Prof. Ambrose Kiprop, Dr. Sarah Chepkwony of Moi University and Dr. Isaac K'Owino of Masinde Muliro University for their guidance, advice and positive criticism during the entire research and write up of thesis. My special gratitude to The World Bank Group through the Africa Centre of Excellence II in Phytochemicals, Textile and Renewable Energy who awarded me a scholarship towards the attainment of this PhD degree in Moi University. My gratitude also goes to the French embassy in Kenya who awarded me a scholarship to do research at Laboratoire d'Etudes et de Recherche sur le Matériau Bois (LERMAB), Université de Lorraine, Faculté des Sciences et Techniques at the University of Lorraine, France. My special appreciation to Prof. Philippe Gérardin, Prof. Christine Gérardin and Prof. Stéphane Dumarçay for the support and guidance during my research stay at University of Lorraine (LERMAB), France.

I acknowledge Egerton University for granting me a study leave for my entire study period. I am also grateful to Vincent Rotich, Enock Langat of Rivatex East African Limited and Bernard Dulo of Moi University for the assistance they granted me in my period of stay at Rivatex East Africa.

Special thanks to Paul Kipkorir of Chemistry laboratory, Moi University and my ACEII-PTRE colleagues, Florence Opondo, Caroline Nakiguli Kiwanuka, Wilson Kosgey, Michael Cheloti, Abigael Jepchirchir, Decra Moraa, Lucy Nyambura, Papias Nteziyaremye and Timothy Omara.

CHAPTER ONE

INTRODUCTION

1.1. Background Information

Up until the second half of the 19th century, organic colorants derived from natural sources like plants and insects were used as textile dyes or lake pigments for paintings, sculptures, and other polychrome works of art. However, the discovery of the synthetic dye "mauve" revolutionized fashion and was indirectly responsible for enormous advances in the food and pharmaceutical industries. This led to an explosion of research within synthetic chemistry, which enabled a rise in commercial applications of chemistry (Gupta *et al.*, 2019).

Nevertheless, the usage of synthetic dyes has had a detrimental effect on the ecology through excessive use of coal for the production of pigments (Ardila-Leal *et al.*, 2021). Although these fossil fuels occur through natural processes and take millions of years to form, they deplete much faster than new ones generated. This negative effect on natural resources has caused natural dyes popularity, and their potential use as suitable alternatives to synthetic dyes (Saxena & Raja, 2014). Synthetic dyes have also been known to release enormous amounts of hazardous chemicals through textile wastewater that are harmful to health and many organisms (Das & Mondal, 2012). These azo dyes, when they find their way to the water system are toxic. Their toxicity have been reported in fish, crustaceans, algae and bacteria (Ferraz *et al.*, 2011; Hernandez-Zamora & Martinez-Jeronimo, 2019).

As a result, strict environmental and economic regulations for the use of chemicals have been adopted recently, including the prohibition of various consumer goods, particularly those using synthetic azo dyes (-N=N-) (Shahid & Mohammad, 2013). Due to the negative impact

that synthetic dyes pose on the environment, developed countries and advanced countries are investing huge amounts in research related to natural dyes because of safety and eco-friendliness (Bafana *et al.*, 2011; Kabir *et al.*, 2019; Roy Choudhury, 2013). Consumers globally on the other hand are looking for safe and eco-friendly textile fabrics (Brosdahl *et al.*, 2010; Eifler *et al.*, 2013). Thus shifting focus to naturally dyed fabrics.

Natural colors usually referred more often to as "dye". Specifically, pigments are made by living organisms hence natural colourants are from native sources origin (Aberoumand, 2011). These dye sources are renewable and sustainable and known as environmentally friendly though sometimes negatively because they are less reliable compared to synthetic dyes (Fröse *et al.*, 2019; Stoyanova *et al.*, 2016).

A large number of diverse plant genera, are historically said to be used by various ethnic communities. The practice of dyeing has been across the diverse civilization. The blend of substances taken from the European madder plant (*Rubia tinctorum L*), which produced an orange-red dye was one of the ancient dyes utilized. Anthraquinone derivatives can be found in significant concentrations in madder plants. Alizarin, purpurin, xanthopurpurin, rubiadin, pseudopurpurin, munjistin, lucidin, indigo, saffron, and their derivatives are some of the fifteen chemicals identified in madder roots that have been determined to play a significant role in dyeing (Chengaiyah *et al.*, 2010; Drivas *et al.*, 2011).

The vast population of plant species possesses enormous economic potential. Plants are a known natural source adding colourants. *Embelia schimperi*, a member of the Myrsinaceae family of plants, is one of the recognized species. It is used by the Maasai people of Tanzania and Kenya to cure adult *Taenia saginata* commonly known as the beef tapeworm (Rondevaldova *et al.*, 2015). As it is well known to contain antifungal and antimicrobial

fighting abilities (Paul *et al.*, 2011), compounds called embelinone and schimperinone were discovered in chloroform extract solvents (Machocho *et al.*, 2003). Flavonol glycoside has been isolated from the methanolic extracts (Manguro *et al.*, 2004) of *Embelia schimperi*, and the 2,5-dihydroxy-3-methyl-1,4-benzoquinone molecule was isolated after the chromatographic separation of an ethyl acetate extract from *Embelia schimperi*, commonly known as embelin (Atlabachew *et al.*, 2017; Awino *et al.*, 2008). Embelin is a naturally occurring alkyl-substituted hydroxyl benzoquinone and a major constituent of *Embelia ribes* and is a known polyphenolic (Hsueh *et al.*, 2019). Because plants contain such large amounts of polyphenolic chemicals, they are reported in the literature and their modification for synthetic phenols is known (Pawar *et al.*, 2018). Among the polyphenols, a varied class of phenolic chemicals with a variety of biological functions are quinone (Martínez & Benito, 2005). Among them, benzoquinones and naphthoquinones are frequently found in nature. Embelin (2, 5-dihydroxy-3-undecyl-1, 4-benzoquinone), an orange pigment, has been isolated from the berries of the Indian shrubs *Embelia ribes* (Radhakrishnan & Gnanamani, 2014) and *Embelia schimperi* (Rondevaldova *et al.*, 2015) and it has become important in medicine due to its anthelmintic and analgesic abilities. Although its dyeing abilities have long been recognized, virtually little research has been done on using embelin or dyes for these applications. Figure 1.1 shows the structure of the embelin.

The use of natural dyes was revived as a result of the aforementioned considerations, which boosted the demand for research into the development of colours that are safe for both people and the environment. Despite the fact that embelin's use as a natural dye has been documented in the literature, little is known about its fastness when used for dyeing or embelin-related

activities (Radhakrishnan *et al.*, 2011) therefore studies in the present work aims to derivatize embelin to achieve dyes with good fastness property.

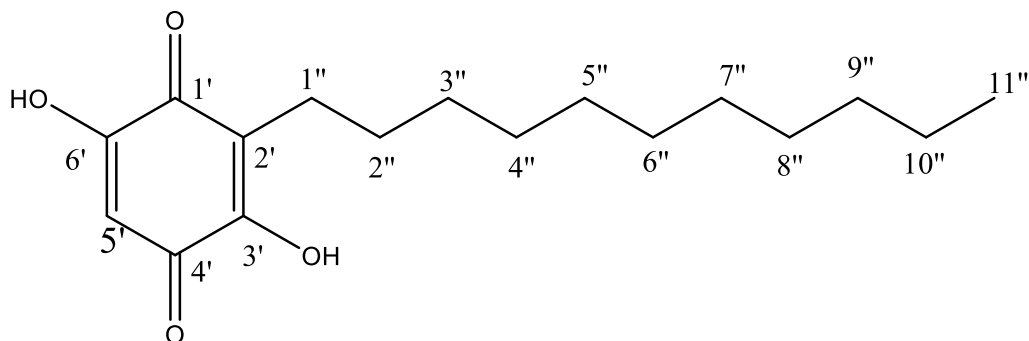


Figure 1.1: Embelin structure

1.2. Statement of the problem

Natural colourants and dyes are very important in the textile, food, and pharmaceutical industries, producing confectionery, cosmetics, medicines, leather, paper, paint and ink (Křížová, 2015). The last decade has seen a global shift in research on natural dyes as a possible replacement for synthesized dyes which have proved to have a widespread negative impact on both the environment and people (Yusuf & clothing, 2019). Natural dyes are eco-friendly and provide tolerance to human health. However, these natural dyes have associated problems such as non-reproducible shades, poor fastness properties (Saxena *et al.*, 2014) and insoluble in water (Ghaheh *et al.*, 2014). Embelin a benzoquinone, according to Samantha *et al.*, (1996) isolated from *E.ribes* on acid hydrolysis dyed cotton, silk, wool, nylon and hair (Samatha *et al.*, 1996). However upon examination retention of colour was found to be of poor quality and has poor solubility (Radhakrishnan *et al.*, 2014). Singh *et al.*, developed a beauty cream from embelin isolated from *Embelia ribes* however the embelin was only soluble in an organic solvents like; alcohol, benzene chloroform and insoluble in water (Singh *et al.*, 2015). These organic solvents are associated with health hazards such as

allergies. The purpose of this work was to chemically modify embelin to create semi-synthetic dyes with improved colorfastness and water solubility that would retain colour better in textile fibers.

1.3. General objective

The study aimed to chemically modify embelin compound from *Embelia schimperi* and assess their dyeing properties on textile fibers.

1.3.1. Specific objectives

The precise specific objectives were to:

1. Isolation and characterization of embelin from *E. schimperi* plant parts
2. Chemically modify embelin and characterize the derivatized embelin compounds.
3. Evaluate dyeing properties of derivatized embelin compounds on cellulose, silk and wool fibers.

1.4. Hypotheses

1. Embelin can be isolated and characterized using *E. Schimperi*
2. Chemical modification and characterization of derivatized embelin compounds can be done
3. Evaluation of dyeing properties of derivatized embelin compounds on cellulose, silk, and wool fibers can be determined.

1.5. Justification

In an effort to counter the negative effects that synthetic dyes have on the environment, a number of commercial dyers and small textile export firms have recently begun exploring the potential of regularly dyeing and printing fabrics with natural colours. Chemical

modification of natural dyes leads to adequate reproducibility of shades, superior fastness properties and improved fiber fixation among other inherent challenges (Pawar *et al.*, 2018). Pawar (2018), synthesized various azo compounds (modified dyes) using epicatechin as a precursor which is a polyphenolic compound a plant-based polyphenolic ingredient called areca nut extract to create semi-synthetic colours with good colour fastness (Pawar *et al.*, 2018). Embelin a benzoquinone has been known to have dyeing properties according to Radhakrishnan *et al.*,(2011) however retention of colour and water solubility are poor (Radhakrishnan *et al.*, 2011). .In this study, various embelin-derivatized dyes were synthesized chemically by modifying isolated embelin from *Embelia schimperi*. The chemical modification added functional groups which made the compounds more polar and water-soluble at adjusted pH, thus being cost-effective, and eco-friendly and the textile fabrics attained had excellent colour fastness.

CHAPTER TWO

LITERATURE REVIEW

2.1. History of natural dyes

Natural dyeing is an old technique, used for a time in the memorial as natural colorants for various occasions like ceremonial, body painting, decorative art, and food and textile decoration Figure 2.1. In the ancient days, people used crushed wild fruits especially berries for pigments and paintings (Toerien & Khumalo, 2010). Natural dyeing practice was widespread during the Bronze Age in Europe (Kulkarni *et al.*, 2011). Japanese artisans were known to weave fabric using wood and fiber such as hemp, paper, mulberry and wisteria that grew naturally in their country (Yoshioka & Creativity, 2010). We may never know where the art of dyeing originated, and the first people to dye their textiles (Abdel-Kareem & Apparel, 2012). However the use of synthetic food colorants is widespread both in globally especially the United States (Sharma *et al.*, 2011). The Egyptians were known to derive dyes from vegetables and it is acknowledged that they learned the culture of dyes from Chinese people in a period dating to pre-3000 BC (Before Christ) (Abel, 2012).

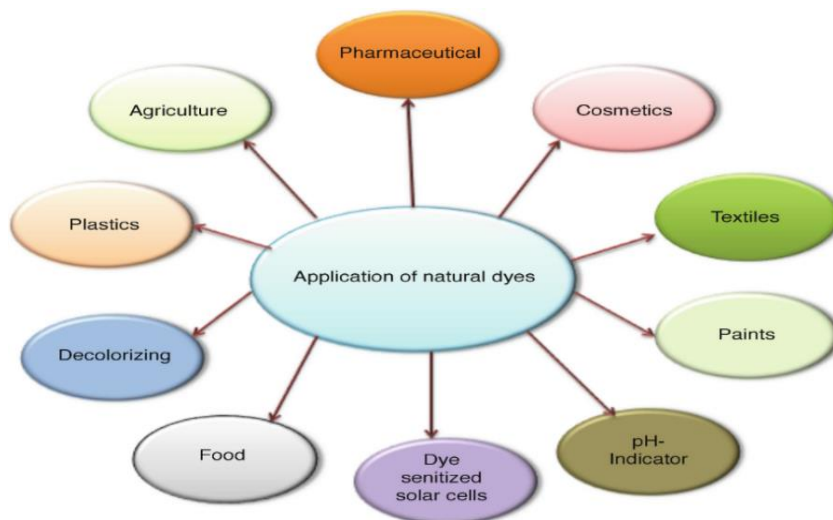


Figure 2.1: Application of natural dyes

The expansion of Mare Nostrum, the location for the first worldwide dye, Tyrian purple probably between the 5th-6th millennium BC enabled material trade with the Romans, the industrious Phoenicians, the Etruscans and the Greeks. Indians have been considered to have quite a history of use of dyes (Melo, 2009). There are more than 450 plants in India that can produce dyes, which has been supported by the discovery of coloured clothing and madder dye traces in the ruins of the Mohenjo-Daro and Harappan civilizations (3500 BC) (Das, 2018). Yellow thread's dye sources were found to be weld, juvenile fustic, and soluble redwood dye in the 16th-century carpets manufactured in Cairo (Otlowska *et al.*, 2018). A wide variety of items, including textiles from medieval Europe have been discovered to have been dyed using the ancient brazil wood dyes (Peggie *et al.*, 2018). Some of the natural dyes and their uses are shown in Table 2.1.

2.2. Application of dyes

Natural dyes have been used to colour leather and feathers, adorn shells, and feathers and in cave paintings. Figure 2.1 shows the various application of natural dyes. The ochre-based

black, white, yellow, and reddish paints that prehistoric man used in his cave drawings have allowed cognitive scientists to date them. Mummies have been discovered in Egypt wrapped in colored clothing (Alawa *et al.*, 2013). Tests done on crimson materials in the tomb of Kings of Egypt revealed the existence of natural organic dyes and pigments, identified to a madder-derived pigment called alizarin (Sharma & Jain, 2013). In more recent history, Alexander the Great reported discovering purple robes from 541 BC in the royal treasury after capturing Susa, the capital of Persia.

Table 2.1: List of natural dyes, their application and sources

Species (Family name)	Traditiona l name	Part Used	Colour obtained	Colour Application	Reference
<i>Acacia catechu</i> (Mimosaceae)	Tilatilayet	Heart wood	Red	Textile (shipsails, mailbags), Calico printing	(Prabhu & Bhute, 2012)
<i>Aegle marmelos</i> (Rutaceae)	Bael,Brel tree (Hindi)	Fruit	Yellow- orange	Food colourant	.
<i>Alcea rosea</i> (Malvaceae)	Meswot	Flower	Red	Food colourant	(Tyub <i>et al.</i> , 2016)
<i>Bidens pilosa</i> (Asteraceae)	Chepkoloit et(Kalenjin)	Leaf	Yellow	Textile dye	(Gautam & Sharma, 2018)
<i>Curcuma longa</i> (Zingiberaceae)	Haldi,Turm eric	Rhizome	Yellow	Food,cosmetic, textile colourant	(Sigrist <i>et al.</i> , 2011)

<i>Dahlia indica</i> (Asteraceae)	Dahlia	Petals	Peech gold	Textile dye	(Gupta <i>et al.</i> , 2006)
<i>Embelia schimperi</i> <i>E.ribes</i> (Myrsinaceae)	Kibong'on g'inik (Kalenjin)	Fruit	Red	Textile dye	(Shankar <i>et al.</i> , 2012)
<i>Fagopyrum esculentum</i> (Polygonaceae)	Buckwheat ,Kota	Grain	Yellow	Textile dye	

The Bible's Book of Exodus makes mention of scarlet-colored linen, which is known as Kermes (after the Kermes insect). Saffron is referenced in the Bible, although henna has been used since 2500 BC (Sharma *et al.*, 2013).

Several natural dyes substance have been extracted from plants variety since the ancient past. Roots, stems, bark, wood, leaves, flowers, and fruits are among the many plant parts which serve as antibacterial (Verma *et al.*, 2017), as natural dye sources for textile and food colouration. Natural colours were extracted from the dry seed endosperm of *Syzygium cumini* (L.) Jambolan fruit using aqueous, acidic, alcoholic, and alkaline extraction methods and investigation for their phytochemicals characteristics assessed. The dye was incorporated into cloth to provide antibacterial fabric (Mariselvam *et al.*, 2017). The root from *Rheum emodi* extracts has been used to yield natural dye which resulted in a range of natural tones on woolen yarn when mixed with metal mordants (Arvindekar *et al.*, 2016). Indigo provides a cooling effect, while turmeric, one of the brightest naturally occurring yellow colours, is a potent antibacterial that revitalizes the skin (Arvindekar *et al.*, 2016).

2.3. Plants as natural sources of dyes

Plant elements that can be found in farming areas in the temperate climate of Austria were looked into as potential sources for natural colors in textile dyeing processes; by using blends of natural dyestuffs in different ratios of iron- and alum-mordants, adequate fastness qualities were obtained for more than 60% of the tested colors (Bechtold *et al.*, 2003). In addition to being planted for its medical properties, the African marigold (*Tagetes erecta* L.), a significant source of carotenoids and Lutein, is also grown as a cut flower and a garden flower. Lutein, a carotenoid pigment, can be found in large amounts in the marigold flowers (*Tagetes*) that gives the yellow to orange-red (Jothi, 2008). Some dyes consist of indigoids, anthraquinones, dihydropyrans, carotenoids and benzoquinone structures. Among the benzoquinone, Myrsinaceae plants have been widely studied.

2.4. Techniques for extracting natural dyes

The use of natural dyes is becoming more prevalent, in the society and their extraction method is equally important (Shi *et al.*, 2005). Natural dyes are extracted using a variety of techniques some are classical methods such as maceration and others are modern-day methods such as ultrasonic-assisted extraction, Soxhlet extraction, and supercritical extraction (Borges *et al.*, 2012; Kasiri & Safapour, 2014). Method consideration is important because of environmental issues and maximum recovery required in the preparation of the dyes. Studies carried out explained that a suitable method of extraction depends on the stability of natural pigments during their extraction, processing, and storage based on specific techniques. Depending on the type of pigments, a suitable pretreatment process of interest must be chosen (Ngamwonglumlert *et al.*, 2017). Using the microwave-assisted extraction technique, natural colours from a wood waste of mahogany powder were successfully

recovered compared to reflux and soxhlet extraction because it gave maximum yield compared to the later methods used (Gala *et al.*, 2020). Simple mixing of various solvents with the plants in a soxhlet extractor or refluxing system will provide dyes from these natural sources. Using a mixture of maceration, soxhlet, and reflux procedures, a study on the extraction of natural colours from sappan wood and mango leaf was conducted. The yield of dyes served as the response factor in experiments to investigate the effects of extraction time and solvent to material ratios revealed that the ideal material to solvent ratio for all materials was 1: 6. And the results demonstrated that the maceration approach, which was followed by the reflux procedure, did indeed yield colours that may be used for fabric colouring on a commercial scale (Sutrisna *et al.*, 2020).

2.5. Qualities of a good dye

Good quality dyes used are the ones considered safe, and ecofriendly (Aggarwal, 2021). The ones with ability to fix itself to fabric without complexity like need of strong acids or heavy metals and soluble (Silva *et al.*, 2020). They should possess different shades bright or dull excellent fastness to light, rub and wetting properties (Silva *et al.*, 2022).

2.6. Chemical modification of natural dyes

The research has shown the utilization of chemically modifying of plant sources as precursor platform for sustainable suitable alternatives to synthetic dyes. Drivas *et al* (2011) chemically modified madder derivatives and used in the dyeing of polyesters (Drivas *et al.*, 2011). Pawar *et al*, (2018) chemically modified polyphenolic compounds from areca nuts and used in the dyeing of polyester and nylon fabrics (Pawar *et al.*, 2018).

2.7. Limitations of natural dyes

Natural dyes possess no limitation in terms of disposal, but their shortcomings are mainly poor colour strength (Prabhavathi *et al.*, 2014). Natural dyes have a small range of colours available (Saxena & Raja, 2014; Tambi *et al.*, 2021) and low solubility (Zhou *et al.*, 2016). Indigo is known to be water-insoluble and sodium hydrosulphite has to be added first before use (Blackburn *et al.*, 2009). Natural resources are also not available in many countries and even where they are present they present complexity in dyeing such as difficulty in blending to produce compound shades (Patel, 2011). Natural dyes usually take longer to dye compared to synthetic dyes (Merdan *et al.*, 2017) and they possess poor fastness properties (Ghaheh *et al.*, 2014). Samantha and Vasudevan in their study revealed that embelin has been used to colour hair, silk, cotton, and wool however it has poor colour retention power (Radhakrishnan *et al.*, 2011). They have been reported to be water-insoluble and soluble in alcohol, chloroform and benzene according to a study conducted by Shankar *et al.*, (2012) which gave reports that embelin had been used to colour silk and wool using alcoholic solution (Shankar *et al.*, 2012).

2.8. Cellulosic fibers: Cotton

A fluffy staple fiber that is almost entirely made of cellulose is cotton. All plants have cells that are mostly made of cellulose which has 1, 4-glucoopyranose connection (Rahman, 2020). It has two types of groups at the ends of the structure: one is a non-reducing group that is present, as shown in Figure 2.2, where a closed ring structure is discovered, and the other is a reducing group that has an aliphatic structure as well as a carbonyl group. The cellulose's - (1-4) linkage distinguishes it from starch's -(1-4) linkage glucose residues (Festucci-Buselli *et al.*, 2007).

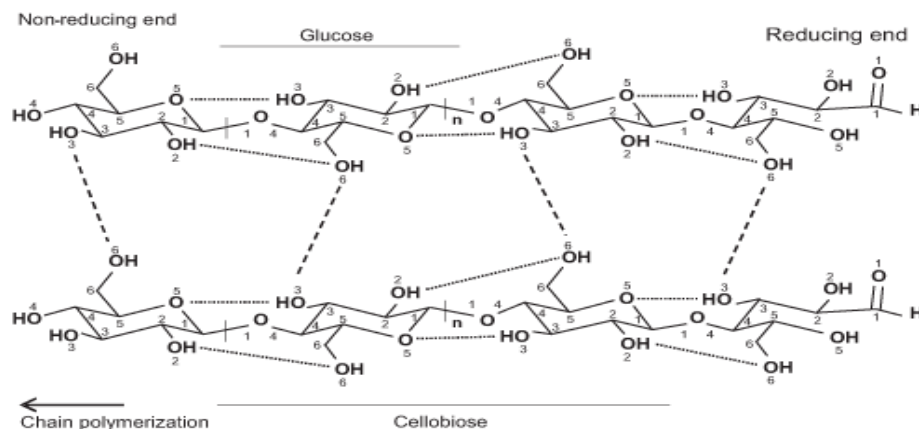


Figure 2.2 Illustrates the structure of cotton with intermolecular and intramolecular hydrogen bonds.

Depending on the reactive group available, dye fixation can occur by nucleophilic substitution or nucleophilic addition processes resulting in the creation of a covalent bond. Reactive dyes that have a halogenated nitrogen heterocyclic ring go through nucleophilic substitution. The aryl ring is made more vulnerable to nucleophilic assault by the electronegative heteroatoms. As the labile group departs with an electron pair, the electron pair on the nucleophile forms a connection with the positively charged, or partially positively charged, electrophile.

2.9. Protein fibers (silk and wool)

In nature, there are several protein fibers. They come from arachnids, insect larvae that spin silk, human hair, bird feathers, and spider webs. Protein is created by linking together numerous amino acid residues (NH-CH(R)-CO) to form a biopolymer, from which it obtains its naturally occurring amino acids. While silk is derived from silkworm cocoons, wool is a textile material that is often obtained from sheep. Wool fibers are formed of the incredibly complex, cross-linked keratin proteins, which include a wide variety of amino acids. The main protein in wool, keratin, is crosslinked using disulfide bonds (Aluigi *et al.*, 2008).

Because wool's amino acid distribution is ionic in nature, the potential of hydrogen (pH) has a significant impact on the fiber's characteristics. Contrarily, silk is made up of fibroin protein made up of amino acids with glycine and alanine being the main constituents (Wani *et al.*, 2020).

Wool can be dyed using acid, metal-complex, mordant, reactive, and a few vat dyes. In addition to one to three sulfonic acid groups per molecule, other water-soluble groups like carboxyl and phenolic can be found in sodium salts of sulfonic acid-based chromogens. Silk's functional groups are protein-like, therefore any dye that works on wool also works on silk. This includes acidic, basic, reactive, and vat dyes. By utilizing mordants-concentrated solutions of basic salts-natural colours can be applied to silk. The fiber is coloured in an acidic dye bath following mordanting..

2.10. Mordants

A mordant is a substance that chemically induces a reaction between the dye and the fabric (Haddar *et al.*, 2014; Mozaffari *et al.*, 2018). Especially for fabrics made from plants, mordants are employed in textiles to stabilize the colour during dyeing or fabric printing (cotton) (Arora *et al.*, 2017). It is usually known that textile fibers can be dyed through the development of a coordinate bond interaction between dye material and the dyed textile fabric. There are different metal mordants tested and in use such as alum, ferrous and chrome because they are accepted environmentally and natural mordants such as tannic acid (Arifeen *et al.*, 2021).

2.11. Improving natural dyes' quality

The capacity of dyes to withstand fading when subjected to end-use treatments including light, crocking, bleach, perspiration, and water is known as their fastness. This quality is divided into light and wash fastness categories.

2.11.1. Light fastness

When compared to synthetic dyes, natural dyes more frequently exhibit poor light fastness due to a chromophoric shift in the dye structure after light absorption because these chromophoric groups are typically insufficient to disperse the energy absorbed resonance (Gupta *et al.*, 2019). The natural dyes fade quickly when subjected to different light fastness standards with an exception of a few dyes such as cochineal, and madder (Degani *et al.*, 2017). The qualities of the cloth being used, the dye's chemical make-up, its physical condition, the type of mordant being used, and the wavelength of the light source being exposed are a few elements that affect a dye's light fastness (Hasan *et al.*, 2016).

The chromophore's photo-oxidation causes the poor light fastness that some natural dyes are known for. By creating a compound of the dye with a transition metal, several researchers have attempted to prevent or limit such photo-oxidation (Vankar, 2000). Alum, stannic chloride, stannous chloride, and ferrous sulphate are examples of eco-friendly mordants that have been used to treat natural dyes to increase their washing fastness (Annapoorani *et al.*, 2014). Tannins with mordants have also been used to minimize photo-oxidation (Prabhu *et al.*, 2011). In addition to rendering tannins insoluble in water and altering their light absorption properties, treatment with metal salts gives a fabric washing fastness. Anthraquinone dyes have good light fastness properties, light fastness of hydroxyanthraquinones was shown to decrease as the number of hydroxyl groups increased

(Cristea *et al.*, 2006). Studies are currently being conducted to find a solution to this inherent problem because light fastness is one drawback of natural dyes in comparison to the more light stable synthetic ones. The light fastness of dye extracts from madder, weld, and wood applied to cotton yarn was increased by using additions such UV (ultraviolet) absorbers in fibers (Lee *et al.*, 2001) furthermore to antioxidants, such as vitamin C and gallic acid (Thiagarajan & Nalankilli, 2013) enhanced the light fastness of cotton yarn dyed with madder, weld, and wood extracts.

2.11.2. Wash Fastness

When compared to synthetic dyes, it has been noted that natural dyed textiles frequently do not have good wash fastness features (Ali *et al.*, 2007). By using various metal salts to improve the wash fastness features, direct natural colors, including as turmeric, annatto, and safflower, are attached to the fiber by weak van der Waals forces or hydrogen bonds that are easily destroyed even when washing is done under gentle conditions (Ding & Freeman, 2017).

2.12. Evaluation of fastness properties

The dyes resistance to fading through washing, rubbing and exposure to light was assessed using developed protocols by different organizations and associations. One such is (International Standard Organization (ISO) PROTOCOL (ISO 105-C02:1989, ISO 105 A02:1993, ISO 105-X12:2000) (Hosseinnezhad *et al.*, 2017; Manyim *et al.*, 2021). This ISO 105 specifies a test for a series of washing fastness it describes how a sample of the textile is mechanically agitated in a soapy solution under specified time and temperature circumstances while in contact with one or two specified adjacent fabrics, one of which is blank, and then rinsed with water and dried. The grey scales for evaluating the color shift of

the dyed sample and the staining of the nearby blank fabric(s) are evaluated using the grey scales for monitoring change (Manyim *et al.*, 2021). The dyed fabrics' reflectance values concerning their CIELAB colour space (L^* , a^* and b^*) indices are measured using SpectroFlash X-rite SP62 spectrophotometer under illumination of D65 (North sky daylight). Where the colour parameters are indicative of L^* (lightness-darkness), a^* (red/green) b^* (blue/yellow), C^* (Chroma) and h^0 (hue angle) respectively (Sinha *et al.*, 2016).

2.13. Evaluation of colour strength

Applying the Kubelka-Munk equation (K/S value), where K is given as the absorption coefficient (K) and S is supplied as the light scattering coefficient (S), allows one to determine the brightness of a colour (Wang *et al.*, 2021) given by Equation (2.1)

$$\frac{K}{S} = \frac{(1-0.01R)^2}{2(0.01R)} \dots\dots\dots\text{Equation 2.1}$$

Where (R) is a certain surface reflectance value at a given wavelength (Sadeghi-Kiakhani *et al.*, 2020). The colour strength (K/S) values typically rise as more dye is absorbed by the coloured fabric . Mordants are also known to improve colour fastness and strengths properties (Sheikh *et al.*, 2016).

The characteristics of the lighting source, how it interacts with the object to change its behavior, and the observer's reaction all affect how colourful an object looks. The L^* (lightness) a^* (Red/Green value) and b^* (Blue/Yellow value) colour space values are calculated by the CIELAB, an opposing colour system, using the same stimulus while taking these factors on account (Bae, 2020).

The changes in the Grey scale from 0 (black) to 100 are represented by the middle vertical axis (L^*), which stands for brightness (white) (Ibraheem *et al.*, 2012).

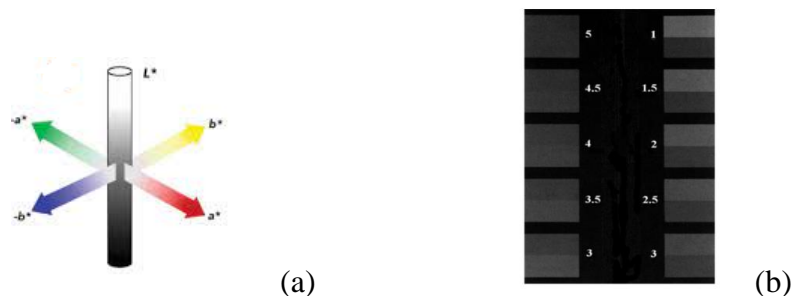


Figure 2.3: (a) CIELAB coordinates (b) Grey scale for colour change

Red and green, as well as blue and yellow, are opposite colours; hence, a colour cannot be both (red and green, for example) at the same time. This is the basis for the colour axis or coordinates in Figure 2.3 (a) (Witzel & Gegenfurtner, 2018). Positive values on the "a" axis represent amounts of red, whereas negative values represent amounts of green. Green is positive and blue is negative on the "b" axis. Zero is a neutral grey area on both axes (Ma *et al.*, 2020). In Grey scale Figure 2.3 is used to measure the fastness characteristics (b).

2.14. Factors controlling the dyeing process

Several factors, such as the material-to-liquor ratio, are necessary for successful dye application to cellulose and proteinous materials (Samanta *et al.*, 2019; Shin & Yoo, 2010). The temperature of experiment in the dye bath (Banchero, 2020; Ma *et al.*, 2020), pH and the time required for dyeing (Arora *et al.*, 2017; Gupta *et al.*, 2019; Kovačević *et al.*, 2021) the fiber's structure, the dye's physical properties, such as its diffusion coefficient, and the fiber's surface features control the affinity between the dye used and the test fiber (Bai *et al.*, 2019; Liu *et al.*, 2020; Pisitsak *et al.*, 2016), the properties of the fiber's surface and the physical features of the dye, such as its diffusion coefficient (Grishanov, 2011; Khattab *et*

al., 2020; Samanta & Konar, 2011). The effectiveness of the dyeing process has been significantly influenced by the equipment utilized (Arputharaj *et al.*, 2016; Banchero, 2020; Ghaly *et al.*, 2014; Saxena *et al.*, 2014).

2.15. Semi-synthetic dyes

Synthetic mauve discovered by William Perkin which revolutionized the industry (Kane, 2014) since the mid nineteenth century. However, these high costs of materials in that period prevented them from commercialization. The production of azo dyes later became a milestone in the textile industry (Hamidian *et al.*, 2013). Several series of indanthrene vat dyes were synthesized in the period between 1901-and 1911 (Stadler & Harrowfield, 2011).

Semi-synthetic dyes are natural dyes modified with new functional groups introduced to improve the dye properties (Nambela *et al.*, 2020). Studies by Pawar *et al.*, (2018) improved the polyphenolic compound from Areca Catechu nuts' dyeability capabilities by combining it with diazonium salts from various primary amines (Pawar *et al.*, 2018). After being used on polyester and nylon fabrics, the resulting modified dyes were discovered to have outstanding overall fastness qualities (Pawar *et al.*, 2020). Alizarin and purpurin were utilized as precursors to modify natural anthraquinonoid dyes, which they then used to colour polyester garments (Drivas *et al.*, 2011).

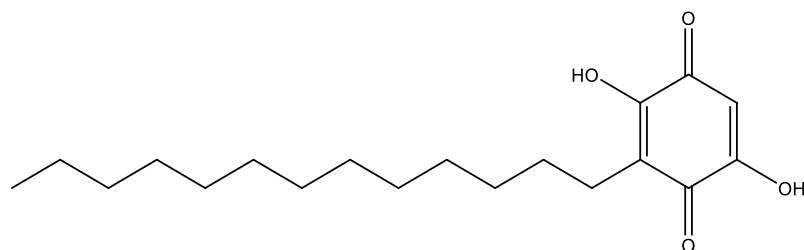
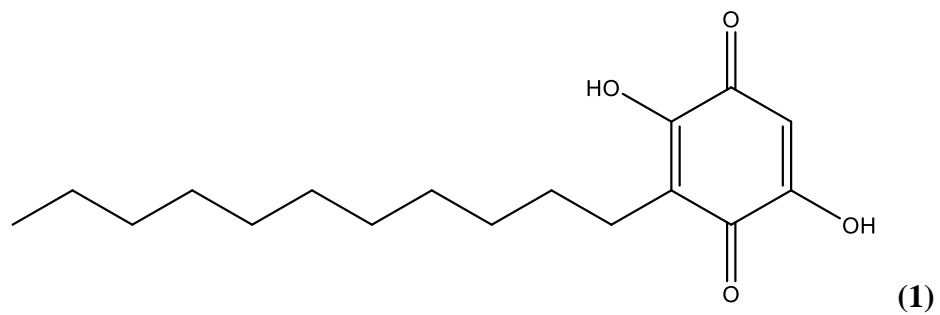
2.16. Benzoquinone dyes from Myrsinaceae plants

More than 1000 plants have been categorized as Myrsinaceae, which is a subfamily of Primulales. Despite being widely distributed around the world, they are primarily found in southern Japan. As seen in Figure 2.4 below, 3,6-dihydroxy-2-alkylbenzoquinones from the Myrsinaceae species have been isolated, and their chemistry has been well studied. Examples

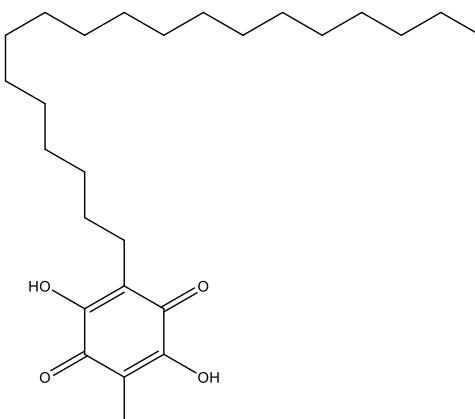
include embelin (1), rapanone (2), maesaquinone (3), and the methylene dimer, vilangin (4) (Andreu *et al.*, 2020; Asha *et al.*, 2017; Omosa *et al.*, 2016; Shuveksh *et al.*, 2017).

2.17. Extraction of embelin

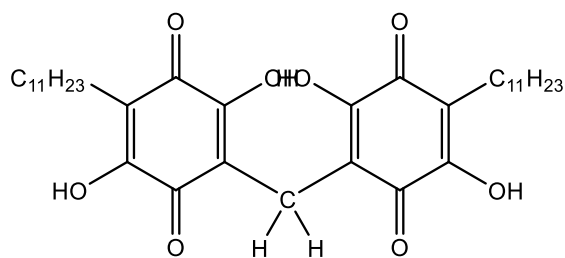
Embelin was discovered to be present in the berries of *Embelia ribes* after being cold-macerated and extracted with n-hexane (yield 3 g, 0.3%) (Mahendran *et al.*, 2011). Additionally, embelin has been discovered in an ethanol extract of *Embelia ribes* leaves (Afzal *et al.*, 2012; Swamy *et al.*, 2007). Benzoquinone pigments have been found in Myrsinaceae plants in Kenya (Omosa *et al.*, 2016).



(2) Rapanone



(3) Maesaquinone



(4) Vilangin

Figure 2.4: Examples of isolated benzoquinones (1-4)

After being dissolved in acetone and separated using High performance thin layer liquid chromatography (HPTLC), leaves from *Myrsine laetevirens* (Myrsinaceae) plants growing in the marginal rain forest of Punta Lara (Buenos Aires, Argentina) were discovered to possess hydroxybenzoquinone pigments (Otegui *et al.*, 1998). Five Oleanane-type pentacyclic triterpenoids (5,6) were isolated from the stem bark of *E. schimperi* that was obtained from Ngong Hills, some 30 kilometers south of Nairobi. There was a methylenedioxy bridge in three of these molecules. Embelinone and Schimperinone, two of the five isolated pentacyclic triterpenoids (shown in Figure 2.5 below), were discovered for the first time (Machocho *et al.*, 2003).

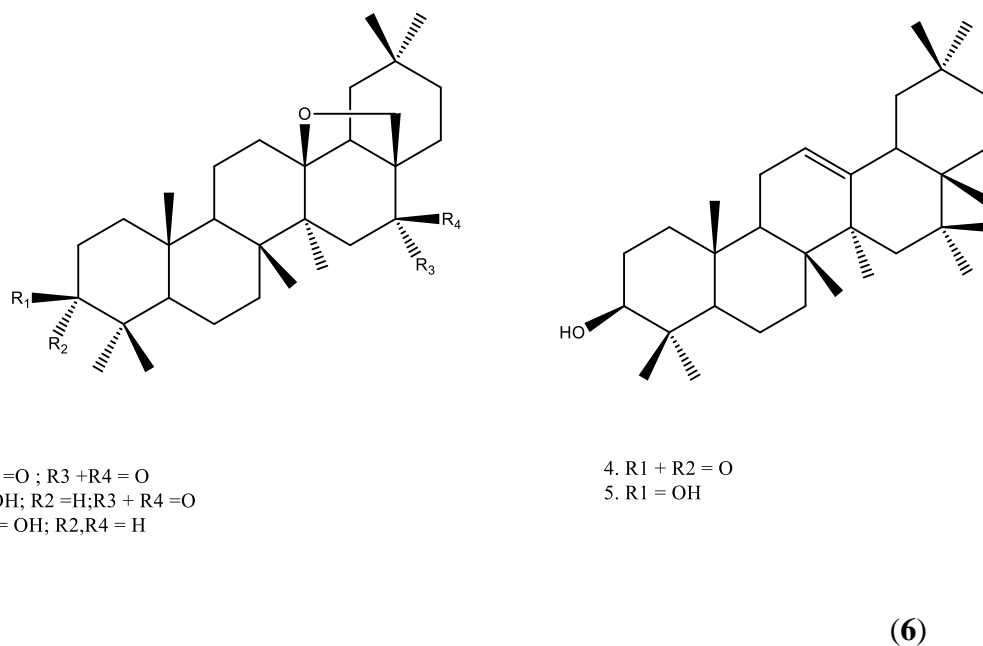
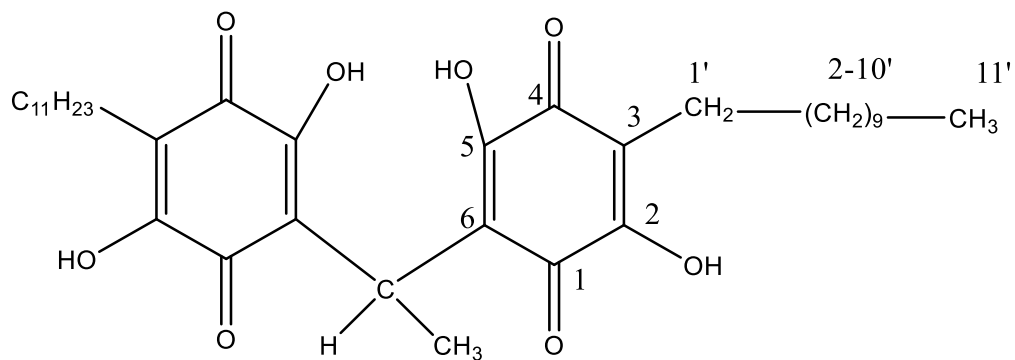
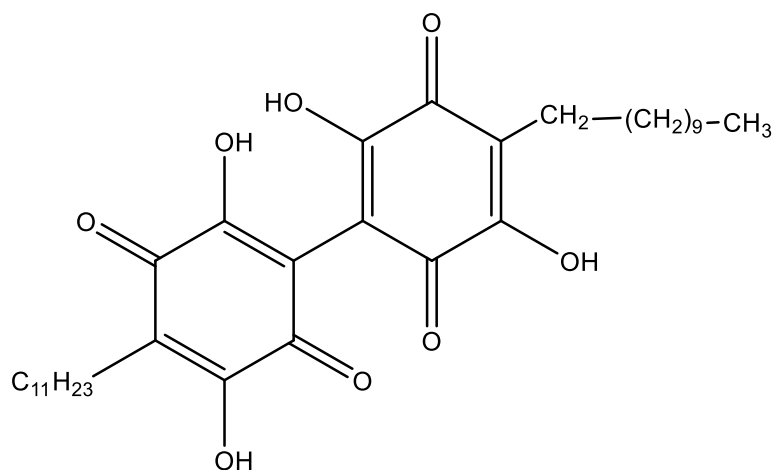


Figure 2.5: Pentacyclic triterpenoids from *Embelia schimperi*

Methyl vilangin was discovered through chromatographic examination of the air-dried berries of *Embelia schimperi* (7), shown in Figure 2.6 below, which was orange in colour, the obtained yield was 50 mg. Embelin (1) shown in Figure 1.1 and biembelin (8) shown in Figure 2.7, were also isolated from *Myrsine Africana* (Kiprono *et al.*, 2004).



(7)

Figure 2.6: Structure of Methyl vilangin

(8)

Figure 2.7: Structure of biembelin

Embelia Schimperii fruits that were gathered from the surroundings in Gonder, Northwest Ethiopia yielded yellow crystals of embelin (Debebe *et al.*, 2015). Berries purchased from Kharibabli, Delhi *Embelia ribes* yielded golden yellow 8.4 % with melting point 142-145°C upon isolation with n-hexane and washing with petroleum ether (Kaur *et al.*, 2015). Coarse powder of *Embelia ribes* fruits was extracted with n-hexane and purification was passed over Silica gel in column chromatography yielding embelin (Chitra *et al.*, 1994). Elution of

column with benzene yielded embelin, which was recrystallized using ether. Embelin was isolated from *Embelia ribes* and the extract achieved 79 and 98 % at 1.0 mg/mL of water and methanol extracts (Hattori *et al.*, 1993). The fresh stem bark of the herbal plant *Embelia schimperi* collected from the Western slopes of Mau ranges in Kericho District which is about 300 km west of Nairobi isolated using ethyl acetate yielded embelin [1]. The 1 kg of coarsely powdered berries were cold-macerated for 72 hours to extract the n-hexane, and the extract was then dried in a rotavapor and chromatographed on silica gel (100–200 mesh). Orange plates of embelin were obtained by elution with benzene and re-crystallization with ether (yield 6.5 g, 0.325%). The percentage purity of embelin was checked by HPTLC when separated using the solvent system ethyl acetate: benzene (70:30) (Thippeswamy *et al.*, 2011).

Fruits from *E. ribes* were air dried at 38 °C and ground into a coarse powder. Cold percolation was used to remove the powdered material (5 kg) for 48 hours while occasional shaking was used. Benzene was used to elute the crude extract (25.8 g), which produced a yellow-orange crystalline powder that was then washed with diethyl ether to produce embelin (Gandhi *et al.*, 2013). Ethiopian scientists discovered the identified substance embelin (1) from hydroalcoholic crude extract of *Embelia schimperi* (Debebe *et al.*, 2015). The total level of embelin was determined to be 3022.6 g/mL in twigs and 1476.5 g/mL in seeds extract, both of which were produced from ethanolic extracts of leaves and seeds obtained in Ethiopia (Rondevaldova *et al.*, 2015).

2.18. Embelin derivatives

The last ten years have seen a significant increase in interest in the synthetic transformations of the biologically active heterocyclic precursor molecule embelin (2,5-dihydroxy-3-

undecyl-1,4-benzoquinone). This has been attributed to the strong reactivity of its carbonyl groups, the active methylene group, and the hydroxyl groups, which have combined to provide difficulties for a number of chemical processes leading to numerous synthetic embelin derivatives (Gudala *et al.*, 2018). Due to the presence of two intramolecular bonds of hydrogen between the quinone and hydroquinone groups on the same ring (Joy *et al.*, 2014) semiquinone radicals are predicted to be produced in both oxidation and reduction reactions. A lengthy alkyl chain (undecyl) substituted on the ring of embelin also gives it solubility in the non-polar phase (Joshi *et al.*, 2009). Embelin can participate in pi-pi stacking interactions and various weak and strong hydrogen bonds with nearby chemical species (Gudala *et al.*, 2018).

The electron charge density in embelin (Shuveksh *et al.*, 2017) is depicted in Figure 2.8 below. They can bind to several transition metals and do exhibit a bidentate nature, according to reports (Cherutoi *et al.*, 2005).

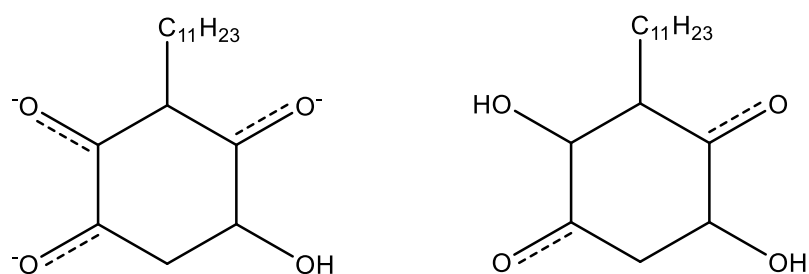


Figure 2.8: Electron density in 2,5-dihydroxy-3-undecyl-1,4-benzoquinone

2.19. Reactions of embelin

Due to the presence of both the quinone and phenolic functional groups on the same ring, embelin is a particularly intriguing molecule. Embelin possesses a lengthy (undecyl) substituent that contributes to its non-polar phase solubility. For instance, the synthesis of amine-substituted derivatives is facilitated by the reaction's carbonyl groups at the C1 and

C4 locations (Mahendran *et al.*, 2011). Different metal complexes are formed by the presence of hydroxyl groups at the C2 and C5 locations (Aravindhana *et al.*, 2014).

According to studies carried out vilangin can be produced by condensation of embelin with formaldehyde in acetic acid solution (Balachandran *et al.*, 2013). Considering that modifications reported in the literature showed that, on the embelin scaffold, the polarity of the linear chain was not affected, embelin analogues bearing a lipophilic chain attached to a hydrophilic benzoquinone moiety **9** shown in Figure 2.8 below, were synthesized to improve water solubility and bio disposability with a potential for anti-cancer activity (Lamblin *et al.*, 2012).

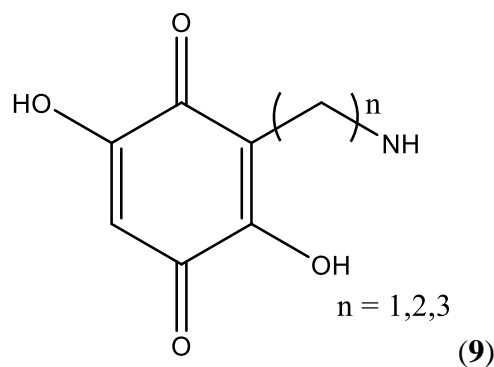
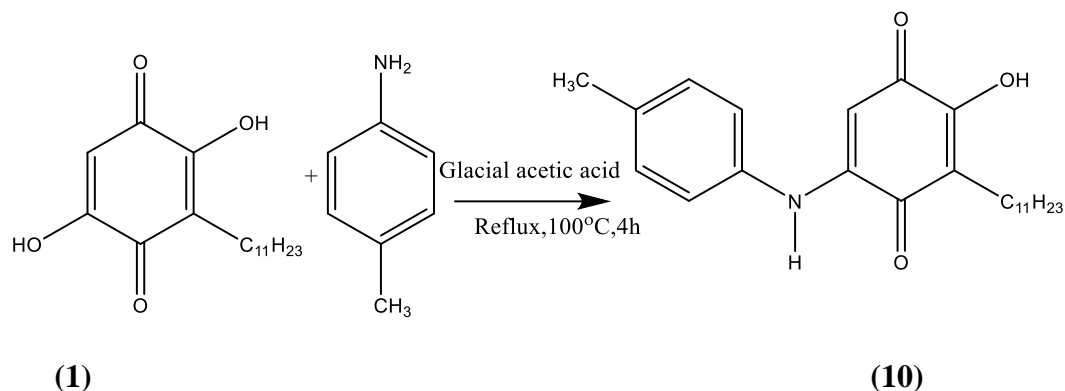


Figure 2.9: Embelin derivative with lipophilic chain

Another synthetic process involved dissolving p-toluidine in glacial acetic acid, which was then refluxed in a water bath for four hours with the mixture of embelin (**1**) obtained from *Embelia schimperi* and p-toluidine, as indicated in Scheme 2.1. The reaction mixture was brought to room temperature before being added to diluted ice-cooled HCl. The purified solid was obtained by recrystallizing the separated solid from a chloroform/ethanol mixture (4:1) after it had been filtered, washed with ethanol, dried, and purified.



Scheme 2.1: Scheme for the formation of embelin derivative (10)

For the therapy of cancer, new embelin analogues have been created, giving 1a-g as the X-Linked inhibitor of apoptosis protein (XIAP) (11) depicted in Figure 2.10 below (Chen *et al.*, 2006). Dihydropyrans and dihydropyridine embelin derivatives that are effective against clinical isolates of multiresistant staphylococcus aureus as well as α -glucosidase inhibition have been created (Penas *et al.*, 2013) and α -glucosidase inhibition (Chen *et al.*, 2020) have been synthesized.

(11) Where R is given below

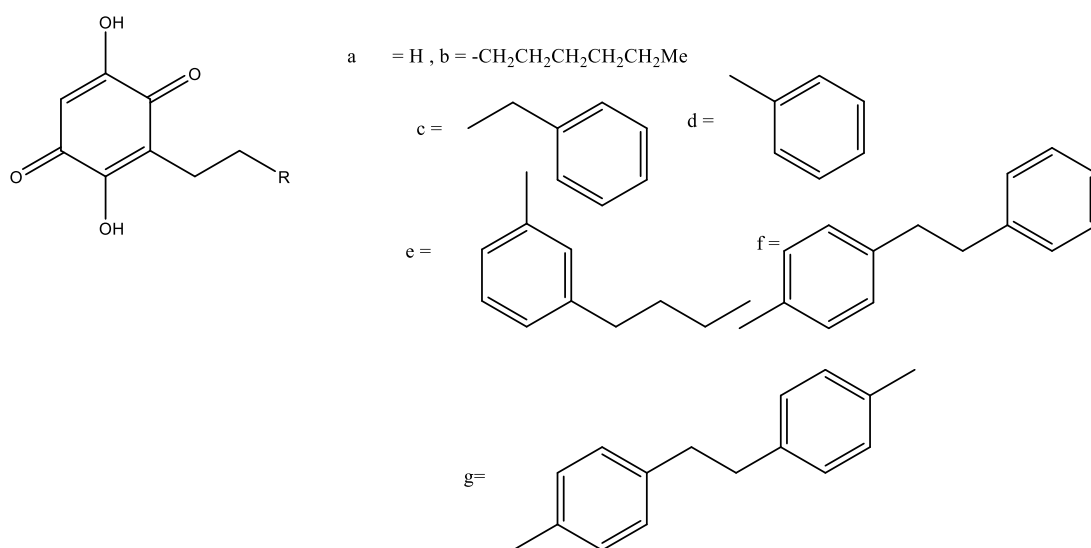
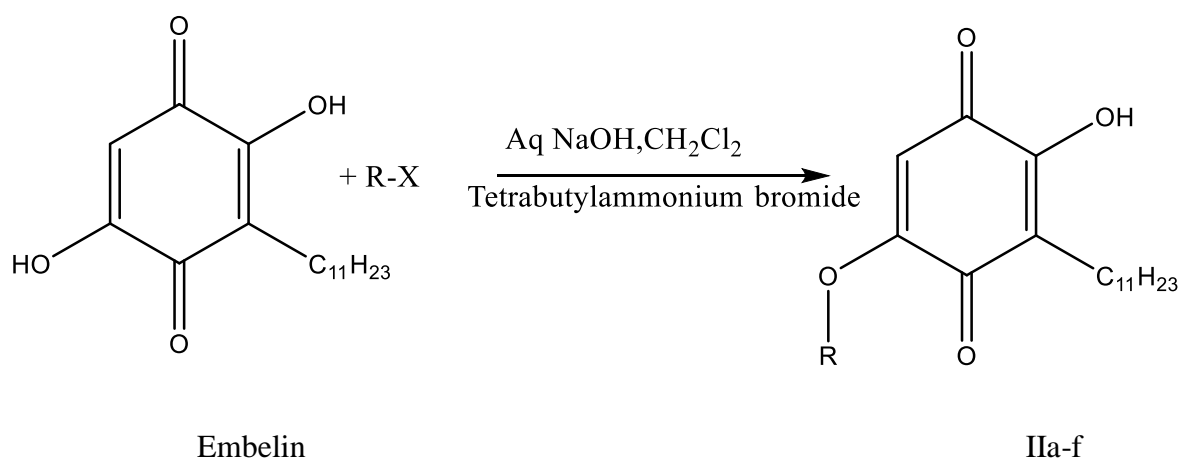


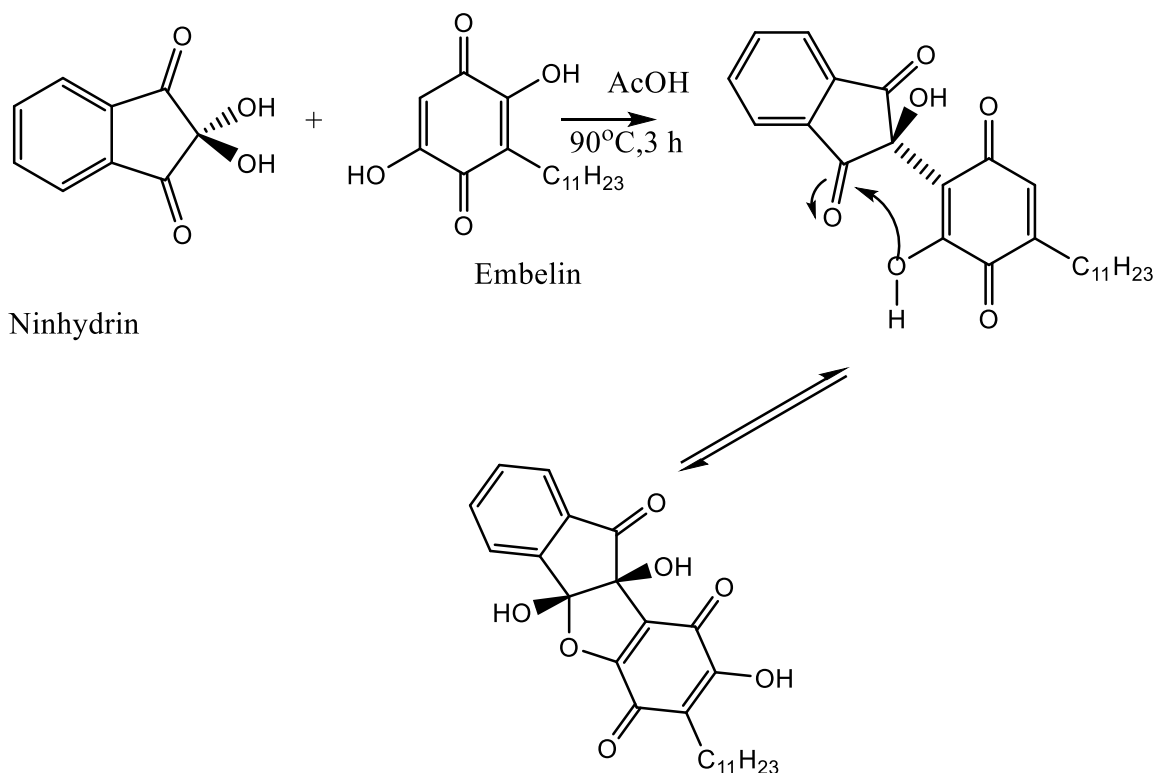
Figure 2.10: embelin analogs as inhibitors of —X-Linked inhibitor of apoptosis protein (XIAP) derivatives

Reports of derivatives of embelin with antimitotic activity have been reported (Srinivas *et al.*, 2010). The reaction to form its respective derivative is shown in Scheme 2.2 where the hydroxyl group was chemically modified to an –OR group for the purpose of studying the impact of derivatized embelin on the lipid status involving cancer as it serves as an indicator of regression or progression of cancer by decreasing testosterone levels. Where R is methylene groups (Srinivas *et al.*, 2010).



Scheme 2.2: Synthetic scheme of 2-hydroxy-5-substituted-3-undecylcyclohexa-2,5-diene-1,4-diones (embelin derivative)

Embelin isolated from *Embelia ribes* berries and condensed with ninhydrin in acidic conditions has been reported (Mahendran *et al.*, 2011). The embelin-ninhydrin adduct was synthesized to improve the biological agent, the adduct contained better antioxidant properties and DPPH compared to the parent embelin compound. The scheme of synthesizing the embelin-ninhydrin adduct is shown in Scheme 2.3 below.



Scheme 2.3: Embelin ninhydrin adduct synthesis

A hydroxy group was added to the side chain of embelin in the embelin ninhydrin adduct to boost the polarity and water solubility for the lead chemical while leaving the scaffold of the 2,5-dihydroxy-1,4-benzoquinone intact.

Aldehydes undergo the Knoevenagel condensation reaction, in which the active methylene molecules create the most beneficial carbon-carbon bonds (Opanasenko *et al.*, 2013). These condensation reactions are usually catalyzed by bases or Lewis acids, with induced temperature elevations (Adimule *et al.*, 2022; Khandelwal *et al.*, 2016). Aldehydes are useful in synthetic reactions by providing means of covalent linkages through condensation reactions (Wang *et al.*, 2021) these reactions involving aldehydes have the advantage that alkylation reactions that can be achieved in a one-pot process (Takeshita *et al.*, 2017). It is

easy to use aldehydes in synthesis without the application of chemical or mechanical forces (Bolm & Hernández, 2019).

2.20. Uses of embelin and its derivatives.

Embelin from *Embelia schimperi* has been studied and found to possess good biological activities and serve as an antifertility agent (Agrawal, 2015) anti-implantation (Kavya *et al.*, 2015) anti-tumor (Xu *et al.*, 2016) anti-inflammatory, analgesic and antioxidant (Mahendran *et al.*, 2011) wound healing (Coutelle *et al.*, 2014) antibacterial (Gupta *et al.*, 2013) and anticonvulsant (Poojari, 2014). They neutralize scorpion-sting, snake-bite and toothache activities (Mahendran *et al.*, 2011). One of the ancient medicines found in India is *Embelia ribes*, which has long been used as a cosmetic to treat skin conditions. An embelin-derived quinone is present in the berries (Radhakrishnan *et al.*, 2011) *E. ribes* is used specifically for dying hair, treating vitiligo and leukoderma, removing pimples, treating acne, and treating carbuncle infections. According to reports, embelin can colour hair, silk, and wool when dissolved in alcohol (Radhakrishnan *et al.*, 2011). They act like polygenetic dyestuffs like alizarin or purpurin (Singh *et al.*, 2014) and this is due to the widespread use of quinonic chemicals. They have a role in a variety of cellular processes and in the mechanics of electron and hydrogen exchanges (Misra *et al.*, 2012).

Compared to embelin, the p-Sulfonylamine phenylamino derivative of embelin showed higher anti-inflammatory efficacy (Mahendran *et al.*, 2011). It was discovered that new compounds created by adding aromatic groups directly connected to the benzoquinone core had enhanced anti-diabetic action and had good anticancer capabilities (Viault *et al.*, 2011) and improved anti-diabetic activity (Maithili *et al.*, 2011). They do have good antioxidant properties (Sekar, 2019) and improved antibacterial activity (Peña *et al.*, 2016).

2.21. Response surface methodology (RSM)

Response surface methodology involves a number of variables and their interactions which have an impact on the response. This is a sophisticated statistical approach or technique that is frequently used to optimize a process. Box and Wilson invented this method in 1951 (Ranganath *et al.*, 2014). This mathematical approach makes it possible to plan experiments that investigate output variables that are influenced by a number of input variables. RSM aids in overcoming issues with conventional optimization techniques. It is a time-saving strategy because it aids in the reduction of experimental experiments. The optimization of dyeing of wool with cotton pod extracts and the dyeing of modified cotton fiber with natural *Terminalia arjuna* dye have both made extensive use of this technology (Haji *et al.*, 2016) which is another use was the dyeing of cotton fiber using natural *Terminalia arjuna* dye (Sinha *et al.*, 2016).

2.22. Physical and spectroscopic techniques

Several spectroscopic determinations have been carried out to determine structures of embelin and synthesized compounds.

2.22.1. Melting point determinations

Melting point is a significant factor in the formulation of various products in the manufacturing sector because the dissolution factor is dependent on it. Correlation is usually expected between structure and melting points (Batisai *et al.*, 2014) because the forces holding the structure influence the solubility of the compound. The melting point gives the purity of a compound and hence becomes a secondary identification indicator

2.22.2. UV-VIS Spectroscopy

It is one of the oldest known methods in spectroscopic analysis (Falcão & Araújo, 2013; Tomaszewska *et al.*, 2013). It entails the study of molecules, where the molecule's absorption range is crucial for identifying the material's advantageous usage (Chandralekha *et al.*, 2020). When molecules absorb light with enough energy from photons, the light is converted into kinetic energy as the electrons accelerate to higher states of excitation (Aslam *et al.*, 2018; Brongersma *et al.*, 2015). Although some stimulation wavelengths produce a transition in the electronic energy states, Ultra-Violet/Visible light's energy is still absorbed (Kumar & Devi, 2011; Mathew *et al.*, 2012). The electronic energy levels are excited by ultraviolet and visible light in the 100 nm to 700 nm wavelength range (Mizoguchi *et al.*, 2004; Zhu *et al.*, 2010). Embelin has been analyzed using Ultra-Violet/Visible spectroscopy (UV/VIS) and maximum absorbance was found at around 290-295 nm (Aravindhana *et al.*, 2014).

2.22.3. Attenuated Total Reflectance-Fourier Transform Infra-Red Spectroscopy

The Attenuated Total –Fourier Transform Infra-Red Spectroscopy (ATR – FTIR) is a very potent tool for investigating functional groups (Depciuch *et al.*, 2016; Khan *et al.*, 2018). The FTIR frequency is somewhere between (700 nm to 1000000 nm or 1 mm). Compared to the energy in the ultraviolet and visible ranges, this region has less energy (Norgard & Best, 2017; Whittemore *et al.*, 2017). Instead of the electrical transitions that take place in the ultraviolet-visible region, the transitions in this region are caused by the rotational and vibrational motions of a molecule (Cozzolino & Agriculture, 2015; Guan *et al.*, 2020). The wavelength measurements are made in wavenumbers (cm^{-1}), which are detectable between 12800 cm^{-1} and 10 cm^{-1} , to facilitate analysis (Boonmung, 2003; Vaz, 2019). It is simpler to ascertain the structure of a molecule when light with appropriate energy interacts with it and the vibrational mode of the molecule matches a bond within the molecule (Bakker & Skinner,

2010). The dipole moment of the molecule under consideration must have undergone a net change. Unless it is not "IR active," the molecule (Kim & Cho, 2013; Mollica Nardo *et al.*, 2020). Fourier Transform Infra-Red (FTIR) spectra of isolated and conventional embelin demonstrated striking similarities, according to spectroscopic experiments that have been conducted (Shaikh *et al.*, 2016; Sivasankar *et al.*, 2017). The Infrared spectrum of crude powder of *E. ribes* stem, leaves, and berries are shown to confirm the presence of phenol at a peak of 3775.23/cm. Amines and amides functional groups are present at 3305.54/cm. The peak at 2918.20 and 2854.03/cm confirms the presence of alkanes (Kamble & Gaikwad, 2016).

2.22.4. Nuclear Magnetic Resonance

Structure elucidation uses the potent spectroscopic method known as nuclear magnetic resonance (NMR) (Silva & Pinto, 2005; Simpson *et al.*, 2012). It is a physical phenomenon whereby nuclei under the influence of a powerful constant magnetic field are agitated by a weakly oscillating magnetic field, and the response produced is an electromagnetic signal equivalent to the frequency of the magnetic field at the nucleus (Ross & medicine, 2019; Timmel *et al.*, 2004). When the oscillation frequency is identical to the inherent frequency of the nuclei, this occurrence takes place close to the resonance (Ananthapadmanaban, 2018; Chen *et al.*, 2015) depends on the precise static magnetic field's strength, the chemical makeup of the nuclei, and the isotope's torsional magnetic characteristics (Hore, 2015; Kleckner *et al.*, 2011). Nuclear magnetic resonance spectroscopy is a method that has been widely applied to the study of non-crystalline materials as well as the determination of the structure of organic molecules found in solution and in the study of molecular physics and

crystals. ^1H and ^{13}C are the nuclei most frequently employed (Chalbot & Kavouras, 2014; Hameed *et al.*, 2017; Martineau, 2014; Stebbins & Melts, 2018).

NMR spectroscopy verified the embelin component obtained from the Ethiopian medicinal plant *Embelia schimperi*. The purified sample's ^1H -NMR and ^{13}C -NMR spectra proved that the substance was embelin. The results of ^1H -NMR (400 MHz, CDCl_3) (400 MHz, CDCl_3) revealed (Debebe *et al.*, 2015).

2.22.5. Scanning Electron Microscopy

Scanning electron microscopy (SEM) is a versatile technique where electron microscope that produces morphology of a sample (Rozina *et al.*, 2022) by imaging the outer layer with a focal array of electrons. Atoms in the sample are in contact with these electrons. These atoms create a number of signals that reveal details about the sample's surface topography and chemical composition. The electron beam scans quickly in a pattern, and the combination of position and intensity yields an image (Zhou *et al.*, 2006).

2.22.6. Elemental analyzer

An elemental analyzer is a kind rapid and sensitive equipment that gives information on the elemental composition in a compound of interest. A sample is superheated to gaseous form for it to be swept through the analyzer by a carrier gas. The samples are converted to carbon dioxide, water and nitrogen oxides in presence of enriched oxygen after conversion they are later reduced, separated and determined using a detector

2.22.7. Thermal Gravimetric Analysis

Thermogravimetric Analysis (TGA) is a method for calculating how much and how quickly a material's weight changes as a function of temperature or time in a controlled environment.

CHAPTER THREE

MATERIALS AND METHODS

3.1. Study area

Embelia schimperi stem together with the bark (stem bark) was collected from three Counties; Kericho County (0°20'13.3"S 35°22'43.4"E), Narok County (1°50'02.3"S 35°55'14.6"E) and Nandi County (0°06'25.38"N 35°01'0.43"E). Kericho County is 2400m above mean sea level and 260 Km west of Nairobi, Kenya. Narok County is 2300 m above sea level and 150 Km West of Nairobi situated in the southern part of the Great Rift Valley. Nandi County is 1800 m above sea level and 400 Km West of Nairobi situated in the southern part of the Great Rift Valley. *Embelia schimperi* berries were sampled from the Western slopes of Mau ranges in Kericho County only. The berries could not be collected from other counties due to geographic and seasonal variations. The sampling locations are coloured highlights in Figure 3.1.

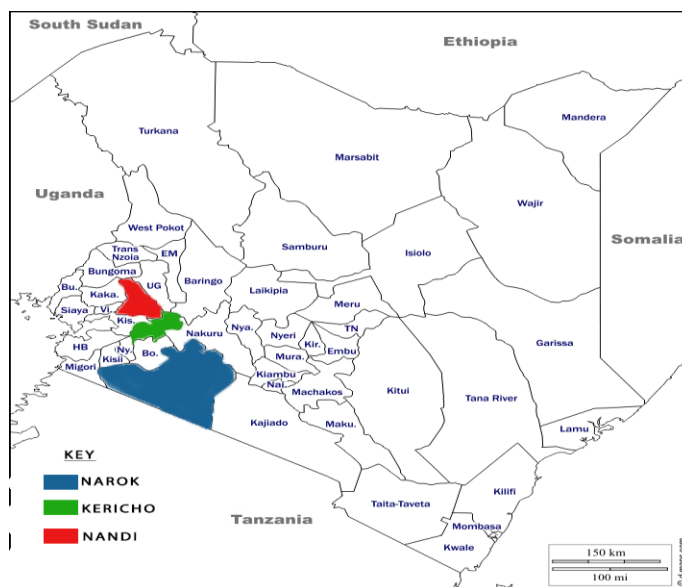


Figure 3.1: Sampling area Map; Kericho, Narok and Nandi Counties

The local geographical positioning system (GPS) details and additional notes of sampling locations are recorded with google coordinates.

3.2. Preparation of plants for extraction

The taxonomic identity and authentication of the study plant were done ,where pressed and identified specimens were deposited in the herbarium of University of Eldoret for future reference under Voucher No MK/KRC/11/20/001. The stem barks and berries samples drying of *Embelia schimperi* was done in the shade. After being dried, the samples were pulverized, tagged, and kept at room temperature until extraction.

3.3. Materials and reagents

The textile fibers utilized in this research included (cotton, silk and wool). Cotton fibers were sourced from Rivatex East Africa outlet in Eldoret. The fibers were already scoured and bleached. Silk and wool were obtained from CETELOR (Centre d'Essais Textile Lorrain, France).

Chemicals reagents and solvents used were ethyl acetate, diethyl ether, hexane, acetone, chloroform, dichloromethane, ethanol, formaldehyde, acetaldehyde, ninhydrin, vanillin, embelin standard, 2,4 dihydroxy benzaldehyde, acetonitrile, hydrochloric acid, sodium chloride, sodium hydrogen carbonate, methanol, phosphomolybdic acid,dioxane, magnesium sulphate and Pre-coated Thin Layer Chromatography Alugram® Xtra SIL G/UV254 silica gel plates for thin layer chromatography were purchased from Merck Millipore.

3.3.1. Instruments

The following instruments were used; Buchi Melting point apparatus,) Carbon,hydrogen,nitrogen,Sulphur CHNS) Elemental Analyzer Carlo Erba 1108 CHNS

(SARM, CRPG), ATR Nicolet 6700 (Thermo Scientific, USA). Beckham Coulter DU 720 UV/Visible spectrophotometer, UV-2550 (PC) SHIMADZU, Shimadzu (Noisiel, France) LC-20A, Clarus 500 GC gas chromatograph, Clarus 500 MS quadrupole mass spectrometer, all from Perkin Elmer Inc. of the United States, Avance DRX 400, NMR spectrometer (Bruker, Germany,(Nutribullet, NB-101B model), ON TESCANA, Vega 3 SBU Scanning electron microscope, Mettler Toledo (Thermogravimetric analyzer) and Radley's equipment MR He: - Tec Ø 135 Radleys EU, P/N: RR 91203/EURO.

3.4. Extraction of *Embelia schimperi* stem bark

The dried powder of *Embelia schimperi* were extracted using maceration method, ultrasonication technique and soxhlet method.

3.4.1. Extraction using maceration method

250 g of the Kericho, Nandi and Narok samples were weighed and extracted using maceration extraction method dissolved in 500 mL solvent (hexane, dichloromethane, ethyl acetate, acetone, chloroform, diethyl ether and ethanol) the solvents were used individually with periodic shaking over 72 hours. Whatman paper No. 1 filter paper was used to filter the macerate, and it was then concentrated in vacuo (HAHNVAPOR Rotary evaporator, HS-2005S model, Korea).

3.4.2. Stem bark extraction using ultrasonication technique

For extraction using the ultra-sonication method, 20 g of dry powder samples of each sample were weighed and extracted using four separate 100 mL extraction times with the following solvents: hexane, dichloromethane, ethyl acetate, acetone, chloroform, and ethanol (10, 20, 30, and 40 minutes) at room temperature (Kamble *et al.*, 2020). The extracts were then decanted, filtered, then the solvent was rotary vaporized under low pressure (HAHNVAPOR Rotary

evaporator), HS-2005S model, S/N: S-01183, Korea, at respective temperature to afford crude extracts (Panichayupakaranant *et al.*, 2010). After that, the combination of the solvents was done and the solution was allowed to cool to room temperature.

3.4.3. Soxhlet extraction

Soxhlet method of extraction was done by weighing 20 g of the sample and placing it in a thimble. Extraction with solvent was done individually (hexane, dichloromethane, ethyl acetate, acetone, chloroform, and ethanol). Extraction was done at four different extraction times (120, 180, 240, 300 and 360 minutes) until given time was achieved with the help of a regulator, the temperature was kept at 60 °C. All the obtained crude extracts were stored at 4 °C awaiting analysis.

3.5. Preparation of crude extracts from *Embelia schimperi* berries

The berries were extracted using the maceration method, using acetone solvent based on the results obtained from section 3.5.1-3.5.3 giving the highest yield.

For extraction of the berries, the sample weighed was 250 g and dissolved in 500 mL of acetone and shaken intermittently for 72 hours. Whatman paper No. 1 filter paper was used to filter the macerate, and it was then concentrated in vacuo (HAHNVAPOR Rotary evaporator, HS-2005S model, Korea). The crude extract was purified using classical column chromatography with solvent system of ethyl acetate and hexane at a ratio of 6:4. Purity of embelin was confirmed by melting point determination and Thin Layer Chromatography (TLC) methods. The TLC solvent solution was composed of ethyl acetate and hexane 6:4 ratio with vanillin as the visualizer. Standard embelin was used to compare to that of isolated embelin in the TLC determination. UV/Vis spectroscopy, FTIR spectroscopy, GC-MS and LC-UV-MS were carried out for acetonic crude extracts

3.6. Qualitative phytochemical screening of *Embelia schimperi* crude extract

A qualitative phytochemical screening was conducted to determine whether or not certain groups of phytochemicals were present (Adedayo *et al.*, 2001; Mohajer *et al.*, 2016). The prepared stem barks and berries crude extract were subjected to different phytochemical tests (Zebeaman & Gebeyehu, 2018).

3.6.1. The Wagner's reagent Test for Alkaloids

The Wagner test 1 mL of diluted HCl acid were added to 50 mg of crude extract after stirring. A few drops of Wagner's reagent were added by the side of the tube to a 1 mL of filtrate (Patil & SA, 2012). The resultant orange-red colour appeared upon the addition of Wagner's reagent indicated presence of alkaloids (Jones & Kinghorn, 2012).

3.6.2. Detection of phenol (Ferric Chloride determination)

About 2 mg of extract was dissolved in 2 mL of distilled water. To the resultant solution, 3 drops of 10% ferric chloride solution was added. A dark green colour indicated the presence of Phenolic compounds (Tamilselvi *et al.*, 2012).

3.6.3. Terpenoid testing (Salkowski test)

Concentrated sulphuric acid (3 mL) was gently added to form a layer after the extracts (5 mg) were thoroughly combined in 2 mL of chloroform. Terpenoids are present when reddish-brown coloration forms at the contact (Wong *et al.*, 2014).

3.6.4. Salkowski test for steroid detection

For these test, 10 mg of the crude extract were dissolved in 1 mL of chloroform and treated with 1 mL of concentrated sulfuric in order to test for the presence of steroids in the mixture.

A chloroform layer precipitate that is reddish-brown and an acid layer fluorescence that is green indicates the presence of steroids (Shukla *et al.*, 2013).

3.6.5. Test for Flavonoids

To 1mL of the extract was placed in a test tube then a few drops of a diluted NaOH solution were added to check for flavonoid content (Zou *et al.*, 2004).

3.6.6. Test for Tannins

Extracts weighing one mg were combined with water, boiled, filtered, and ferric chloride solution. The presence of tannins in the test samples is indicated by emergence of a strong green color (Bate-Smith, 1962).

3.6.7. Detection for Saponins:

The crude extract sample was forcefully shaken with 10 mL of water to conduct a test for saponins and a foam test. Formation of soapy lather is indicative test for presence of saponins. The Brain & Turner, 1975 modified approach was used for this test (Ndukwe *et al.*, 2007).

3.6.8. Test for Glycosides (Cardiac glycoside Keller-Killani Test)

Three drops of 5% ferric chloride and concentrated sulphuric acid were carefully applied around the test tube's containing cooled test sample. Glycosides are present when a reddish-brown color ring appears at the intersection of two layers. The operation was carried out using the modified Daniel and Daniel 1991 approach (Kawale & Choudhary, 2009).

3.7. Quantification of embelin from crude extracts using LC/UV/PDA

Embelin contained in the acetonetic crude extracts was quantified using the liquid chromatography (LC) coupled with the Ultra-Violet (Ultra-Violet/Photo Diode Array detector 9UV/PDA). It is anticipated that the embelin absorption will take place between 230 and 280 nm (Arora, 2012). Dried acetone crude samples (2 mg) were diluted in methanol and

subjected to a 10-minute sonication process before being filtered and reduced to a final volume of 10 mL for LC analysis. Each sample (20 μ L) was analyzed by an LC-PDA method that was optimized and validated using a reversed-phase Chromatopak Peerless basic C18 column (4.6 x 250 mm, 5 mm), detection/monitoring wavelength of 280 nm, column temperature of 25 °C, solvents A and B of water and acetonitrile (adjusted with 5% v/v acetic acid) using isocratic elution at a flow rate of 0.32 mL/min and 10% B in A. By directly comparing the relative retention duration and the UV/Vis absorption maxima of the corresponding peak of the embelin standard, the presence of embelin in *Embelia schimperi* samples was identified. Embelin in the samples was measured using the relative peak area of an integrated curve created using an embelin standard.

3.8. Thin-layer chromatography

The ideal solvent system for isolating the target sample was determined using thin layer chromatography (TLC), the compounds present in *Embelia schimperi* extracts, using TLC separation as per the methods in literature (Bouzeko *et al.*, 2019; Debebe *et al.*, 2015; Harborne, 1998). Different solvents of different polarities were prepared and the TLC method was used to find suitable solvents for separation with good resolution. The solvents used were ethyl acetate (E.A) and hexane (H). Acetic acid (A) was used to avoid the tailing of peaks (Li *et al.*, 2021). Solvents with different polarities were used: (H:E.A: A) 85:10:5, (H:E.A: A) 80:15:5, (H: E.A) 8:2,7:3,6:4, 5:5, and (E.A: H) 7:3 and 6:4. Different visualization techniques used, are the UV lamp and vanillin to visualize the TLC plates. Embelin standard was also used as a reference material in the TLC plates

3.9. Isolation and purification of embelin

The column was packed under n-hexane and ethyl acetate (4:6 ratio) by a slurry method using silica gel particle size (70-230 mesh ASTM), following the method used in literature (Alipieva *et al.*, 2017; Bouzeko *et al.*, 2019). The sample was then loaded into the column, and the solvent system determined by TLC analysis was used to elute the material (ethyl acetate: hexane; 6:4). The compounds with weak affinity to the stationary phase were eluted faster (Dou *et al.*, 2021). The eluate samples were collected in the 20 cm³ test tubes. TLC profiles analysis of each fraction was done and those with the same retardation factor (Rf) values were kept in the same pool and concentrated in vacuo. Pooled fractions with the same Rf value as the embelin standard were subjected to crystallization. The obtained crystals of embelin (**1**) were kept at room temperature and underwent several characterization methods for structure elucidation.

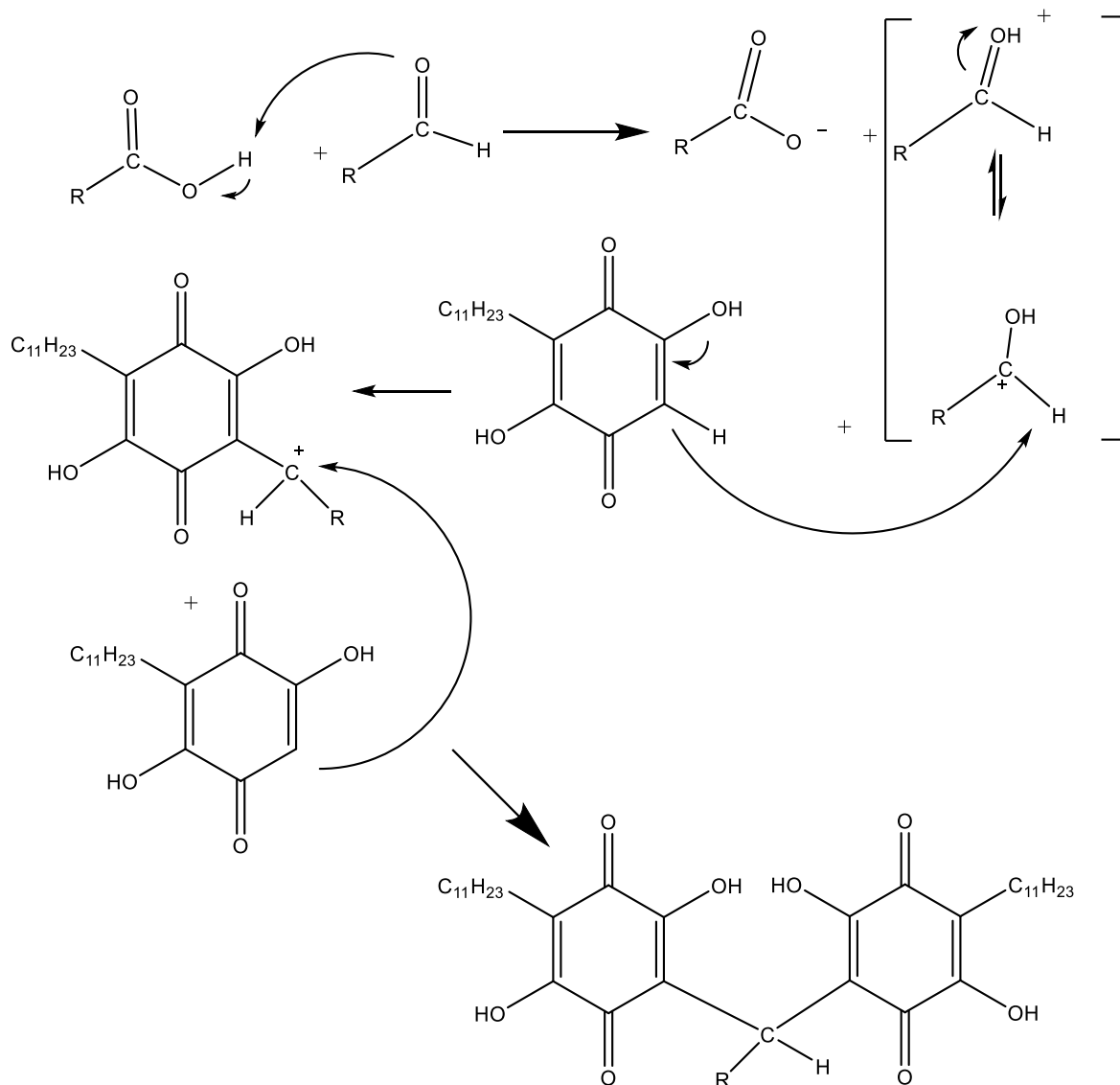
3.10. Characterization of embelin

Different spectroscopic methods, such as ultra-violet, Fourier transform infrared (FTIR), gas chromatography tandem mass spectrometry (GC-MS), liquid chromatography-mass spectrometry, nuclear magnetic resonance, and elemental analysis, were utilized to analyze embelin.

3.11. Chemical modifications of embelin

Chemical modifications were carried out using embelin (**1**) as the precursor compound. Four different types of derivatives were then synthesized namely; vilangin (**3**), methyl vilangin (**4**), embelin-2, 4-dihydroxybenzaldehyde (**5**) and embelin ninhydrin (**6**). Their synthetic procedures are outlined below. Embelin standard was used as a reference and labeled (**2**).

Embelin (**1**), Figure 1.1, has an active methylene group at the C₆ position useful for condensation reactions. The schematic synthetic reaction of 3,4 and 5 is shown in Scheme 3.1.



Scheme 3.1: Mechanistic formation of embelin derivatives from different substituted aldehydes

3.11.1. Synthesis of vilangin (3)

Synthesis of vilangin was done by the method of condensing embelin with formaldehyde in presence of acetic acid solution as per the method described by Balachandran *et al.* (2013) with modification. The isolated embelin (1 g) was weighed and 30 mL of glacial acetic acid solution was added, after which it was gently warmed at 30 °C for 10 minutes. Afterwards 5 mL of 40 % formaldehyde were added. The resultant solution was warmed in a heating bath at 40 – 45 °C while continuously stirring at a constant rate for 10 minutes. The solution obtained was left to stand at ambient temperature to cool. Re-crystallization in dioxane and chromatographic column purification followed (Balachandran *et al.*, 2013). The synthetic set up is displayed in Appendix 1.

3.11.2. Synthesis of methyl vilangin (4)

Methyl vilangin synthesis was carried out by the condensation reaction of embelin with acetaldehyde as shown in Scheme 3.1 in solution of acetic acid solution as per the ascribed method of Balachandran *et al.* (2013) with modification. Isolated embelin (1000 mg) was weighed and 30 mL solution of glacial acetic acid added followed by gentle warming at 30 °C. Thereafter followed by the addition of 5 mL of 40 % acetaldehyde. The resultant solution was warmed in a heated bath at 45 °C while being continuously stirred at a constant rate for 10 minutes. The resulting solution obtained cooled to room temperature and crystallized from dioxane,

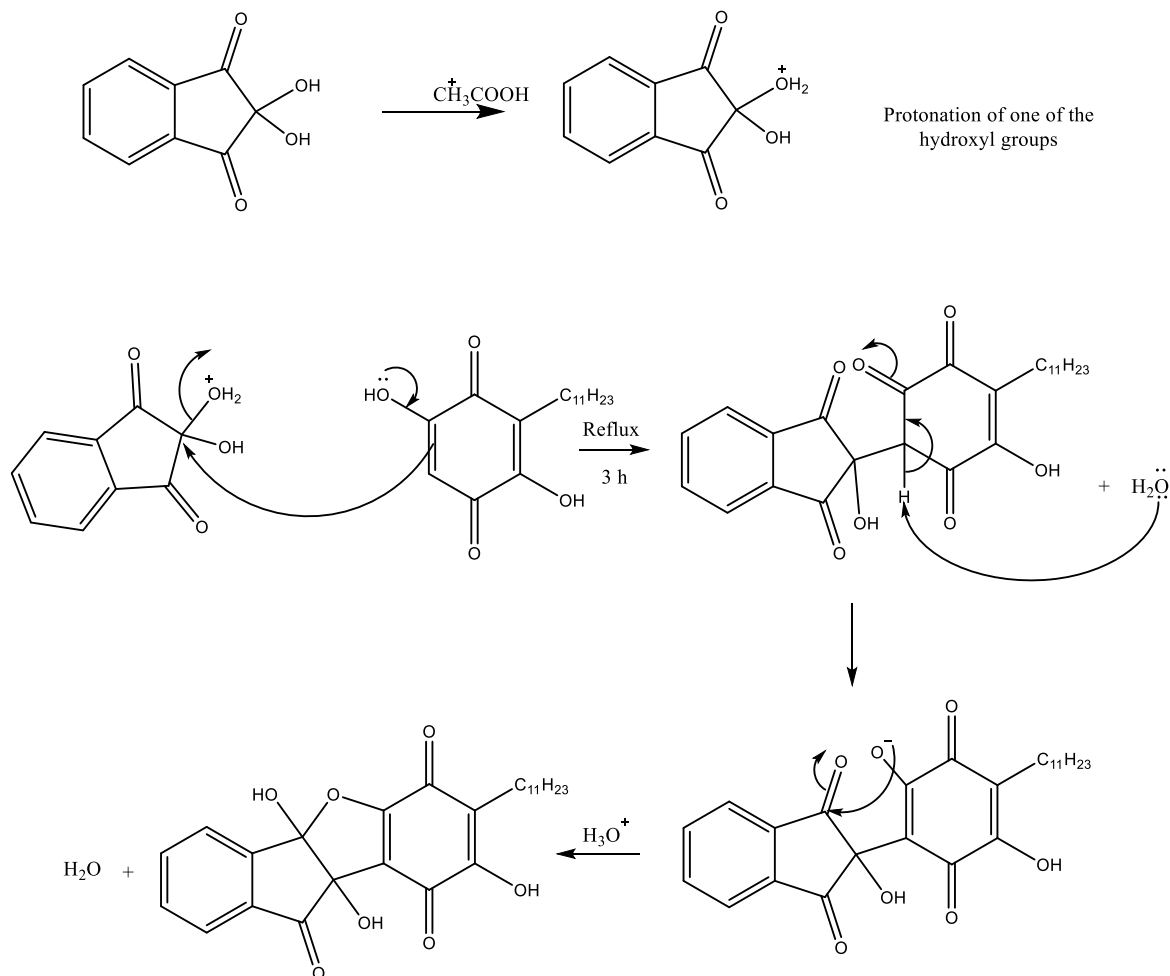
3.11.3. Synthesis of embelin-2,4-dihydroxy benzaldehyde derivative (5)

The embelin-2,4-dihydroxy benzaldehyde (6,6'-((2,4-dihydroxy phenyl)methylene)bis(2,5-dihydroxy-3-undecylcyclohexa-2,5-diene-1,4-dione)) derivative synthesized by the condensing embelin with 2,4 dihydroxybenzaldehyde in presence of ethanoic acid solution

as per the modified method of Balachandran *et al.* (2013) with modification. Embelin (3 g) was weighed and dissolved in 100 mL of acetic acid solution after which it was gently warmed at 30 °C. Thereafter 100 mL 40 % 2,4-dihydroxybenzaldehyde solution was added. The resultant solutions were consequently warmed in a water bath at 45 °C while continuously being stirred at a constant rate for 10 minutes. The resultant mixture obtained thereafter was left to stand at room temperature to cool. This was followed by recrystallization and purification using column chromatography.

3.11.4. Synthesis of embelin ninhydrin derivative (6)

Embelin-ninhydrin (4bS, 9bS)-8-hydroxy-4b, 9b-dimethyl-7-undecyl-4b, 9b-dihydro-9*H*-indeno [1, 2-*b*] benzofuran-6, 9, 10-trione was prepared, as per the modified method of (Mahendran *et al.*, 2011) as shown in Scheme 3.2. Embelin (0.6171g, 2.1 mmol) was weighed and transferred to a flask containing ninhydrin (125 mg, 0.7 mmol) in a solution of 0.01 L acetic acid. Refluxing of the mixture was carried out at 85 °C for 3 hours in an oil bath. TLC was continuously used to monitor the completion of the reaction. After transferring the mixture to a separating funnel addition of 25 mL ethyl acetate was added. The resulting product was purified using conventional column chromatography, producing a brown product called embelin ninhydrin (ENn).



Scheme 3.2: Mechanistic formation of embelin ninhydrin derivative .

3.12. Chemical and physical characterization of embelin derivatives

Several physical and spectral characterizations were done out to confirm and characterize derivatized from embelin (**3-6**). UV-Vis spectroscopy, FTIR spectroscopy, Liquid Chromatography-electrospray ionization tandem mass spectroscopy (LC-ESI/MS), elemental analysis and NMR spectroscopy was carried out for each derivative.

3.12.1. Melting point determination

The introduction of a little amount of the sample substance into a capillary tube was carried out by inverting the open side of the sealed capillary tube with gentle tapping. Heating and observation were done when the solid started to melt and when it had finally melted. The sample-containing glass capillary tube was put into the heating block. The samples were heated swiftly to temperatures about 10 °C below their projected melting points, guided by preliminary determinations, but the actual melting points were measured by heating the samples slowly to a rise in temperature of about 1 °C per minute. This guaranteed the correctness of the data by ensuring that the sample and the block were in thermal balance.

3.12.2. UV-Visible spectrophotometric spectroscopy

UV-Visible spectroscopy characterization of compounds (**1-6**) was done to identify the molecular species by generating bands on the interaction of electromagnetic radiation within the Ultra violet-visible region. The electronic spectra of the samples were obtained in dichloromethane using the Beckham Coulter DU 720 Ultraviolet/Visible Spectrophotometer. Blank samples were prepared by filling the cuvette (1 cm path length) with a suitable solvent (dichloromethane). The spectrophotometer scanning range was 200-800 nm . The blank solution (dichloromethane) was scanned and thereafter the prepared sample solution according to the laid down procedures (Gupta *et al.*, 2014; Sekar, 2019) and the changes in absorbance recorded and an absorption spectrum curve was generated.

3.12.3. Fourier Transform Infra-Red spectroscopy

Using OMNIC version 9.1.24 software, ATR-FTIR spectra were captured on a Nicolet 6700 (Thermo Scientific, USA) spectrometer (Thermo Fisher Scientific). The dry solid samples were placed in the ATR-FTIR equipment and the knob was closed. Background correction

was done before analysis which collected background spectra after 16 periodic scans at 4 cm^{-1} and resolution data recorded at room temperature. The scan range was $4000 - 500\text{ cm}^{-1}$. Appendix 2 shows the ATR-FTIR equipment which was used in the analysis.

3.12.4. Liquid chromatography-Mass Spectrometry

The Agilent 1200 HPLC, which included an Agilent G1329A high-performance autosampler (hp-ALS-SL), an Agilent G1312A binary pump (BIN-SL), an Agilent G1379B vacuum degasser, an Agilent G1316A thermostated column compartment (TCC-SL), and an Agilent G1314B variable wavelength detector, was used for the LC/MS analysis (VWD-SL).

The atmospheric pressure electrospray ionization (API-ES) source was used to run the quadrupole mass spectrometer in positive mode. A Kromasil RP C18 column (particle size of $5\text{ }\mu\text{m}$, column size of $150\text{ mm} \times 4.6\text{ mm}$, Alltech Associates, Inc. Deerfield, IL) was used with an HPLC flow rate of 1 mL/min . In an isocratic elution, methanol and water with 0.1% formic acid made up the mobile phase ($v/v = 87:13$). Mass spectra between 100 and 1000 m/z were captured. For MS, the nebulizer pressure was 30 PSIG , the dry gas temperature was $350\text{ }^\circ\text{C}$, and the Vcap voltage was 3500 V . The dry gas flow for MS was 13.0 L/min . Software developed by Agilent Lab chromatography/mass selective detector (LC/MSD) ChemStation was used to collect and process the data.

A quadrupole time-of-flight micro mass spectrometer (Q-TOF-MS) from Waters Corp. in Milford, Mississippi, with electrospray ionization (ESI) in both ESI-MS and ESI-MS-MS modes, and the Masslynx software, were used to get the mass spectrum (V4.0, Waters Corp., Milford, MS). At a flow rate of 1.5 L min^{-1} , each separated and purified sample was directly injected from the sample vial into the ESI source. For acquisitions in the positive and negative ion modes, the ion source voltages were set at 3000 V . The mass spectrum was scanned from

100 to 1000 m/z in continuum mode at a speed of 1 second while the source temperature was held constant at 100 °C. Precursor ion scans on negative ion modes using low energy collision-induced dissociation (CID) resulted in more structural fragments, which helped the structural identification of compounds of interest. Appendix 3 shows the LC-MS equipment used in the analysis.

3.12.5. Gas chromatography-Mass spectrometry (GC-MS)

The analysis was conducted using a Clarus 500 GC gas chromatograph (Perkin Elmer Inc., USA) connected to a Clarus 500 MS quadrupole mass spectrometer (Perkin Elmer Inc., USA). A 5% diphenyl/95% dimethyl polysiloxane fused-silica capillary column (Elite-5 s, 60 m0.25 mm, 0.25 mm film thickness, Perkin Elmer Inc., USA) was utilized for the gas chromatographic separation. A split/split-less injection port with electronic control was used for the gas chromatograph injection method. The injection (volume of 1 L) was carried out in split mode with a split flow of 20 mL/min at a temperature of 250 °C at the interface. As a carrier gas, helium was employed at a constant flow rate of 1.2 mL/min. The oven's temperature program began with a steady temperature of 200 °C for 4 minutes, then was raised progressively to 330 °C at a rate of 5 °C/min, and was then maintained at 330 °C. The electron impact mode produced ionization (ionization energy of 70 eV). The temperatures of the source and transfer lines were 250 °C and 330 °C, respectively. Scan mode was used to detect mass, from m/z 35 to m/z 700 a.m.u. Before being aspirated into the GC-MS, the samples were silylated with BSTFA 1% TMCS. The show lasted 40 minutes in total.

3.12.6. Nuclear Magnetic Resonance spectroscopy

The spectra of ^1H and ^{13}C NMR of the target samples were run using the Avance DRX 400 NMR Spectrometer (Bruker, Germany). The solvents used were CDCl_3 and DMSO-d_6 in 5

mm tubes at ambient room temperature. Chemical shifts were measured in units of parts per million (ppm) (Geng *et al.*, 2020; Hao *et al.*, 2021; Kandhasamy *et al.*, 2021).

3.12.7. Elemental analysis

Carlo Erba's 1108 CHNS Elemental Analyzer was used for elemental analysis (SARM, CRPG). The samples were placed in capsule-like tin vials encapsulated and put into the elemental analyzer. The heating furnace where combusting of samples occurs was set to a temperature of process 1030 °C left oven, right oven, 650 °C. Helium gas (carrier gas) at 100 kpa, reference gas (R) at 70 Kpa, dry air at 55 psi and oxygen at 30 psi. Samples were loaded on the autosampler wheel using pair of tweezers and when the wheeler was pushed in the clockwise direction the samples were loaded into the deeply recessed hole and the start button was pressed after the wheel was covered. Acetanilide was the reference standard.

3.13. Application of embelin and derivatives on textile fibers

3.13.1. Dyeing processes

The cotton fibers dyeing was carried out using the laboratory type-dyeing machine (PARAMOUNT Digi wash i2). Silk and wool were dyed utilizing using Radley's equipment MR He: - Tec Ø 135 Radleys EU, P/N: RR 91203/EURO. The textile fibers were moistened with a non-ionic surfactant, 30 minutes prior to dyeing (Wang *et al.*, 2020). According to the modified methodology, dyeing tests were conducted, and the dyes were made in dyeing conical flasks with a material to liquor ratio of 1:50. With the help of 0.1 M HCl and 0.1 M NaOH, the pH was changed. The samples were taken from the dye bath and rinsed in cold water to remove the unfixed dyestuff once the dye bath had finished cooling. After adding the non-ionic soapy solution to the dyed materials, they were washed with water, dried by air, and then tested for color fastness. The materials were washed with enough water after the

dyeing procedure was finished, and then allowed to dry before measurements of color strength and fastness qualities were taken. Grey scale was used as the basis for assessments of color fastness to track change (ISO 105-C02:1989, ISO 105 A02:1993, ISO 105-X12:2000). A SpectroFlash X-rite SP62 spectrophotometer was used to measure the reflectance values of the dyed cotton to its CIELAB color space (L^* , a^* , and b^*) values under the illumination of D65 (Manyim *et al.*, 2021). Where L^* (lightness-darkness), a^* (red/green), b^* (blue/yellow), C^* (chroma), and h^0 (hue angle).are indicated in the color parameters.

3.13.2. Mordanting

Dyeing was performed with alum, copper sulphate, nickel and ferrous mordants, employing, pre-, post and simultaneous treatments of the textile fibers. In the pre-treatment, the textile fibers were first submerged in the solution containing mordants for 20 minutes followed by thorough rinsing with water before the dyeing process. In simultaneous dyeing, the textile fibers were introduced to the dye bath containing the dyes and the mordants. In post-mordanting, the textile fibers were then dyed before being treated with respective mordants thereafter whereas with pre-mordants the textile fibers were first treated with the mordants before the dyeing process (Karabulut *et al.*, 2020). The derivatized dyes and embelin were also employed in the textile fibers without mordanting.

3.14. Method optimization for dyeing procedures

Using the response surface methodology, Central Composite Design (Omorieg *et al.*, 2017) created by a Design Expert, the dyeing of particular textile fibers was optimized. pH, time, and temperature were the dyeing variables that were taken into consideration, and the evaluation of both the individual and combined effects was based on the response (colour

strength). The values for the three aforementioned variables were chosen under the direction of single-factor preliminary tests. Twenty experiments were done as a result of the optimization. Optimization design resulted in twenty experiment runs. Table 3.1 displays the experimental designs and independent variables.

3.14.1. Model validation

The optimization was conducted to establish the dyeing conditions variables giving maximum colour strength. Experiments under the given optimized conditions were carried out to determine the obtained model validity (Haji *et al.*, 2016).

Table 3.1: Actual levels of independent variables (Design Experts software)

For cotton dyed fibers					
LEVEL	$-\alpha$	-1	0	1	$+\alpha$
pH	4	6	9	12	13
TIME (s)	10	30	60	90	110
TEMPERAT	9.32	40	85	130	160.68
URE					
LEVEL	$-\alpha$	-1	0	1	$+\alpha$
For Embelin ninhydrin dye with silk and wool					
LEVEL	$-\alpha$	-1	0	1	$+\alpha$
pH	4.98	6	7.5	9	10.02
TIME (s)	9.55	30	60	90	110.45
TEMPERAT	22.96	40	65	90	107.04
URE					

Where levels are represented as: $-\alpha$ (Lower level axial points), -1(lower limits), 0 (center level point), 1(upper level), $+\alpha$ (upper level axial point).

3.15. Testing of Colour Fastness

The capacity of the colour to be retained during washing, rubbing or when the textile fiber which has been dyed is subjected to light is referred to as colour fastness. The colourfastness testing in this study was done to evaluate the colourfastness qualities for the semi-synthesized dyes compared to the parent dye embelin. The dyed textile fibers were evaluated for washability, rub (dry and wet) and fastness to light properties.

3.15.1. Colour fastness to rubbing

The assessment of rubbing fastness property was evaluated using a Crockmeter machine (AATCC Model, M238AA SDATLAS) and the procedure was carried in accordance with ISO 105-X12:2001 protocol by placing the dyed textile fibers onto the crock meter machine, the fabrics were rubbed, to and fro in both wet and dry methods. The samples were evaluated for stains on white blank fabric using the grey scale after they had air dried.

3.15.2. Colour fastness to washing

The dyeing operations for the dyed fabrics were carried out in accordance with ISO 105-C02:1989, ISO 105 A02:1993, and ISO 105-X12:2000 regulations, and the wash fastness of the dyed fabrics was tested in a Gyro wash machine for wet conditions. This was done by attaching the blank fabric and the dyed material after the wash fastness procedure was finished the fabrics were detached, dried, and evaluated for staining Non-ionic soapy solution was added into the liquor ratio and the samples were placed in the steel containers and preheated to 60 °C for 30 minutes , with gentle agitation. After which the samples were rinsed. The colour change in the dyed fabrics and the stained blank fabric were evaluated regarding the original specimen using the grey scales (Ayele *et al.*, 2020).

3.15.3. Colour fastness to Light

Evaluation of fastness to light was assessed in accordance to ISO 105-C02:1989, ISO 105 A02:1993, and ISO 105-X12:2000 protocol. The fibers dyed at optimum dyeing conditions were simultaneously exposed to daylight for 5, 10, 15 and 20 hrs. Grading was evaluated between 1 and 8, where 1 is exceptional poor and 8 being excellent. The evaluation of change in colour change was in comparison to the original undyed fiber and assessed by Grey scale analysis.

3.15.4. Evaluation of colour strength using CIELAB

Colour strength measurements of fabrics were done by employing a SpectroFlash X-rite SP62 spectrophotometry technique using D65 (Manyim *et al.*, 2021). The dyed fabrics were assessed for their L^* , a^* , b^* , C^* , and h^0 values of the dyed fibers as per the CIELAB colour scale. The data of C^* and h^0 were calculated using Equations 3.1 and 3.2 below.

The Chroma values are given by

$$\text{Chroma } (C^*) = \sqrt{a^2 + b^2} \dots\dots\dots \text{Equation 3.1}$$

$$\text{Hue angle } (h) = \tan^{-1} b/a \dots\dots\dots \text{Equation 3.2}$$

L^* indicates luminosity, a^* shows redness/greenness, and b^* describes yellowness/blueness co-ordinate, C^* , h^0 represent the chroma and hue angle respectively. The blank fabric was the undyed fabric. The (K/S) value determination was done based on Kubelka–Munk equation as shown in equation 3.3 below.

$$\frac{K}{S} = \frac{(1-0.01R)^2}{2(0.01R)} \dots\dots\dots \text{Equation 3.3}$$

Where (K) is given as the respective absorption coefficient, scattering coefficient(S) and (R) is the minimum reflectance of complete capacity (Sadeghi-Kiakhani *et al.*, 2020).

3.16. Thermal stability and surface characterization of dyed textile fibers

Thermal stabilities and surface characterization of dyed textile fibers were studied using Thermo-gravimetric analysis technique (TGA)/Differential scanning calorimetry (DSC) technique. This was to investigate the thermal stabilities of mordanted textile fibers while surface characterization was evaluated using scanning electron microscopy (SEM) and FTIR of dyed fibers.

3.16.1. Thermogravimetric analysis

Thermal stabilities and behavior of dyes, blank and mordanted cotton were studied with a Mettler Toledo (Thermogravimetric analysis/Differential scanning microscopy) equipment. Seven (7) mg samples were placed in 70 μ L alumina pans. One alumina (standard grade) was used as a blank and placed in cell number one. The pans were hence sealed with lids that are drilled by use of a pressing device cased in Mettler Toledo equipment to form a capsule. A dynamic model at a temperature range from (30 to 600) °C with heating rates of 10 °C per min was used to determine the initial decomposition temperatures. The nitrogen carrier gas at a flow rate of 50 mL per minute was employed.

3.16.2. Scanning electron microscopy

Scanning electron microscopy (SEM) imaging was performed ON TESCAN, Vega 3 SBU at magnifications of 1500X on undyed and dyed textile fabrics was done. The textile fibers were lodged onto the aluminum holding stub supported with double-sided tape for support. The support tape was held to the stub and the sample was carefully placed on top of the tape

after it had been secured to the stub. To make the sample conductive, a very tiny layer of gold was applied to the stub with the sample on it.

3.17. Statistical analysis

The effects of the different combinations of the factors on colour strength were studied using statistically designed experiments analysis. This analysis was done to establish a functional relation involving independent variables and the output response surface to fit the model shown below in Equation 3.4

$$y = \beta_0 + \beta_1X_1 + \beta_2X_2 + \beta_3X_3 + \beta_{11}X_1^2 + \beta_{22}X_2^2 + \beta_{33}X_3^2 + \beta_{12}X_1X_2 + \beta_{22}X_2X_2 + \beta_{32}X_3X_2 \dots \dots \dots \text{Equation 3.4}$$

Where X1, X2, and X3 are the input factors that influence the response Y, β_0 β_1 β_2 , β_3 , β_{12} , β_{22} and β_{32} are constant parameters.

The findings were both qualitative and quantitative nature. The experiments were performed out in triplicate. The means and standard deviations of replicated quantitative data were used to express the data (Moreira *et al.*, 2020; Ramaraj & Unpaprom, 2019).

3.18. Model validation

Validation of the values obtained was confirmed by experimental runs based on the evaluations of the models achieved and measurements of the colour strength. The statistical values from the model were then compared to experimental values obtained (Sinha *et al.*, 2013; Yadav *et al.*, 2021).

CHAPTER FOUR

RESULTS AND DISCUSSION

4.1. Extraction Yields

Stem bark was extracted with different solvents by maceration method and the percent yield are shown in table 4.1. The acetonic extraction yields exhibited the highest yield of 1.6 ± 0.02 percent followed by ethanolic extraction of 1.124 ± 0.03 and chloroform 1.122 ± 0.03 all from Kericho county while the hexane extract gave the least percent yield amount of 0.3 ± 0.08 . (Laraib *et al.*, 2021). The acetone extraction yields exhibited the highest yield of 1.06 ± 0.34 , percent followed by dichloromethane extraction of 1.14 ± 0.02 and thirdly ethanolic crude gave a yield of 1.04 ± 0.05 in the Nandi county stem bark samples. While the chloroform extract gave the highest percent yield amount of 1.06 ± 0.09 , followed by ethanol extracts with a yield of 1.05 ± 0.05 , whereas the dichloromethane extraction of 0.97 ± 0.04 in the Narok County stem bark samples was the third highest. From the results in Table 1, the stem barks collected from Nandi and Narok Counties were found to contain very low yield upon extraction and were therefore not subjected to further analysis beyond phytochemical screening. The low yield could be due to the intraspecific variation as a result of soil chemistry, seasonal changes and weather patterns, it was discovered that the *Albizia coriaria* leaves from some agro-ecological zones of Uganda had different yields which could have been caused by different geographic variations (Omara *et al.*, 2021).

The Kericho County stem barks were further extracted with other methods in an effort to find out suitable solvent and method that will maximize the yield and the results are presented in Table 4.2. From the results in Table 4.1 and Table 4.2 maceration method was most effective

and the acetone solvent was the best solvent that gave the highest yield. The acetone crude extract samples gave the highest in yield this could be due to their non-polar nature expected to extract most of the non-polar secondary metabolites. A comparison of maceration extraction methods and microwave-assisted polyphenols and tannins extracted from *Acacia mollissima* barks from Morocco showed that the maceration method gave the highest yield (Naima *et al.*, 2015).

Table 4.1: Percentage yield of stem bark crude extracts by maceration method .

County	Solvent	[% Mean (gm/gm) \pm SD]
Kericho	Hexane	0.5 \pm 0.02
	Diethyl ether	0.35 \pm 0.01
	Chloroform	1.122 \pm 0.05
	Acetone	1.6 \pm 0.02
	Dichloromethane	0.84 \pm 0.03
	Ethyl acetate	0.624 \pm 0.02
	Ethanol	1.124 \pm 0.03
Nandi	Hexane	0.35 \pm 0.12
	Diethyl ether	0.24 \pm 0.01
	Chloroform	0.63 \pm 0.05
	Acetone	1.06 \pm 0.34
	Dichloromethane	1.14 \pm 0.02
	Ethyl acetate	0.24 \pm 0.12
	Ethanol	1.04 \pm 0.05
Narok	Hexane	0.3 \pm 0.08
	Diethyl ether	0.45 \pm 0.06
	Chloroform	1.06 \pm 0.09
	Acetone	0.7 \pm 0.07
	Dichloromethane	0.97 \pm 0.04
	Ethyl acetate	0.44 \pm 0.04
	Ethanol	1.05 \pm 0.05

Table 4.2: Kericho County Samples extraction based on different techniques

Method of extraction	Solvent	Time	% Yield
Ultrasonication Extraction	Hexane	10 mins	0.63 ± 0.08
		20 mins	0.76 ± 0.11
		30 mins	0.23 ± 0.19
		40 mins	0.92 ± 0.08
	Chloroform	10 mins	1.77 ± 0.13
		20 mins	1.80 ± 0.17
		30 mins	1.5 ± 0.35
		40 mins	1.02 ± 0.09
	Dichloromethane	10 mins	0.69 ± 0.03
		20 mins	0.71 ± 0.16
		30 mins	0.95 ± 0.04
		40 mins	0.62 ± 0.15
	Acetone	10 mins	0.91 ± 0.19
		20 mins	0.68 ± 0.20
		30 mins	1.19 ± 0.13
		40 mins	0.99 ± 0.24
	Ethyl acetate	10 mins	0.20 ± 0.08
		20 mins	0.28 ± 0.11
		30 mins	0.36 ± 0.15
		40 mins	0.71 ± 0.34
Ethanol	10 mins	1.03 ± 0.10	
	20 mins	0.94 ± 0.24	
	30 mins	1.51 ± 0.34	
	40 mins	1.62 ± 0.26	
Soxhlet extraction	Hexane	120mins	0.32 ± 0.02
		180 mins	0.47 ± 0.17
		240 mins	0.69 ± 0.11
		300 mins	0.61 ± 0.13
	Chloroform	120mins	0.75 ± 0.21
		180 mins	0.54 ± 0.13
		240 mins	0.60 ± 0.25
		300 mins	0.81 ± 0.12
	Dichloromethane	120mins	0.71 ± 0.27
		180 mins	0.27 ± 0.16
		240 mins	0.68 ± 0.22
			300 mins
Acetone	120mins	0.97 ± 0.18	
	180 mins	0.85 ± 0.03	

		240 mins	0.83 ± 0.04
		300 mins	0.87 ± 0.02
	Ethyl acetate	120mins	0.13 ± 0.02
		180 mins	0.17 ± 0.01
		240 mins	0.22 ± 0.06
		300 mins	0.37 ± 0.12
	Ethanol	120mins	0.75 ± 0.16
		180 mins	1.26 ± 0.18
		240 mins	$1.20. \pm 0.20$
		300 mins	1.37 ± 0.28

Taking into consideration that these findings showed that acetonic extract from the maceration method gave the highest percent yield the berries samples were extracted using the maceration technique and the consequent results displayed in Table 4.3.

Table 4.3: Percentage yield of acetonic extracts from berries crude extraction by maceration method

County	Solvent	[% Mean (gm/gm) \pm SD]
Kericho	Acetone	40 ± 1.21

The Kericho berries samples gave a high yield compared to stem bark samples observed in Table 4.1 and Table 4.2.

4.2. Phytochemical screening results

All the stem bark crude extracts and berries were subjected to phytochemical screening which was done according to stipulated protocols. The results in Table 4.4 are for the stem barks extraction by maceration method whereas the results in Table 4.5 are for the stem barks extraction by soxhlet and ultrasonication method while for Table 4.6 are for the berries samples extraction by maceration method respectively. All the stem bark crude extracts by maceration method showed the presence of alkaloids metabolites, tannins, phenolic saponins, flavonoids, glycosides and steroids present in the Kericho sample but the

terpenoids and steroids were present in acetone and chloroform extracts and were absent in diethyl ether, ethyl acetate, hexane, DCM and ethanolic extracts according to the results in Table 4.4. Terpenoids and cardiac glycosides are all absent in Narok samples. This result was consistent with the findings from stem bark analysis of *Embelia schimperi* dichloromethane/methanol crude extracts by Guyasa *et al* (2018), who collected stem bark samples of *Embelia schimperi* from the region of Oromia a distance of 381 km west of Addis Ababa (Guyasa *et al.*, 2018) where alkaloids and terpenoids were also observed in acetic berries crude extract of *Embelia schimperi* berries according to the studies that have been carried out (Zebeaman *et al.*, 2018).

The crude stem bark extracts from the three geographical regions' stem barks contained tannins, flavonoids, saponins, and phenolics, according to the phytochemical screening that was done in stem barks and in berries extracts from Kericho county. There was the presence of intense tannins in acetic and ethanolic extracts. Flavonoids were intense in acetone and chloroform extracts. Cardiac glycosides were only present in Kericho and Nandi samples but absent in Narok samples, with Kericho showing intense cardiac glycosides in chloroform, and acetic extracts. Terpenoids were only available in Kericho acetone and chloroform stem bark extracts. In Nandi samples, Terpenoids were only observed in acetone extracts. These findings are in agreement with the studies by Guyasa *et al.*, (Zebeaman *et al.*, 2018). However, the terpenoids, cardiac glycosides and steroids were not detected in Narok extracts. The indifference found in phytochemical content could be due to intraspecific variation (Corrado *et al.*, 2021) occurrence of different weather patterns (Zubay *et al.*, 2021) different soil types (Salomon *et al.*, 2021), seasonal variations (Flamini *et al.*, 2021) and salinity fluctuations (Sibero *et al.*, 2020).

Table 4.4: Phytochemical Screening Test Results of *Embelia schimperi* stem bark crude extracts by maceration method

Region	Secondary metabolites	Hexane	Acetone	DCM	Chloroform	Diethyl ether	Ethyl Acetate	Ethanol
Kericho	Tannins	+	++	++	+	+	+	++
	Alkaloids	-	+	-	+	+	+	+
	Flavonoids	+	++	++	++	+	+	++
	Terpenoids	-	+	-	+	-	-	-
	Cardiac glycosides	-	++	-	++	+	+	-
	Saponins	+	+	+	+	+	+	+
	Phenolics	++	++	++	+	+	+	++
	Steroids	-	+	-	+	-	-	-
	Narok	Tannins	+	+	+	+	+	+
Alkaloids		+	+	+	+	+	+	+
Flavonoids		+	++	+	++	+	+	+
Terpenoids		-	-	-	-	-	-	-
Cardiac glycosides		-	-	-	-	-	-	-
Saponins		+	+	+	+	+	+	+
Phenolics		+	+	+	+	+	+	+
Steroids		-	-	-	-	-	-	-
Nandi		Tannins	+	+	+	+	+	+
	Alkaloids	+	+	+	+	+	+	+
	Flavonoids	+	++	+	++	+	+	+
	Terpenoids	-	+	-	-	-	-	-
	Cardiac glycosides	+	+	+	+	+	+	+
	Saponins	+	+	+	+	+	+	+
	Phenolics	+	+	+	+	+	+	+
	Steroids	-	-	-	-	-	-	-

Table 4.5: Phytochemical Screening Test Results of *Embelia schimperi* stem bark (Kericho county) crude extracts by ultrasonic and soxhlet method

Method	Secondary metabolites	Hexane	Acetone	DCM	Chloroform	Ethyl Acetate	Ethanol
Ultrasonication	Tannins	+	++	+	+	+	++
	Alkaloids	+	+	+	+	+	+
	Flavonoids	++	++	++	++	+	++
	Terpenoids	-	+	-	+	-	-
	Cardiac glycosides	-	++	-	++	+	-
	Saponins	+	+	+	+	+	+
	Phenolics	++	++	++	+	+	++
	Steroids	-	+	-	+	-	-
	Soxhlet method	Tannins	+	+	+	+	+
Alkaloids		+	+	+	+	+	+
Flavonoids		+	+	+	+	+	+
Terpenoids		-	-	-	-	-	-
Cardiac glycosides		-	-	-	-	-	-
Saponins		+	+	+	+	+	+
Phenolics		+	+	+	+	+	+
Steroids		-	-	-	-	-	-

Table 4.6: Phytochemical Screening Test Results of *Embelia schimperi* Kericho County berries acetonc crude extracts

Kericho berries	Tannins	+
	Alkaloids	+
	Flavonoids	++
	Terpenoids	+
	Cardiac glycosides	+
	Saponins	+
	Phenolics	++
	Steroids	+

KEY ++ = intense phytochemicals presence

+ = the phytochemical presence ; - = the phytochemical absence

The berries of *Embelia schimperi* found in Kericho County contained steroids, alkaloids, flavonoids, terpenoids, cardiac glycosides, saponins, and phenolics presence of phenolics and flavonoids is intense. Among the studies carried out of the Myrsinaceae species reported, the species that have been widely studied were *Embelia ribes*. The study carried out using *Embelia ribes* seeds showed the presence of alkaloids, tannins, and glycosides extracted using ethanol, chloroform, diethyl ether, n-hexane and acetone extract (Agrawal *et al.*, 2021) A report by, Arthanareeswari *et al.*, (2021) showed containment of tannins, alkaloid and phenolic acids (Arthanareeswari *et al.*, 2021) in chloroform extract of *Embelia ribes*. The studies done revealed the presence of steroids and glycosides, saponins tannins and anthraquinones in *Embelia ribes* (Zeeshan *et al.*, 2018). Reports by (Lal *et al.*, 2013) revealed containment of alkaloids, saponins and tannins in *Embelia ribes* fruits sampled from indigenous forests with an altitude of 1500 M in central and lower Himalayas, in several states throughout India.

Phytochemical constituents in plants are related to the effectiveness of dyes. Reports carried revealed that brilliant colours and fragrant smell emanating from plants are a result of specific phytochemicals present (Gupta *et al.*, 2013). These consists of tannins, flavonoids, glycosides, saponins, steroids and alkaloids observed in phytochemicals present in the roselle plant were related to its dyeing properties (Ozougwu & Anyakoha, 2016). It has been observed that the presence of flavonoids and tannins in the bark of *Castanopsis indica* makes them good organic dyes (Bhandari *et al.*, 2021). Quality and quantity of natural dyes present in Argy wormwood was observed to depend on the phytochemicals present (Shafiq *et al.*, 2021).

Based on the findings that acetonc extract from the *Embelia schimperi* berries gave a high yield and revealed the presence of most of the phytochemicals it was further chosen for further chemical, physical and spectroscopic profiling and isolation of embelin.

4.3. UV/Vis spectra of Kericho sample crude extract

UV-Vis spectra of the acetonc extract, Figure 4.1 of *Embelia schimperi* was selected from 285 nm to 300 nm due to its broadness and distinctive peaks and also proper baseline. The phytochemicals present can be detected by identification of compounds that contain pi-bonds, lone pair electrons, sigma bonds, presence of aromatic rings and even available chromophores in the UV-Vis between 200 and 750 nm on the electromagnetic spectrum. Figure 4.1 UV-VIS spectrum shows peaks at 292, 294, and 296 nm, respectively, which indicate the presence of phenolics, aromatic ring and flavonoids with absorption ranging from 0.1 to 0.8. These absorption bands are characteristic of alkaloid, tannin, flavonoid and phenolic compounds present in the sample (Mabasa *et al.*, 2021).

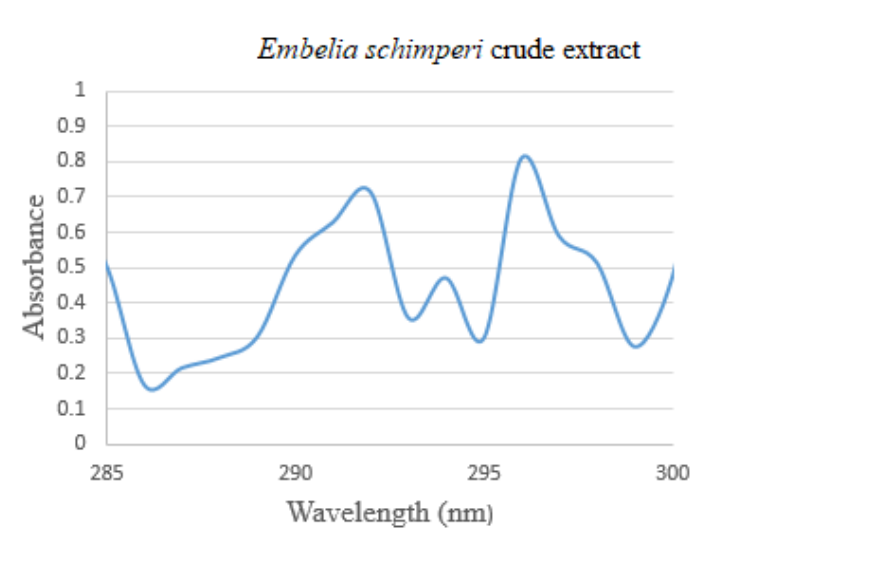


Figure 4.1: UV-VIS spectrum of acetonc crude extract from Kericho County

4.4. GC-MS spectra from Kericho County berries crude samples

The Gas Chromatography-Mass Spectrometry (GC-MS) analysis was conducted on the acetonic crude extracts. The chromatogram, Figure 4.2 revealed several bioactive compounds. The most abundant bioactive compounds in *Embelia schimperi* are shown in Figure 4.3-Figure 4.5 which include embelin.

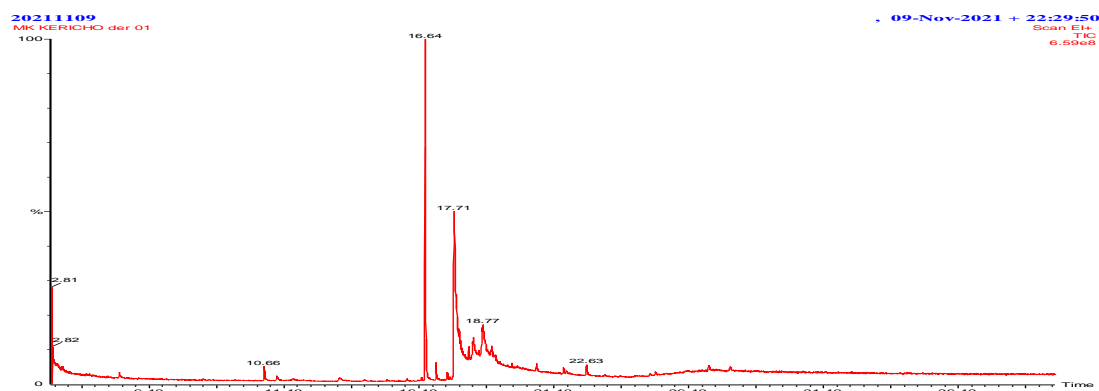


Figure 4.2: GC-MS chromatogram from Kericho County *Embelia schimperi* acetonic extract

The GC chromatogram showed presence of 2 major peaks at retention time 16.81 and 17.71 minutes. The observed peak at 16.81 was assigned to embelin compound as its M/S spectrum showed m/z fragments of 142 and m/z 154 and 294 observed in Figure 4.3 fragment with a m/z of 142 was due to 2,4,6-trihydroxycyclohexa-2,4-dien-1-one .

The m/z 154 is undec-1-ene which is a fatty acid responsible for emulsification characteristics. The observed peak at a retention time of 17.71 min is a squalene observed in Figure 4.3, it is a natural triterpene and is known to aid water "solubilization" of poorly water-soluble molecules (Babič *et al.*, 2017). The squalene structure is what is observed in UV-VIS spectra, Figure 4.1 to be causing $\pi \rightarrow \pi^*$ transitions. A study by Lozano-Grande *et al.* (2018) described squalene as a fixative agent in perfumes and lipsticks because of its ability to

accelerate dispersion of dyes resulting in greater brightness (Fernandes & Maharani, 2022; Lozano-Grande *et al.*, 2018).

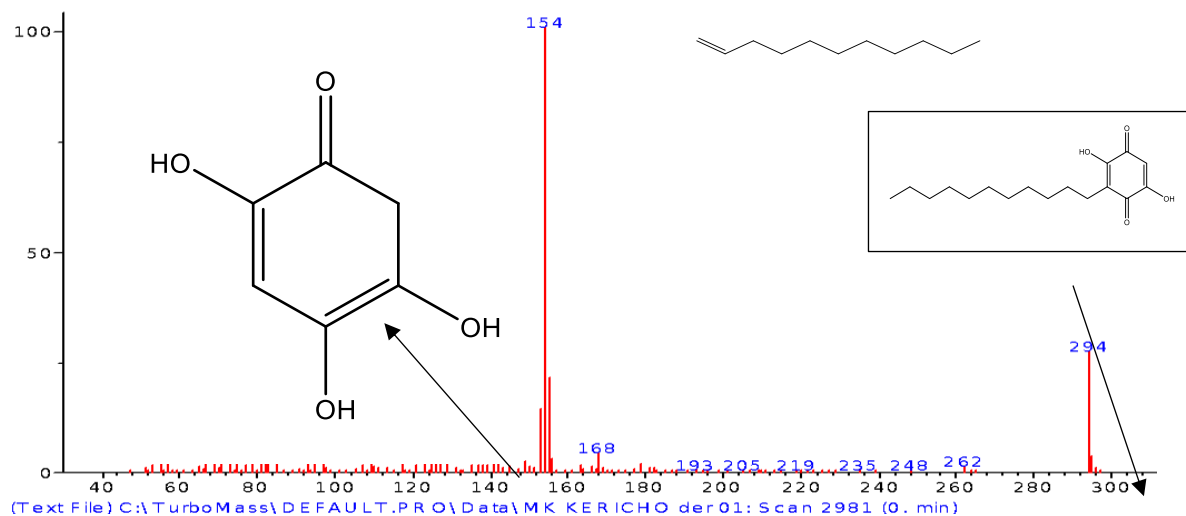


Figure 4.3: GC-MS Spectrum of embelin

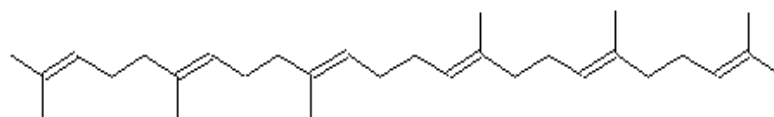


Figure 4.4: Squalene

4.4.1. Quantification of embelin from Kericho berries sample extract

LC/MS was used to perform quantitative analysis on an acetonic extract from Kericho County. By contrasting their retention times with those of typical embelin, an evaluation was conducted. The values were represented in percentages and quantified using an embelin standard calibration curve. Therefore, a 40% embelin concentration was discovered in the extracts from Kericho County.

The concentration of embelin in the samples was calculated by integrating the peak area of the samples and comparing it to the peak areas of the standard. The Kericho samples of *Embelia schimperi* were eluted at a retention time (tR) of 4 min with a UV λ_{max} of 280 nm.

All the samples analyzed showed characteristic peaks of embelin at the same retention time shown by that of standard embelin.

Figure 4.5(a) shows the embelin standard single peak at a retention time of 4 min. Figure 4.5 (b) shows that there is no interference from other compounds.

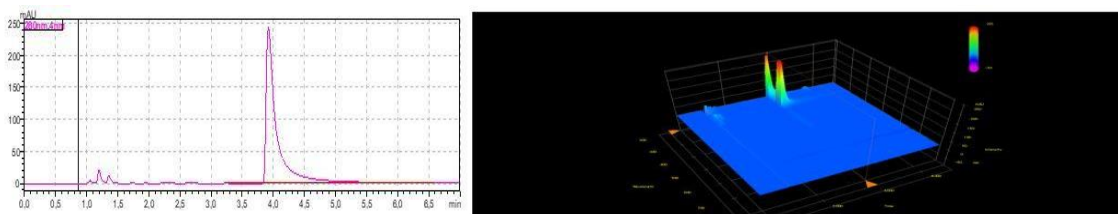


Figure 4.5: (a) Embelin standard chromatogram (b) Embelin standard 3D chromatogram

The Kericho County samples Figure 4.6 (a) showed the presence of embelin at a retention time of 4 min.

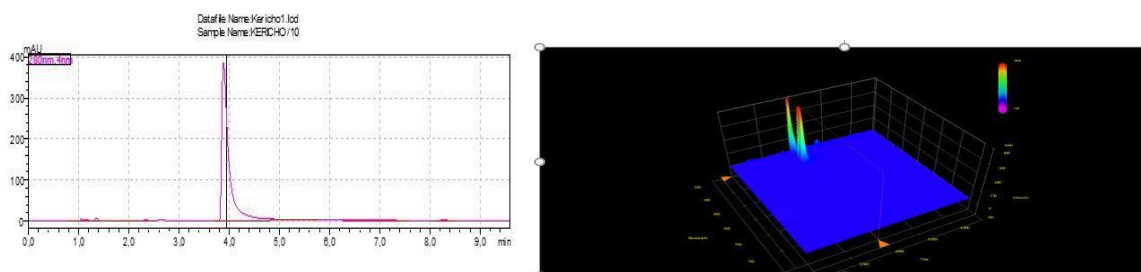


Figure 4.6: (a) LC-UV-MS chromatogram and (b) 3D at 280 nm of crude *Embelia schimperi* fruit acetonc extract, Kericho County sample

The 3D chromatogram is shown in Figure 4.6(b) and it shows a clear image of no interference from other substances.

4.5. FT-IR Spectroscopic characterization of crude extracts

The FTIR spectrum of the Kericho county crude sample extract Figure 4.7. Revealed several peaks

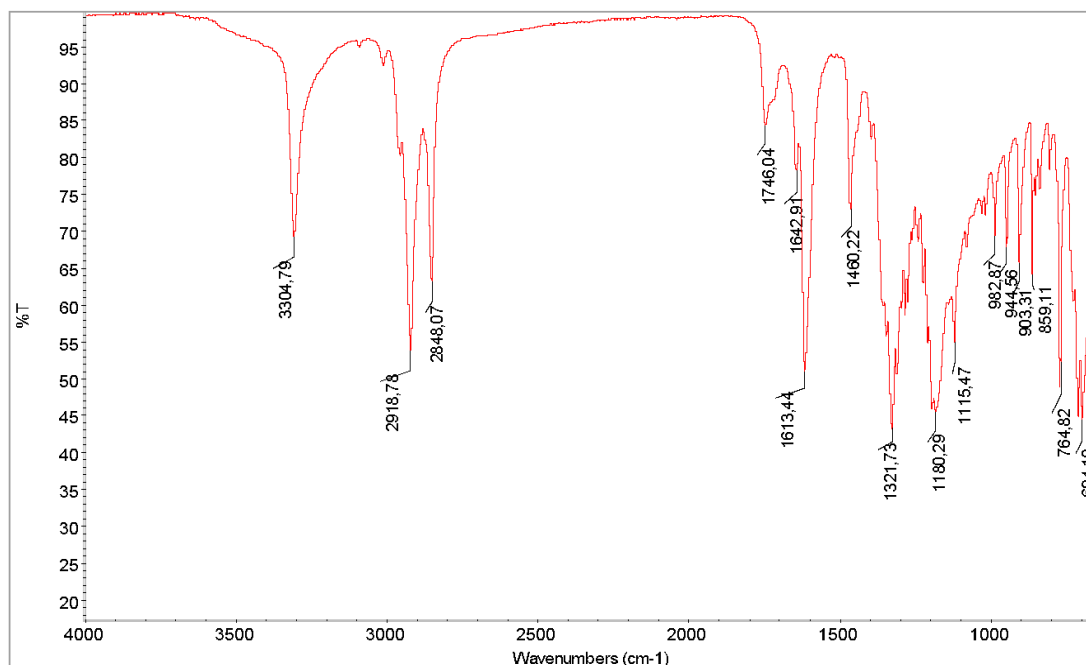


Figure 4.7: The FTIR spectra of Kericho crude acetonetic extract

The spectral data shown in Figure 4.7. reveals IR: cm^{-1}): 3304.79 (hydroxyl), 2918.78 H stretch, 2848.07 (-C-H stretch;), 1748.04 (carbonyl), 1613.44 (C=C bond), responsible for $\pi \rightarrow \pi^*$ transitions 1460.22 (CH_2 bend) , 1180.29, due to -C-O-H. The peaks observed at 2918.78 cm^{-1} and 2848.07 cm^{-1} are the -C-H bands and the peaks observed at 1748.04 cm^{-1} ascribe to the $n \rightarrow \pi^*$ observed in the UV/VIS spectra in Figure 4.1.

4.6. Isolation and purification of embelin

Isolation and purification of the acetonetic crude extract from the berries were done using column chromatography. The solvent system used was ethyl acetate and hexane at a ratio of 6:4. This was chosen as the best solvent system for isolation of compounds in the extracts based on the preliminary findings of separation using TLC chromatography. Figure 4.8 shows TLC profiles of separations of compounds from the crude extract, Embelin was identified using the reference embelin standard.

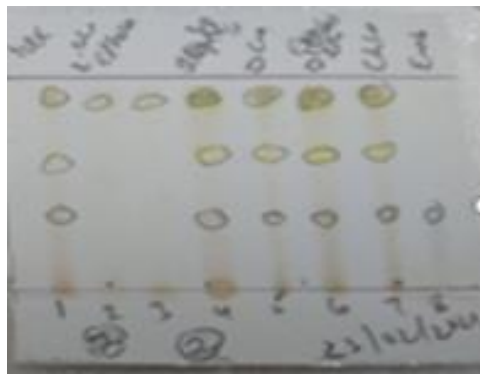


Figure 4.8: various TLC profiles of *Embelia schimperi* crude extract

4.6.1. Column chromatography

Purification was done using column chromatography. The eluates collection was done in 50 cm³ test tubes. The fractions consisting of similar compounds with the same R_f were pooled together after verification with TLC, and excess solvents were evacuated using rota vapor shown in Figure 4.9 below. This was done according to the methods available in the literature (Chiang *et al.*, 2021; Devi, 2021; Ebrahim & Ebada, 2021). The isolated embelin was confirmed by comparing it with the embelin standard using Thin layer chromatography, in Figure 4.10.



Figure 4.9: Removal of the excess solvent from embelin crude sample



Figure 4.10: TLC of isolated embelin compound (a) and embelin standard (b)

4.7. Structure elucidation of characterized embelin

Various physical and spectral characterizations of embelin confirmed the successful isolation of embelin. All characterizations done were compared to the standard embelin carried out under the same conditions.

4.7.1. Melting point determination

The melting point assessment of the embelin was observed in the range of 142-145 °C consistent with the melting point of standard embelin (142-144°C). The determination shows that there is no significant variation and hence embelin was isolated in the pure form. These findings are consistent with studies carried out by Srinivas *et al.* (2010) and Shrimali *et al.*, (2019) where embelin isolated from *Embelia ribes* was reported to have a melting point of 142-144°C (Shrimali *et al.*, 2019; Srinivas *et al.*, 2010).

4.7.2. UV-Visible spectroscopy of Embelin

The ultraviolet absorption analyses of embelin (**1**) and embelin standard (**2**) were done using dichloromethane solvent and the spectra obtained are displayed in Figure 4.11. The spectra showed presence of two bands with λ max of 292 nm due to $\pi \rightarrow \pi^*$ transitions with an absorptivity of 0.8 and a weak shoulder at λ max 336 with an absorptivity of 0.05, this is due

to $n \rightarrow \pi^*$ transitions of the carbonyl in the embelin structure. The band at λ_{max} 292 nm are associated with phenolic and flavonoids and the band at 336 nm are associated with the presence of aromatic ring.

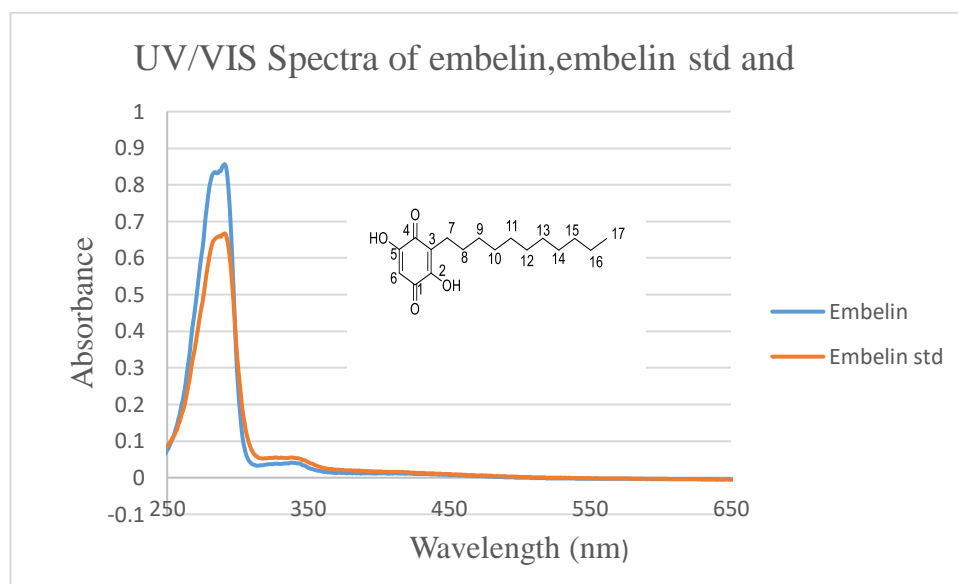


Figure 4.11: UV-VIS spectra of embelin and embelin standard in dichloromethane, scan 200-800 nm

4.7.3. FTIR spectroscopy of embelin and embelin standard

The FTIR spectrum of embelin and embelin standard are shown in Figure 4.12. The FTIR spectra for the two compounds exhibited intense absorption peak at 3301.84 cm^{-1} , which is due to the $-\text{OH}$ group and is associated with the absorption of the phenolic compound observed at 2918.78 cm^{-1} and 2851.01 cm^{-1} peaks are due to sp^2 and sp^3 C-H stretch. A peak at 1610.49 cm^{-1} is due to C=O, whereas the absorptions at 1324.67 cm^{-1} and 1188.13 cm^{-1} were due to CH_2 bend and $-\text{C}-\text{O}-\text{H}$ stretch respectively. Similar results were observed in the embelin isolated from *Embelia ribes* (Shaikh *et al.*, 2016). FTIR Studies done by Badamaranahalli on embelin isolated from *Embelia ribes* revealed an intense absorption peak at 3304 cm^{-1} which was characteristic of the $-\text{OH}$ group and similar results for embelin isolated in this study, revealed absorption peak at 3304.84 cm^{-1} (Badamaranahalli *et al.*,

2015). The aromatic ring in the benzoquinone structure causes the $\pi \rightarrow \pi^*$ and the C=O group in embelin causes the $n \rightarrow \pi^*$ transitions observed in the UV/VIS spectra Figure 4.11.

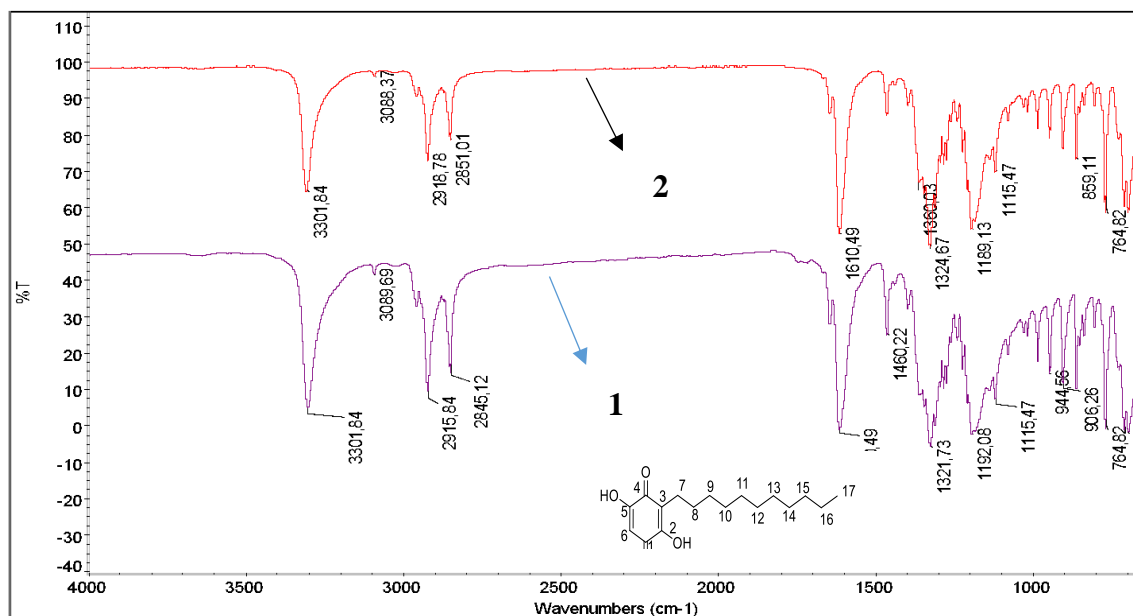


Figure 4.12: FTIR of isolated embelin and embelin standard

4.7.4. ESI-MS spectrum of embelin in the negative mode

The Electro Spray Ionization-Mass Spectrometry spectrum of embelin (**1**) and the embelin standard (**2**) were both carried out in the negative-ion mode. They both showed a molecular ion peak at m/z 292.9 [M-H]⁻ which is the molecular formula of embelin (C₁₇H₂₆O₄), Figure 4.13 and Figure 4.14. The ESI-MS confirms the structure of embelin which consists of the observed functional groups in FTIR spectra in Figure 4.13 like the -C=C-, C=O-, C-H functional groups and further complements the results obtained in the GC-MS.

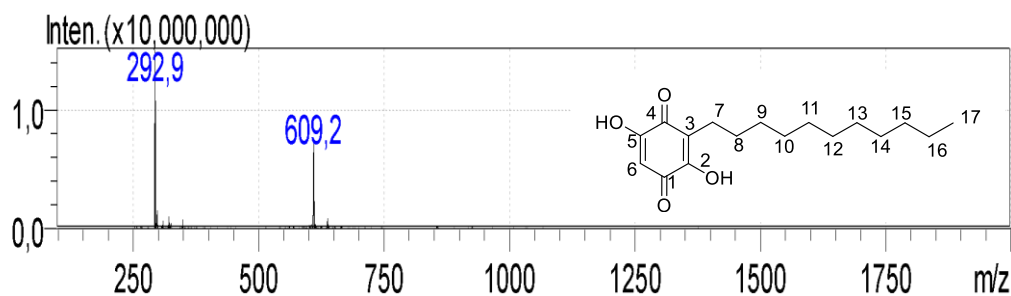


Figure 4.13: ESI-MS spectrum of embelin in the negative mode

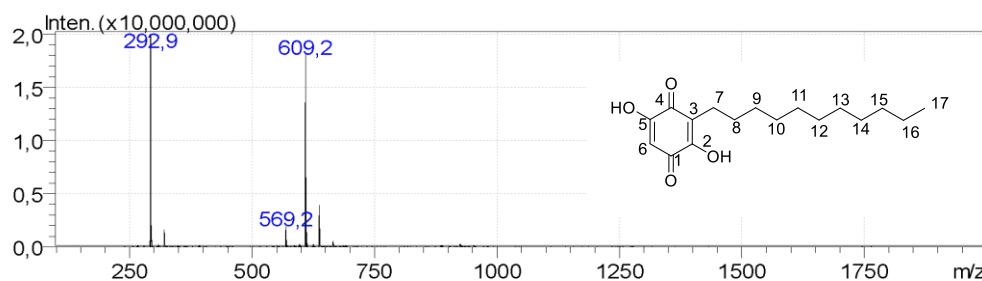


Figure 4.14: ESI-MS spectrum of embelin standard in the negative mode

These findings confirmed the molecular ion mass of embelin. The theoretical value of embelin exhibit a molar mass of 294 g/mol. These results are in agreement with the findings of Li *et al.*(2019), where High-resolution ESI-MS data of embelin isolated from *Aegiceras corniculatum* reported the m/z 295.1914 in the positive mode (Li *et al.*, 2019). One other peak was observed at m/z 609.2 in the embelin spectra and two peaks are observed at m/z 569.2 and m/z 609.2 in the embelin standard. The m/z 569.2 corresponds to a dimer formed from the m/z 292.9 which losses a hydroxyl group (Wong-Paz *et al.*, 2021). The hydroxyl fragment is not observed because it is eliminated as a water molecule (Musharraf *et al.*, 2013) The m/z 609.2 corresponds to the dimer formed from the m/z 292.9 which combines with sodium atom to form an adduct $[2M-2H+Na]^-$ according to reports in the literature (Schug & McNair, 2003). The observed fragments provide better identification of the resultant product by giving signatures of the compound (Delcambre & Saucier, 2012). The molecular

ion was produced without fragmentation and then the gaseous analyte (embelin) was allowed to collide with the gaseous target (nitrogen gas) found in the collision cell resulting in energy gain which is distributed among vibrational degrees of freedom (internal energy) in the embelin compound. Thus, the excited state of the embelin compound was populated resulting in the observed fragments in the process of CID (Banerjee & Mazumdar, 2012; Ortiz *et al.*, 2014). The hydroxyl fragment is not observed because it is eliminated as a water molecule (Musharraf *et al.*, 2013). The confirmed embelin structure contains the, -C=O (1610.49 cm^{-1}) and -C-H (2915.84 cm^{-1}) and -O-H (3301.84 cm^{-1}) functional groups observed in the FTIR.

4.7.5. ^1H and ^{13}C NMR spectroscopy

The ^1H NMR spectrum of the embelin, Figure 4.15, showed a peak at 11.03 ppm (H2,H5), singlet peak at δ 5.79 ppm which corresponds to the proton at position H-6, the signal at δ 0.85 ppm corresponds to a triplet corresponding to the methyl proton in position H-17 with a coupling constant of 7 Hz (t,-CH₃, for H-17, $J=7$ Hz), the multiplet at δ 1.25-1.34 (m, 18 H at H 8-H 16) and a signal at δ 2.23ppm (d,2H, $J=7.8$, H-7) showed the protons H-7 connected to the undecyl chain of the embelin. The Distortionless Enhancement Polarization Transfer) DEPT ^{13}C NMR for embelin is shown in Figure 4.16. It showed a signal at δ 104.45 ppm (C-6) and a signal at δ 118.04 (C-3) which corresponds to the carbon bearing the decyl group, the carbons between 31.92 - 22.75 ppm (C-7-C16) are found in the undecyl chain and the chemical shift at 14.70 ppm (C-17) belongs to the methyl carbon bearing the triplets.

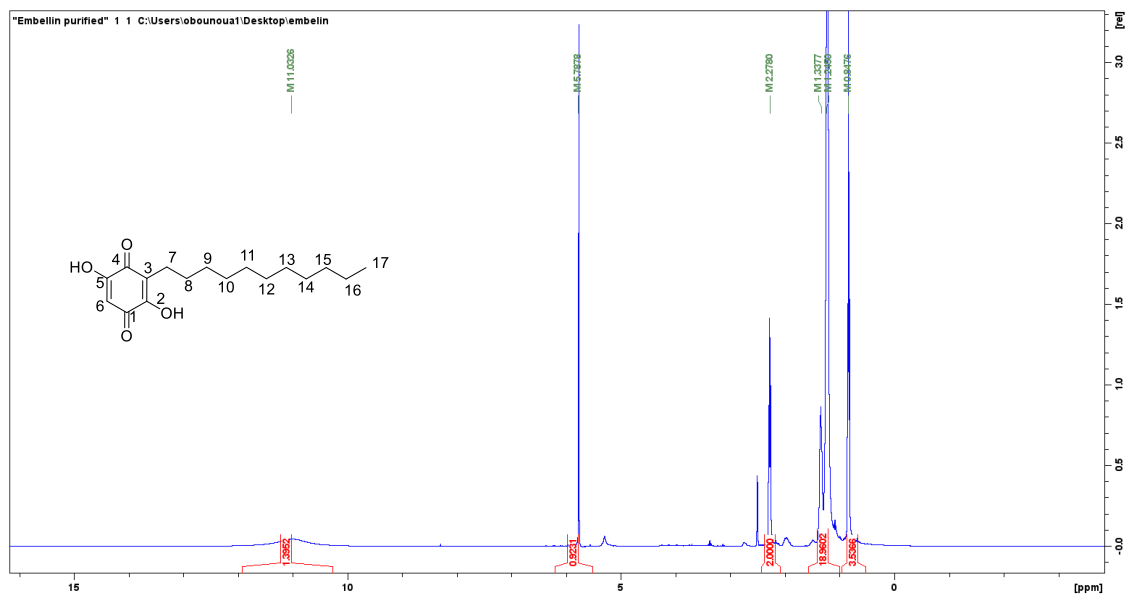


Figure 4.15: ^1H NMR of embelin (1) (400 MHz, DMSO, ppm)

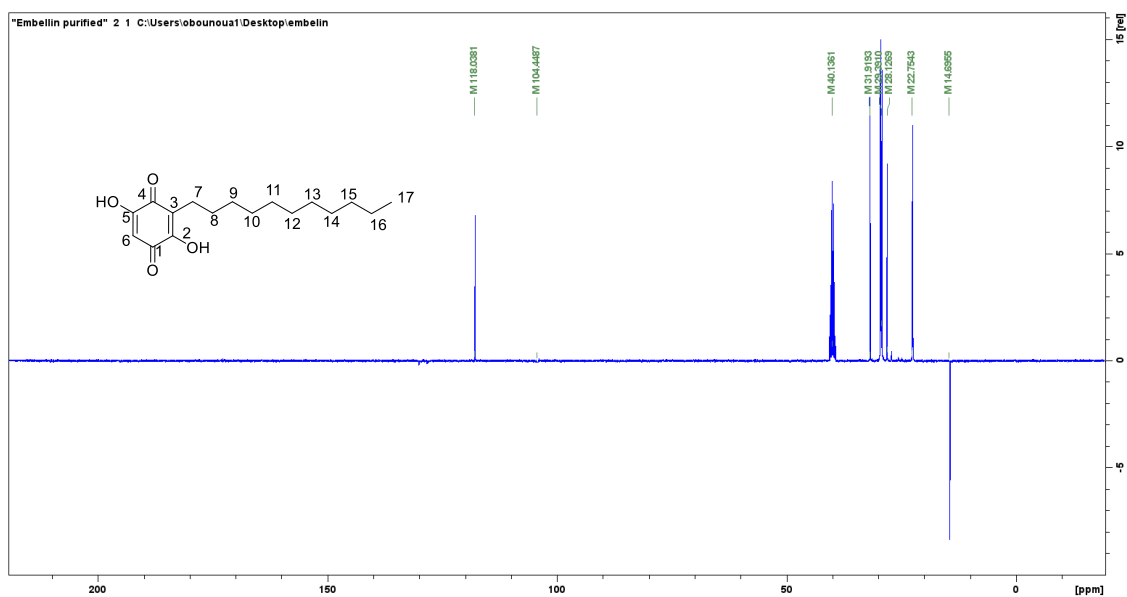


Figure 4.16: Dept NMR of embelin (1) (400 MHz, DMSO, ppm)

The chemical shifts of the standard embelin compare well with data of the isolated embelin.

The ^1H NMR data for the standard embelin are shown in Figure 4.17 it shows a chemical shift at 0.84 ppm which is a triplet associated with the methyl protons in position H-17 with a coupling constant of $J=7$ Hz. A multiplet was observed at 1.23 ppm associated with 18

protons in position H 8-H 16. A chemical shift which is a doublet was observed at 2.27 ppm with a coupling constant of 7.8 Hz associated with 2 H in position H-7 of the undecyl chain. A broad singlet was observed at 11.06 ppm associated with the protons in positions H2, and H5. The DEPT ^{13}C NMR for embelin standards, Figure 4.18, showed a chemical shift at 117.37 ppm associated with the C-3 position, 103.80 ppm (C-6) and a chemical shift at 22-31.28 ppm associated with carbon for position C-7-C-17. The chemical shift at 13.89 ppm belongs to the methyl carbon in C-17.

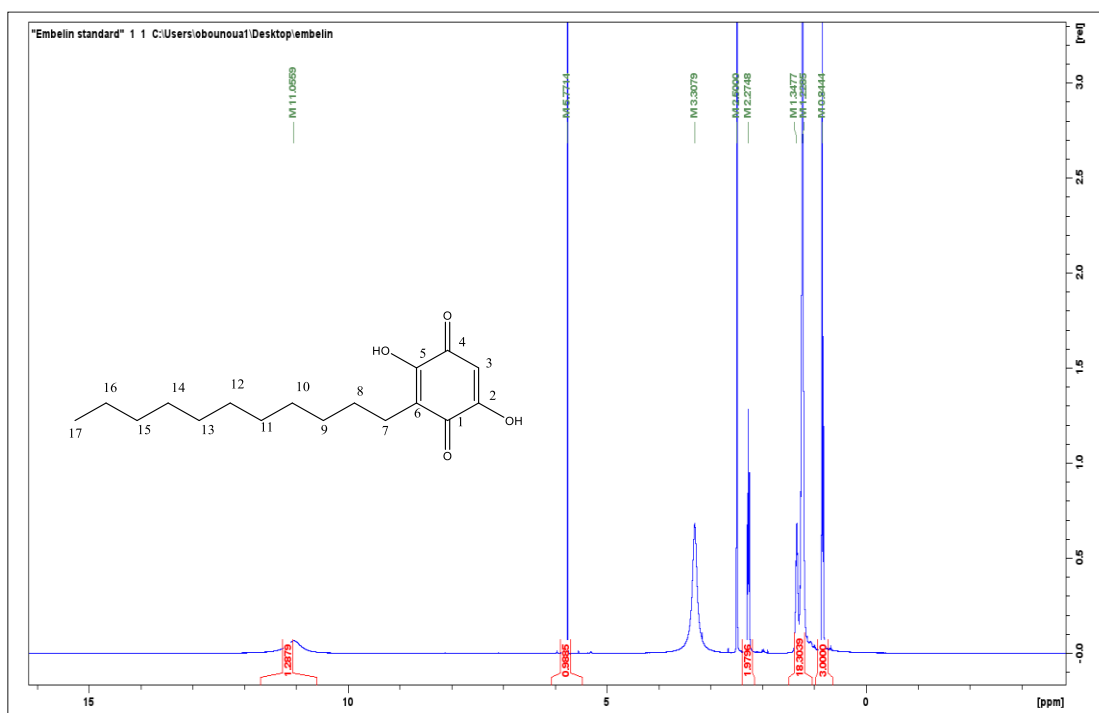


Figure 4.17: ^1H NMR of embelin standard (2) (400 MHz, DMSO, ppm)

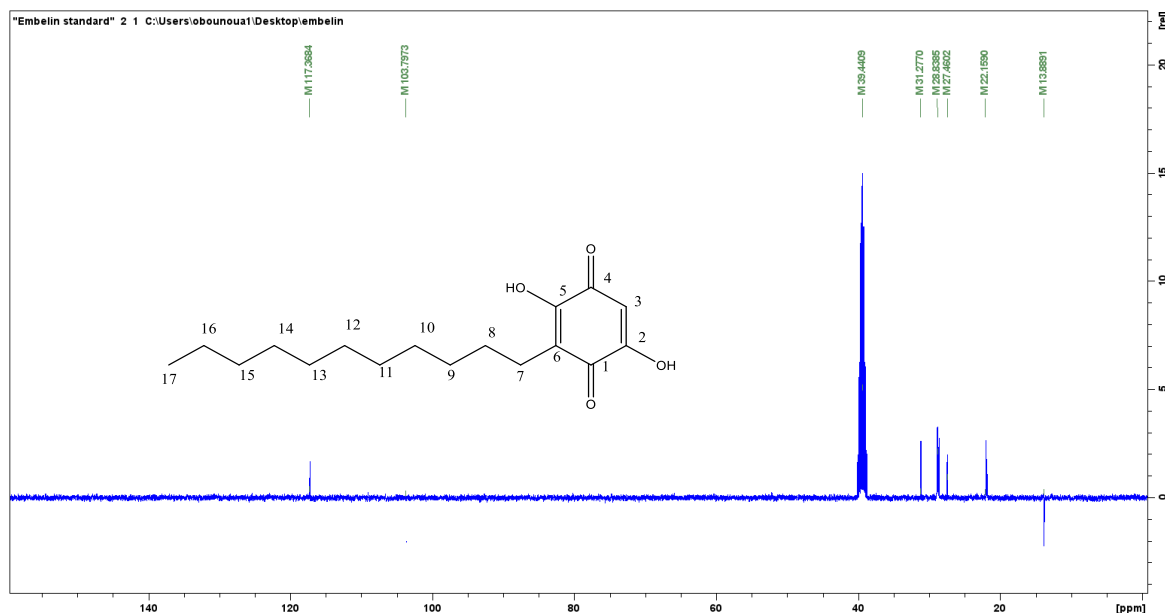


Figure 4.18: Dept NMR of embelin standard (**2**) (400 MHz, DMSO, ppm)

4.7.6. Elemental analysis of embelin

Table 4.7 shows the basic analytical information about the embelin chemical. It is clear that the experimentally determined (found) and theoretically predicted proportions of carbon, hydrogen, and oxygen (CHO) match.

Table 4.7: Elemental analysis of embelin compound

COMPOUND	CALCULATED			FOUND		
	C	H	O	C	H	O
C ₁₇ H ₂₆ O ₄	69.36	8.90	21.74	69.39	8.93	21.68

4.8. Derivatives of embelin

The chemical modification of embelin yielded derivatives namely: Vilangin (**3**) Figure 4.20, methyl vilangin (**4**), Embelin -2,4-dihydroxy benzaldehyde (**5**) and Embelin ninhydrin (**6**). The derivatives were characterized to confirm the successful modification.

4.8.1. Characterization of vilangin

The derivatized vilangin dyes are shown in Figure 4.19. The dye captured in Figure 4.19 was orange in colour obtained after successful modification.



Figure 4.19: Synthesized vilangin dyes

4.8.1.1. Melting point determination

The melting point of the vilangin dyes was found in the range of 264-265 °C. These values were consistent with the findings of Balachandran *et al.*, (2013) who synthesized vilangin with a melting point of 262 °C (Balachandran *et al.*, 2013).

4.8.1.2. UV-VIS spectra of vilangin (3)

The ultraviolet absorption spectra of the vilangin (**3**), shown in Figure 4.20 was scanned between the wavelength of 200 and 800 nm. The spectroscopic analysis of **3** in dichloromethane, revealed presence of two peaks at λ max of 292 nm these peaks are present in both embelin (**1**) and vilangin (**3**). The peak at 292 nm ascribes to $\pi \rightarrow \pi^*$ transitions. Upon modification of embelin to form compound (**3**) the peak initially observed at 336 nm in (**1**) embelin has undergone a red shift to a λ max 417 nm, this is because of an added hydroxyl groups (Opata & Dreuw, 2021) and the resultant vilangin structure underwent an increased conjugation because of the substituents hence increasing bathochromic shifts ascribed to $n \rightarrow \pi^*$ transitions due to -C=O in the vilangin structure (Hayashi *et al.*,

2009) . In addition to that, the favourable interaction between the oxygen atom of the carbonyl and aromatic ring has been found to lead to lower energy (Gautrot *et al.*, 2006). The peaks of embelin (1) are similar to those of the embelin standard (2).

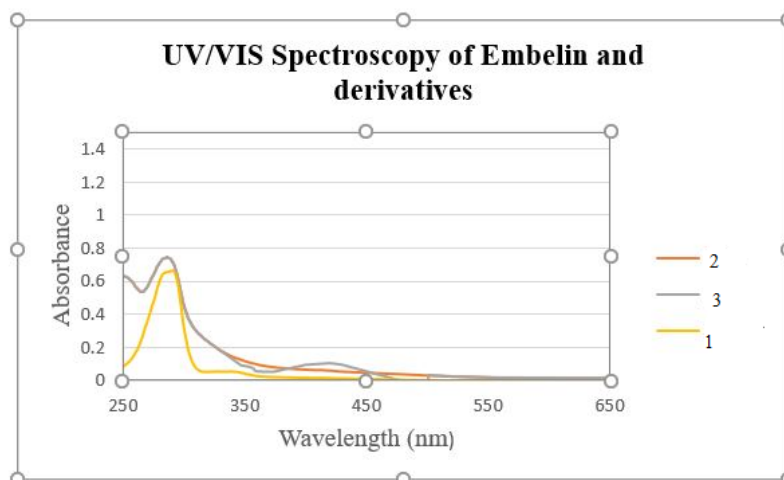


Figure 4.20: UV-VIS spectra of embelin and embelin standard and vilangin in Dichloromethane, scan 200-800 nm

4.8.1.3. FTIR spectra of vilangin

The ATR-FTIR frequency of vilangin, Figure 4.21, was scanned between the frequencies of 4000-500 cm^{-1} . The precursor embelin consists of a hydroxyl group and carbonyl group in the same ring resulting in an intramolecular hydrogen bond that brings stability to the group. The -OH peaks observed in embelin (1) at 3301.04 cm^{-1} are shifted to a peak at 3313.63 cm^{-1} on modification to the vilangin compound. The -OH peak is sharp and it was due to intramolecular hydrogen bonds which reduces the -O-H stretching band, these patterns are similar in embelin pure compounds (Dreesen *et al.*, 2001; Mondal *et al.*, 2012; Sivasankar *et al.*, 2017). The other peaks show, that the C-H stretch in the range of 2918.78–2848.07 cm^{-1} , the peak at 1610.49 cm^{-1} is due to C=O stretch (quinine carbonyl) and are fingerprints similar to those of embelin. An absorption peak is observed at 1427 cm^{-1} which is due to the

intensity of the $-C-O-H$ stretch, the wavenumbers of the $-O-H$ group are further shifted left thus confirming the formation of vilangin. Other characteristic peaks observed are similar to peaks in embelin. These results are consistent with similar results found in literature (Balachandran *et al.*, 2013). The peaks at 1610.49 cm^{-1} are related to $\pi \rightarrow \pi^*$ and $n \rightarrow \pi^*$ transitions observed in the UV-VIS spectra, Figure 4.20. The observed fingerprint shifts from embelin to vilangin are evidence that successful chemical modification from embelin to vilangin occurred and a new compound formed.

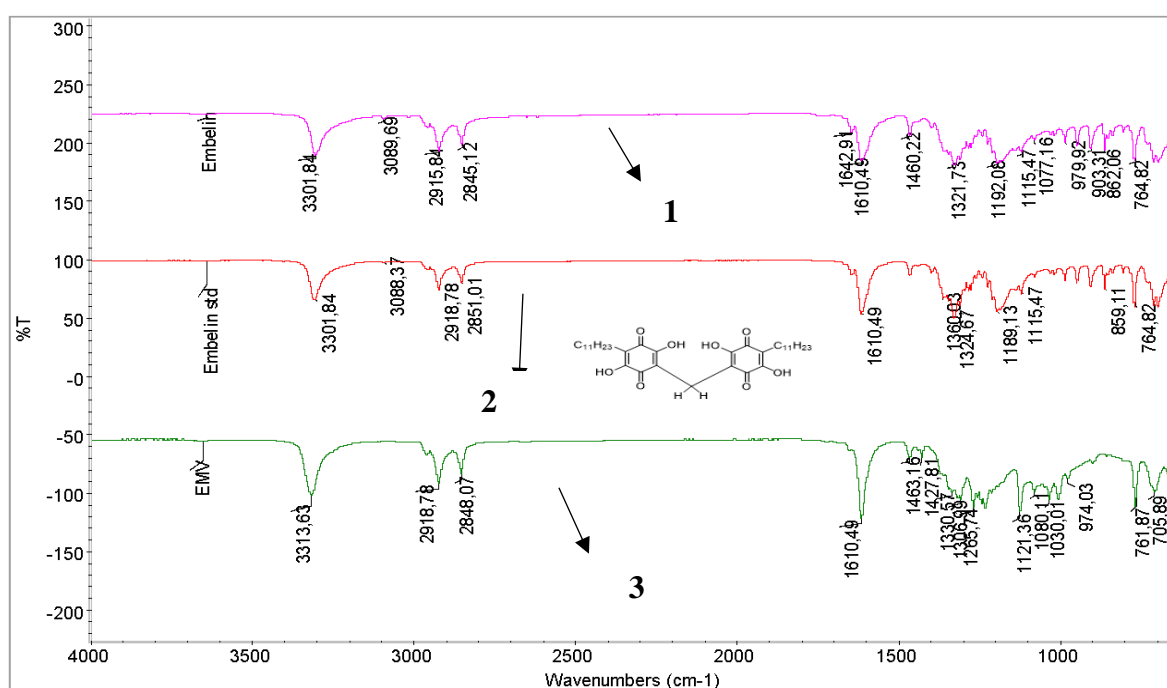


Figure 4.21: FTIR of vilangin (3)

4.8.1.4. LC-ESI-MS of Vilangin (3)

The LC-ESI-MS spectrum was obtained in negative-ion mode, Figure 4.22, to identify the semi-synthesized vilangin compound (3). The spectra showed the molecular ion peak at m/z 599.4 which confirmed the structure of vilangin which has a molar mass of 600 g/mol. These findings are in agreement with reports found in the literature (Balachandran *et al.*, 2013).

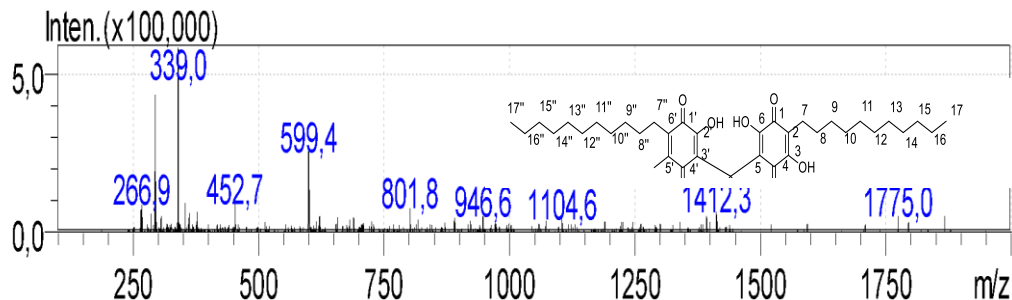


Figure 4.22: LC-ESI-MS spectrum of vilangin (3) in the negative mode

Some three other major fragment peaks were observed at m/z 266.9 which corresponds to the ($C_{16}H_{26}O_3$) fragment, m/z 339.0 corresponding to the ($C_{20}H_{35}O_4$) fragment and m/z 452.7 corresponding to ($C_{25}H_{40}O_7$) fragment. The fragments occur as a result of rearrangements within the molecule in the process of analysis leading to the loss of small molecules (Callemien & Collin, 2008). The structure of vilangin is made up of functional groups; $-C-H$ at 2918.78 cm^{-1} , $-C=O$ at 1610.49 cm^{-1} and $-O-H$ at 3313.63 cm^{-1} , observed in the FTIR spectra shown in Figure 4.21 above.

4.8.1.5. 1H and ^{13}C NMR spectroscopy of vilangin

The 1H NMR spectrum of the embelin, observed in section Figure 4.15, shows the signal at 0.85 ppm which is a triplet from the methyl group in position 17 (H-17) with a coupling constant of $J = 7$ Hz. In vilangin, Figure 4.23, the triplet from two sets of methyl protons is observed at 0.86 ppm in positions H-17 and H-17', with a coupling constant of $J = 8$ Hz. The broad singlet in embelin is observed at 1.25-1.34 ppm with a coupling constant of $J = 7$ Hz, consisting of 18 H at positions H 8-H 16, these signals were present in vilangin at 1.25 – 1.34 ppm with a coupling constant of $J = 7.1$ Hz, consisting of 36 H protons at positions H-8-H 16 and H 8'-H 16'. The chemical shift observed at 2.23 ppm is a doublet with a coupling constant $J = 7.8$ and is associated with two protons in position H-7 connected to the undecyl

chain of the embelin, the corresponding observation shifts to a signal at 2.26 ppm which is a doublet with a coupling constant $J=7.8$, associated with four protons in position H-7, H-7' of the undecyl chain in the vilangin compound. The singlet peak at 5.79 ppm which corresponds to the proton at position H-6, observed in embelin was not observed in the ^1H NMR spectrum of the vilangin (**3**) and new protons at position H-18 at 2.5164 ppm are observed in vilangin, this shows the disappearance of quinonoid proton and formation of bridging protons that bridge between two embelin groups. These are evidence of formation of a vilangin compound from proton NMR

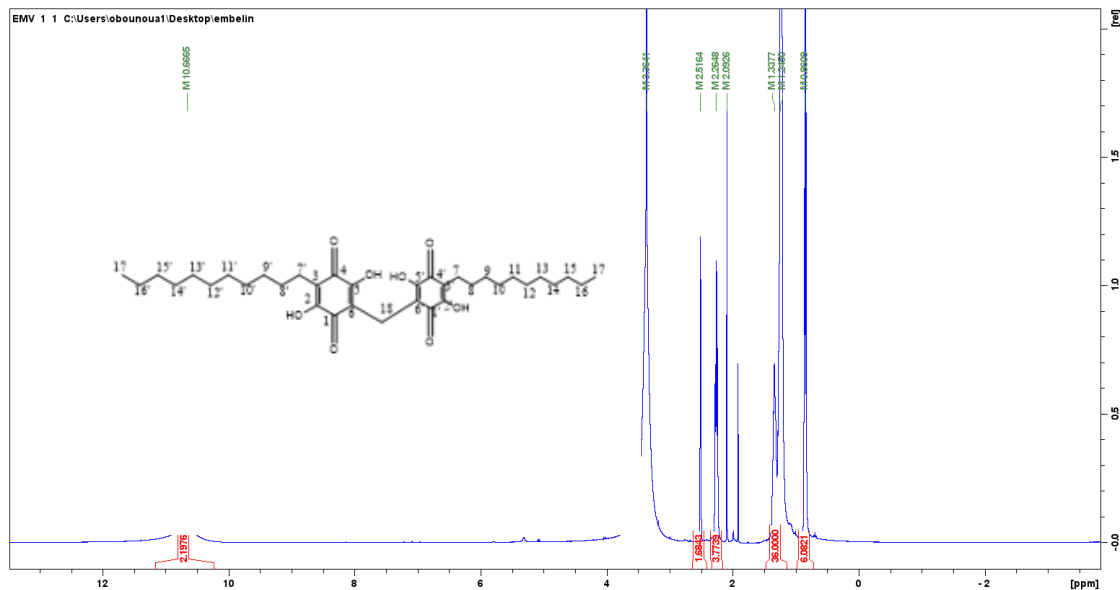


Figure 4.23: ^1H NMR of vilangin (**3**) (400 MHz, DMSO, ppm)

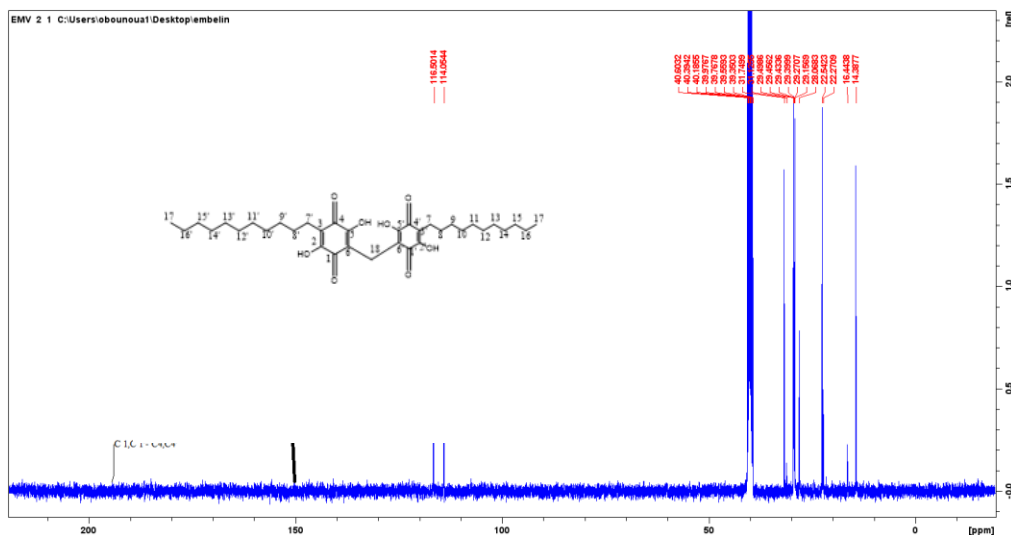


Figure 4.24: ^{13}C NMR of vilangin (3) (400 MHz, DMSO, ppm)

The DEPT ^{13}C NMR for embelin is shown in Figure 4.16 and presents a C-3 peak at 118.04 ppm which corresponds to the carbon bearing the decyl group. In vilangin, Figure 4.24, the chemical shift, was observed at 116.50 ppm corresponding to (C-3, C-3') of the vilangin, the signals observed at 104.45 ppm (C-6), 31.92-22.75 ppm (C-9-C 14) and 14.70 ppm (C-17) in the embelin were observed at 31.06-22.58 ppm (C-9-C 14, C-9'-C-14') and 14.42 ppm in position (C-17, C-17') respectively in vilangin. The C-6 carbon in embelin with 104.45 ppm was not observed in vilangin and the new chemical shift was observed at 16.44 ppm (C-18) which evidenced successful chemical modification of embelin to form vilangin. Because of the complexation between the two embelin groups, a chemical shift at approximately 150 ppm related to C-2 and 200 ppm related to carbonyl peaks in positions C-1, C-4 and C-1', C-4' related to the carbonyl carbons was observed. These chemical shifts at 200 ppm are the peaks observed at 1610.49 cm^{-1} in the FTIR and they are the consequences of $n \rightarrow \pi^*$ transitions in the UV-VIS spectra Figure 4.20.

4.8.1.6. Elemental analysis of vilangin

The elemental analytical data of the vilangin compound are depicted in Table 4.8. It is evident that the experimental (found) and theoretical percentages values of carbon, hydrogen and oxygen (CHO) supported the molecular formulae of the new synthesized complexes.

Table 4.7: Elemental analysis of vilangin compound

COMPOUND	CALCULATED			FOUND		
	C	H	O	C	H	O
C ₃₅ H ₅₂ O ₈	69.97	8.72	21.31	69.13	8.72	22.15

4.8.2. Characterization of methyl vilangin (4)

Characterization of methyl vilangin (4) was carried out to confirm its successful formation from embelin. Various techniques were involved to determine its structural components.

4.8.2.1. Melting point determination

The melting point of the methyl vilangin was determined and found in the range of 130-132 °C these results are consistent with the findings of Kiprono *et al.*, (2004) who determined melting point of methyl vilangin berries isolated from *Embelia schimperi* berries with 129-131 °C (Kiprono *et al.*, 2004).

4.8.2.2. UV-Visible spectroscopy of methyl vilangin (4)

The ultraviolet absorption spectra of the methyl vilangin(4), Figure 4.25 was scanned between the wavelength of 200 and 800 nm. The UV-VIS spectra of 4 revealed the presence of two peaks at λ max of 292 nm. These peaks were present in both embelin (1) and methyl vilangin (4). The peak at 292 nm ascribes to the benzoquinone with -C=C- chromophore which causes the $\pi \rightarrow \pi^*$ transitions. Upon modification of embelin to form compound (4) the peak initially observed at 336 nm in (1) embelin had a slight shift to 337 nm upon the

formation of methyl vilangin. The lack of significant change between the two compounds 1 and 4 could be due to the lack of strong electronic coupling of the chromophores in the new compound 4 formed (Guo *et al.*, 2007).

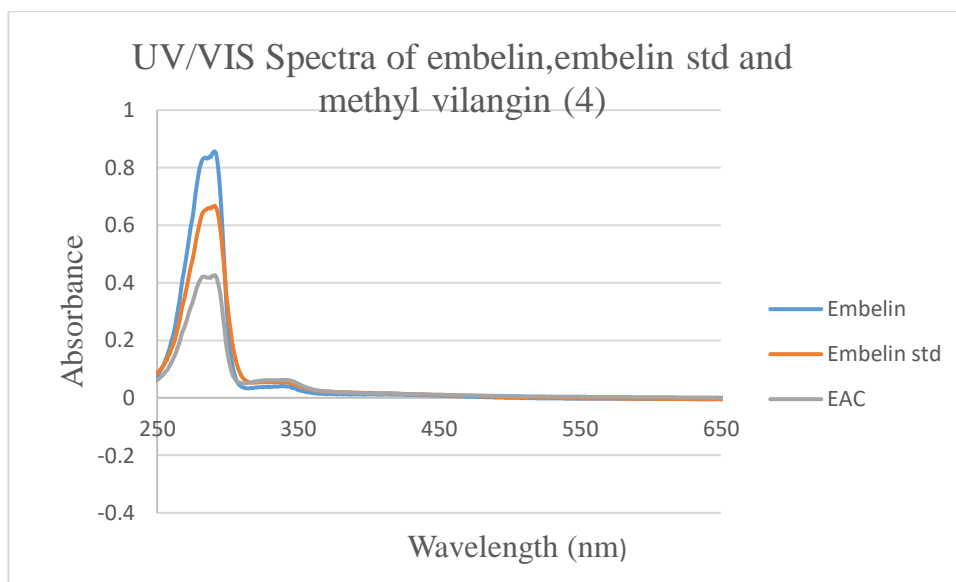


Figure 4.25: UV-VIS spectra of embelin and embelin standard and methyl vilangin in dichloromethane, scan 200-800 nm

4.8.2.3. FTIR of methyl vilangin

ATR-FTIR of methylvilangin was scanned between the frequencies of 4000-500 cm^{-1} . The starting material embelin is known to have a quinone and a hydroxyl functional group on the same aromatic ring resulting in intramolecular hydrogen bonds, which causes stability in the compound. Figure 4.26 shows an intense absorption peak at 3316.57 cm^{-1} which is due to –OH group. The other observed peaks shows, that C-H stretch in the range of 2918.78–2853.93 cm^{-1} , the peak at 1713.63 cm^{-1} and 1616.39 cm^{-1} are due to C=O stretch (quinone carbonyl) and are similar to that of embelin. An absorption peak is observed at 1466.11 cm^{-1} which is due to the intensity of the –C-O-H stretch. The wavenumbers of the –O-H group are further shifted left thus confirming the formation of methyl vilangin. Other characteristic peaks observed are similar to peaks in embelin. These findings are consistent with similar results

by Kiprono et al., (Kiprono *et al.*, 2004). The methyl vilangin compound experiences the intramolecular hydrogen bonding between the carbonyl and hydroxyl group and resonance between hydroxyl and $\text{C}=\text{C}$ groups in the aromatic ring causes sharp peaks in 3316.57 cm^{-1} . Other signals observed are 1324.67 cm^{-1} , 1283.42 cm^{-1} due to $\text{C}-\text{O}-\text{H}$, 1124.31 cm^{-1} , 1056.53 cm^{-1} due to $\text{C}-\text{O}$ alcohol, 950.86 cm^{-1} (rocking methylene), 773.66 cm^{-1} and 676.42 cm^{-1} (methylene bending). The peaks observed at 1713.63 cm^{-1} and 1616.39 cm^{-1} are related to α, β unsaturated $\text{C}=\text{O}$ and are evidence of formation of new compound they also shows ($\pi \rightarrow \pi^*$ and $n \rightarrow \pi^*$) transitions observed in the UV-VIS spectra, in Figure 4.25,

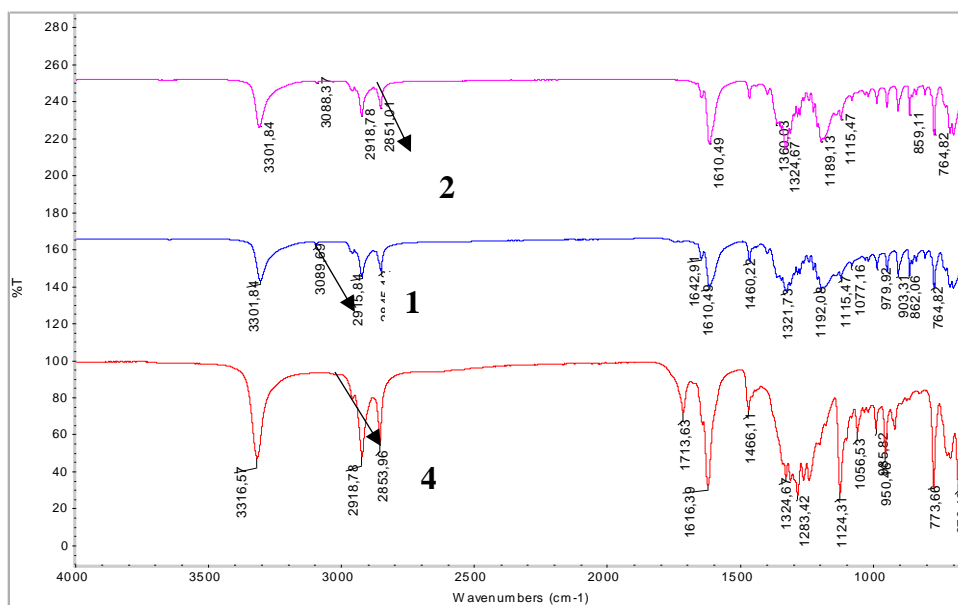


Figure 4.26: FTIR of embelin and embelin standard and methyl vilangin

4.8.2.4. LC-ESI/MS of methyl vilangin (4)

The LC-ESI-MS spectrum of methyl vilangin obtained in negative-ion mode was used to identify the semi-synthesized methyl vilangin compound (**4**), Figure 4.27. The spectrum had a molecular ion peak at m/z 613.2 which confirmed the structure of methyl vilangin which has a molar mass of 614.9 g/mol . Two other peaks at m/z 240.9 and m/z 292.9 were observed

in the spectra. The first fragment at m/z 292.9 corresponds to $[M-H]^-$ a fragment of embelin ($-C_{17}H_{26}O_4$) from compound **4**. The fragment at m/z 240.9 corresponds to the ($-C_{14}H_{23}O_4$) group from compound **4**. The fragments occur as a result of rearrangements within the molecule leading to the loss of small molecules (Callemien *et al.*, 2008). All the generated fragments occurred as a result of rearrangement within the compound in the process of ionization (Demarque *et al.*, 2016; Vessecchi *et al.*, 2010). These observed fragments identify the methyl vilangin because of the accurate signatures obtained from the fragments (Delcambre *et al.*, 2012; Hsu *et al.*, 2003).

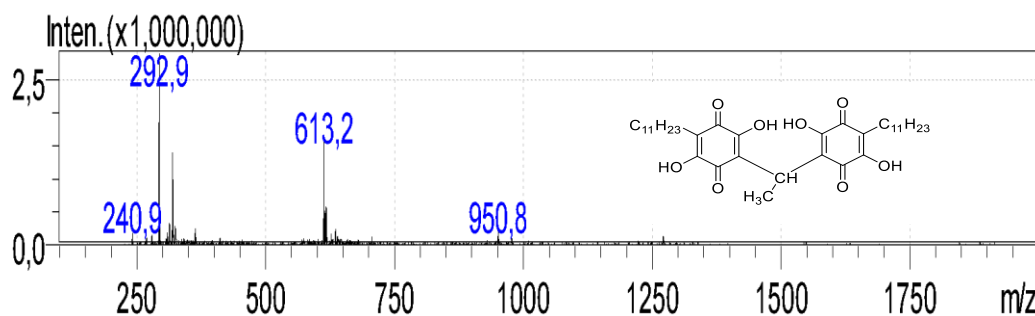


Figure 4.27: LC-ESI/MS spectrum of methyl vilangin (**4**) in the negative mode

4.8.2.5. 1H and ^{13}C NMR spectroscopy

The 1H NMR spectrum of the embelin, Figure 4.15, showed the signal at 0.85 ppm which is a triplet from the methyl group in position 17 (H-17) with a coupling constant of 7 Hz. In methyl vilangin, Figure 4.28, the triplet from two sets of methyl protons is observed at a chemical shift of 1.26 ppm in positions H-17 and H-17', with a coupling constant of $J = 8$ Hz. The broad singlet in embelin is observed at 1.25-1.34 ppm with a coupling constant of $J = 7$ Hz, consisting of 18 H at positions H 8-H 16, these protons are present in methyl vilangin at a chemical shift of 1.63 ppm with a coupling constant of $J = 8$ Hz, consisting of 36 H protons at positions H-8-H 16, H 8'-H 16'. A chemical shift was observed at 2.23 ppm which is a

doublet with a coupling constant $J = 7.8$, associated with two protons in position H-7 in embelin in the undecyl chain, these observations shifted to a signal at 2.15 ppm which is a doublet with a coupling constant $J = 7.8$, associated with four protons in position H-7, H-7' of the undecyl chain in methyl vilangin. The singlet peak at 5.79 ppm which corresponds to the proton at position H-6, observed in embelin was not observed in the methyl vilangin (4). There is formation of new protons at position H-18 with a chemical shift of 2.91 ppm and a chemical shift at 1.84 ppm is observed and this is evidence of the disappearance of quinonoid proton and formation of bridging protons that bridge between two embelin groups which led to the formation of methyl vilangin.

The DEPT ^{13}C NMR for embelin that was shown in Figure 4.16 it showed a C-3 peak at 118.04 ppm which corresponds to the carbon bearing the decyl group in methylvilangin Figure 4.30, this signal was observed at 118.00 ppm corresponding to (C-3, C-3'), the signals observed at 104.45 ppm (C-6), 31.92-22.75 ppm corresponding to C-9-C 14 and 14.70 ppm corresponding to C-17 were shifted to 31.70-22.58 ppm, C-9-C 14, C-9'-C-14' and 14.42 ppm corresponding to C-17 .C-17' respectively in methyl vilangin, Another signal was observed at 17.71 ppm which was associated C-18 formed on bridged formed on the formation of methyl vilangin. The C-6 carbon in embelin at 104 45 ppm is not observed in methyl vilangin is evidence that a new compound was formed. Because of the complexation between the two embelin groups a chemical shift is observed at approximately 172 ppm related to carbonyl peaks in positions C-1, C-4 and C-1', C-4'. These peaks at 172 ppm are due to the $-\text{C}=\text{O}$ group and they are associated with the peak observed at 1713.63 cm^{-1} in the FTIR, Figure 4.26 and they cause $n \rightarrow \pi^*$ transitions in the UV/VIS spectra Figure 4.25. The $-\text{C}=\text{O}$ group was observed in GC-MS Figure 4.3.

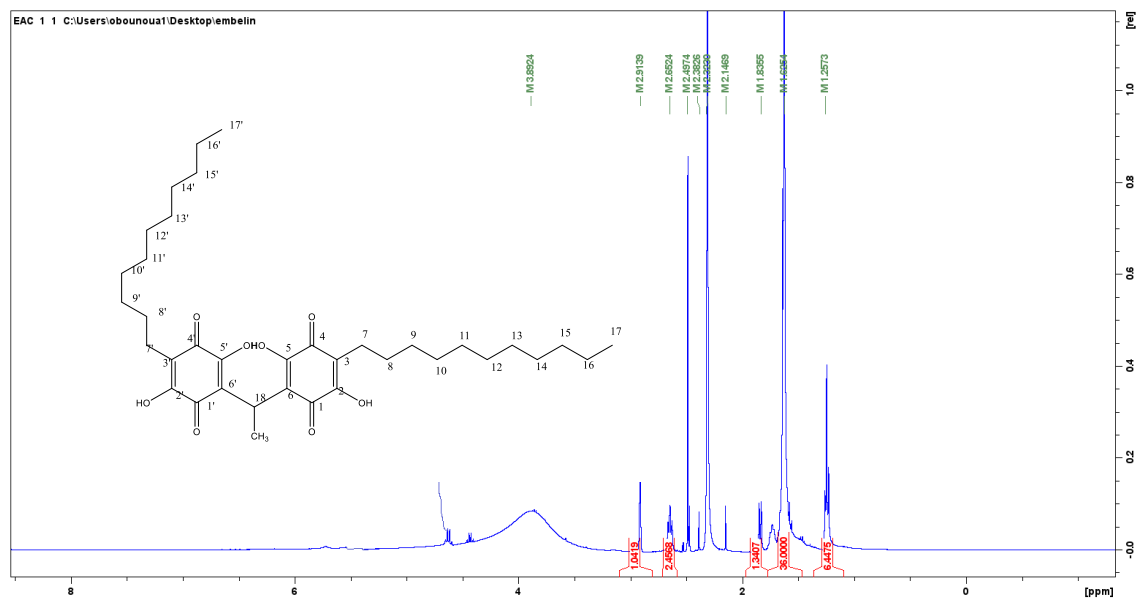


Figure 4.28: ^1H NMR of methyl vilangin (**4**) (400 MHz, DMSO, ppm)

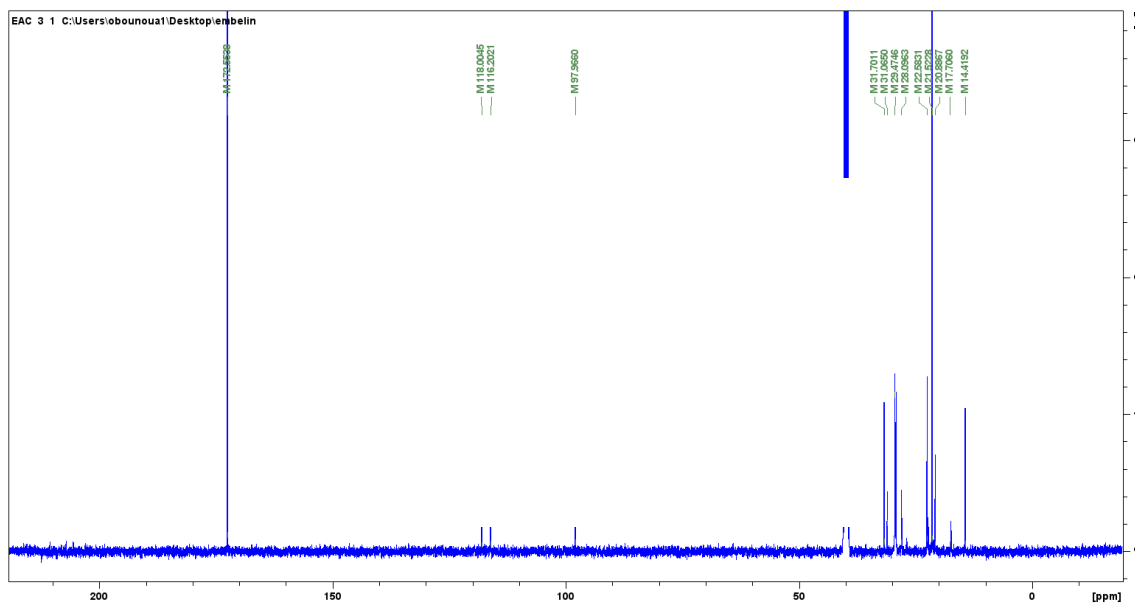


Figure 4.29: ^{13}C NMR of methyl vilangin (**4**) (400 MHz, DMSO, ppm)

4.8.2.6. Elemental analysis of methyl vilangin

The elemental analytical data of the methyl vilangin compound are depicted in Table 4.9.

Values found in the experiment were in agreement with theoretical (CHO) values.

Table 4.8: Elemental analysis of methyl vilangin compound

COMPOUND	CALCULATED			FOUND		
	C	H	O	C	H	O
C ₃₅ H ₅₄ O ₈	70.31	8.87	20.82	70.25	8.91	20.84

4.8.3. Characterization of Embelin-2,4 -dihydroxybenzaldehyde derivative

Characterization of Embelin-2,4 -dihydroxybenzaldehyde (**5**) was carried out to confirm its successful formation from embelin. Various techniques were involved to determine its structural components.

4.8.3.1. Melting point determination of (**5**)

The melting point of the (**5**) was found in the range of 261-264°C.

4.8.3.2. UV-Visible spectroscopy of embelin-2,4 -dihydroxybenzaldehyde derivative (**5**)

The ultraviolet absorption spectra of the compound (**5**), Figure 4.30 was scanned between the wavelength of 200 and 800 nm. The UV-VIS of **5**, revealed the presence of one peak at λ max of 292 nm, these peaks are present in both embelin (**1**) and compound (**5**). The peak at 292 nm ascribes to the aromatic ring with -C=C- chromophore which causes the $\pi \rightarrow \pi^*$ transitions. Upon modification of embelin to form compound (**5**). Compound **5** did not show other peaks. There seems to be a lack of different electronic coupling of the chromophores in the new compound **5** apart from what has been witnessed in embelin (**1**) formed (Lukhele, 2012).

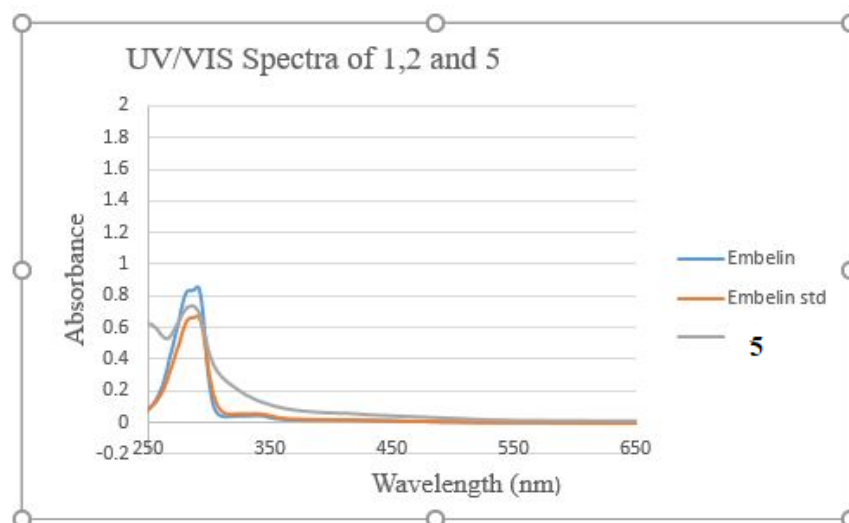


Figure 4.30: UV-VIS spectra of embelin and embelin standard and compound **5** in dichloromethane, scan 200-800 nm

4.8.3.3. FTIR of Embelin-2,4 -dihydroxybenzaldehyde

The structure of compound **5** was confirmed by spectral data, Figure 4.31. FTIR-ATR: cm^{-1}): 3298.90 (hydroxyl), 2918.78 (bridged -C-H stretch), 2848.07 (-C-H stretch; alkyl), 1613.44 (quinine carbonyl), 1460.22, 1324.67, 1183.21, 982.87 (rocking methylene) and 708.64 (methylene bending).

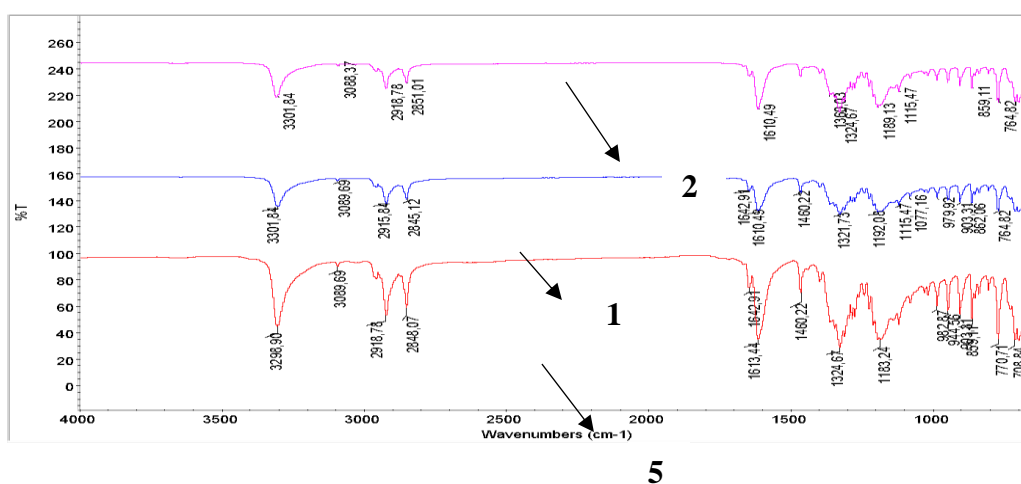


Figure 4.31: FTIR of embelin and embelin standard and embelin-2,4 -dihydroxybenzaldehyde (**5**)

4.8.3.4. LC-ESI-MS of embelin-2,4 -dihydroxybenzaldehyde derivative

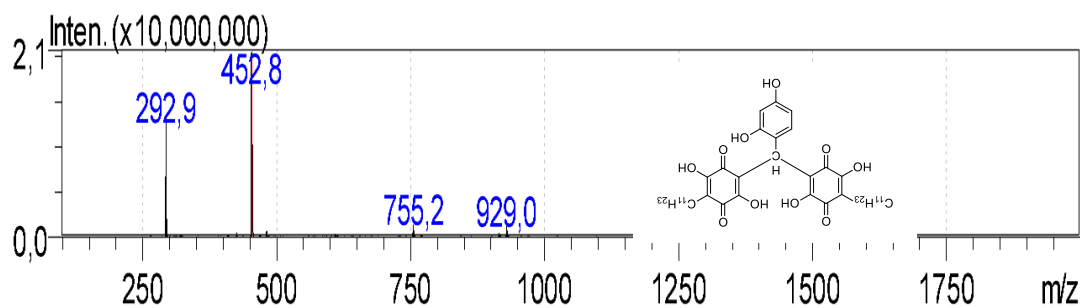


Figure 4.32: LC-ESI/MS spectrum of embelin 2,4-dihydroxybenzaldehyde derivative

The spectra shown in Figure 4.32 showed the molecular ion peak of $C_{17}H_{26}O_4$ (**1**) at m/z 292.9 which corresponds to the structure of embelin. These findings using ESI/MS showed that the structure of compound **5** was not formed based on the theoretical value of compound **5** which has a molar mass of 705.94 g/mol.

4.8.3.5. 1H and ^{13}C NMR spectroscopy of embelin-2,4 -dihydroxybenzaldehyde derivative(**5**)

The 1H NMR spectrum of the embelin observed in Figure 4.15, showed the chemical shift at 0.85 ppm which is a triplet associated with the methyl group in position H-17 with a coupling constant of 7 Hz. In compound **5**, Figure 4.33, a chemical shift was observed at 0.64 ppm with a coupling constant of $J = 8$ Hz associated with the methyl protons at H-17. The broad singlet in embelin was observed at 1.25-1.34 ppm with a coupling constant of $J = 7$ Hz, consisting of 18 H observed at positions H 8-H 16 in embelin. In compound **5a** these chemical shifts were observed at 0.99 – 1.12 ppm with a coupling constant of $J = 7.1$ Hz, consisting of 18 H protons at positions instead of 36 H expected to be observed H-8-H 16, H 8'-H 16'. A chemical shift was observed at 2.05 ppm with a coupling constant of $J = 7.8$ associated with two protons in position H-7 in embelin in the undecyl chain. These observation shifts to a

signal at 2.07 ppm which is a doublet with a coupling constant $J = 7.8$ in compound 5. The singlet peak observed at 5.79 ppm in embelin is retained in compound 5 at 5.54 ppm.

The DEPT ^{13}C NMR for embelin is shown in Figure 4.16 showed a C-3 peak at 118.04 ppm which corresponds to the carbon bearing the decyl group, in compound 5 in Figure 4.34. This signal was observed at 117.83 ppm corresponding to (C-3, C-3') in compound 5. The chemical shift observed at 104.45 ppm corresponds to (C-6), 31.74-22.75 ppm corresponding to C-9-C 14 and 14.70 ppm corresponding to C-17 in the embelin were shifted to 31.08-21.45 ppm, C-9-C 14, C-9'-C-14' and 14.36 ppm corresponding to C-17 .C-17' respectively in compound 5. The C-6 carbon in embelin with 104 45 ppm is observed in compound 5 at 104.26 ppm and the carbonyl signal observed at 172.45 is related to carbonyl peaks in positions C-1, C-4. These results show that compound 5 was not formed as expected. This is supported by UV-VIS spectra which showed only a single peak observed in Figure 4.30. There is not much significant effect in the FTIR structure in Figure 4.31 whose functional group replicated that of embelin. The ESI-MS spectra showed the molecular ion at m/z 452.8 which deviated from the theoretical value of compound 5. The singlet peak observed at 5.79 ppm in embelin is retained in compound 5 at 5.54 ppm implying that no substitution occurred in the bridging proton. The chemical shift observation of the signal at 104.26 ppm is evidence that compound 5 was not successfully formed. The main reason for unsuccessful modification could be due to the steric hindrance due to the bulky substituent in the aldehyde (Zhou *et al.*, 2020).

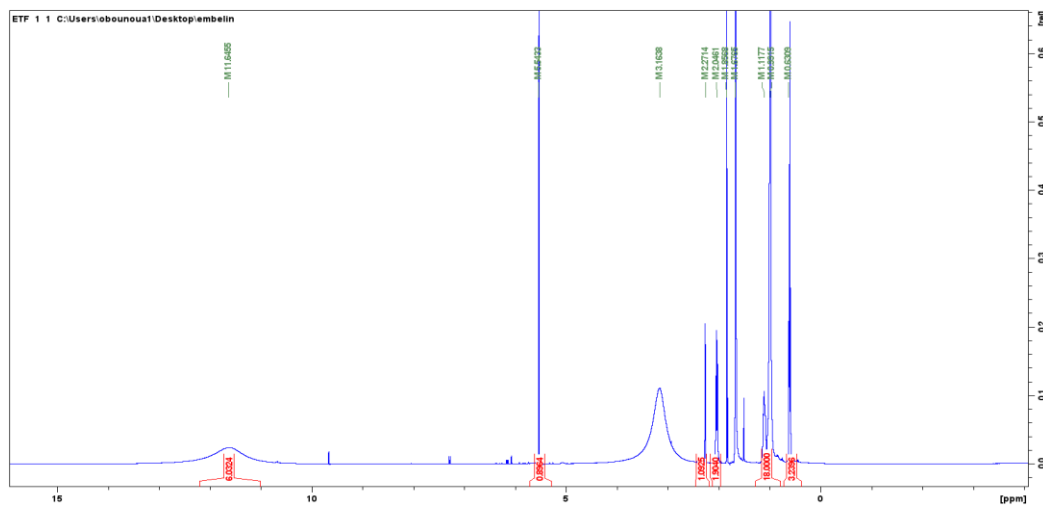


Figure 4.33: ^1H NMR of embelin-2,4 -dihydroxybenzaldehyde (**5**) (400 MHz, DMSO, ppm)

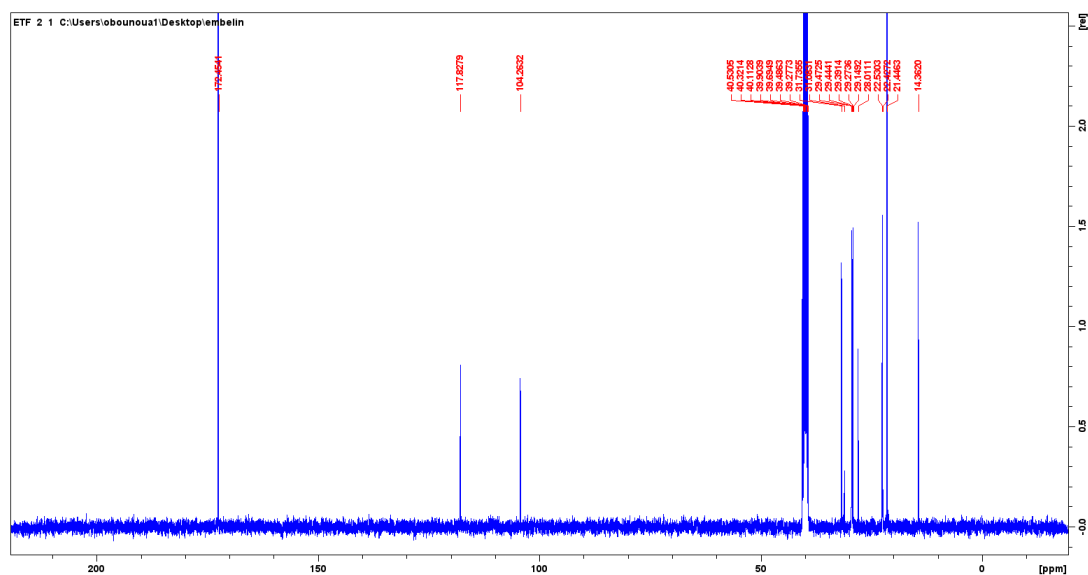


Figure 4.34: ^{13}C NMR of embelin-2,4 -dihydroxybenzaldehyde (**5**) (400 MHz, DMSO, ppm)

4.8.3.6. Elemental analysis of compound embelin-2,4 -dihydroxybenzaldehyde (**5**)

The elemental analytical data of compound **5** are depicted in Table 4.10. It is evident that values found in the experimental were not in agreement with theoretical (CHO) values.

Table 4.9: Elemental analysis of compound embelin-2,4 -dihydroxybenzaldehyde (5) compound

COMPOUND	CALCULATED			FOUND		
	C	H	O	C	H	O
C ₄₁ H ₅₃ O ₁₀	69.75	7.58	22.67	68.93	8.72	22.37

4.8.4. Characterization of embelin with ninhydrin derivative(6)

Various physical and spectral characterizations were carried out to confirm the successful chemical modification of embelin to embelin ninhydrin.

4.8.4.1. Determination of melting point

The melting point of embelin ninhydrin was found to be in the range of 176-178°C, these values were consistent with the finding in the literature where embelin ninhydrin was found with a melting point of 178-180°C (Mahendran *et al.*, 2011).

4.8.4.2. UV-Visible spectroscopy of embelin ninhydrin (6)

The ultraviolet absorption spectra of the embelin ninhydrin (6), Figure 4.35 was scanned between the wavelength of 200 and 800 nm. Spectroscopic analysis of embelin ninhydrin in dichloromethane revealed the presence of two peaks at λ max of 292 nm due to $\pi \rightarrow \pi^*$ transitions of the dienes in the embelin structure and a shoulder at λ max 336, this is probably due to $n \rightarrow \pi^*$ transitions. Upon the chemical modification of embelin with ninhydrin, there was an increased conjugation which led to a bathochromic shift from λ max 336 to λ max 498 nm (Sutradhar & Misra, 2018). Furthermore, the added hydroxyl groups and carbonyl which contain oxygen increases the electron density in the compound which lowers the energy gap and increases the wavelength to λ max 498 nm due to $n \rightarrow \pi^*$ (Liu *et al.*, 2020).

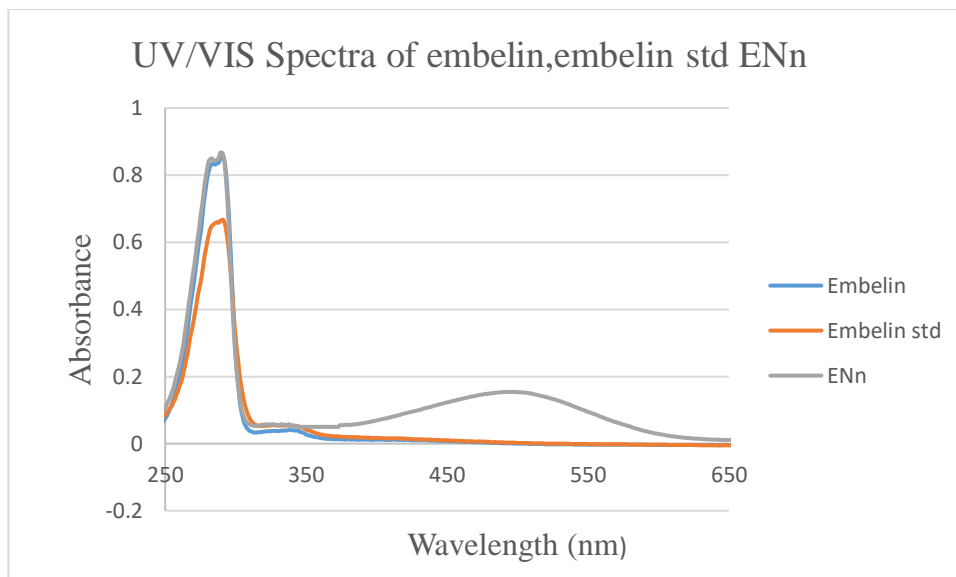


Figure 4.35: The UV-Vis absorbance spectra for embelin, embelin standard and embelin ninhydrin

4.8.4.3. FT-IR spectroscopy of embelin ninhydrin

The ATR-FTIR frequency was scanned between the frequencies of 4000-500 cm^{-1} . The starting material embelin has a quinone and a hydroxyl quinone on the same aromatic ring causing it to have intra-molecular hydrogen bonds, which stabilizes this compound. The FT-IR spectra Figure 4.36 for both the isolated embelin and the standard shows intense sharp –OH groups at 3301.84 cm^{-1} . These findings are consistent with the FTIR spectrum of embelin isolated from *Embelia ribes* in other related studies (Radhakrishnan *et al.*, 2011). The sharp OH peaks in the compounds are due to the existence of the intramolecular hydrogen bonds which resulted from hydrogen connected to the electronegative oxygen atom and the –C=O bond because of the electronegative difference in the two atoms (Anitha *et al.*, 2015). These resonance effects between –C=O and -O-H groups led to sharp intense absorption at 3301.84 cm^{-1} . The peak observed at 1610.49 cm^{-1} is due to the stretching frequency of the carbonyl present. These results are consistent with the findings by Radhakrishnan and Chepkwony

where the -C=O group in embelin was observed at 1610 cm^{-1} (Chepkwony *et al.*, 2014; Radhakrishnan *et al.*, 2013).

In contrast, the derivatized compound, embelin ninhydrin shows the -OH groups at 3307.73 cm^{-1} . This is evidence enough that -OH exists in a different chemical environment. The absorption frequency of -C=O is also evident at 1716.57 cm^{-1} and at 1616.37 cm^{-1} the vibrational frequency is due to α, β unsaturated C=O . This shows that a new compound has been formed. These peaks at 1615 cm^{-1} , are probably due to carbon-carbon double bonds, which merge with the lower frequency carbonyl peaks and are then only detectable under conditions of high spectral resolution (Echeverría *et al.*, 2018). Although not much shift was observed in the fingerprints, the deviations from corresponding vibration frequencies of embelin are evident enough that a new compound has been formed. The -C=O functional groups are observed as $n \rightarrow \pi^*$ transitions in the UV-VIS spectra Figure 4.35

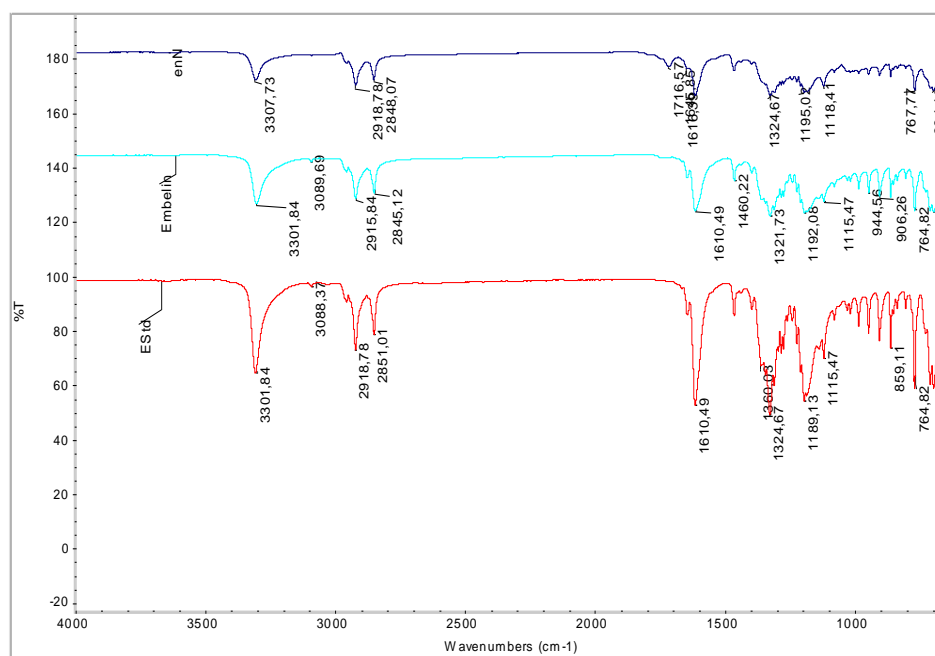


Figure 4.36: The ATR- FT-IR spectra of embelin, embelin standard and embelin ninhydrin in the range $4000\text{-}500\text{ cm}^{-1}$

4.8.4.4. LC-ESI-MS of embelin ninhydrin

The LC-ESI-MS spectrum of embelin ninhydrin obtained in negative-ion mode was used to identify the semi-synthesized embelin ninhydrin compound (**6**), Figure 4.37. The spectrum had a molecular ion peak at m/z 452.9 which confirmed the structure of embelin ninhydrin which has a theoretical molar mass of 453 g/mol. Two other peaks at m/z 292.9 and m/z 569.2 were observed in the spectra. The first fragment at m/z 292.9 corresponds to $[M-H]^{-a}$ fragment of embelin ($-C_{17}H_{26}O_4$) from compound **6**. The m/z 569.2 corresponds to an embelin dimer formed during the ionization process but has lost a hydroxyl group (Wong-Paz *et al.*, 2021). The observed fragments provided better identification of the resultant product by giving signatures of the compound (Delcambre *et al.*, 2012). The peak at m/z 452.9 was produced without fragmentation and the other fragments are a result of the gaseous analyte (ENn) which was allowed to collide with the gaseous target (nitrogen gas) found in the collision cell resulting in energy gain which is distributed among vibrational degrees of freedom (internal energy) in the ENn compound. Thus, the excited state of ENn compound was populated resulting in the observed fragments in the process of CID (Banerjee *et al.*, 2012; Ortiz *et al.*, 2014). The hydroxyl fragment is not observed because it is eliminated as a water molecule (Musharraf *et al.*, 2013).

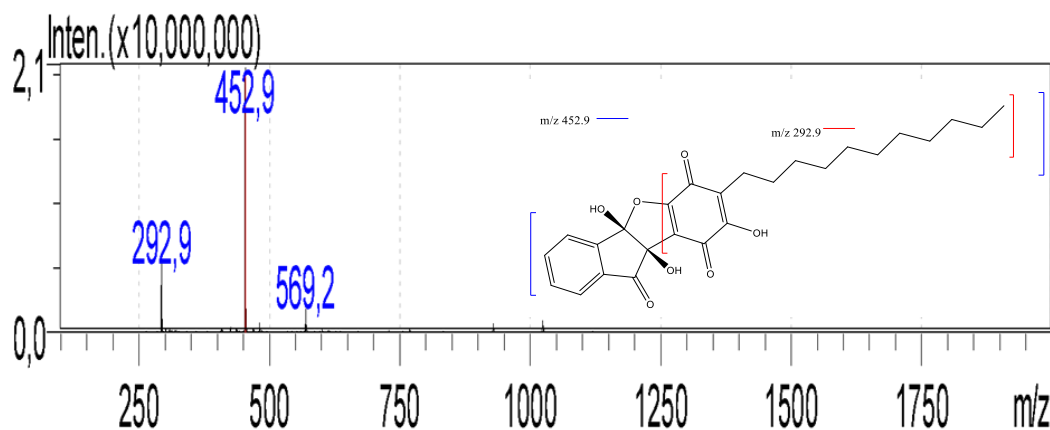


Figure 4.37: LC-ESI/MS spectrum of embelin ninhydrin in the negative mode

4.8.4.5. ^1H and ^{13}C NMR spectroscopy of embelin ninhydrin (6)

The ^1H NMR spectrum of the embelin, observed in Figure 4.15, shows the signal at 0.85 ppm which is a triplet from the methyl group in position 17 (H-17) with a coupling constant of $J = 7$ Hz. In Embelin ninhydrin (ENn) (6), Figure 4.38, the triplet from the methyl group is observed at 0.60 ppm in position H-17 with a coupling constant of $J = 8$ Hz. The broad singlet in embelin is observed at 1.25-1.34 ppm with a coupling constant of $J = 7$ Hz, consisting of 18 H at positions H 8-H 16. These signals were present in embelin ninhydrin as a multiplet at 0.97 ppm with a coupling constant of $J = 8$ Hz, consisting of 16 H protons at positions H-9-H 16. The signal observed at 2.23 ppm which is a doublet with a coupling constant $J = 7.8$, is associated with two protons in position H-7 connected to the undecyl chain, the corresponding observation shifts to a signal at 2.25 ppm which is a doublet with a coupling constant $J = 7.1$ associated with two protons in position H-7 of the undecyl chain in embelin ninhydrin compound another proton at H-8 which is a multiplet with 2.04 ppm in ENn. A singlet peak at 5.79 ppm which corresponds to the proton at position H-6, was observed in embelin. Other protons observed in embelin ninhydrin upon modification are H-20 at 5.52 ppm (-OH), aromatic protons 6.86-7.73 ppm (4H). The successful formation of

embelin ninhydrin is evidenced by the disappearance of protons at H-6 and H-5 which are not observed in embelin ninhydrin.

The DEPT ^{13}C NMR for embelin is shown in Figure 4.16 and presents a C-3 peak at 118.04 ppm which corresponds to the carbon bearing the decyl group. In embelin ninhydrin Figure 4.39, this signal was observed at 117.83 ppm corresponding to (C-3), the signals observed at 104.45 ppm (C-6), 31.92-22.75 ppm corresponding to C-9-C 14 and 14.70 ppm corresponding to C-17 in embelin were shifted to 131 ppm (C-6), 31.76-22.44 ppm, C-7-C 16, and 14.38 ppm in position C-17 respectively in embelin ninhydrin. Other carbon signals were observed at 198.63 ppm (C-18) due to carbonyl from the substituent ninhydrin, 172.42 ppm (C-1,4), 156 ppm (C-3), 152 ppm (C-6), 142 ppm (C-25), 136 ppm (C-22), 130 ppm (C-5). These signals of 124.10 ppm (C-24, C-25) and 124.13 ppm (C-23) are associated with carbons in the benzene ring of the substituent. Other signals present were 117.83 ppm (C-21), 116 ppm (C-2) 54 ppm (C-19). The carbon-13 signals from the substituent are evidence of successful modification of embelin to embelin ninhydrin. The observed chemical shifts at 172 ppm are due to the $-\text{C}=\text{O}$ group and they are associated with the peak observed at 1716.57 cm^{-1} observed in the FTIR, Figure 4.36 and they cause $n \rightarrow \pi^*$ and $\pi \rightarrow \pi^*$ transitions in the UV/VIS spectra Figure 4.35. The $-\text{C}=\text{O}$ group was observed in GC-MS Figure 4.3.

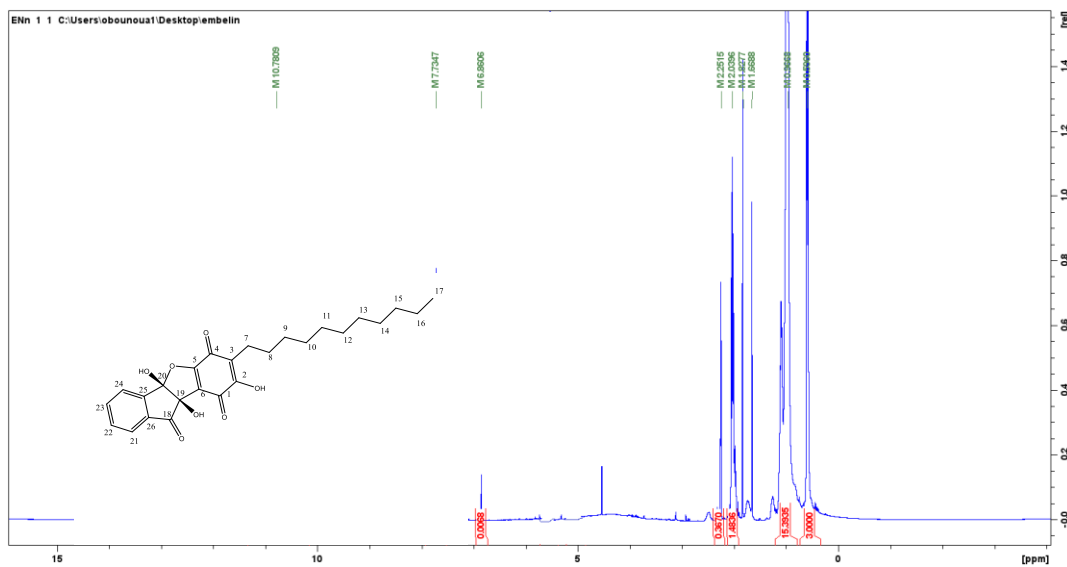


Figure 4.38: ^1H NMR spectra of embelin ninhydrin (**6**) (400 MHz, d-DMSO, ppm)

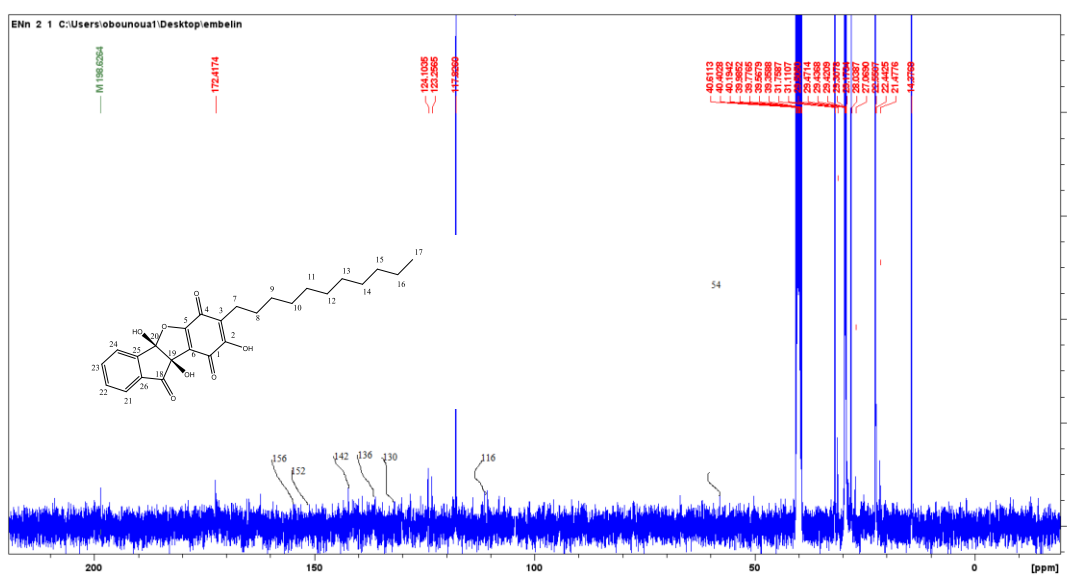


Figure 4.39 : ^{13}C NMR spectra of embelin ninhydrin (**6**) (400 MHz, DMSO, ppm)

4.8.4.6. Elemental analysis of compound Embelin ninhydrin (**6**)

The elemental analytical data of the compound ENn are depicted in Table 4.11 It is evident that values found in the experimental were in agreement with theoretical (CHO) values.

Table 4.10: Elemental analysis of compound ENn compound

COMPOUND (M.F)		CALCULATED			FOUND		
C ₂₆ H ₃₀ O ₇	C	H	O	C	H	O	
	68.70	6.66	24.64	68.74	6.64	24.62	

4.9. Effect of semi-synthetic derivatives on textile fibers

The semi-synthetic derivatives all supports successful modification of the embelin compound except derivative (5) which showed characteristics of embelin suggesting its modification was not successful. The functional groups introduced are chromophores that enhances hydrophilicity behavior of the dye and enhances adhesion to the textile fibers

4.10. Dyeing of textile fibers

Dyeing experiments were performed using embelin (1) and all the compounds (3-6) to the textile fibers (cotton, wool, and silk). Preliminary dyeing experiments were carried out, compounds 4 and 5 did not exhibit dyeing properties. This was not possible probably because of the bulky group of the substituent which causes dye aggregation. Hence dyeing was further performed with compounds 1, 3 and 6 only.

4.10.1. Dyeing of textile fibers with embelin dyes (1)

Embelin dyes were applied to cotton, silk and wool fibers and their colour strength was evaluated alongside dyed textile fibers using synthesized derivatives and results shown in comparison to each derivatized dye.

4.10.2. Dyeing of textile fibers with vilangin dyes (3)

Vilangin dyes were applied to cotton, silk and wool fabric. The effect of pH, time and temperature parameters on colour strength was evaluated. The cotton fibers showed relatively

weak colour strength whereas silk and wool fibers faded instantly and their colour strengths could not be evaluated. The three variations were found to have an impact on colour strength of cotton fibers.

4.10.2.1. Effect of dyeing pH on cotton vilangin dye

The effect of dyeing pH on colour strength is shown in Figure 4.40. The colour strength increases with the increase of dyeing pH and reach a maximum value at approximately 8.5 then it decreases. The increased colour strength can be attributed to better dye exhaustion at alkaline pH resulting from hydrogen bond formation between the dye molecule and cellulose fibers. However, at pH higher than 9 there is a decrease in colour strength, resulting in an anionic character increase causing repulsion to occur between the dye molecule and fabric leading to low colour strength.

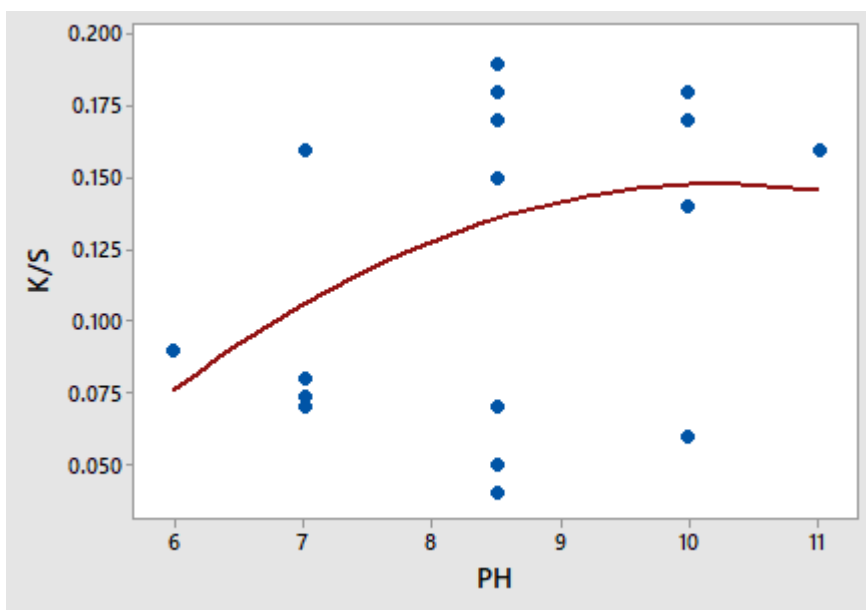


Figure 4.40: Effect of pH on colour strength of cotton dyeing with vilangin

4.10.2.2. Effect of dyeing time on cotton vilangin dye

Effect of dyeing time on colour strength of vilangin dyed cotton fabric is shown in Figure 4.41. The more the dyeing time the higher the colour strength until dye equilibrium is

attained. An increase in time over 60 min causes a decrease in colour strength. The low colour strength is attributed to the desorption of dye components from the cotton fiber into the dye bath during a longer dyeing time (Adeel *et al.*, 2009).

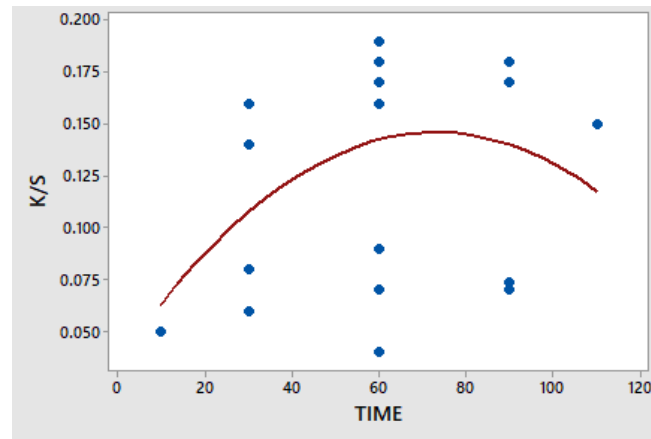


Figure 4.41: Effect of time on colour strength of cotton dyeing with vilangin

4.10.2.3. Effect of dyeing temperature on cotton vilangin dye

The effect of dyeing temperature on colour strength is demonstrated in Figure. 4.42. As it can be observed, the colour strength increases with the increase of dyeing temperature and reaches a maximum value at 85 °C where the aggregate of the vilangin dye molecule is fully broken down. The fiber also swells leading to dye uptake. Beyond this temperature, there is a decrease in colour strength, which may be attributed to a decrease in dye molecule stability at higher temperatures.

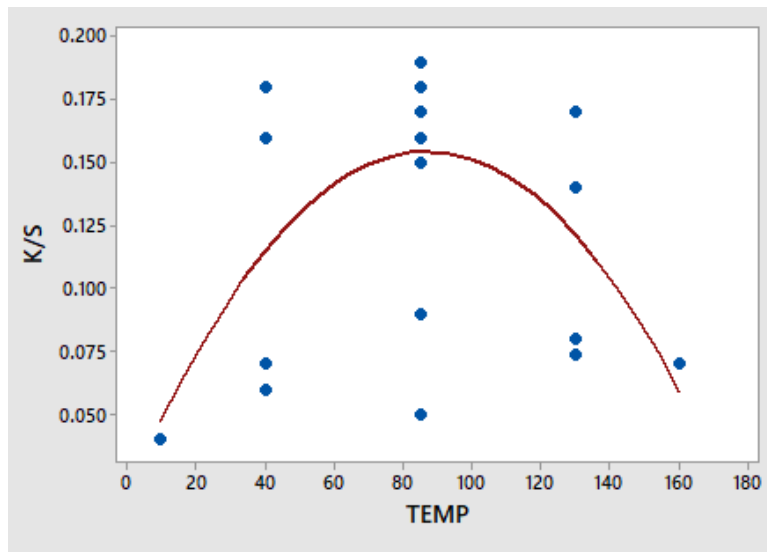


Figure 4.42: Effect of temperature on dye exhaustion of cotton dyeing with vilangin

4.10.2.4. Response surface methodology optimization

The dyeing of cotton fibers was optimized by using the Response surface methodology. The factors considered were pH, temperature and time. The experimental conditions for dyeing cotton fabric using vilangin dye were designed by using Design Expert. The effects of the different parameters on colour strength of cotton were measured and evaluated using statistically designed experiments as shown in Table 4.12 below.

The experimental factors of consideration and color strengths (K/S) of the dyed cotton samples are shown in Table 4.12. The regression model equation (Equation 4.1) and analysis of 3D response plots showed the optimum dyeing conditions and the variation of dyeing conditions on the colour strength.

Table 4.11: Experimental design and results for the colour strength of cotton fibers dyed with vilangin (3)

Run	X1	X2	X3	K/S
1	-1	-1	-1	0.08
2	$-\infty$	0	0	0.09
3	-1	-1	-1	0.16
4	1	1	1	0.17
5	1	1	-1	0.18
6	0	0	0	0.19
7	0	0	$+\infty$	0.07
8	0	0	0	0.18
9	1	-1	0	0.14
10	0	$-\infty$	0	0.05
11	1	-1	-1	0.06
12	$+\infty$	0	0	0.16
13	-1	1	-1	0.07
14	0	$+\infty$	0	0.15
15	-1	1	1	0.07
16	0	0	$-\infty$	0.04
17	0	0	0	0.19
18	0	0	0	0.18
19	0	0	0	0.17
20	0	0	0	0.19

The obtained data were fitted to various models and their respective ANOVA showed in Table 4.13.

Table 4.12: Analysis of Variance

Factor	F-Value	P-value
Model	6.13	0.0045
X ₁ .(pH)	6.67	0.0273
X ₁ .X ₂ (pH.Time)	8.56	0.0152
X ₂ ² (Time.Time)	8.90	0.0137
X ₃ ² (Temperature.Time)	25.15	0.0005

Model summary results are in Table 4.14. The effect of all variables and their interactions on the response are tabulated. The model reduction was done to eliminate insignificant models. If there are many insignificant model terms, the model reduction can improve the model. In this study, in this case, X₁, X₁.X₂, X₂² and X₃² are significant model terms. The "Pred R-Squared" of 0.8466 was in reasonable agreement with the "Adj R-Squared" of 0.7085.

$$K/S = 0.18 + 0.021 X_1 + 0.016 X_2 + 3.255E-003 X_3 + 0.031 X_1.X_2 + 0.018 X_1.X_3 - 7.500E-004 X_2.X_3 - 0.015 X_1^2 - 0.023 X_2^2 - 0.039 X_3^2 \dots \dots \dots \text{Equation 4.1}$$

Table 4.13: Model Summary

S	R-sq	R-sq (adj)
10.7976	84.66 %	70.86 %

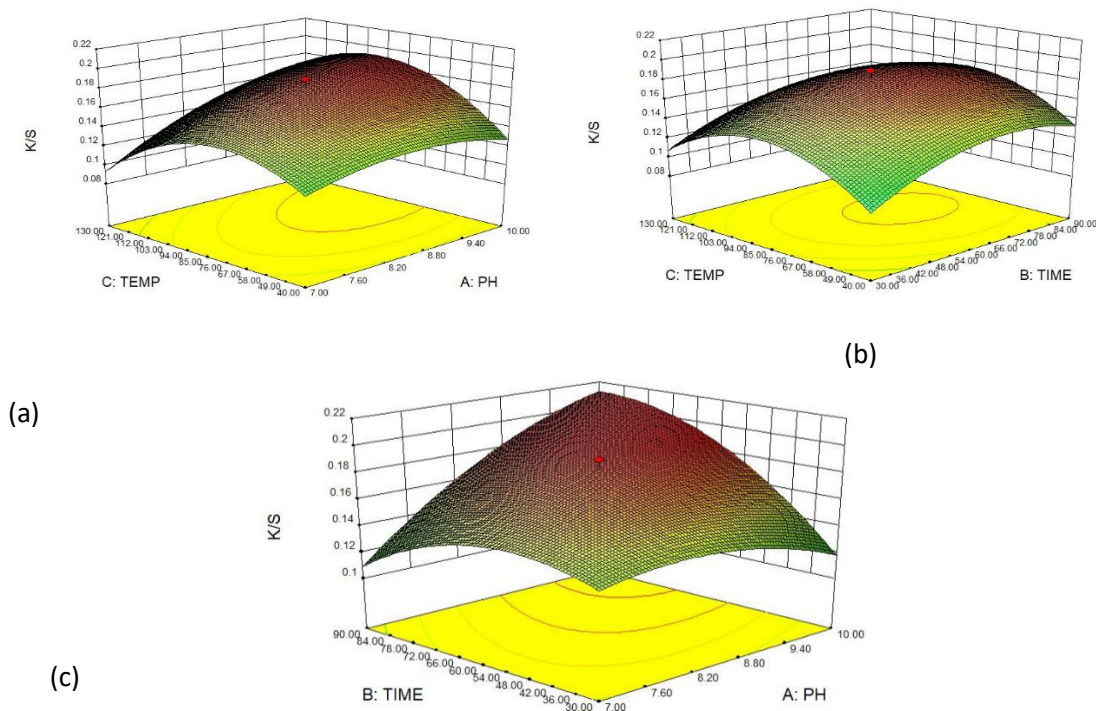


Figure 4.43: Plot of 3-D (a) Temperature vs pH (b) Temperature vs time (c) Time vs pH
 This model can be used to navigate the design space, and the 3D plots are shown in Figure 4.43. From the response plots, the optimal conditions are the pH of 8.5, time of 60 min and temperature of 85°C.

4.10.2.5. Validation of RSM for dyeing of cotton fibers with vilangin dye

Optimized dyeing conditions were used to validate the suitability of the model for the prediction of response values (colour strength). Optimized dyeing conditions were validated by performing experiments under the optimized conditions. The optimized dyeing values are the colour strength of 0.19 whereas the experimental values gave the colour strength of 0.18 for the vilangin dyed cotton fabric.











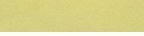



4.10.2.6. Variation on unmordanted and mordanted dyed cotton fibers with vilangin dye

The Alum ($\text{Al}_2\text{K}_2(\text{SO}_4)_4 \cdot 24\text{H}_2\text{O}$) mordanted cotton fabrics showed, light yellow shades in all the pre-, post and simultaneous mordanting methods (Odero *et al.*, 2020) From Table 4.15 it

is observed that all the value of a^* are negative and the values of b^* , are positive this clearly results in a clear shift to yellowness according to CIELAB protocols (Zhang *et al.*, 2019). This explains the yellowish colour achieved experimentally. The Iron ($\text{FeSO}_4 \cdot 7\text{H}_2\text{O}$), mordanted exhibits significant variations, a^* values for pre-mordanted cotton fabric is -1.13 and +14.74 for b^* . For post-mordanted cotton fabric, a^* value was + 0.11 and +21.53 for b^* and the simultaneous mordanted cotton fabric gave a^* value of + 1.54 and + 30.24 for giving yellow shades. These shades were observed in the red-yellow region of the CIELAB protocol, resulting in the formation of darker shades (Shabbir *et al.*, 2019). The copper mordanted cotton fabrics in the pre, simultaneous and post-mordanting resulted in the negative $-a^*$ values and positive b^* , displaying the green-yellow colour shades in the CIELAB colour space. The same case applies to nickel-mordanted cotton fabrics, where they fall in the green-yellow colour space with lighter shades. The variability in mordants results in the formation of different shades of colours (Ayele *et al.*, 2020).

The low colour strengths (K/S) values were observed by using simultaneous, pre-, and post-mordanted methods with vilangin on cotton fibers. These resulted in significant variation in color strength which was attributed to the fact of weak interactions between mordants and functional groups of dye molecules and cotton fabric (Karabulut *et al.*, 2020). Another reason could be due to the structural relationship of the vilangin dye and the rate of diffusion of the dye to the cellulosic fabric under the given dyeing conditions. Studies carried out by Zhao *et al.*, and Zhou *et al.*, reported the interactions between dye-dye, dye-fiber and dye- Na^+ , observed that the main interactions in a dye molecule are a result of $\pi \rightarrow \pi^*$ stacking (Zhao *et al.*, 2021; Zhou *et al.*, 2021).

Table 4.14: Colour strength and shades of modified vilangin dye cotton fabrics

Method	Mordant	L*	a*	b*	ΔE	C*	H°	K/S	Shades
Embelin	NO	77.4	-2.47	+18.30	12.66	18.47	7.68	0.18	
Vilangin	NO	77.8	-2.69	+19.02	12.99	19.21	8.05	0.19	
PRE	Ferrous	79.9	-1.13	+14.74	16.93	14.78	4.38	0.23	
	Copper	80.62	-2.38	+13.02	15.47	13.24	10.35	0.19	
	Alum	80.18	-1.33	+12.65	19.00	12.72	6.00	0.20	
	Nickel	80.23	-1.54	+14.75	17.00	14.83	5.96	0.23	
POST	Ferrous	77.24	+0.11	+21.53	23.62	21.53	5.11	0.32	
	Copper	79.23	-1.36	+17.48	19.63	17.53	4.45	0.26	
	Nickel	80.22	-2.73	+12.22	14.72	12.52	12.6	0.19	
	Alum	80.99	-1.63	+12.16	14.58	12.27	7.63	0.20	
SIMULT.	Nickel	79.22	-0.06	+18.38	20.49	13.38	0.19	0.27	
	Ferrous	75.23	+1.54	+30.24	32.47	30.28	2.92	0.52	
	Copper	78.30	-2.69	+25.33	27.55	25.47	6.06	0.34	
	Alum	79.56	-1.41	+17.51	19.67	17.57	4.60	0.28	

4.10.2.7. Colour fastness properties of dyed cotton

The colour fastness properties were done according to ISO 105-C02:1989, ISO 105 A02:1993, and ISO 105-X12:2000. The results obtained for washing, rubbing and light fastness are summarized in Table 4.16. The results show excellent fastness properties for the vilangin dyes compared to embelin dye. The fastness tests suggest that vilangin dyes have good dyeability for cotton fabrics. The colour fastness is improved by the use of mordants, this may be due to the formation of coordinate bonds which promotes the wash, rubbing, and light fastness (Gong *et al.*, 2020).

Table 4.15: Colour fastness of the vilangin dyed fabric using different methods of mordanting

Method	Mordant	Wash fastness		Rubbing fastness		Lightfastness
		C.C	C.S	Dry	Wet	
Vilangin	Without	2-3	2	3	3	4
Embelin	Without	2-3	2	2	2	1
Simultaneous	Alum	3-4	3	4	4	4
	Copper	3	4	5	4	4
	Ferrous	4	4	5	4	5
Pre-mordanting	Nickel	3	3	4	4	4
	Alum	3	3	4	4	4
	Copper	3	3	4	4	4
Post-mordanting	Ferrous	4	3-4	3	4	4
	Nickel	3	3-	3	3	4
	Alum	4	4	3-4	4	5
	Copper	4	4	4	4	4
	Ferrous	5	4	4	4	5
	Nickel	4	4	4	4	5

C-C-Colour change, Colour stain. 1-Poor; 2-Fairly good 3- Good, 4-Very good, 5-Excellent

4.10.3. Dyeing of cotton fabric with embelin ninhydrin dye optimization

Embelin ninhydrin dyes shown in Appendix 4, were applied to cotton, silk and wool fabric. The effect of three parameters, pH, time and temperature on the colour strengths are given below.

4.10.3.1. Effect of dyeing pH on cotton ENn dye

The effect of dyeing pH is shown in Figure 4.44. There is an increase in colour strength, K/S 1.8 to 4 when pH increases from 4 to 10 and then an equilibrium is reached. After the equilibrium, a decrease is observed from 10 to 13. These findings revealed that there is a great dependency of pH on the interaction of cellulose fiber with embelin ninhydrin dye. The embelin ninhydrin dye has hydroxyl and quinone functional groups.

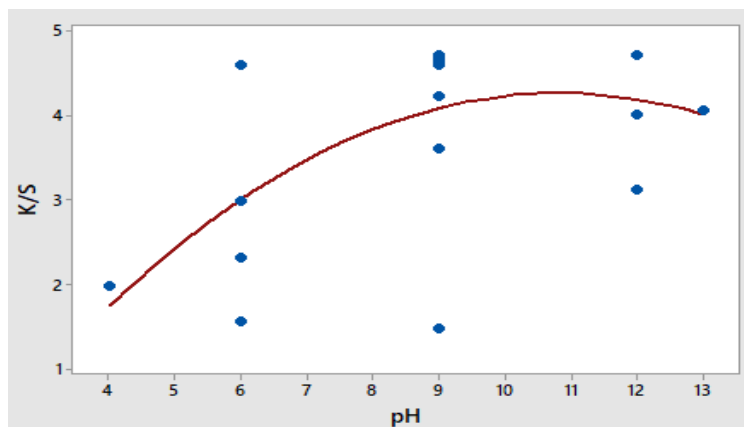


Figure 4.44: Effect of pH on dye exhaustion with ENn cotton dyeing

Hydrogen bonds are formed between hydroxyl groups of the embelin ninhydrin dye and the hydroxyl groups of the cellulosic fabric dye and the hydroxyl groups of cellulose. Secondly, Covalent bonds are also formed on the interaction of the quinone functional groups present in embelin ninhydrin dye with appropriate functional groups in the cellulosic polymer of the fabric. This shows that at high alkaline conditions the embelin ninhydrin dye gets activated and on interaction with O-nucleophile in the cellulose fabric, a covalent bond forms according to Michael's addition mechanisms (Lewis, 2014). In this study dyeing of cotton fabric was carried out under the influence of different pH values. It was observed that dye maximum colour strength at pH 9 Figure 4.46. This showed that at pH 9, water molecules and the ions such as Na^+ and -OH ions diffuse into the inner part of the cellulosic fabric, swelling the fabric and leading to increased dye intake (Naveed *et al.*, 2020; Shu *et al.*, 2020).

4.10.3.2. Effect of dyeing time on cotton ENn dye

The effect of dyeing time is shown in Figure 4.45, which shows that there is an increase in dye exhaustion with an increase from 18 min to 80 minutes and the colour strength increases exponentially from K/S value 2.2 to 4.3 in ENn dyeing of cotton fabrics. Then an exponential decrease in time is observed from 85 min to 110 min and colour strength of the dye is also decreased after the equilibrium is reached.

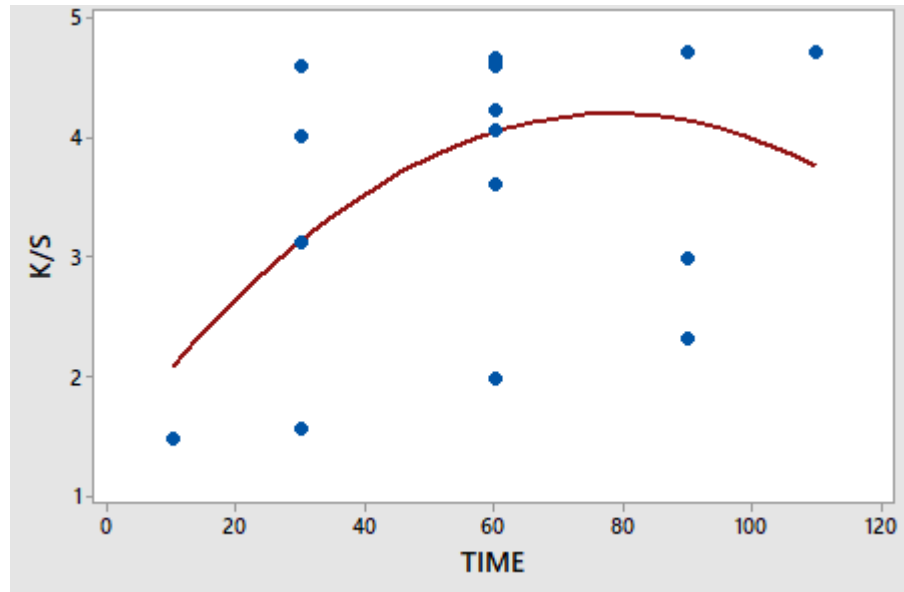


Figure 4.45: Effect of time on colour strength of cotton dyeing with ENn

After the equilibrium is reached it shows that a long time causes a shift from the cotton-dyed fabric to the dye bath causing colour strength to decrease (Irfan *et al.*, 2018; Khan *et al.*, 2014). This shows that the optimum time for swelling the cotton fabric is 80 min and is sufficient to transfer the ENn to the outer surface of the cellulosic fabric.

4.10.3.3. Effect of dyeing temperature on cotton ENn dye

The effect of dyeing temperature in Figure 4.46 shows that the dye colour strength increases with an increase in temperature from 35°C to 90°C. It is known that temperature is one important factor that greatly influences the dyeing rate (Repon *et al.*, 2016; Sinha *et al.*, 2016). There is a small retardation observed at around 90°C. These showed that dye molecules' movement and pore sizes of the cellulosic fiber increase with increased temperature enhancing the colour strength of the dyed fabric (Hassan & Bhagvandas, 2017; Tissera *et al.*, 2016).

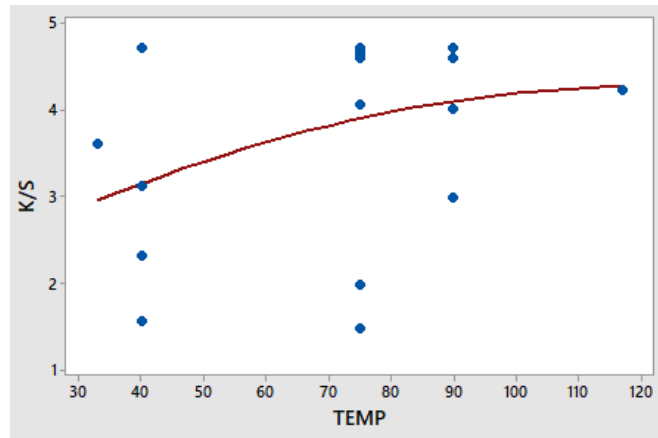


Figure 4.46: Effect of temperature on dye exhaustion of cotton dyeing with ENn

4.10.3.4. Response surface methodology optimization

The standard response methodology for dyeing cotton fabric using embelin ninhydrin dye was designed using Design-Expert software by application of Central Composite Design, Table 4.17. The process variables represented by X_1 , X_2 and X_3 , were the codes for pH, Time (min) and Temperature ($^{\circ}\text{C}$). The (K/S) colour strength was the response factor considered in the dyeing process. The regression model equation (Equation 4.2) and analysis of 3D surface plots showed the optimum dyeing conditions and the variation of dyeing conditions on colour.

Table 4.16: Effect of dyeing variables on dye exhaustion of ENn on cotton fabric

pH	TIME	TEMPERATURE	K/S	
0	0	0	-1	2.98
0	0	0	0	4.71
0	0	0	0	4.6
1	1	-1	1	2.31
1	1	-1	-1	1.98
-1	0	0	-1	4.63
0	0	0	0	4.01
0	0	0	+∞	1.48
0	0	0	0	4.06
0	0	-∞	0	4.52
+∞	0	0	0	1.56
1	1	1	1	3.11
0	0	0	-∞	4.62
-1	0	0	1	4.61
0	0	0	0	3.61
-∞	0	0	0	4.41
-1	1	-1	1	4.64
0	0	0	0	4.67
0	0	1	0	4.6
1	1	1	-1	4.23

$$K/S = 4.27 + 0.73 X_1 + 0.35 X_2 - 0.32 X_3 - 0.44 X_1^2 + 0.12 X_2^2 - 0.42 X_3^2 + 0.18 X_1 * X_2 - 0.30 X_1 * X_3 - 0.39 X_2 * X_3 \dots\dots\dots \text{Equation 4.2}$$

Table 4.17: Model Summary

S	R-sq	R-sq (adj)
10.5794	75.79 %	64.00 %

Where, K/S is the colour strength value (output K response); X1 is the dye bath pH, X2 is the time of dyeing and X3 is the temperature of the dye bath. The analysis of variance (ANOVA) showed statistical significance displayed in Table 4.19. The Fisher's F-value of 3.58 with a low probability value (P < 0.0326) shows that the regression model is significant. The model

summary, Table 4.18 shows R-sq shows that 75.79 % of the variation of the model shows a good correlation.

Table 4.18: ANOVA of cotton dyed embelin ninhydrin

Source	Sum of squares	DF	Mean Square	F-Value	P-Value
Model	18.09	9	2.07	3.58	0.0326
X1	7.36	1	7.36	12.73	0.0051
X2	1.69	1	1.69	2.92	0.1180
X3	1.44	1	1.44	2.49	0.1459
X1*X2	0.26	1	0.26	0.44	0.5211
X1*X3	0.74	1	0.74	1.28	0.2848
X2*X3	1.22	1	1.22	2.12	0.1762
X1*X1	2.80	1	2.80	4.85	0.0523
X2*X2	0.19	1	0.19	0.34	0.5754
X3*X3	2.52	1	2.52	4.35	0.0635
Residual	5.78	10	0.58		
Lack-of-Fit	4.77	5	0.95	4.73	0.0568
Pure Error	1.01	5	0.20		
Cor Total	23.87	19			

4.10.3.5. Three-dimensional-surface plots and response optimization

The surface plots (RSM) in three-dimensional (3D) showed the effect of dyeing variables (X1, X2, and X3) on dyed fabrics are shown. In Figure 4.47, the surface plots show the effect of two factors while the third variable is held constant (Barani *et al.*, 2012). Colour strength is at an increasing time and temperature with a hold time of 85 °C, the response, K/S increases.

Figure 4.47(a) shows the response surface plot between pH and temperature while holding the time constant, at a hold time of 60 mins, and the increase in colour strength K/S, is observed. Figure 4.47 (b) shows the response surface plot between pH and time while holding the temperature constant, at a hold temperature of between 85 °C an increase in colour strength K/S, is observed. Figure 4.47 (c) shows the response surface plot between temperature and time while holding the time constant, at a pH of 9 and an increase in colour strength is observed.

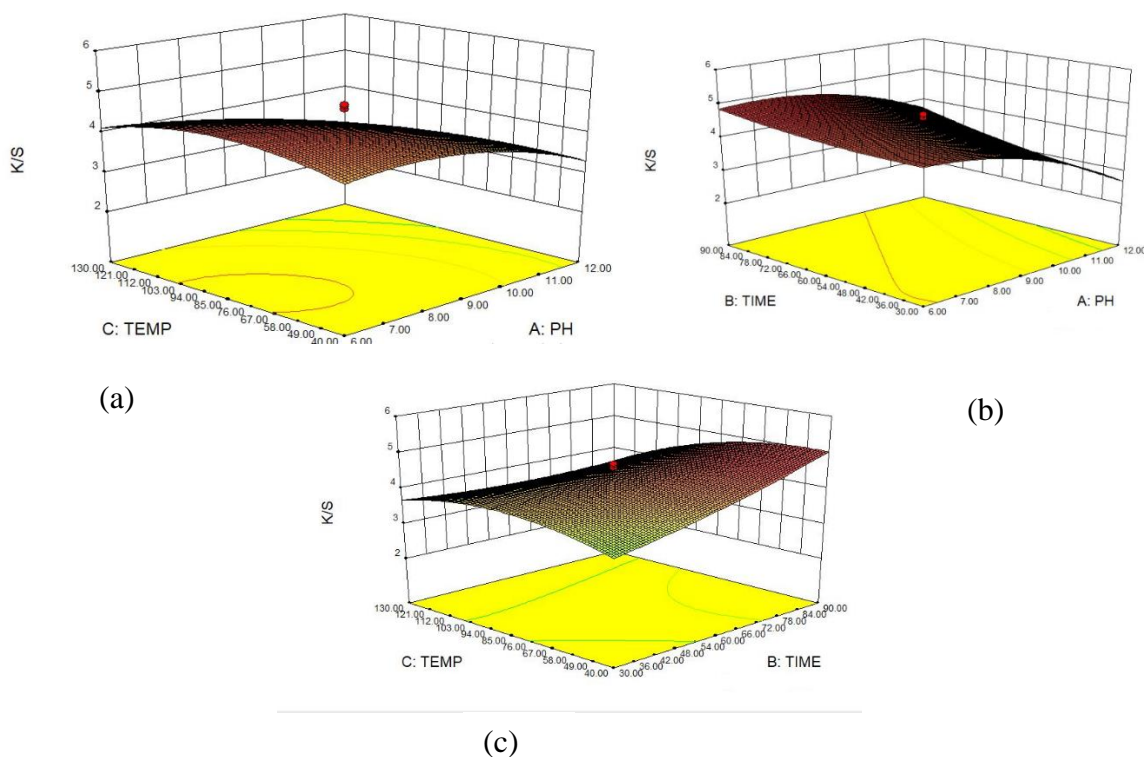


Figure 4.47: Plot of 3-D (a)- Temperature vs pH (b) time versus pH (c) temperature versus time

The increase in colour strength K/S values could be due to the crosslinks that occur between the dye and cellulose polymer due to ionic interactions because of the presence of hydroxyl groups (Haji, 2020; Mongkholrattanasit *et al.*, 2021).

4.10.3.6. Optimized dyeing conditions of embelin ninhydrin with cotton fiber

From the response surface methodology and the design applied (CCM) generated by the Design Expert. It is observed that dyeing of cotton fabric with increased colour strength (K/S) values occurs at pH of 9 temperature of 80 °C and time of 60 minutes.

4.10.3.7. Validation of RSM for dyeing of cotton fibers with embelin ninhydrin dye

Optimized dyeing conditions were validated by performing the experiments using values from optimized conditions. The optimized conditions gave a colour strength of 4.71 whereas the dyeing carried out at a pH of 9, time of 60 mins and temperature of 80 °C gave a colour strength of 4.02 experimental. These showed that there is no significant variation between the predicted and actual values.

4.10.3.8. Effect of mordants on dyeing of cotton with embelin ninhydrin dye

Mordanting is useful in semi-synthetic dyeing because the process results in the acquisition of a new shade and also provides excellent colour fastness ratings. For the interest of the environment and global interest, it becomes necessary to use ecofriendly chemical mordants example salts of aluminum and Iron (Zia *et al.*, 2019). Embelin ninhydrin dyeing of cotton fabrics was subjected to the use of four different mordant salts; ferrous, alum, copper and salt of nickel.

4.10.3.9. Variation on unmordanted and mordanted dyed cotton fabrics

The colorimetric properties following the CIELAB colour coordinate space (L^* , a^* and b^*) protocol were used to study the colour measurements and effect of mordants of dyed cotton fabric using embelin ninhydrin dye. Figure 4.48 shows the variation of embelin dyed cotton fabric with embelin ninhydrin cotton fabric both unmordanted.

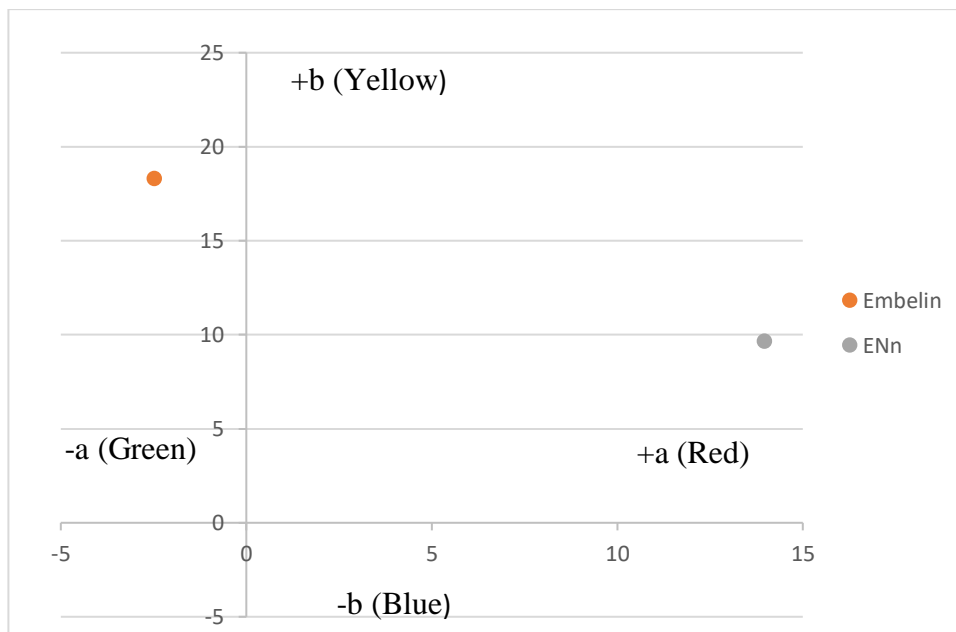


Figure 4.48: Plot of un-mordanted and mordanted ENn cotton dyed fabric

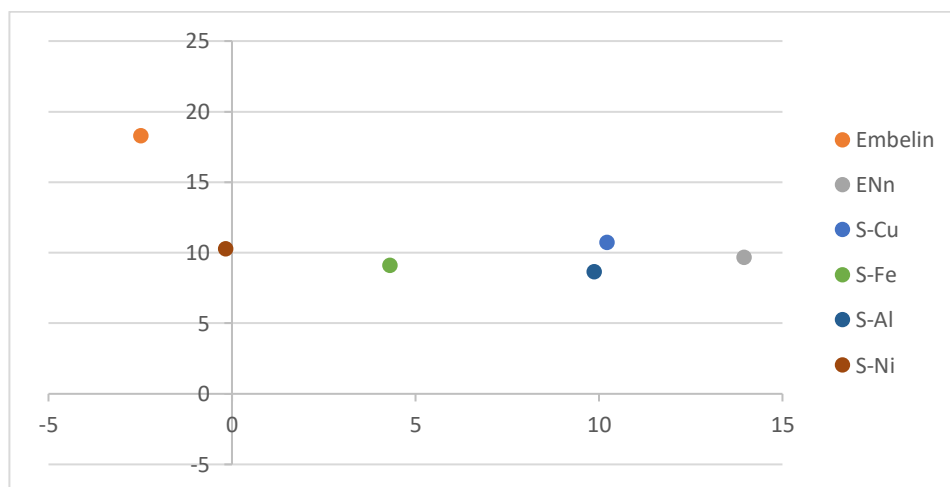


Figure 4.49: Plot of un-mordanted and simultaneous mordanted ENn cotton dyed fabric

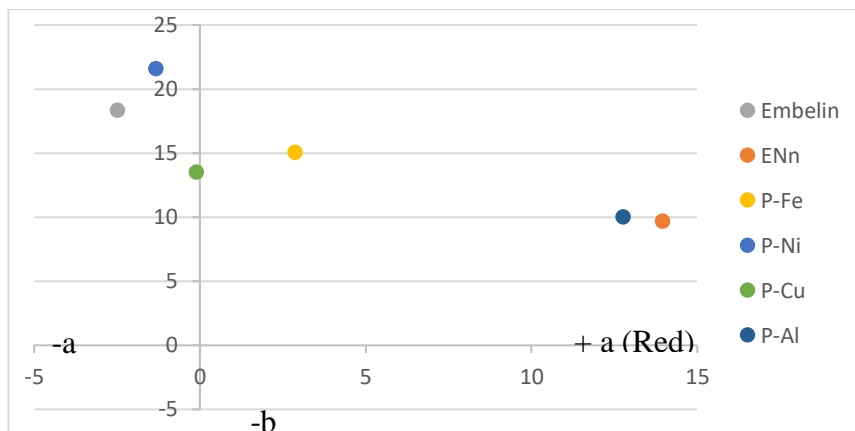


Figure 4.50: Plot of unmordanted and post mordanted ENn cotton dyed fabric

The cotton fabrics mordanted by alum ($\text{Al}_2\text{K}_2(\text{SO}_4)_4 \cdot 24\text{H}_2\text{O}$) gave different shades using simultaneous post and pre-mordanting methods Figure 4.49-4.51. The color coordinates are within the toward red-yellow quadrant with values b^* being low and high a^* values, (Table 4.20) an exception is in Pre-mordanted cotton fiber where the b^* value is higher than a^* resulting and the color tends towards the achromatic region (Ding *et al.*, 2021; Ohno & Applications, 2017). The Ferrous ($\text{FeSO}_4 \cdot 7\text{H}_2\text{O}$) mordanting showed that simultaneous and post-mordanted samples tend towards the red –yellow colour space, but are shifted towards the achromatic region, the pre-mordanted is shifted towards yellow but is at the achromatic region. The colour strength range is 2.74 - 4.09, with the pre-mordant having the highest colour strength. The L^* -luminosity values of ferrous mordanted are in the range of 46-56, this explains why they are darker shades. The interaction between Ferrous mordant and the ENn dye molecule mordanted could be due to coordinative unsaturated sites offered by Iron metal which enables the formation of a chelate effect (Repon *et al.*, 2017; Shabbir *et al.*, 2016; Yan *et al.*, 2021) which results in better colour strength compared to embelin dyed cotton fabric with colour strength of K/S value 0.18.

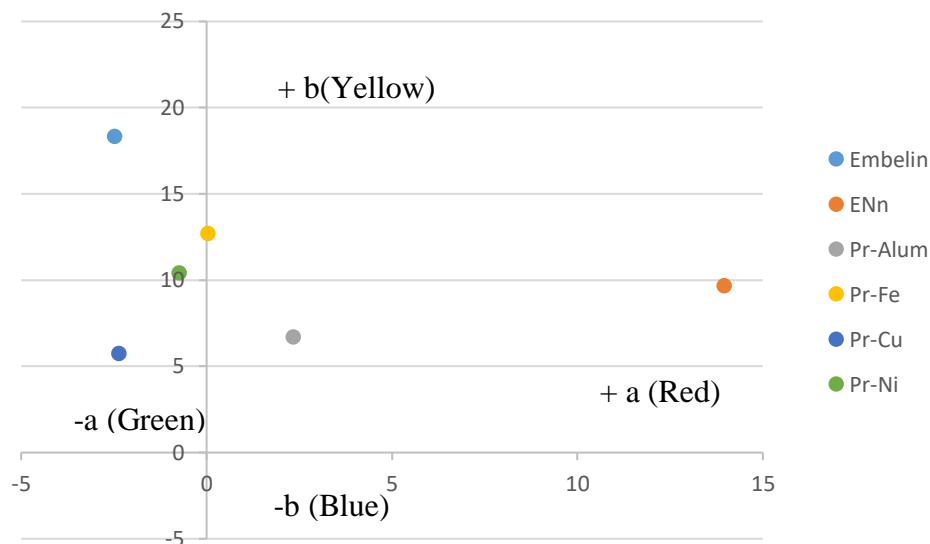







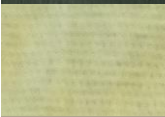


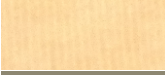





Figure 4.51: Plot of un-mordanted and pre-mordanted ENn cotton dyed fabric

The copper metal simultaneous mordant Figure 4.49 shows that the colour falls in the yellow-red quadrant with a^* value +10.24 and +10.74 and $+b^*$, their L^* values is 55,68. The post-mordanted shows that the colour falls in the achromatic region with a^* value -0.10 and +13.48 and $+b^*$, their L^* value is 68. The pre-mordanting shows that the colour falls in the yellow-green quadrant with a^* value of -2.36 and +5.73 and $+b^*$ falls within the yellow-red quadrant. The shades are very close in appearance however the colour strength of copper mordanted taking into consideration methods is in the range of, K/S 2.3-2.7 compared to ENn dyed cotton fabric with a K/S value of 4.02. The nickel metal dyed cotton fabric simultaneous mordant shown in Figure 4.49 shows that the colour falls in the yellow-green quadrant but very near to the achromatic region with a^* value -0.16 and +10.26 b^* , their L^* values are 37 and the colour strength at 2.51. The post mordanted, Figure 4.50, shows that the colour falls in the achromatic region with a^* value -1.31 and +21.57 and $+b^*$, their L^* values is 66. The pre-mordanting, Figure 4.51, shows that the colour falls in the yellow-green quadrant with a^* value -0.74 and +10.38 and $+b^*$, their L^* value is 74. Compared with the control embelin,

the unmordanted embelin ninhydrin dyed cotton fabric with L^* value of 57.70, shown in Table 4.20. The cotton ENn dyed fiber has a colour strength (K/S) value of 4.02 which is

Table 4.19: Evaluated colour measurements of the ENn cotton dyed fabric with mordants

Meth od	Mord ant	L^*	a^*	b^*	ΔE	C^*	H°	K/S	Shades
ENn dye	NO	57.70	+13.97	+9.65	27.40	16.97	55.36	4.02	
Embe lin	NO	77.4	-2.47	+18.30	12.66	18.46	7.79	0.18	
Simul taneo us	Copp er	55.68	+10.24	+10.74	27.88	14.84	43.64	2.30	
	Ferro us	53.19	+4.32	+9.10	27.82	10.07	25.39	2.74	
	Alum	57.74	+9.88	+8.63	25.12	13.12	48.86	2.31	
	Nicke l	36.94	-0.16	+10.26	43.20	10.26	0.89	2.51	
POST	Ferro us	46.22	+2.89	+15.04	36.49	15.32	10.88	4.04	
	Nicke l	65.96	-1.31	+21.57	26.73	21.61	3.48	2.14	
	Copp er	67.98	-0.10	+13.48	18.69	13.48	0.43	2.68	
	Alum	62.80	+12.77	+10.01	23.73	16.23	51.91	3.73	
Pre	Alum	70.71	+2.34	+6.69	11.80	7.09	19.28	2.46	
	Ferro us	56.11	+0.05	+12.67	27.78	12.67	0.23	4.09	
	Copp er	76.94	-2.36	+5.73	8.34	6.20	22.39	2.27	
	Nicke l	74.11	-0.74	+10.38	13.18	10.41	4.08	2.32	

greater than embelin dyed cotton fiber with colour strength of 0.18. This shows that the cotton

ENn dyed fiber has a higher colour strength close to the highest mordanted cotton ENn post mordanted ferrous fiber.

Generally the metallic mordants and salt; (alum, nickel, copper and ferrous) with different methods of application affected the color characteristics of the cellulosic fabrics dyed with embelin ninhydrin dye. These can be associated with the ability of metal under use in dyeing. Alum and copper have shown weak binding ability whereas nickel coordinates moderately fair to cotton fabrics and ferrous binds strongly in all the methods used.

Table 4.20: The Colourfastness of dyed fabric with different methods of mordant used

Method	Mordant	Wash fastness		Rubbing fastness		
		C.C	C.S	Dry	Wet	Light fastness
Embelin	NO	2-3	2	2	2	1
Embelin ninhydrin	NO	4	5	5	3	4
Simultaneous	Alum	5	5	5	4	4
	Copper	5	5	5	5	4
	Ferrous	4	5	5	4	5
	Nickel	5	5	4	4	4
Pre	Alum	5	5	4	4	4
	Copper	5	5	4	4	4
	Ferrous	5	5	5	4	4
	Nickel	5	5	5	4	4
Post	Alum	4	5	5	4	5
	Copper	4	5	5	4	4
	Ferrous	5	5	5	4	5

Key: Colour change (C.C), Colour stain (C.S)

The reason could be due to greater available vacant sites for coordinative unsaturation in ferrous metal that allows for bond formation upon interaction with cellulosic fiber (Schneider-Coppolino *et al.*, 2022; Wan & Lee, 2021).

4.10.3.10. Colour fastness properties

The fastness rating properties were carried out according to the ISO 105-C02:1989, ISO 105 A02:1993, and ISO 105-X12:2000 approved protocol. The data in Table 4.21 shows the ratings of colour fastness of the dyed embelin ninhydrin dyed cotton fabrics against washing fastness, rubbing fastness and light fastness applying the simultaneous, pre-mordant and post mordanting methods to cotton fabrics. The embelin ninhydrin cotton dyed fabric without mordants also showed excellent fastness properties which were observed according to the rating values on the grey scale. The dyed fabrics exhibited, 4-5 ratings on a Grey scale which was good to excellent. The embelin-dyed cotton fabric exhibited poor fastness properties.

4.10.4. Dyeing of silk with embelin ninhydrin

Embelin ninhydrin dyes were applied to silk and the effect of each parameter was evaluated based on the colour strength.

4.10.4.1. The effect of temperature on dye exhaustion

The effect of dyeing temperature is shown in Figure 4.52 shows that the dye exhaustion increases with an increase in temperature from 35°C to 70 °C. The dye's exhaustion decreases beyond the temperature of 80 °C . This shows that ENn dye becomes more soluble with an increase in temperature. Studies carried out by Ren et al., concluded that the most important thing in the dyeing effect of silk fabric is the temperature (Ren *et al.*, 2018). Dye is known to exist in solution in aggregate forms at different sizes which are broken down to maintain and these aggregates break down to maintain an overall dynamic equilibrium of dye solution (Shokoofehpoor *et al.*, 2020). The kinetic energy Increase in temperature leads to increased penetration of dyes in fabrics (Rather *et al.*, 2020). An increase in temperature causes an increase in the porosity of the dyed fabric structure by increasing the numbers and their size, thus the small dye particles penetrate the fabric pores at high temperatures leading to an

increase in the dye uptake. Beyond 70 °C there is a decrease in dye exhaustion and fixation of dyes this is because alkaline hydrolysis occurs (Oh & Park, 2020; Rehman *et al.*, 2021).

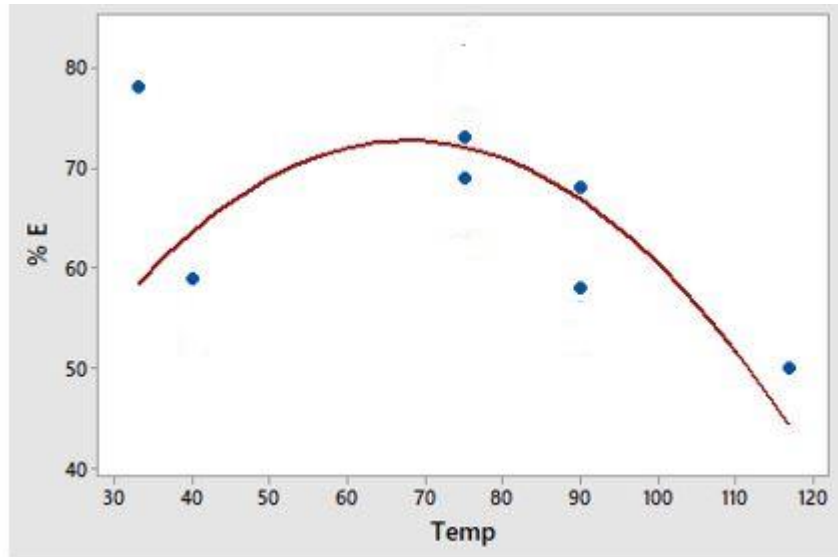


Figure 4.52: Effect of temperature on dye exhaustion silk dyeing with ENn

4.10.4.2. The effect of time on dye exhaustion

The effect of dyeing time is shown in Figure 4.53, it shows that there is an increase in dye exhaustion with an increase from 18 to 60 minutes and the exhaustion increases exponentially from 60 % to 68 % in ENn dyeing of silk fabrics. This is because when silk fabric is immersed in a dye solution, it absorbs dye till an equilibrium is reached (Diarsa & Gupte, 2020). After equilibrium, the dye exhaustion decreases with dyeing time from 62 to 110 min. This is because the dyes got hydrolyzed due to prolonged time and unavailability of adsorption sites (Verma *et al.*, 2012).

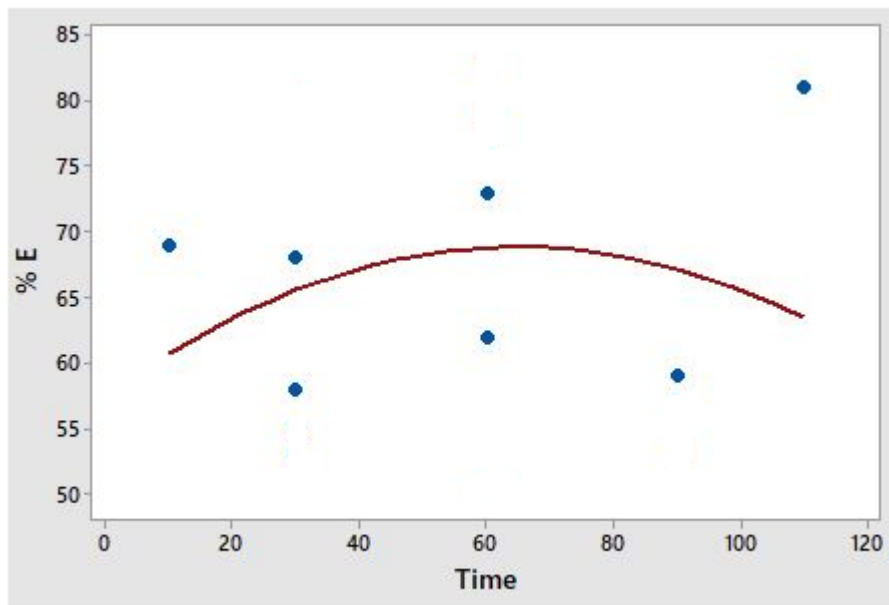


Figure 4.53: Effect of time on dye exhaustion with ENn silk dyeing

4.10.4.3. The pH on dye exhaustion

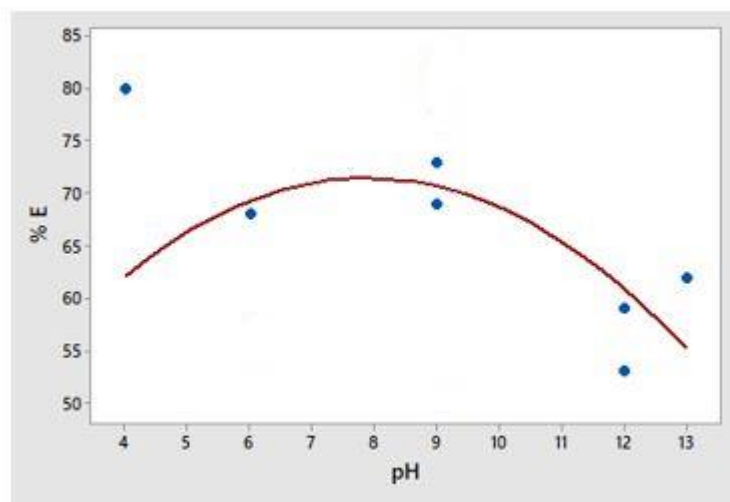


Figure 4.54: Effect of pH on dye exhaustion with ENn silk dyeing

The effect of dyeing pH is shown in Figure 4.54. There is an exponential increase in dye exhaustion when pH is increased from 4 to 7.5 from 63 % to 70 % and then an equilibrium is reached. After the equilibrium, a decrease is observed from 8 to 13. This explains the

increase in colour strength from acidic to alkaline conditions (Bhavsar *et al.*, 2020). This shows that there is minimum repulsion between the dye and fabric in acidic conditions going to alkaline conditions (Adeel *et al.*, 2020). Dye exhaustion is at 55 % under acidic conditions showing that the presence of $-\text{COOH}$ and $-\text{NH}_2$ in silk fibers influences the bonding with functional colorant. Bath gives good colour strength. While moving towards alkaline conditions the exhaustion of dye is lowered.

4.10.4.4. Dyeing of silk fabric with embelin ninhydrin dye optimization

The standard response methodology for dyeing silk fabric using embelin ninhydrin dye was designed by using Design expert software by application of central composite design, Table 4.22. The process variables represented X_1 , X_2 and X_3 , were the codes for pH, Time (min) and Temperature ($^{\circ}\text{C}$). Colour strength (K/S) was the response factor considered in the dyeing process.

Where, K/S is the colour strength value (output response); X_1 is the dye bath pH, X_2 is the time of dyeing and X_3 is the temperature of the dye bath. The analysis of variance (ANOVA) showed statistical significance displayed in Table 4.24. The Fisher's F-value of 23.82 with a low probability value ($P < 0.0001$) shows that the regression model is significant. The model summary, Table 4.23 shows R-sq shows that 95.54 % of the variation of the model shows a good correlation.

Table 4.21: Experimental design and results for dye exhaustion of silk fibers dyed with Embelin ninhydrin dye

Run	X1	X2	X3	K/S	
1		0	0	9.9	
2		$-\alpha$	0	13.4	
3		1	1	12.6	
4		$+\alpha$	0	8.8	
5		-1	-1	14.2	
6		-1	1	13	
7		-1	-1	12	
8		1	-1	11.9	
9		1	-1	8.2	
10		1	1	9.8	
11		0	0	10.8	
12		0	$-\alpha$	9.8	
13		0	0	10.4	
14		0	0	10.3	
15		0	0	$+\alpha$	13.8
16		0	0	0	10.7
17		0	0	$-\alpha$	10
18		0	0	0	10.2
19		-1	1	1	15.8
20		0	$+\alpha$	0	12.3

$$\text{K/S SILK EN}_n = 31.67 - 4.05 X_1 - 0.02 X_2 - 0.13 X_3 + 0.19 X_1^2 + 4.45 \times 10^{-4} X_2^2 + 1.12 \times 10^{-3} X_3^2 - 8.33 \times 10^{-4} X_1 * X_2 + 5.0 \times 10^{-3} X_1 * X_3 - 5.0 \times 10^{-5} X_2 * X_3 \quad \text{-----Equation 4.3}$$

Table 4.22: Model summary of ENn silk dye

S	R-sq	R-sq (adj)
10.3053	95.54 %	91.53 %

Table 4.23: Analysis of variance

Analysis of variance					
Source	Sum of	Mean		F-Value	P-Value
	squares	DF	square		
Model	69.95	9	7.77	23.82	< 0.0001
X1	29.99	1	29.99	91.88	< 0.0001
X2	6.07	1	6.07	18.60	0.0015
X3	23.44	1	23.44	71.82	< 0.0001
X1*X2	0.011	1	0.011	0.034	0.8564
X1*X3	0.28	1	0.28	0.86	0.3751
X2*X3	0.011	1	0.011	0.034	0.8564
X1*X1	2.51	1	2.51	7.71	0.0196
X2*X2	2.31	1	2.31	7.07	0.0240
X3*X3	7.07	1	7.07	21.67	0.0009
Residual	3.26	10	0.33		
Lack-of-Fit	2.72	5	0.54	4.95	0.0519
Pure Error	0.55	5	0.11		

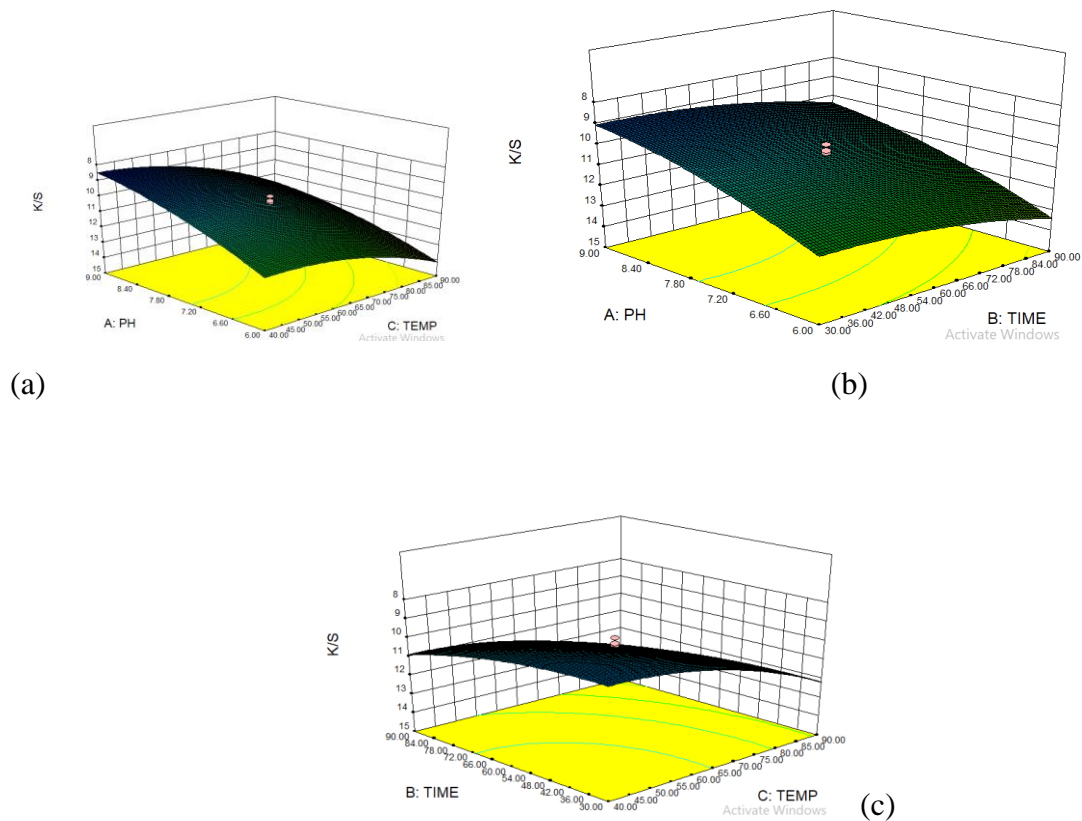













Figure 4.55: Plot of 3-D (a)- pH vs Temperature (b) pH vs time (c) Time vs temperature. The surface plots (RSM) in a three-dimensional (3D) plot showing the effect of dyeing variables (X1, X2, and X3) on silk-dyed fabrics are shown. The effect of two process variables while a third is held constant is observed, Figure 4.55 (a) shows the response surface plot between pH and temperature while holding the time constant, 60 min, the response plot shows that the colour strength is increased on increasing the pH and the temperature until an optimum is achieved where the colour strength decreases. Figure 4.55 (b) shows the response surface plot between pH and time while holding the temperature constant, at 65 °C, the relationship shows that there is an increase in colour strength K/S when the pH increases are

observed. Figure 4.55 (c) shows the response surface plot between time and temperature while holding the pH constant at 7.5, the increase in colour strength (K/S) was observed.

4.10.4.5. Validation of RSM for dyeing of silk fibers with Embelin ninhydrin dye

Optimized dyeing conditions were used to validate the suitability of the model for the prediction of response values (colour strength). Optimized dyeing conditions were validated by performing experiments under the optimized conditions. The optimized dyeing values are the colour strength of 15.8 whereas the experimental values gave the colour strength of 14. The experimental response values were well in agreement with predicted response values.

Table 4.24: Colour measurements of the silk dyed fabric using different methods of mordanting

Method	Mordant	L*	a*	b*	ΔE	C*	H°	K/S	Shades
Embelin	NO	55.89	-5.47	13.12	29.65	14.21	22.63	1.13	
ENn	NO	70.73	10.00	-1.05	12.66	10.05	84.00	13.98	
PRE	Ferrous	41.87	+7.59	+18.83	22.43	5.14	21.95	2.98	
	Copper	73.39	-11.87	+34.65	27.28	36.63	18.91	5.69	
	Alum	78.84	5.94	+6.46	17.50	8.77	42.60	2.43	
POST	Ferrous	45.64	+8.14	+22.26	19.69	23.7	20.09	3.45	
	Copper	84.78	-12.88	+44.59	40.04	46.41	16.11	8.68	
	Alum	95.90	+5.70	+3.17	34.30	6.52	60.92	1.75	
SIMUL.	Ferrous	60.88	+18.20	+45.11	32.41	48.64	21.97	3.25	
	Copper	80.75	+0.16	+0.83	22.93	0.84	10.91	4.39	
	Alum	97.59	+5.54	+1.06	36.65	5.64	79.17	2.11	

4.10.4.6 Variation on unmordanted and mordanted dyed silk fabrics

Mordanting was carried out on silk fibers by using the material to liquor ratio at 1:50. The CIELAB colour space (L^* , a^* and b^*) values of silk fabric dyed with embelin ninhydrin dye under optimal conditions are shown in Table 4.25. The L^* range from 42-96 chroma (c^*) values range from 5-46. The observations made from the a^* - b^* plot (Figure 4.56-Figure 4.58), show that embelin dyed without mordanting tends towards yellow and the embelin ninhydrin dyed silk fabric without mordants tends to red, showing a different shade of colour from yellow-green to red after dyeing with modified dye.

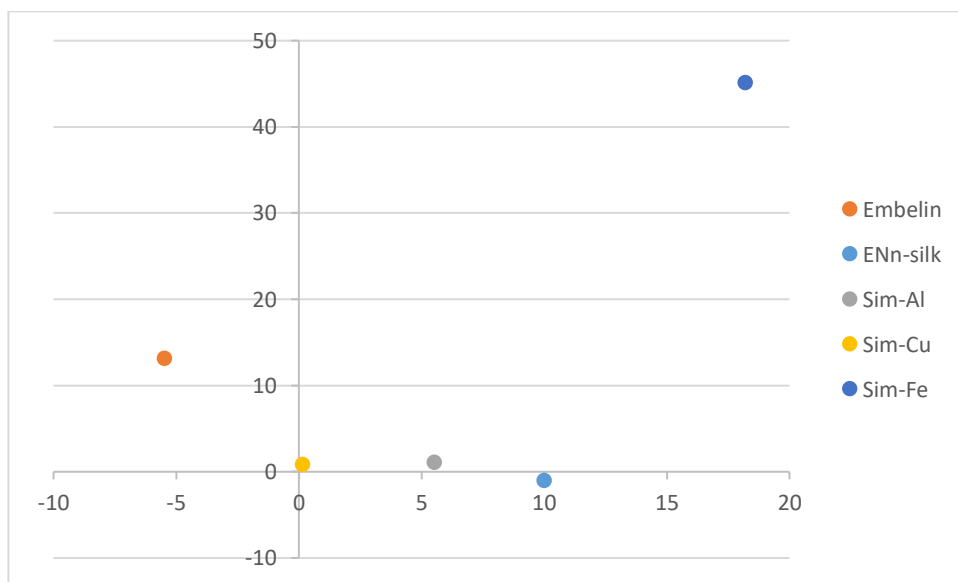


Figure 4.56: Plot of colour coordinates for simultaneous mordanted silk fibers

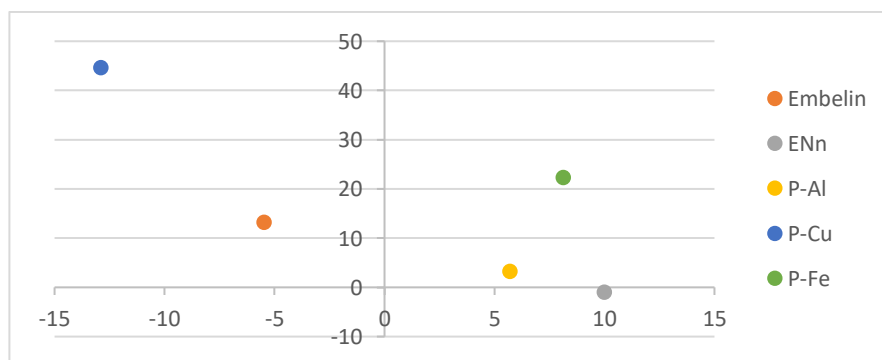


Figure 4.57: Plot of colour coordinates for post-mordanted silk fibers

Alum mordanted silk fiber samples ($\text{Al}_2\text{K}_2(\text{SO}_4)_4 \cdot 24\text{H}_2\text{O}$) shades obtained in simultaneous mordanting, Figure 4.56, shows shifts towards red, with low b^* of +1.06 and high a^* values of +5.54 and the K/S of 2.11 (Table 4.20). The Post mordanted fibers show (Figure 4.57) that a^* is +5.70 which is higher, than b^* at +3.17, and the K/S of 1.75 resulting in less color saturation because it is towards the achromatic region but the difference is insignificant. The pre-mordanted alum has a^* value of 5.94 and b^* values of 6.46 and the K/S of 2.43. Out of the three observed mordanting methods, the pre-mordanting, Figure 4.58, has better colour saturation. Generally, alum mordanting in silk fibers has low colour saturation and gives pale shades (Miah *et al.*, 2017) evidenced by the observed colour strengths between (K/S 1.75-2.43). This could be due to low adsorption by silk fibers. Another reason could be due to the accumulation of the alum metal dye complex in both simultaneous and post-mordanting in the form of aggregates resulting in poor penetration of the dyes compared to the pre-mordanting process (Ganesan & Karthik, 2017; Ohno *et al.*, 2017). For the Ferrous ($\text{FeSO}_4 \cdot 7\text{H}_2\text{O}$) mordanted shades obtained in simultaneous mordanting, Figure 4.56, shows shifts towards red, with a high b^* of +45.11 and low a^* values of +18.20 and the K/S of 3.25 (Table 4.25). The post mordanted fibers (Figure 4.57) showed a^* value of + 8.14 which is lower than b^* at + 22.26, and the K/S of 3.45 which results in a high colour saturation than embelin or embelin ninhydrin dyed silk fabrics. The pre-mordanted ferrous has a^* value of + 7.59 and b^* values of +18.83 and the K/S of 2.98. The colours are within the red and yellow colour spaces. The post mordant gives the best colour strength however the colour strengths are generally low in the dyeing of silk with ferrous mordants. Generally, alum mordanting in silk fibers has low colour saturation and gives pale shades (Miah *et al.*, 2017) evidenced by the observed colour strengths between (K/S 1.75-2.43).

For the Copper ($\text{CuSO}_4 \cdot 7\text{H}_2\text{O}$) simultaneous mordanted shades obtained, Figure 4.56, shows a shift towards the achromatic region, with b^* values of + 0.83 and low a^* values of +0.16 and the colour strength is K/S of 4.39 (Table 4.25) in Post mordanted fibers (Figure 4.57) a^* is - 12.88 which is lower, than b^* , + 44.59, and the K/S of 8.68 resulting in a high colour saturation than embelin or embelin ninhydrin dyed silk fabrics. The pre-mordanted cuprous has a^* value of - 11.87 and higher b^* values of + 34.65 and the K/S of 5.69. The colours are within the green-yellow colour space. The post-mordant gives the highest colour strength of the three mordants, alum, ferrous and cuprous. The copper sulphate gives the highest colour strength followed by ferrous mordanted. This is because Ferrous sulphate and copper sulphate mordants are positively charged metals known for the presence of coordinative unsaturation and ability to form coordination complexes by chelation with dye molecules (Mongkhorrattanasit *et al.*, 2011).

Generally, alum mordanting in silk fibers has low colour saturation and gives pale shades (Miah *et al.*, 2017) evidenced by the observed colour strengths between (K/S 1.75-2.43). Silk fibers also together with dye anions and metal cations from mordants have a relatively strong attraction towards the positive charge of amino and negative charge of carboxyl groups respectively (Patel *et al.*, 2021). Hence, they end up forming an ionic bond between the dye molecule and silk fiber and metal mordant and fiber and in the end with dye and metal ions. The dye-metal chelation process thus results in the formation of coordinate bonds with the uncharged amine ($-\text{NH}_2$) ends of the groups of silk (Teli *et al.*, 2018; Uddin, 2014).

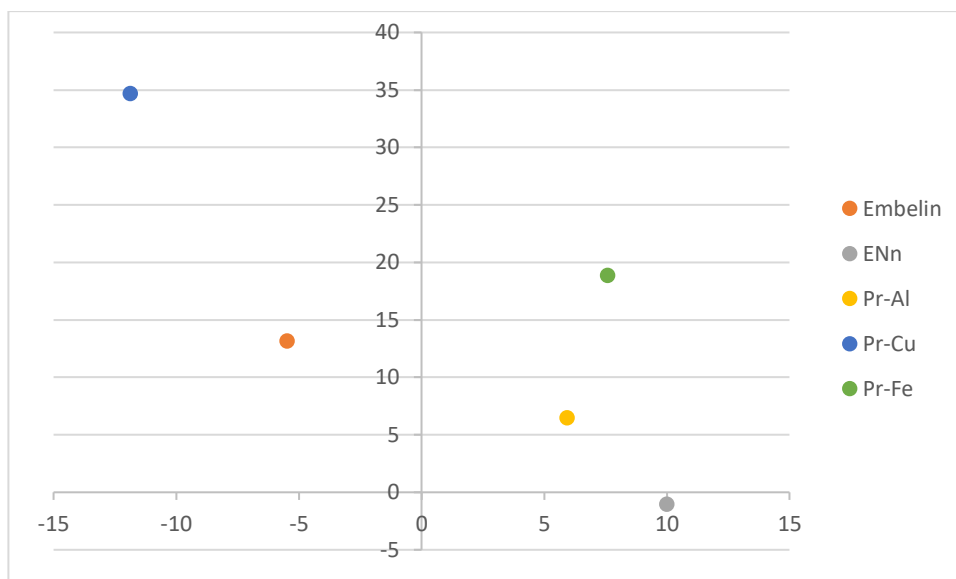


Figure 4.58: Plot of colour coordinates for Pre-mordanted samples

The L^* values range of alum mordanted are in the range of 79-98 meaning the lightness is higher in these regions hence the lighter shades observed in alum mordanted fabrics (Kovačević *et al.*, 2021). The ferrous pre, Figure 4.58 and post-mordanted cotton fabrics have shifted towards L^* values ranging between 42 -61, they present darker shades observed in Table 4.20. The copper mordanted dyed fabrics have L^* Values of the range 73-85.

4.10.4.7 Colour fastness properties of dyed silk

The colour fastness properties were carried out according to ISO 105-C02:1989, ISO 105 A02:1993, and ISO 105-X12:2000. The results obtained for washing, rubbing and light fastness are summarized in Table 4.26.

It is observed that good fastness properties for the embelin ninhydrin dyed fabric are obtained compared to the embelin dye one. The fastness tests suggest that embelin ninhydrin dyes have good dyeability for silk fabrics. From the table of results it is observed that the simultaneous pre and post -mordanting, show good fastness when compared to the embelin ninhydrin sample (without mordant) (Ganesan *et al.*, 2017; Phan *et al.*, 2020). The colour

fastness was improved by the use of approved metal mordants, this may be due to the formation of coordinate bonds which promotes the wash, rubbing and light fastness (Gong *et al.*, 2020).

Table 4.25: Colour fastness of the dyed fabric using different methods of mordanting

Method	Mordant	Wash fastness		Rubbing fastness		Light fastness
		C.C	C.S	Dry	Wet	
Embelin ninhydrin	Without	2-3	2	3	3	2
Embelin	Without	2-3	2	2	2	1
Simultaneous	Alum	3-4	3	4	4	4
Mordanting	Copper	3	4	3	4	4
	Ferrous	4	4	3	4	3
Pre-	Alum	3	3	4	4	4
mordanting	Copper	3	3	4	4	4
	Ferrous	4	3-4	3	4	4
Post-	Alum	4	4	3-4	4	3
mordanting	Copper	4	4	4	4	4
	Ferrous	4	4	4	4	3

C-C-Colour change, Colour stain. 1-Poor; 2-Fairly good 3- Good,4-Very good,5-Excellent

4.10.5. Dyeing of wool with ENn

Preliminary dyeing experiments of wool fibers using embelin ninhydrin dye were carried out and the effect of one parameter was done while holding the other two constants. The response factor was the dye exhaustion strength.

4.10.5.1. Effect of dyeing pH on wool ENn dye

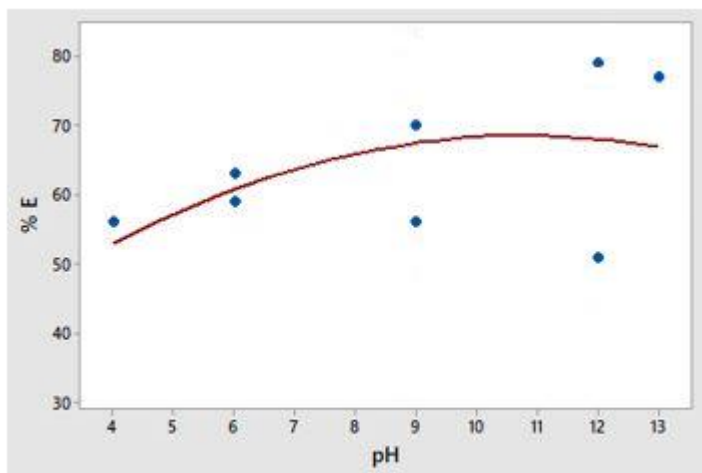


Figure 4.59: Effect of pH on dye exhaustion wool dyeing with ENn

The effect of dyeing pH is shown in Figure 4.59. There is an exponential increase in dye exhaustion when pH is increased from 4 to 9 from 52 % to 68 % and then an equilibrium is reached. After the equilibrium, a decrease is observed from 10 to 13. The pH dyebath has an impact on dye exhaustion in wool, this is because it affects the degree of ionization and surface interaction charge of wool (Haji & Rahimi, 2020). It can be seen that the dye exhaust increases by increasing the pH of the dye bath from 5 to 8. The pH dependence of dye exhaustion can be correlated to the interaction between dye molecules and wool keratin on changing the pH values (Xu *et al.*, 2020). The wool fibers on the other consist of carboxylic groups which also gain a negative charge by ionization on alkaline hydrolysis and a repulsion occur leading to a decrease in dye exhaustion at higher alkaline conditions (Shabbir *et al.*, 2016; Shen, 2019).

4.10.5.2. Effect of dyeing time on wool ENn dye

The effect of dyeing time is shown in Figure 4.60, which shows that there is an increase in dye exhaustion with an increase of time from 20 to 60 minutes and the exhaustion increases exponentially from 54 % to 70 % in ENn dyeing of wool fabrics. Then an exponential

decrease in time is observed from 60 min to 110 min and exhaustion of dye is also decreased from 70 % to 40 %. This shows that an equilibrium is reached (Diarsa *et al.*, 2020). This shows that it takes about 60 min to transfer the ENn to the outer surface of the wool fibers. This is because, at a lower time of 40 min, exhaustion of dyes already occurs and is exponentially increasing until the absorbed dye diffuses to the outer surface of the fiber resulting in the decrease of dye exhaustion upon reaching the equilibrium (Zheng *et al.*, 2017).

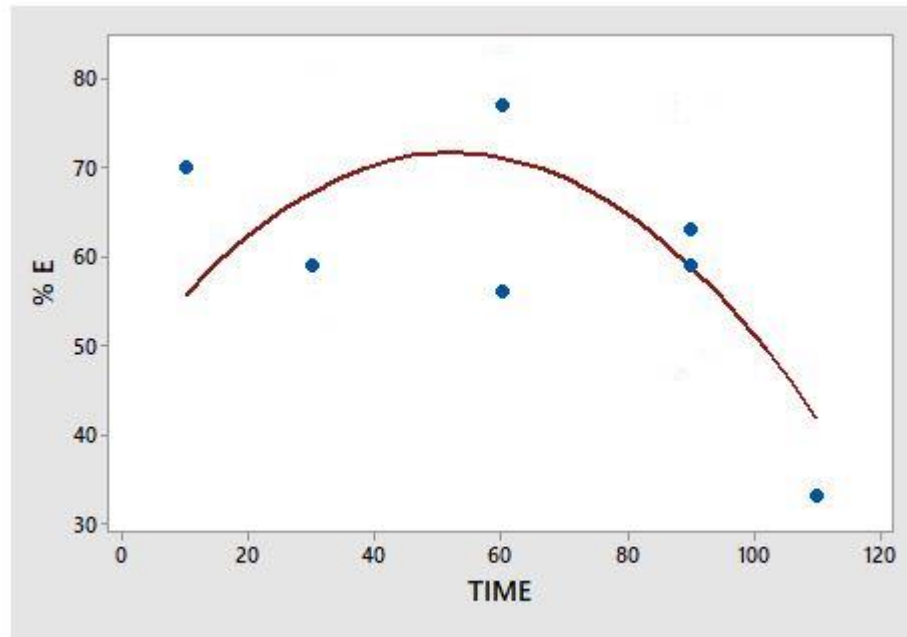


Figure 4.60: Effect of time on dye exhaustion of wool dyeing with ENn

4.10.5.3. Effect of dyeing temperature on wool ENn dye

The effect of dyeing temperature shown in Figure 4.61 shows that the dye exhaustion increases with an increase in temperature. As it is observed, the color strength of the dyed samples increased with the increase of dyeing from 33 °C temperature up to 70°C.

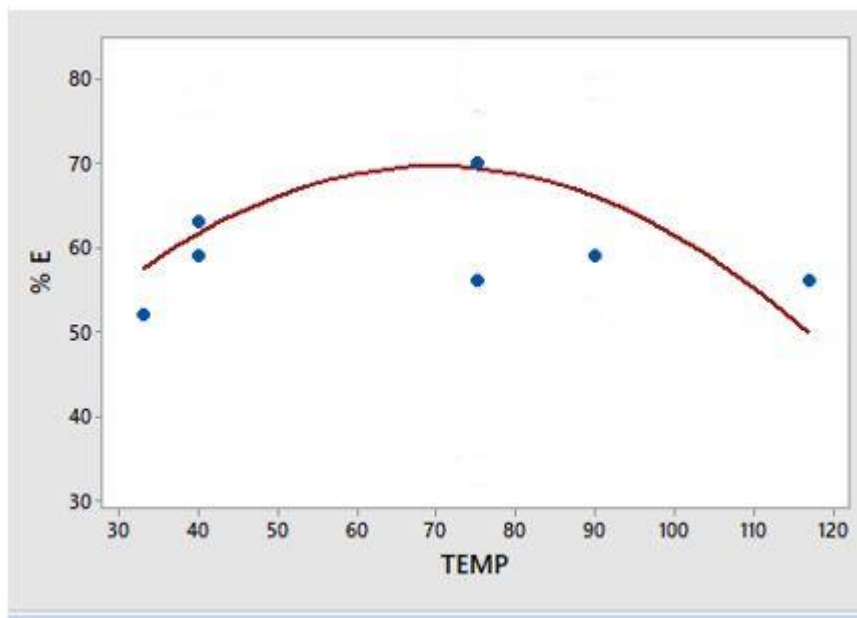


Figure 4.61: Effect of temperature on dye exhaustion of wool dyeing with ENn

This reveals that wool dyeing with ENn is done best at 70°C. It can be observed that at low temperature there is no acceleration of dyeing kinetics whereas too high temperatures results in low dye exhaustion in the dye bath (Adeel *et al.*, 2018; Safapour *et al.*, 2018; Xiao *et al.*, 2018). Beyond the equilibrium, there is a decrease in dye exhaustion from 80°C to 120°C.

4.10.5.4. Dyeing of wool fabric with embelin ninhydrin dye optimization

The dyeing of wool fabric was optimized by using the Response surface methodology. The factors considered were pH, temperature and time. The experimental conditions for dyeing wool fabric using ENn dye were designed using Design Expert software Table 4.27.

Table 4.26: Experimental design and results for dye exhaustion of wool fibers dyed with Embelin ninhydrin dye

Run	X1	X2	X3	K/S
1	0	0	0	5.2
2	-1	-1	1	8.9
3	$+\infty$	0	0	13.9
4	0	0	0	5.3
5	0	0	0	5.2
6	0	0	0	5.3
7	0	0	0	5.6
8	1	1	1	14.4
9	0	$+\infty$	0	9
10	0	0	0	6.4
11	0	$-\infty$	0	4.5
12	0	0	$-\infty$	4.8
13	1	1	-1	10.3
14	-1	1	-1	3.6
15	1	-1	1	8.6
16	-1	-1	-1	5.4
17	0	0	$+\infty$	13
18	$-\infty$	0	0	10
19	-1	1	1	12.7
20	1	-1	-1	5.4

The regression model equation (Equation 4.4) and analysis of 3D response plots showed the optimum dyeing conditions resulting from variation of different dyeing conditions on colour strength.

$$\begin{aligned}
 \text{K/S (Wool)} = & +58.977 - 13.83 X_1 - 0.24 X_2 - 0.05 X_3 + 0.95 X_1^2 + 3.31 \times 10^{-4} X_2^2 + 1.69 \times 10^{-3} X_3^2 \\
 & + 0.02 X_1 * X_2 - 0.02 X_1 * X_3 + 1.08 X_2 * X_3 \dots\dots\dots \text{Equation 4.4}
 \end{aligned}$$

Where, the response factor was, colour strength (K/S); X1 signifies the dye bath pH, X2 is the time of dyeing and X3 signifies the temperature of the dye bath. The analysis of variance (ANOVA) showed statistical significance displayed in Table 4.28. The Fisher's F-value is 41.29 with a probability value ($P < 0.0001$) which is ($P \geq 0.05$) implying that the model is significant. The model summary, Table 4.29 shows that the variation between the three variables in the dyeing of wool fibers with ENn dye has a good correlation.

Table 4.27: ANOVA for wool dyeing with ENn

Analysis of variance					
Source	Sum of squares	DF	Mean square	F-Value	P-Value
Model	223.40	9	24.82	41.29	< 0.0001
X1	15.73	1	15.73	26.17	0.0001
X2	30.08	1	30.08	50.04	< 0.0001
X3	83.11	1	83.11	138.26	< 0.0001
X1*X2	9.46	1	9.46	15.74	0.0027
X1*X3	3.51	1	3.51	5.84	0.0363
X2*X3	5.28	1	5.28	8.79	0.0142
X1*X1	65.79	1	65.79	109.45	< 0.0001
X2*X2	1.28	1	1.28	2.13	0.1750
X3*X3	16.14	1	16.14	26.85	0.0004
Residual	6.01	10	0.60		
Lack-of-Fit	4.92	5	0.98	4.49	0.0625
Pure Error	1.10	5	0.22		
Cor Total	229.41	19			

Table 4.28: Model Summary of wool

S	R-sq	R-sq (adj)
10.7976	97.38 %	95.02 %

The predicted R-squared of 0.8118 is in reasonable agreement with the Adjusted R Squared of 0.9502. The values are close to unity implying that the model is statistically accurate. On the other hand lack of fit was non-significant. The 3-D response plots Figure 4.62

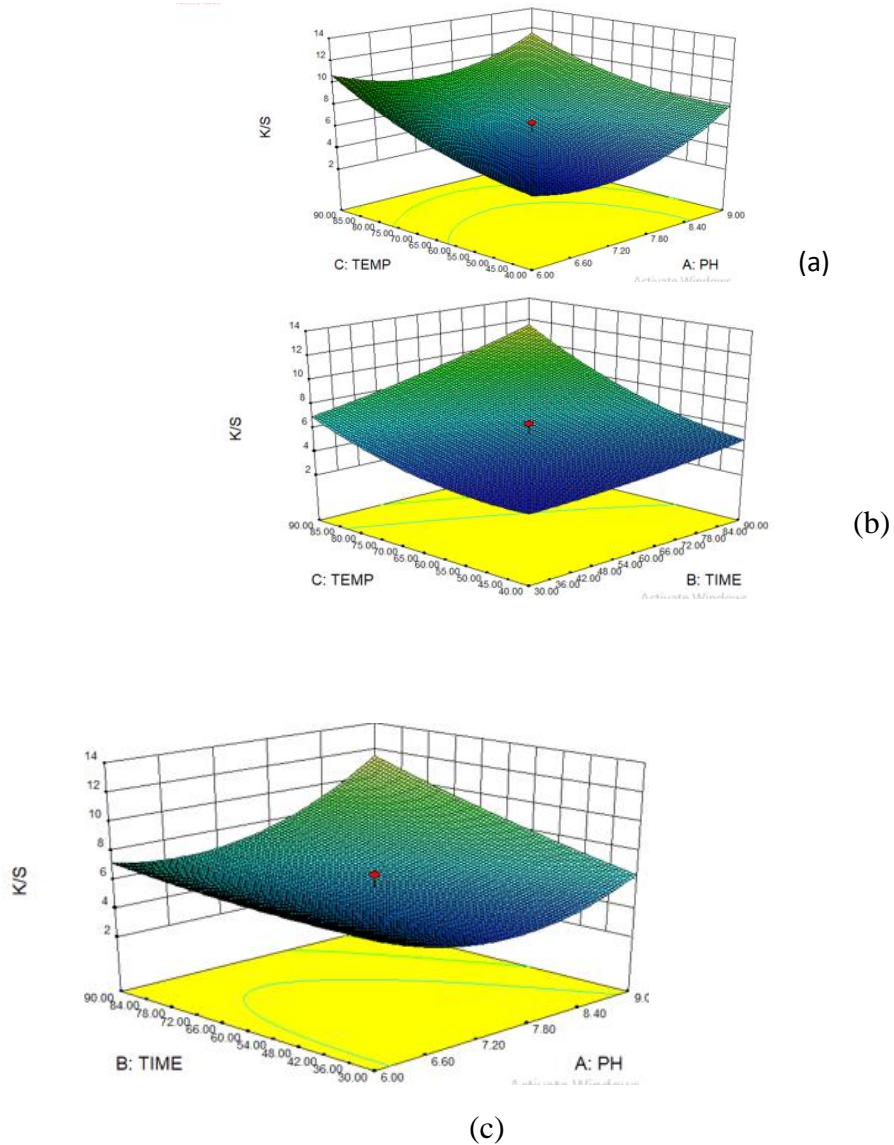


Figure 4.62: 3 D plots of wool ENn dyeing(a)- temp vs pH (b) temp vs time (c) time vs pH strength (K/S), at a temperature of between 65-70 °C Figure 4.79 (a). At a time of 60 min.

4.10.5.5. Validation of RSM for dyeing of wool fibers

Optimized dyeing conditions were used to validate the suitability of the model for the prediction of response values (colour strength). Optimized dyeing conditions were validated by performing experiments under the optimized conditions. The optimized dyeing values are the colour strength of 14.4 whereas the experimental values gave the colour strength of 15.9. The experimental response values were well in agreement with predicted response values.

4.10.5.6. Variation on unmordanted and mordanted dyed wool fibers

Mordanting was carried out on wool fibers with material to liquor ratio at 1:50. The CIELAB scale and colour space (L^* , a^* and b^*) values of wool fabric dyed with embelin ninhydrin dye are shown in Table 4.30. The L^* range from 46-86 chroma (c^*) values range from 3-33. The observations made from the a^* - b^* plot (Figure 4.63-Figure 4.65), show that embelin dyed without mordanting tends towards yellow-red quadrant and the embelin ninhydrin dyed wool fabric without mordants tends to red, showing a clear shift of resultant shade from yellow-green to red after chemical modification. The colour strength of embelin dyed wool K/S is 1.17 and upon dyeing with modified ENn the colour strength increases to a higher colour strength of 15.9.

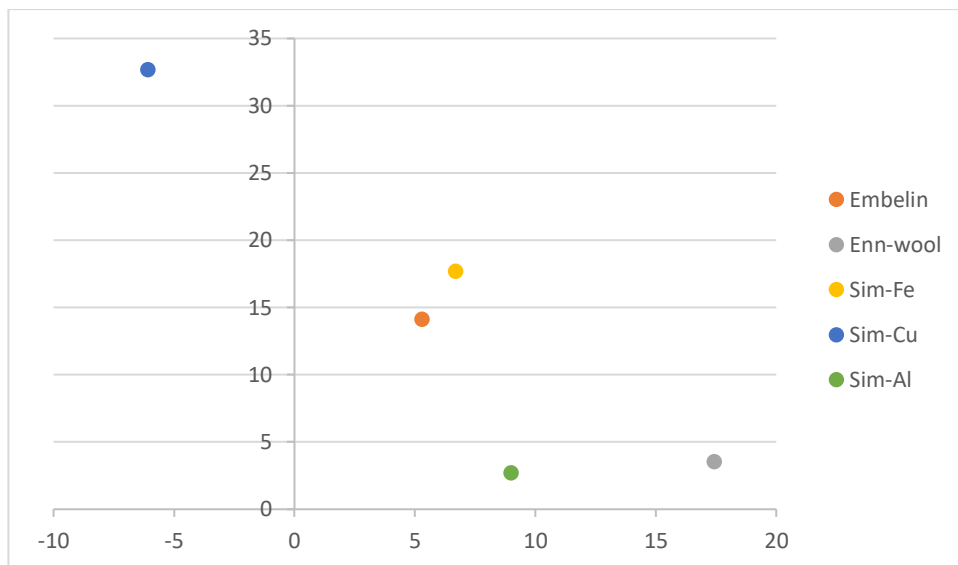


Figure 4.63: Plot of colour coordinates for simultaneous mordanted wool fibers

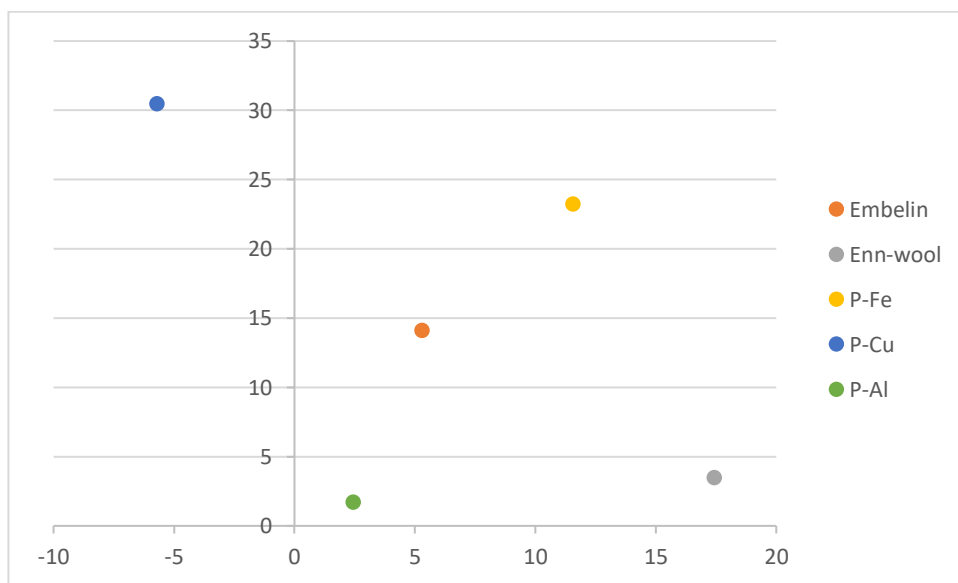


Figure 4.64: Plot of colour coordinates for post-mordanted silk fibers

Alum mordanted wool fibers samples ($\text{Al}_2\text{K}_2(\text{SO}_4)_4 \cdot 24\text{H}_2\text{O}$) shades obtained in simultaneous mordanting, Figure 4.63, shows shifts towards the achromatic region, with low b^* of + 2.66 and high a^* values of +9.00 with K/S of 2.48 (Table 4.30). In post mordanted fibers (Figure 4.64) a^* is + 2.46 which is higher, than b^* , +1.71, and the K/S of 4.88 resulting in less colour saturation. The pre-mordanted alum has a^* value of + 9.75 and b^* values of 5.64 and the K/S

of 2.97. The colour strengths of alum in wool are low. These weak colour strength values could be due to weak coordination between alum and functional groups of woolen fibers (Kovačević *et al.*, 2021; Singha *et al.*, 2018). For the ferrous ($\text{FeSO}_4 \cdot 7\text{H}_2\text{O}$) mordanted shades, simultaneous mordanting, occupied the yellow–red quadrant towards red, with a high b^* of +17.68 and low a^* values of +6.69 with K/S of 5.32 (Table 4.30). In post mordanted fibers (Figure 4.64) a^* is +11.58 which is lower, than b^* , values of +23.23, and the K/S of 14.54 resulted in a high colour saturation compared to embelin but close to the colour strength of embelin ninhydrin dyed wool fibers. The pre-mordanted ferrous has a^* value of +6.30 and b^* values of +17.37 and the K/S of 5.69. The colours are within the red-yellow quadrant of CIELAB colour space. The post mordant gives the best colour strength however the colour strengths with ferrous mordants. This could be due to the highly stable chelate complex formed between the embelin ninhydrin dye molecule and the ferrous mordant (Ammayappan & Shakyawar, 2016; Chakraborty, 2011). This is further evident by the observed colour strengths between (K/S 5.69-14.54).

For the copper ($\text{CuSO}_4 \cdot 7\text{H}_2\text{O}$) mordanted shades obtained with simultaneous mordanting, Figure 4.63, shows a shift towards the yellow-green region, with b^* values of +32.66 and low a^* values of -6.08 and the colour strength is K/S of 7.69 (Table 4.30) in post mordanted fibers (Figure 4.64) a^* is -5.69 which is lower than b^* , +30.59, and the K/S of 11.45 resulting in a high colour saturation than embelin and close to embelin ninhydrin dyed wool fabrics. The pre-mordanted, Figure 4.65, cuprous, showed a^* values of -9.26 and higher b^* values of +17.92 and the K/S of 9.89. All the colours fall within the green-yellow colour space. The ferrous post-mordanted wool fiber gave the highest colour strength followed by post copper mordanted. This is because of the vacant d-orbitals in Ferrous metallic mordant which allows

for coordinative unsaturation resulting in the ability to form coordination complexes with the embelin ninhydrin dye molecules because it will accommodate the active sites of wool fabric ($-\text{COOH}$ and $-\text{CONH}_2$) (Kamel *et al.*, 2011). This ability of coordination results in enhanced interaction between the wool fiber and the dye exhaustion (Shabbir *et al.*, 2017; Zhou *et al.*, 2020). The alum mordanted wool fibers have low colour saturation and give pale shades (Miah *et al.*, 2017) evident by the observed colour strengths between (K/S 2.48-4.88).

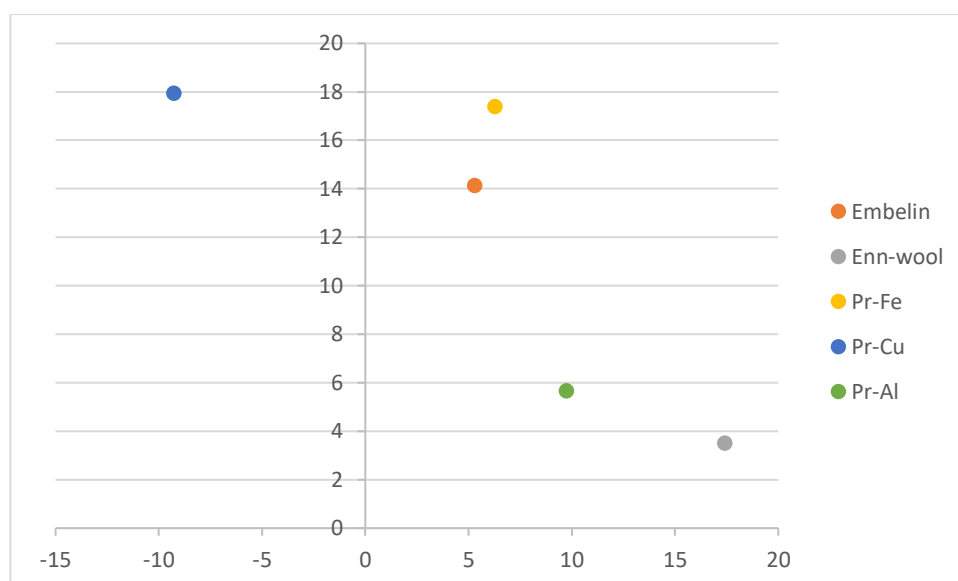


Figure 4.65: Plot of colour coordinates for Pre-mordanted samples

4.10.5.7. Colour fastness properties of dyed wool fibers

The colour fastness properties were carried out according to ISO 105-C02:1989, ISO 105 A02:1993, and ISO 105-X12:2000. It was observed from Table 4.31 that the embelin ninhydrin dyed fabrics showed good fastness properties than that for the embelin dyed. From the table of results, it is observed that the mordanted fibers showed colour fastness of rating 4-5 which is good compared to embelin and embelin ninhydrin dyed fibers without mordants. The fastness tests suggest that mordanted embelin ninhydrin dyes have good dyeability for

wool fabrics. The mordants contributed to good colour fastness properties (Samanta & Agarwal, 2009; Singha *et al.*, 2018).

Table 4.29: Colour measurements of the wool dyed fabric using different methods of mordanting












Metho d	Mordan t	L*	a*	b*	ΔE	C*	H°	K/S	Shades
Embel in	NO	56.08	5.3	14.11	10.82	15.07	20.59	1.17	
ENn	NO	59.85	17.43	+3.50	17.66	17.78	78.65	15.9	
PRE	Ferrous	53.02	+6.30	+17.37	11.11	18.48	19.94	5.69	
	Copper	79.66	-9.26	+17.92	21.50	18.18	27.33	9.89	
	Alum	84.75	9.75	+5.64	23.52	11.26	59.95	2.97	
POST	Ferrous	46.25	+11.58	+23.23	20.29	25.96	26.5	14.54	
	Copper	69.39	-5.69	+30.49	19.25	31.02	10.57	11.45	
	Alum	86.32	+2.46	+1.71	26.48	3.00	55.2	4.88	
SIMU LT.	Ferrous	56.88	+6.69	+17.68	7.50	18.90	20.73	5.32	
	Copper	72.35	-6.08	+32.66	22.13	33.22	10.55	7.69	
	Alum	74.51	+9.00	+2.66	17.12	9.38	73.53	2.48	

Table 4.30: Colour fastness of the dyed fabric using different methods of mordanting

Method	Mordant	Wash fastness		Rubbing fastness		
		C.C	C.S	Dry	Wet	Light fastness
Embelin ninhydrin	Without	2-3	2	3	3	2
Embelin	Without	2-3	2	2	2	1
Simultaneous	Alum	3-4	3	4	4	4
Mordanting	Copper	3	4	3	4	4
	Ferrous	4	4	3	4	3
Pre- mordanting	Alum	3	3	4	4	4
	Copper	3	3	4	4	4
	Ferrous	4	3-4	3	4	4
Post- mordanting	Alum	4	4	3-4	4	3
	Copper	4	4	4	4	4
	Ferrous	4	4	4	4	3

C-C-Colour change, Colour stain. 1-Poor; 2-Fairly good 3- Good,4-Very good,5-Excellent

4.11. Thermal stability and surface characterization of dyed cotton fibers

Cotton is a cellulosic fiber with a semi-crystalline polymer whose thermal properties are determined by its molecular structure, material density, crystallization level, crystal orientation angle and the mobility of molecular arrangements in both the amorphous and crystalline regions. Since dyeing of cotton fiber causes some alteration in chemical, and physical morphological properties of the fiber, changes are also expected in its thermal characteristics (Gashti *et al.*, 2013)

4.11.1. Thermo Gravimetric Analysis (TGA) /Differential Scanning Calorimetry (DSC)cotton blank fabric

Thermal Gravimetric analysis of dyed cotton fabrics was studied because suitable dyes are the ones able to withstand processing conditions and are thermally stable.

Thermogravimetric analysis (TGA) provides information on quantitative weight change

when the heating process occurs (Jeske *et al.*, 2012; Mansa & Zou, 2021). The thermal analysis techniques (TGA/ DSC) were used to analyze the effect of mordants on cotton fabrics dyed using embelin ninhydrin dye (6) and vilangin dye (EMV). The dye mordants' mass sample weights are shown in Table 4.32 below.

Table 4.31: Different cotton dyed and mordanted fabrics weights

Position	Sample	Pan wt (mg)	Sample wt. (mg) manual	Sample wt.(mg) auto	Midpoint degree temperature
101	Blank vial				
102	Blank cotton	174.90	6.59	6.4307	356.30
103	EM-FE	181.89	6.54	6.5464	354.44
104	EM-CU	178.75	7.00	6.9843	347.30
105	EM-ALUM	183.65	6.90	6.7793	354.23
106	EM-NI	180.81	6.75	6.6973	356.08
107	EM-NO-MORD	180.86	6.67	6.4143	359.61
108	ENN COT	177.52	6.57	6.4653	344.07
109	ENN-NI	173.34	6.74	6.5570	313.40
110	ENN-FE	174.20	6.32	6.1411	358.27
111	ENN-CU	189.38	6.85	6.6801	362.27
112	ENN-ALUM	175.40	6.61	6.4005	325.42
113	EMBEL-COTT	186.44	6.98	6.7727	360.41
114	ENN DYE	182.21	6.73	5.0385	379.73
115	EMV DYE	182.97	6.50	6.4460	407.55
116	EMBELIN DYE	179.64	6.38	6.2005	390.26

4.11.2. TGA/DSC of vilangin dyed cotton fabric

The TGA/DSC curves of these studied samples are shown in Figures (4.66-4.70) respectively. The dyed cotton fabrics were mordanted using ferrous, copper, alum and nickel metal mordants.

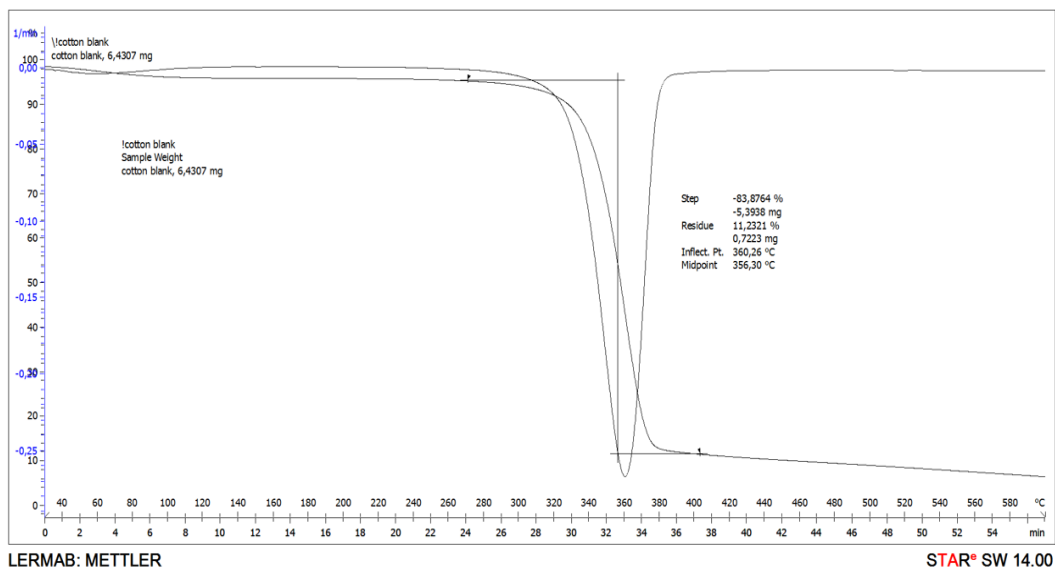


Figure 4.66: TGA/DSC Curve for blank cotton

Figure 4.66 shows the TGA/DSC curve of blank cotton fabric. The recorded thermogravimetric plot shows the existence of two steps involved in the mass loss. One occurs in a region between 40 to 100 °C and the other between 300 to 400 °C. The first temperature loss at a lower value (i.e., the first step) may be attributed to the thermo-oxidative degradation of the blank cotton fabrics which transforms to carbonaceous residues (Koklukaya *et al.*, 2015; Onoji *et al.*, 2016) and the second, higher temperature value may correspond to the subsequent degradation of the cellulosic polymer (Ferreira *et al.*, 2018; Lei *et al.*, 2018). The second observed loss is the most critical one both in terms

of the rate of weight loss and total weight loss (Hu *et al.*, 2019).

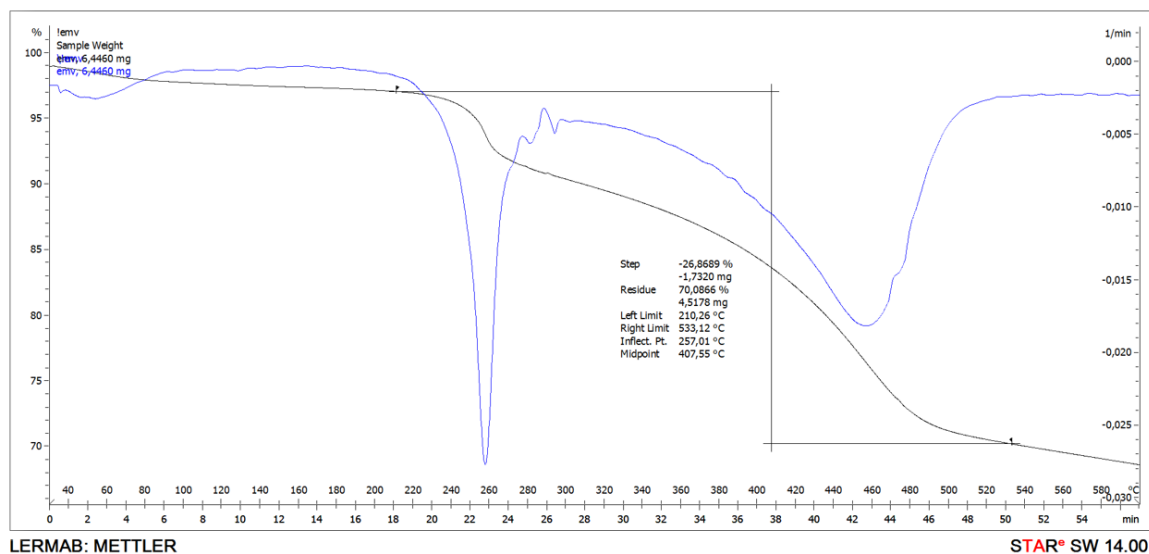


Figure 4.67: TGA /DSC curve of vilangin dye

The thermogravimetric analysis of vilangin shown in Figure 4.67 shows the presence of four mass loss events. The TGA-DSC curves recorded show that the thermal decomposition of semi-synthetic dye exhibited a four-step degradation pattern. The first minor weight loss of the membranes, ranging from 40 to 80°C, may be derived from the evaporation of the residual solvent and the absorbed water. The second mass loss, in the temperature range of 200--240°C, can be attributed to the disintegration of the functional groups, the decomposition of vilangin is observed at between 460 and 500 °C. TGA/DSC curve of embelin is observed in Appendix 5

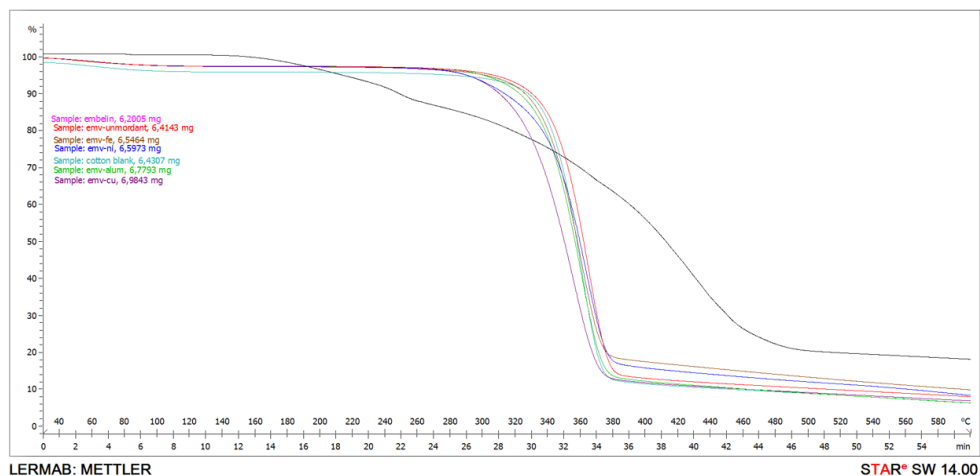


Figure 4.68: Overlay of Vilangin dyed cotton fabrics

Figure 4.68 shows the TGA/DSC for the overlay of vilangin dyed cotton fabrics with different mordants. Individual TGA/DSC curves are shown in Appendix 3-8. From the overlay in Figure 4.68, it can be observed that in the range of 320 and 380 °C there is a huge loss of mass in the cotton samples, which may be related to the thermal degradation of the cellulose, which occurs around 350°C (Chen *et al.*, 2019). At lower temperatures below 300 °C cellulosic damage occurs in its amorphous region (Leng *et al.*, 2018; Santmartí & Lee, 2018) however at higher temperatures between 300 and 380 °C there is a significant mass loss, this being the main stage of pyrolysis of the cellulosic fibers, occurring generally in the crystalline region. The real degradation temperature for mordanted cotton fabrics significantly was higher after the dyeing treatment process. This is because covalent bonds and hydrogen bonding were formed between cellulosic fabric and semi-synthetic dye and mordants used thus thermal stability of dyed fabric is improved. The functional groups of the vilangin dye have a relatively high ability to absorb more water. The third weight loss, starting at 380°C, demonstrates the degradation of the cellulose polymer chains as well as the destruction of cross-linking and weight loss (Asim *et al.*, 2019; Mizera *et al.*, 2019). Appendices 6 -10 shows the TGA/DSC curves of different vilangin dyed cotton fibers.

4.11.3. TGA/DSC of embelin-ninhydrin dye

The thermogravimetric analysis of embelin ninhydrin shown in Figure 4.69 shows the presence of four mass loss events. The TGA-DSC curves recorded show that the thermal decomposition of semi-synthetic dye exhibited a four-step degradation pattern. The first minor weight loss of the membranes, ranging from 40 to 100°C, may be derived from the evaporation of the residual solvent and the absorbed water in the cotton fiber. The second mass loss is the temperature range of 180--240°C, which can be attributed to the disintegration of the functional groups, the decomposition of embelin ninhydrin was observed at between 340 and 420 °C.

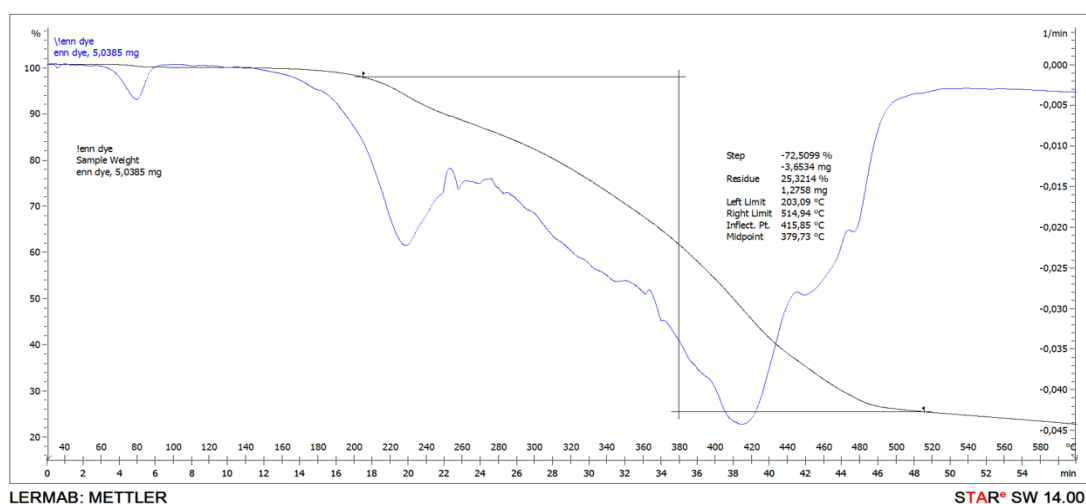


Figure 4.69: TGA/DSC of embelin ninhydrin dye

Figure 4.70 shows the TGA/DSC for the overlay of embelin ninhydrin-dyed cotton fabrics with different mordants. Individual TGA/DSC curves are shown in Appendix 11-15. From the overlay, it can be observed that in the range 240 to 380 °C there is a huge loss of mass in the cotton samples, the occurrence is associated with the rapid thermal decomposition of the cellulose, which usually occurs around 350°C (Abidi *et al.*, 2007). At temperatures below 300°C, there is cellulose damage in its amorphous region associated with the loss of adsorbed

water molecules (Wang *et al.*, 2007). At higher temperatures mass loss occurrence in cellulosic fibers, is generally in the crystalline region but the degradation temperature for mordanted cotton fabrics is significantly higher after the dyeing treatment process. This is because covalent bonds and hydrogen bonding were formed between cellulosic fabric and semi-synthetic dye and mordants used thus thermal stability of dyed fabric is improved (Alihosseini, 2016; Rather *et al.*, 2017). The functional groups of the embelin ninhydrin dye have conferred more hydroxyl groups to cellulosic fabric increasing the thermal stability which is observed as the third weight loss, starting at 380°C, demonstrating the degradation of the cellulose polymer chains as well as the destruction of cross-linking and weight loss (Borsoi *et al.*, 2016). Appendices 8 -12 shows TGA/DSC curves of the different embelin ninhydrin cotton mordanted fibers.

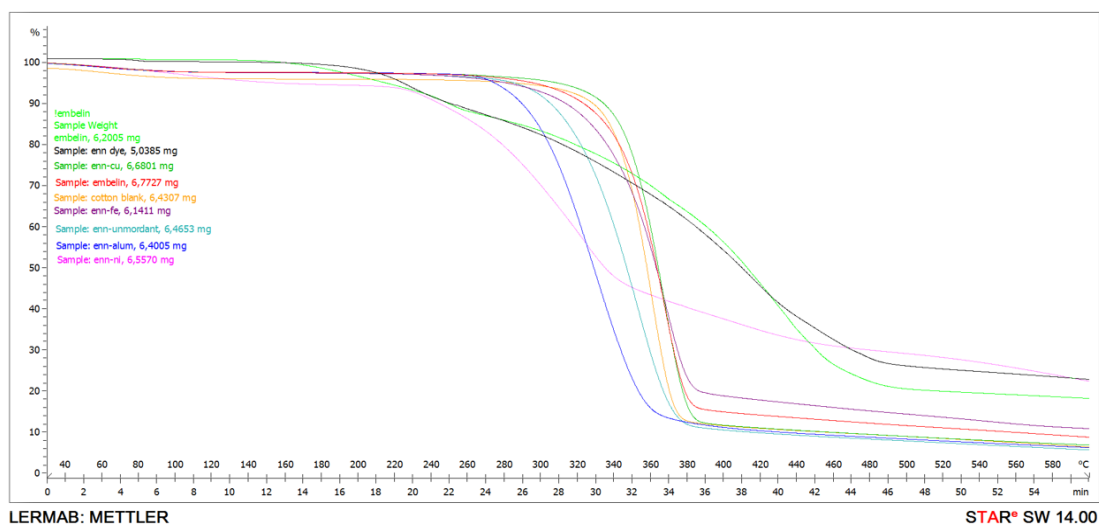


Figure 4.70: Overlay of embelin ninhydrin dyed cotton fabrics

4.12. FTIR spectroscopy and scanning electron microscopy of vilangin dyed cotton fiber

The FTIR spectra of the undyed cotton and vilangin dyed cotton fabric is shown in Figure 4.71. From the spectra, it can be observed that the undyed fabric exhibits the characteristic cellulose polymer structure with peaks at 1027 cm^{-1} (Hospodarova *et al.*, 2018; Sultana *et al.*, 2020). The absorption peaks centered at 3316.57 cm^{-1} for the undyed fabric are shifted to 3325.41 cm^{-1} on dyeing. These peaks are broad and correspond to O–H stretching as a result of interaction with a cellulose polymer. Also the observed broad peak between $3000\text{--}2800\text{ cm}^{-1}$ is due to –C–H stretches (Cao *et al.*, 2021; Chung *et al.*, 2004). However changes and modification in cotton fabrics takes place within 2000 cm^{-1} to 800 cm^{-1} of the cellulose polymer (Wang *et al.*, 2021; Zhang *et al.*, 2019). In the region of 1630 cm^{-1} , it shows –O–H of water absorbed from the cellulose structure (Le Troedec *et al.*, 2008; Zain *et al.*, 2014). The peak at 1457.27 cm^{-1} is due to the –O–H in-plane bending (Che Kamarludin *et al.*, 2014). In the region around 1400 cm^{-1} to 1300 cm^{-1} , there is CH_2 scissoring and –CH bending and –OH in-plane bending (Araujo *et al.*, 2018; Boukir *et al.*, 2018). Plane bending occurs in the region 1200 cm^{-1} due to –CH bending and –O–H in-plane bending (Grancaric *et al.*, 2017). The vilangin dyed cotton fabric exhibits a new peak at 1109.57 cm^{-1} which is absent in undyed cotton fabric. This is due to C–O–C asymmetric stretch between the dye and the cellulose polymer (Jabli *et al.*, 2020). The peaks in the region below 1000 cm^{-1} are due to –C–O valence vibrations of cellulose polymer (Fengel, 1992; Ilyas *et al.*, 2019).

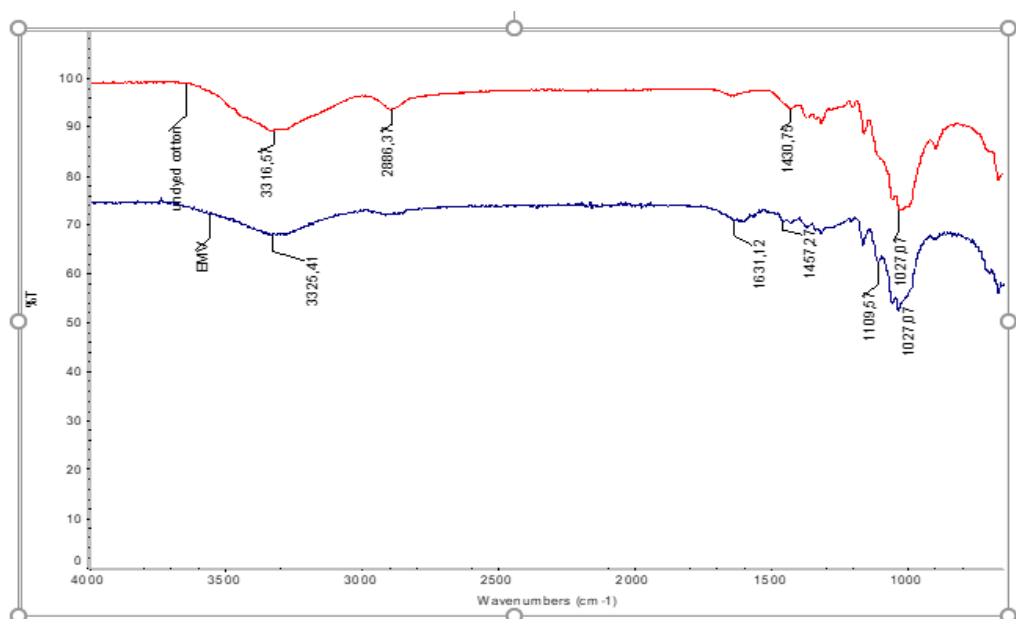


Figure 4.71: FTIR analysis of cotton fabric dyed with vilangin

The SEM images of the undyed and dyed cotton fiber with vilangin are shown in Figures 4.72(a) and (b). It can be seen that the blank cotton fiber has a relatively smooth surface. The high magnification SEM images of the cotton fiber dyed with vilangin dye show a formation of aggregated dye on the surface of cotton fibers. Generally, the ability of the dye to aggregate on the surface of textiles fiber is defined by several factors such as size, mobility, end-group functionalities, relative composition, and molecular architecture. The peak observed at 1631.12 cm^{-1} in vilangin dyed fiber (Figure 4.71) is related to the carbonyl group of the vilangin dye (Figure 4.71) and hydroxyl groups of cotton generate some ionic and Van der Waals interactions with the hydroxyl groups of dye solutions after enhancing their compatibility. These interactions are strong enough to enable the aggregation of semi-synthetic dyes on the cellulose surface as a result of the surface area they possess (Parvinzadeh Gashti *et al.*, 2014; Wang *et al.*, 2016).

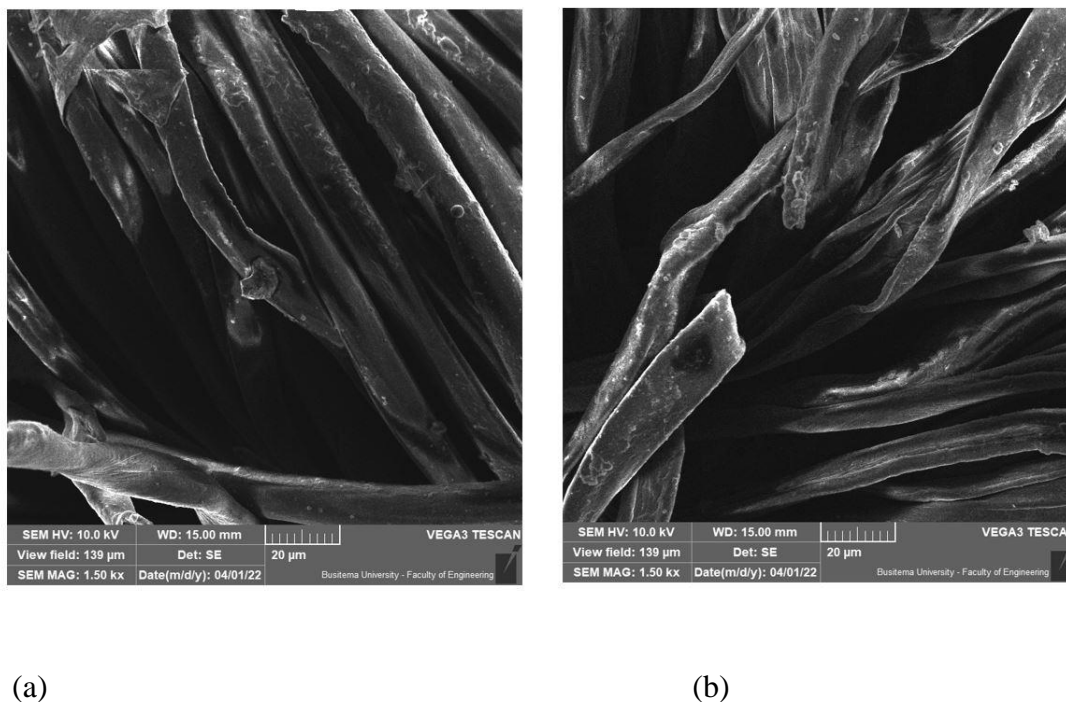


Figure 4.72 (a): SEM of undyed cotton and (b) vilangin dyed cotton fiber

4.12.1. Surface characterization of embelin ninhydrin dyed cotton fiber

The FTIR spectra of the embelin ninhydrin dyed fabric reveal, in Figure 4.73 a broad peak was observed at 3334.25 cm^{-1} , which is a shift from 3316.57 cm^{-1} from the undyed cotton fabric. This peak is attributed to the fundamental stretching vibration of the -OH hydroxyl group (Emam *et al.*, 2018). The peak at 2901.10 cm^{-1} is associated with -C-H stretching (Trache & Tarchoun, 2019). The peak at 1427.81 cm^{-1} and 1313.89 cm^{-1} in the embelin ninhydrin dyed fiber can be assigned to aromatic C-O-H bending mode, the same case with the blank fabric and an additional signal for the dyed fabric at 1159.67 cm^{-1} and 1109.59 cm^{-1} , this is due to the interaction between the dye auxochromes and functional groups present in the cellulose fabric as a result of C-O-C stretch (Salama, 2020). The embelin ninhydrin dyed cotton fabric showed signals of the cellulose structure fingerprints at 1027 cm^{-1} characteristic fingerprint of the undyed fabric (Adebayo *et al.*, 2019; Jacob *et al.*, 2019). The

structure of interaction between the ENn dye and cellulose is observed in Figure 4.76.

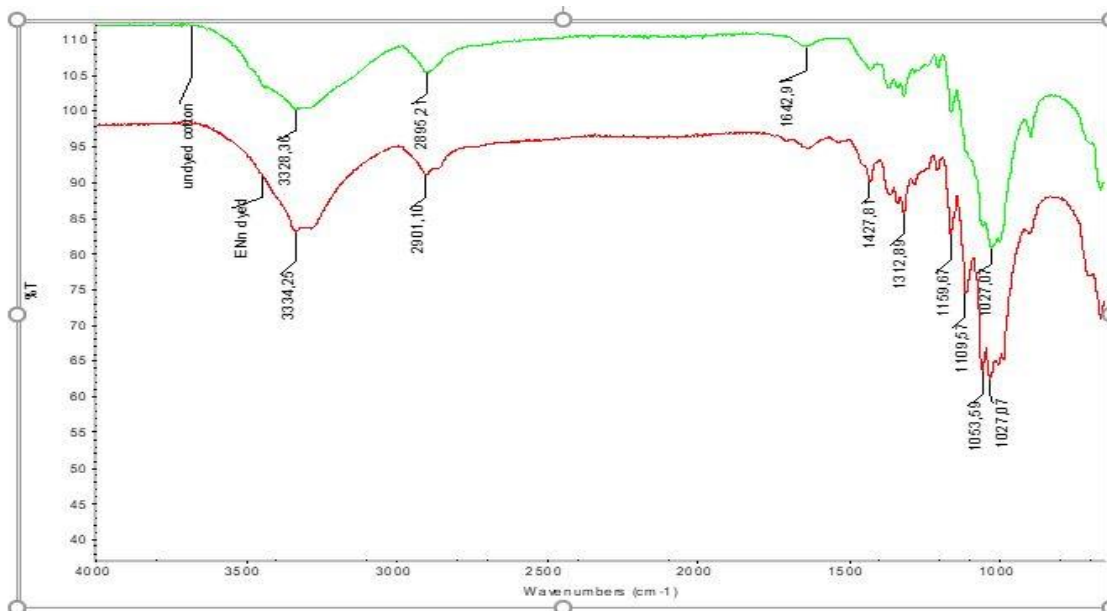
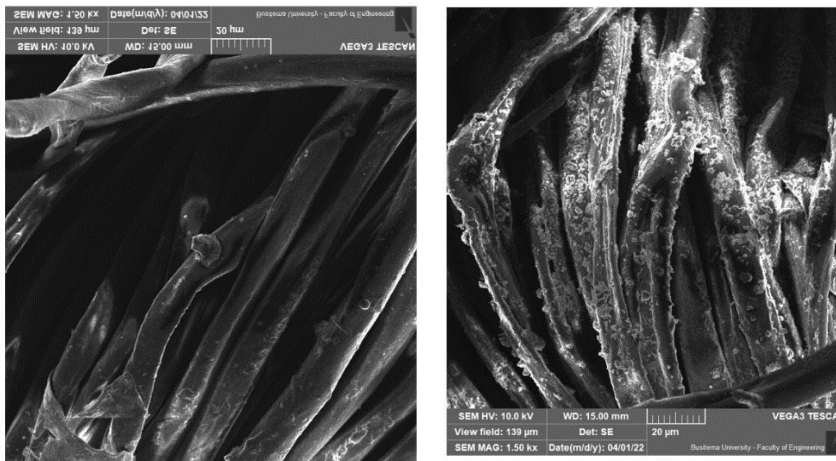


Figure 4.73: ATR-FTIR Spectra of embelin ninhydrin dyed cotton fabric

The SEM images of the undyed and dyed cotton fiber with embelin ninhydrin are shown in Figures 4.74 (a) and (b). The undyed cotton fiber has a relatively smooth surface observed over high magnification SEM. The images of cotton fiber dyed with embelin ninhydrin dye showed a rough surface due to aggregated dye on the surface of cotton fibers. The peak observed at 1644 cm^{-1} in ENn dyed fiber (Figure 4.74) is related to carbonyl group of the embelin ninhydrin dye. Figure 4.75 shows interaction of the embelin ninhydrin dye and cellulosic fiber.



(a)

(b)

Figure 4.74: (a) SEM of undyed cotton and (b) embelin ninhydrin dyed cotton fiber

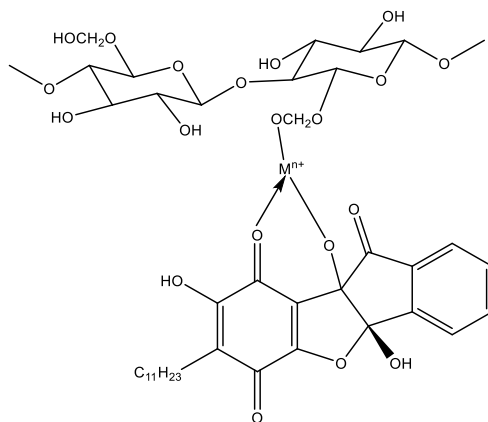


Figure 4.75: Structure of embelin ninhydrin dye and cellulosic structure interaction

4.12.2. Surface characterization of dyed silk with embelin ninhydrin

The FTIR results in Figure 4.76 showed peaks at 3278.27 cm^{-1} that correspond to the OH frequency vibrations, of silk fiber, the sharp peak at 1619.33 cm^{-1} correlates with the CH_3 in the amide group of silk fiber. The absorption bands at 1227.44 cm^{-1} correspond to C-C, C-N, and N-H functional groups between the silk and the dye (Kiran *et al.*, 2020). Figure 4.78 shows the interaction of the embelin ninhydrin dye and silk fiber.

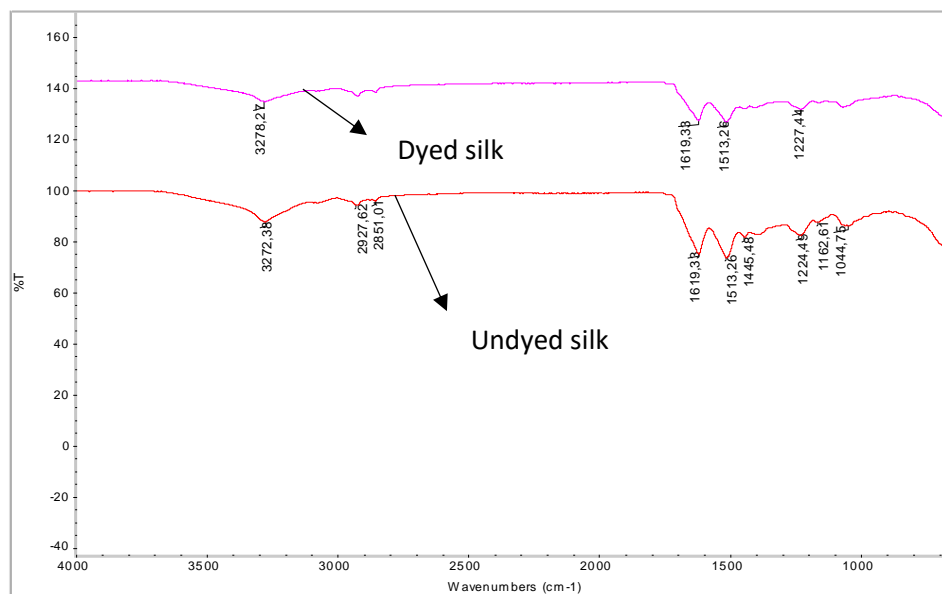
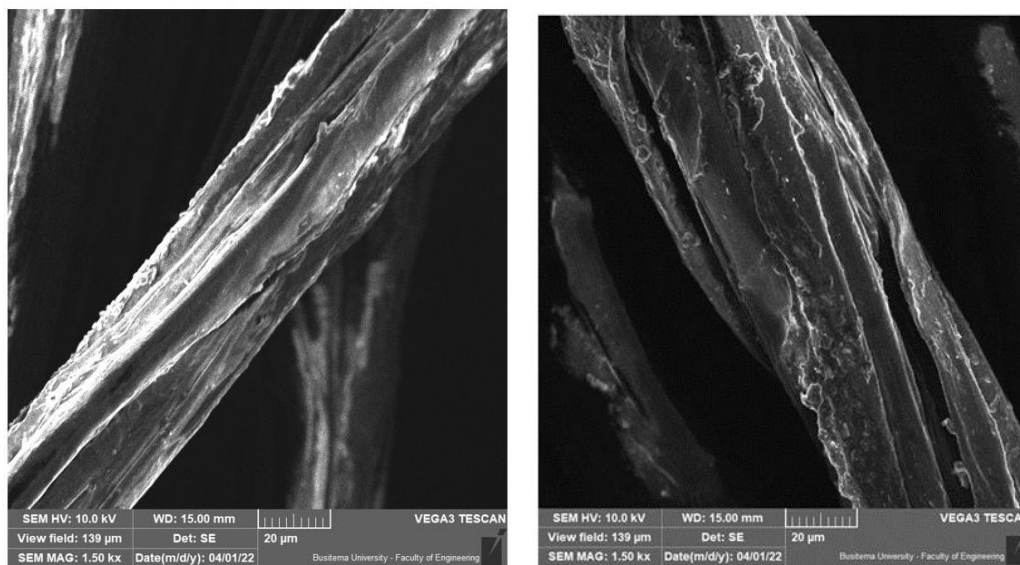


Figure 4.76: FTIR of dyed silk with embelin ninhydrin and undyed silk



(a)

(b)

Figure 4.77: (a) SEM Blank silk fiber (b) SEM ENn silk dyed fiber

Figure 4.77: (a) and (b) shows the SEM Blank silk fiber and ENn silk dyed fiber respectively which shows a soft surface and the dyed silk surface shows a rough surface. The peak observed at 1027 cm^{-1} silk undyed fiber shifts to 1044.78 cm^{-1} upon dyeing (Figure 4.76). Figure 4.78 shows the dye ,mordant,silk fiber interaction.

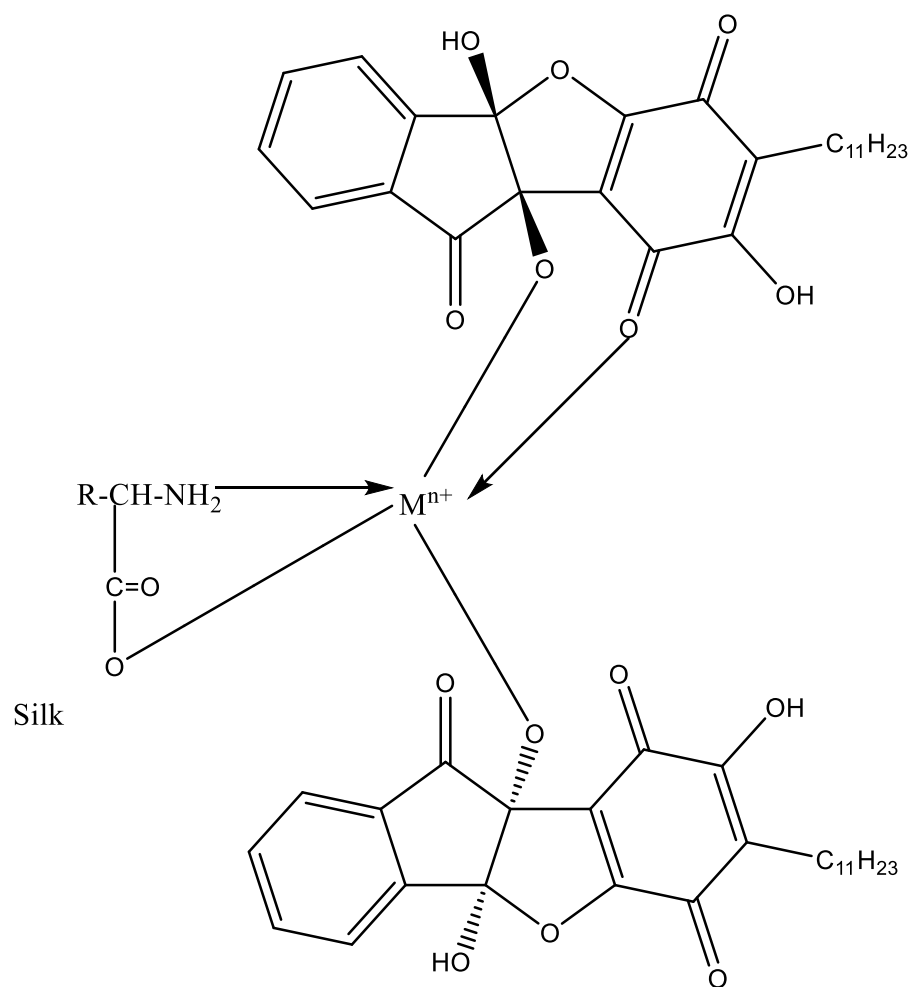


Figure 4.78: Structure of embelin ninhydrin dye and metal mordant on silk

4.12.3. Surface characterization of wool dyed fabric with ENn dye

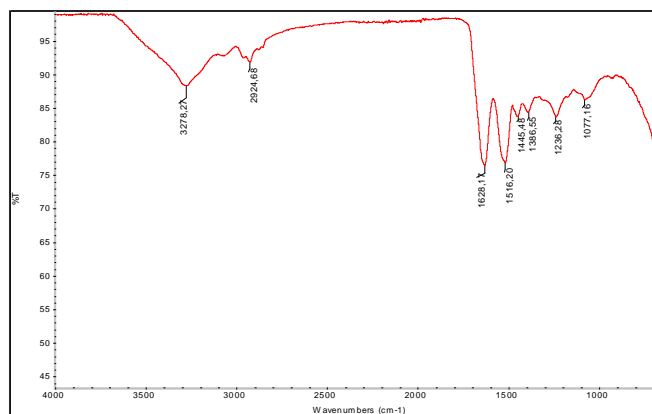


Figure 4.79: FTIR spectrum of wool undyed fiber

The FTIR spectra of plain wool, are shown in Figure 4.79 characteristic absorption frequency expected of the peptide bonds -CONH is observed. The band at around 3278.27 cm^{-1} is characteristic of amide A, which is associated with N-H stretching bonds. At 1628.17 cm^{-1} , the stretching frequency observed is the C-O, connecting to Amide I. The absorption frequency at 1516.20 cm^{-1} is related to amide II C-O stretching frequency vibrations that provide a connection for amide I can be observed in the range of 1628.17 cm^{-1} . The absorption band at 1518.20 cm^{-1} has a relationship with amide II, due to the N-H bend and C-H stretch vibration frequencies, whereas amide III vibrational frequencies are observed at $1236.28\text{-}1386.55 \text{ cm}^{-1}$ which have a relationship to C-N, C-C stretching, N-H and C-O bending stretch vibrations (Abou Taleb *et al.*, 2020; Hassan, 2020). Appendix 2 shows the surface characterization several mordanted embelin ninhydrin wool fibers using FTIR.

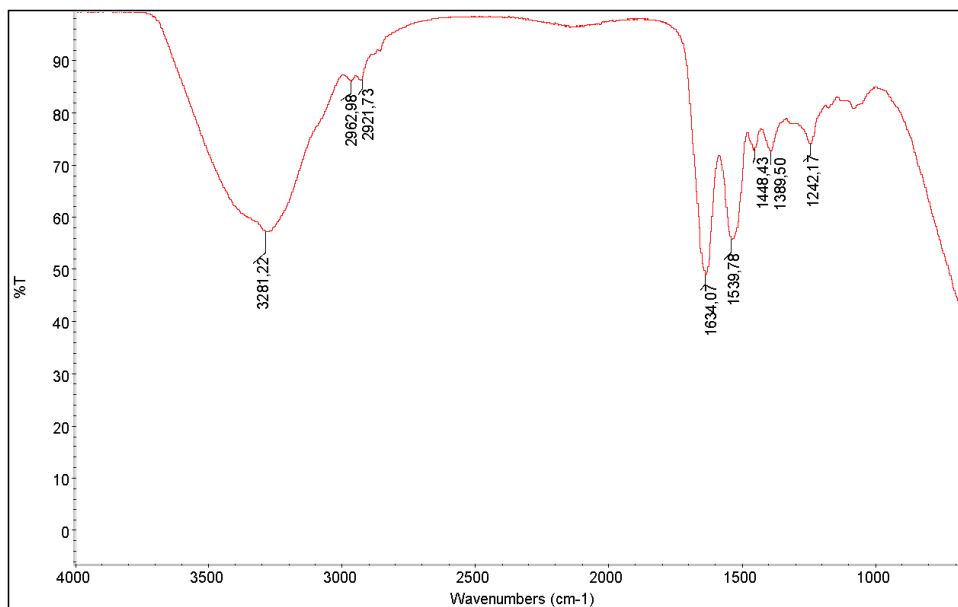


Figure 4.80: Wool ENn dyed without mordants

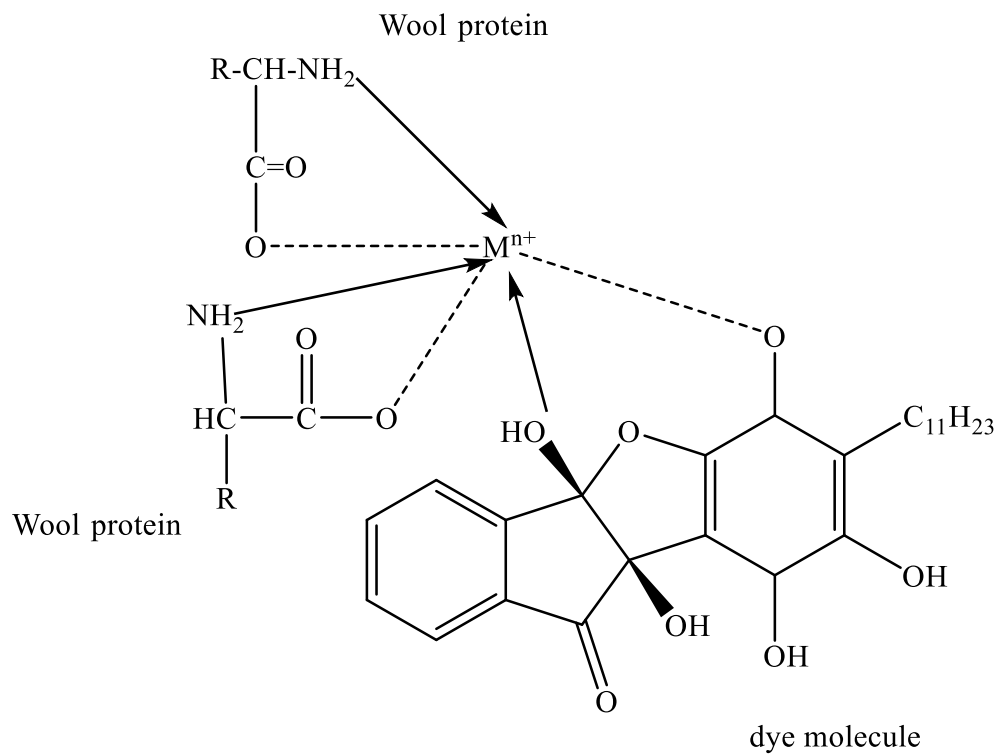


Figure 4.81: Possible mechanism between ENn dye molecule and wool fiber

There is a shift in the primary amide, amide I to 3281.22 cm^{-1} and the intensity is increased in the primary and secondary amide bonds, to 1634.27 cm^{-1} and 1539.78 cm^{-1} respectively Figure 80. The increase in intensity after dyeing procedures confirms the addition of more oxygen groups on the outer surface of wool fibers. Figure 4.81 shows the resultant functional groups were formed on the outer surface of the wool fibers on the interaction between the active functional species from the dyes and wool fabric (Haji *et al.*, 2016). The addition of oxygen groups on the surface groups of wool fabric is responsible for the wettability and dye absorption of wool fiber (Gupta & Basak, 2010; Haji *et al.*, 2020).

The SEM images of the undyed and dyed wool fiber with embelin ninhydrin are shown in Figures 4.82 (a) and (b). The undyed wool fiber has a relatively smooth surface observed over high magnification SEM. The images of the wool fiber dyed with embelin ninhydrin dye showed a rough surface due to aggregated dye on the surface of wool fibers. The peak observed at 1634 cm^{-1} in ENn dyed fiber (Figure 4.81) is related to the carbonyl group of the embelin ninhydrin dye. Figure 4.80 shows the interaction of the embelin ninhydrin dye and wool fiber. The dyed fabrics are rough because of wettability through the introduction of hydrophilic groups (Haji, 2020).

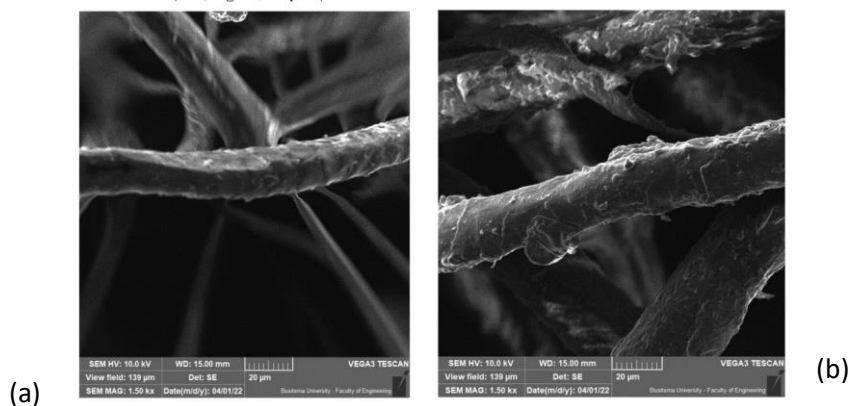


Figure 4.82: (a) SEM Blank wool fiber (b) SEM ENn wool dyed fiber

CHAPTER FIVE

CONCLUSION AND RECOMMENDATIONS

5.1. Conclusion

Embelin from *Embelia schimperi* from berries were successfully isolated. Four derivatives were semi-synthesized, namely; methylenebis- (2, 5-dihydroxy-4-undecyl-3,6-benzoquinone (Vilangin).(3); 6, 6'-(ethane-1,1-diyl)bis(2,5-dihydroxy-3-undecylcyclohexa-2,5-diene-1,4-dione) with common name methyl vilangin (4). The third derivative semi-synthesized was, 6,6'-((2,4-dihydroxyphenyl)methylene)bis(2,5-dihydroxy-3-undecylcyclohexa-2,5-diene-1,4-dione) (5) and (4b*S*, 9b*S*)-8-hydroxy-4b, 9b-dimethyl-7-undecyl-4b, 9b-dihydro-9*H*-indeno [1, 2-*b*] benzofuran-6, 9, 10-trione (embelin ninhydrin) (6).The precursor embelin and derivatives were characterized using spectroscopic and analytical techniques. The semi-synthesized compounds were confirmed using ATR-FTIR, LC/ESI/MS , GC-MS and ¹H NMR and ¹³C NMR and elemental analysis. Compounds 3 and 6 were soluble under alkaline conditions. The dyeing properties of the four derivatives on cellulosic (cotton) and proteinous fibers (silk and wool) were carried out and it was observed that (vilangin) was able to dye cellulosic fibers and embelin ninhydrin had good dyeability towards cotton, silk and wool fibers. The methyl vilangin (4) and embelin-2,4 -dihydroxybenzaldehyde (5) were not able to dye the fibers. Thermal stability of dyed fabrics was carried out using TGA/DSC and surface characterization of dyed fibers was evaluated using scanning electron microscopy and FTIR spectroscopy. The dyed fibers had good colour strength and excellent colour fastness properties compared to embelin dye. Different shades were achieved by using approved environmentally friendly metal mordants.

5.2. Recommendations

This study showed that embelin from *Embelia schimperi* can be used as precursor compound for chemical modification of semi-synthetic dyes. Solubility was enhanced by alkaline condition of the process. Dyeing properties of the semi-synthetic derivatives were enhanced through mordanting with the allowed environmentally metal mordants. These resulted in green, violet and brown shades. In order to further exploit the potential of *Embelia schimperi* samples as source of natural dyes for textile dyeing the following recommendations are made from this study

- (1) There is need to optimize extraction of embelin from stem bark samples
- (2) There is need to optimize extraction of embelin from *Embelia schimperi* berries samples
- (3) There is a need to optimize the extraction conditions to yield a higher amount of embelin by employing other methods which have not been studied here for example the microwave-assisted techniques
- (4) There is a need to exploit the dyeing properties of vilangin and embelin ninhydrin in the synthetic fibers e,g polyester fibers
- (5) There is a need to employ the use of bio mordants instead of metal mordants in search of more shades
- (6) There is a need to employ low-cost alkylation agents from plants and fruits in place of aldehydes used in chemical modification to cut on cost and biocompatibility because they can be found in nature in plant leaves and fruits, for example, hexanal from fresh cut grass.

REFERENCES

- Abdel-Kareem, O. J. R. J. o. T., & Apparel. (2012). History of dyes used in different historical periods of Egypt.
- Abel, A. (2012). The history of dyes and pigments. In *Colour Design* (10.1016/b978-0-08-101270-3.00024-2pp. 557-587).
- Aberoumand, A. J. W. (2011). A review article on edible pigments properties and sources as natural biocolorants in foodstuff and food industry. *6*(1), 71-78.
- Abidi, N., Hequet, E., & Ethridge, D. J. J. o. a. p. s. (2007). Thermogravimetric analysis of cotton fibers: relationships with maturity and fineness. *103*(6), 3476-3482.
- Abou Taleb, M., Mowafi, S., Vineis, C., Varesano, A., Sanchez Ramirez, D., Tonetti, C., & El-Sayed, H. J. J. o. N. F. (2020). Effect of alkali metals and alkaline earth metals hydroxides on the structure of wool fibers. 1-14.
- Adebayo, G. O., Hassan, A., Yahya, R., Rahman, N. A., & Lafia-Araga, R. J. P. B. (2019). Influence of wood surface chemistry on the tensile and flexural properties of heat-treated mangrove/high-density polyethylene composites. *76*(12), 6467-6486.
- Adedayo, O., Anderson, W., Moo-Young, M., Snieckus, V., Patil, P., & Kolawole, D. J. P. b. (2001). Phytochemistry and antibacterial activity of *Senna alata* flower. *39*(6), 408-412.
- Adeel, S., Ali, S., Bhatti, I. A., & Zsila, F. J. A. J. o. C. (2009). Dyeing of cotton fabric using pomegranate (*Punica granatum*) aqueous extract. *21*(5), 3493.
- Adeel, S., Hussaan, M., Rehman, F.-u., Habib, N., Salman, M., Naz, S., Amin, N., & Akhtar, N. J. J. o. N. F. (2018). Microwave-assisted sustainable dyeing of wool fabric using cochineal-based carminic acid as natural colorant.
- Adeel, S., Rehman, F.-u.-., Hameed, A., Habib, N., Kiran, S., Zia, K. M., & Zuber, M. J. J. o. N. F. (2020). Sustainable extraction and dyeing of microwave-treated silk fabric using arjun bark colorant. *17*(5), 745-758.
- Adimule, V. M., Nandi, S. S., Kerur, S., Khadapure, S. A., & Chinnam, S. J. T. i. C. (2022). Recent Advances in the One-Pot Synthesis of Coumarin Derivatives from Different Starting Materials Using Nanoparticles: A Review. 1-31.
- Afzal, M., Gupta, G., Kazmi, I., Rahman, M., Upadhyay, G., Ahmad, K., Imam, F., Pravez, M., Anwar, F. J. B., & Pathology, A. (2012). Evaluation of anxiolytic activity of embelin isolated from *Embelia ribes*. *2*(2), 45-47.
- Aggarwal, S. (2021). Indian dye yielding plants: Efforts and opportunities. *Natural Resources Forum*, *45*(1), 63-86. doi:10.1111/1477-8947.12214

- Agrawal, K. K., Agrawal, N., Jadon, N., Gangwar, K., Jain, S., Sharma, N. J. R. J. o. P., & Technology. (2021). Determination of extractive value, phytochemical constituents and In-vitro anti-urolithiatic activity of *Embelia ribes burm. F.* and *Ipomea hederacea Jacq.* *14*(7), 3566-3570.
- Agrawal, S. J. I. J. o. L. S. (2015). Effect of embelin on reproductive organs of male albino rats. *5*(1), 1.
- Alawa, K., Ray, S., & Dubey, A. J. S. R. R. (2013). Dye yielding plants used by tribals of Dhar district, Madhya Pradesh, India. *3*, 30-32.
- Ali, S., Nisar, N., & Hussain, T. J. J. o. t. T. I. (2007). Dyeing properties of natural dyes extracted from eucalyptus. *98*(6), 559-562.
- Alihosseini, F. (2016). Plant-based compounds for antimicrobial textiles. In *antimicrobial textiles* (pp. 155-195): Elsevier.
- Alipieva, K., Simova, S., Zahmanov, G., Zhou, S., Wolfender, J.-L., & Georgiev, M. I. J. P. L. (2017). New tetraacetylated iridoid glycosides from *Sambucus ebulus L.* leaves. *20*, 429-432.
- Aluigi, A., Vineis, C., Ceria, A., Tonin, C. J. C. P. A. A. S., & Manufacturing. (2008). Composite biomaterials from fibre wastes: Characterization of wool–cellulose acetate blends. *39*(1), 126-132.
- Ammayappan, L., & Shakyawar, D. J. J. o. N. F. (2016). Dyeing of carpet woolen yarn using natural dye from cochineal. *13*(1), 42-53.
- Ananthapadmanaban, D. (2018). Summary of some selected characterization methods of geopolymers. In *Geopolymers and Other Geosynthetics*: IntechOpen.
- Andreu, G. L. P., Dos Reis, F. Z., González-Durruthy, M., Hernández, R. D., D'Vries, R. F., Berghe, W. V., & Alberici, L. C. J. T. i. V. (2020). Rapanone, a naturally occurring benzoquinone, inhibits mitochondrial respiration and induces HepG2 cell death. *63*, 104737.
- Anitha, R., Gunasekaran, M., Kumar, S. S., & Athimoolam, S. J. J. o. C. S. (2015). Structural and vibrational spectral studies on hydrogen bonded salts: 4-chloroanilinium maleate and nitrate. *127*(8), 1435-1450.
- Annapoorani, G., Sundarraaj, D. J. I. J. o. S., & Research. (2014). Dyeing of cotton and wool fabric using *Mirabilis jalapa* flower. *3*(7), 1126-1129.
- Araujo, C., Freire, C., Nolasco, M., Ribeiro-Claro, P., Rudic, S., Silvestre, A., & Vaz, P. J. B. (2018). Hydrogen bond dynamics of cellulose through inelastic neutron scattering spectroscopy. *19*(4), 1305-1313.

- Aravindhan, R., Sreelatha, T., Perumal, P., & Gnanamani, A. J. C. M. (2014). Synthesis, characterization and biological profile of metal and azo-metal complexes of embelin. *I(1)*, 69-79.
- Ardila-Leal, L. D., Poutou-Pinales, R. A., Pedroza-Rodriguez, A. M., & Quevedo-Hidalgo, B. E. (2021). A Brief History of Colour, the Environmental Impact of Synthetic Dyes and Removal by Using Laccases. *Molecules*, *26*(13). doi:10.3390/molecules26133813
- Arifeen, W. U., Rehman, F. U., Adeel, S., Zuber, M., Ahmad, M. N., & Ahmad, T. (2021). Environmental friendly extraction of walnut bark-based juglone natural colorant for dyeing studies of wool fabric. *Environ Sci Pollut Res Int*, *28*(36), 49958-49966. doi:10.1007/s11356-021-14277-8
- Arora, J., Agarwal, P., & Gupta, G. (2017). Rainbow of Natural Dyes on Textiles Using Plants Extracts: Sustainable and Eco-Friendly Processes. *Green and Sustainable Chemistry*, *07*(01), 35-47. doi:10.4236/gsc.2017.71003
- Arora, S. (2012). High-throughput quantification of pharmacologically active isoflavones using LC-UV/PDA and LC-MS/MS. In *Isoflavones* (pp. 218-243).
- Arputharaj, A., Raja, A. S. M., & Saxena, S. (2016). Developments in Sustainable Chemical Processing of Textiles. In *Green Fashion* (10.1007/978-981-10-0111-6_9pp. 217-252).
- Arthanareeswari, M., Harshil, H., Ganesh, M., & Mohankumar, R. J. M. T. P. (2021). Synthesis of Embelin-Fe complex from Embelia ribes fruits and characterization. *40*, S206-S209.
- Arvindekar, A., Laddha, K. J. I. c., & products. (2016). An efficient microwave-assisted extraction of anthraquinones from Rheum emodi: Optimisation using RSM, UV and HPLC analysis and antioxidant studies. *83*, 587-595.
- Asha, A., Mohan, A. S., Suma, S., Sudarsanakumar, M., & Kurup, M. P. J. J. o. M. S. (2017). Facile synthesis and spectral characterization of 2, 5-bis (cyclohexylamino)-1, 4-benzoquinone polymorphs from methyl and ethyl protocatechuic aldehydes. *1141*, 299-308.
- Asim, M., Jawaid, M., Paridah, M. T., Saba, N., Nasir, M., & Shahroze, R. M. J. P. C. (2019). Dynamic and thermo-mechanical properties of hybridized kenaf/PALF reinforced phenolic composites. *40*(10), 3814-3822.
- Aslam, U., Rao, V. G., Chavez, S., & Linic, S. J. N. C. (2018). Catalytic conversion of solar to chemical energy on plasmonic metal nanostructures. *1*(9), 656-665.
- Atlabachew, M., Mehari, B., Combrinck, S., & McCrindle, R. (2017). Single-step isolation of embelin using high-performance countercurrent chromatography and

determination of the fatty acid composition of seeds of *Embelia schimperi*. *Biomed Chromatogr*, 31(12). doi:10.1002/bmc.4018

- Awino, O. S., Kiprono, P. C., Keronei, K. P., Kaberia, F., & Obala, A. A. J. Z. f. N. C. (2008). Antimicrobial activity of 2, 5-dihydroxy-3-methyl-1, 4-benzoquinone from *Embelia schimperi*. 63(1-2), 47-50.
- Ayele, M., Tesfaye, T., Alemu, D., Limeneh, M., Sithole, B. J. S. C., & Pharmacy. (2020). Natural dyeing of cotton fabric with extracts from mango tree: A step towards sustainable dyeing. 17, 100293.
- Babič, A., Pascal, S., Duwald, R., Moreau, D., Lacour, J., & Allémann, E. J. A. F. M. (2017). [4] Helicene–Squalene Fluorescent Nanoassemblies for Specific Targeting of Mitochondria in Live-Cell Imaging. 27(33), 1701839.
- Badamaranahalli, S. S., Kopparam, M., Bhagawati, S. T., & Durg, S. J. E. j. o. p. s. (2015). Embelin lipid nanospheres for enhanced treatment of ulcerative colitis–Preparation, characterization and in vivo evaluation. 76, 73-82.
- Bae, T. W. J. P. o. (2020). Image-quality metric system for color filter array evaluation. 15(5), e0232583.
- Bafana, A., Devi, S. S., & Chakrabarti, T. J. E. R. (2011). Azo dyes: past, present and the future. 19(NA), 350-371.
- Bai, R., Yu, Y., Wang, Q., Shen, J., Yuan, J., & Fan, X. (2019). Chitosan-templated bio-coloration of cotton fabrics via laccase-catalyzed polymerization of hydroquinone. *Eng Life Sci*, 19(9), 643-654. doi:10.1002/elsc.201800132
- Bakker, H., & Skinner, J. J. C. r. (2010). Vibrational spectroscopy as a probe of structure and dynamics in liquid water. 110(3), 1498-1517.
- Balachandran, C., Duraipandiyam, V., Balakrishna, K., Sundaram, R. L., Vijayakumar, A., Ignacimuthu, S., & Al-Dhabi, N. A. (2013). Synthesis and medicinal properties of plant-derived vilangin. *Environmental Chemistry Letters*, 11(3), 303-308. doi:10.1007/s10311-013-0408-4
- Balachandran, C., Duraipandiyam, V., Balakrishna, K., Sundaram, R. L., Vijayakumar, A., Ignacimuthu, S., & Al-Dhabi, N. A. J. E. c. l. (2013). Synthesis and medicinal properties of plant-derived vilangin. 11(3), 303-308.
- Banchero, M. (2020). Recent advances in supercritical fluid dyeing. *Coloration Technology*, 136(4), 317-335. doi:10.1111/cote.12469
- Banchero, M. J. C. T. (2020). Recent advances in supercritical fluid dyeing. 136(4), 317-335.

- Banerjee, S., & Mazumdar, S. J. I. j. o. a. c. (2012). Electrospray ionization mass spectrometry: a technique to access the information beyond the molecular weight of the analyte. *2012*.
- Barani, H., Broumand, M. N., Haji, A., & Kazemipur, M. J. J. o. n. f. (2012). Optimization of dyeing wool fibers procedure with *Isatis tinctoria* by response surface methodology. *9*(2), 73-86.
- Bate-Smith, C. J. C. b. (1962). Flavonoid compounds. 755-809.
- Batisai, E., Ayamine, A., Kilinkissa, O. E., & Báthori, N. B. J. C. (2014). Melting point–solubility–structure correlations in multicomponent crystals containing fumaric or adipic acid. *16*(43), 9992-9998.
- Bechtold, T., Turcanu, A., Ganglberger, E., & Geissler, S. J. J. o. C. P. (2003). Natural dyes in modern textile dyehouses—how to combine experiences of two centuries to meet the demands of the future? , *11*(5), 499-509.
- Bhandari, N. L., Shrestha, S., Bhandari, G., Parajuli, N., Silwal, S. B., & Adhikari, R. J. E. J. o. C. (2021). Extraction of Dye from *Castanopsis indica* for Its Use in Textile Dyeing and Medicinal Purpose with Natural Mordant. *64*(11), 5-6.
- Bhavsar, P., Dalla Fontana, G., Tonin, C., Patrucco, A., Zoccola, M. J. D., & Pigments. (2020). Superheated water hydrolyses of waste silkworm pupae protein hydrolysate: a novel application for natural dyeing of silk fabric. *183*, 108678.
- Blackburn, R. S., Bechtold, T., & John, P. J. C. T. (2009). The development of indigo reduction methods and pre-reduced indigo products. *125*(4), 193-207.
- Bolm, C., & Hernández, J. G. J. A. C. I. E. (2019). Mechanochemistry of gaseous reactants. *58*(11), 3285-3299.
- Boonmung, S. (2003). *Evaluation of DRIFTS technique with PLS regression for determination of added mineral nitrogen in soil*: The University of Arizona.
- Borges, M., Tejera, R., Díaz, L., Esparza, P., & Ibáñez, E. J. F. C. (2012). Natural dyes extraction from cochineal (*Dactylopius coccus*). New extraction methods. *132*(4), 1855-1860.
- Borsoi, C., Zimmermann, M. V., Zattera, A. J., Santana, R., Ferreira, C. A. J. J. o. T. A., & Calorimetry. (2016). Thermal degradation behavior of cellulose nanofibers and nanowhiskers. *126*(3), 1867-1878.
- Boukir, A., Hajji, L., & Zghari, B. (2018). Effect of Moist and Dry Heat Weathering Conditions on Cellulose Degradation of Historical Manuscripts exposed to Accelerated Ageing: ¹³C NMR and FTIR Spectroscopy as a non-Invasive Monitoring Approach.

- Bouzeko, I. L. T., Ndontsa, B. L., Mba Nguekeu, Y. M., Awouafack, M. D., Wong, C. P., Simo Mpetga, J. D., Mbouangouere, R., Tane, P., & Morita, H. J. N. p. r. (2019). A new alkylbenzoquinone from *Embelia rowlandii* Gilg.(Myrsinaceae). *33*(13), 1909-1915.
- Brongersma, M. L., Halas, N. J., & Nordlander, P. J. N. n. (2015). Plasmon-induced hot carrier science and technology. *10*(1), 25-34.
- Brosdahl, D. J., Carpenter, J. M. J. J. o. t., apparel, t., & management. (2010). Consumer knowledge of the environmental impacts of textile and apparel production, concern for the environment, and environmentally friendly consumption behavior. *6*(4).
- Callemien, D., & Collin, S. J. J. o. t. A. S. o. B. C. (2008). Use of RP-HPLC-ESI (-)-MS/MS to differentiate various proanthocyanidin isomers in lager beer extracts. *66*(2), 109-115.
- Cao, H. Z., Yao, Y., Halada, G., Jung, H. J., & Kim, T. J. S. (2021). Impact of NaOH Concentration on Deweaving of Cotton Fabric in Aqueous Solutions. *13*(4), 2015.
- Chakraborty, J. (2011). Metal-complex dyes. In *Handbook of textile and industrial dyeing* (pp. 446-465): Elsevier.
- Chalbot, M.-C. G., & Kavouras, I. G. J. E. p. (2014). Nuclear magnetic resonance spectroscopy for determining the functional content of organic aerosols: A review. *191*, 232-249.
- Chandralekha, B., Hemamalini, R., Muthu, S., & Sevvanthi, S. J. J. o. M. S. (2020). Spectroscopic (FT-IR, FT-RAMAN, NMR, UV-Vis) investigations, computational analysis and molecular docking study of 5-bromo-2-hydroxy pyrimidine. *1218*, 128494.
- Che Kamarludin, S. N., Ubong, S., Idris, N., Azmi, I. S., Jainal, M. S., Jalil, R., Wan Omar, W. S. A., Zainal Mulok, T. E. T., Safaai, N. S. M., & Azizan, A. (2014). *Imidazolium-based Ionic Liquid Dissolution Influence on Crystallinity of Oil Palm Frond, Oil Palm Trunk and Elephant Grass Lignocellulosic Biomass*. Paper presented at the Advanced Materials Research.
- Chen, C., Zhang, F., Barras, J., Althoefer, K., Bhunia, S., Mandal, S. J. I. A. t. o. c. b., & bioinformatics. (2015). Authentication of medicines using nuclear quadrupole resonance spectroscopy. *13*(3), 417-430.
- Chen, J., Nikolovska-Coleska, Z., Wang, G., Qiu, S., Wang, S. J. B., & letters, m. c. (2006). Design, synthesis, and characterization of new embelin derivatives as potent inhibitors of X-linked inhibitor of apoptosis protein. *16*(22), 5805-5808.
- Chen, W.-H., Wang, C.-W., Ong, H. C., Show, P. L., & Hsieh, T.-H. J. F. (2019). Torrefaction, pyrolysis and two-stage thermodegradation of hemicellulose, cellulose and lignin. *258*, 116168.

- Chen, X., Gao, M., Jian, R., Hong, W. D., Tang, X., Li, Y., Zhao, D., Zhang, K., Chen, W., Zheng, X. J. J. o. e. i., & chemistry, m. (2020). Design, synthesis and α -glucosidase inhibition study of novel embelin derivatives. *35*(1), 565-573.
- Chengaiyah, B., Rao, K. M., Kumar, K. M., Alagusundaram, M., & Chetty, C. M. J. I. J. o. P. R. (2010). Medicinal importance of natural dyes-a review. *2*(1), 144-154.
- Chepkwony, S., Kiprono, P., & Lutta, S. J. I. J. A. C. (2014). Structure determination of nickel-embelin complex. *7*(7), 21-24.
- Cherutoi, J., Cheruiyot, L., & Kiprono, C. J. B. o. t. C. S. o. E. (2005). Synthesis and characterization of Zinc (II) and Copper (II) complexes of embelin. *19*(2), 295-299.
- Chiang, N., Ray, S., Lomax, J., Goertzen, S., Komarnytsky, S., Ho, C.-T., & Munafo, J. P. J. I. j. o. m. s. (2021). Modulation of Brain-Derived Neurotrophic Factor (BDNF) Signaling Pathway by Culinary Sage (*Salvia officinalis* L.). *22*(14), 7382.
- Chitra, M., Sukumar, E., Suja, V., & Devi, S. J. C. (1994). Antitumor, anti-inflammatory and analgesic property of embelin, a plant product. *40*(2), 109-113.
- Chung, C., Lee, M., & Choe, E. K. J. C. P. (2004). Characterization of cotton fabric scouring by FT-IR ATR spectroscopy. *58*(4), 417-420.
- Corrado, G., De Micco, V., Lucini, L., Miras-Moreno, B., Senizza, B., Zengin, G., El-Nakhel, C., De Pascale, S., & Roupheal, Y. J. F. i. P. S. (2021). Isosmotic Macrocation Variation Modulates Mineral Efficiency, Morpho-Physiological Traits, and Functional Properties in Hydroponically Grown Lettuce Varieties (*Lactuca sativa* L.). *12*, 1010.
- Coutelle, O., Hornig-Do, H. T., Witt, A., Andree, M., Schiffmann, L. M., Piekarek, M., Brinkmann, K., Seeger, J. M., Liwschitz, M., & Miwa, S. J. E. m. m. (2014). Embelin inhibits endothelial mitochondrial respiration and impairs neoangiogenesis during tumor growth and wound healing. *6*(5), 624-639.
- Cozzolino, D. J. J. o. t. S. o. F., & Agriculture. (2015). Sample presentation, sources of error and future perspectives on the application of vibrational spectroscopy in the wine industry. *95*(5), 861-868.
- Cristea, D., Vilarem, G. J. D., & pigments. (2006). Improving light fastness of natural dyes on cotton yarn. *70*(3), 238-245.
- Das, P. K. (2018). Aquatic and Marshland Dye Yielding Plants and Their Ethno-Medicinal Uses From Jhargram District, West Bengal, India.
- Das, P. K., & Mondal, A. K. J. I. J. o. C. R. (2012). Evaluation Of Antimicrobial Screening And Antimutagenic Activity Of Ethanolic Extract Of Some Selected Dye Yielding Plants Of South West Bengal, India. *4*(11), 145-153.

- Debebe, Y., Tefera, M., Mekonnen, W., Abebe, D., Woldekidan, S., Abebe, A., Belete, Y., Menberu, T., Belayneh, B., Tesfaye, B. J. B. c., & medicine, a. (2015). Evaluation of anthelmintic potential of the Ethiopian medicinal plant *Embelia schimperi* Vatke in vivo and in vitro against some intestinal parasites. *15*(1), 1-6.
- Degani, L., Gulmini, M., Piccablotto, G., Iacomussi, P., Gastaldi, D., Dal Bello, F., & Chiantore, O. J. J. o. C. H. (2017). Stability of natural dyes under light emitting diode lamps. *26*, 12-21.
- Delcambre, A., & Saucier, C. J. J. o. M. S. (2012). Identification of new flavan-3-ol monoglycosides by UHPLC-ESI-Q-TOF in grapes and wine. *47*(6), 727-736.
- Demarque, D. P., Crotti, A. E., Vessecchi, R., Lopes, J. L., & Lopes, N. P. J. N. P. R. (2016). Fragmentation reactions using electrospray ionization mass spectrometry: an important tool for the structural elucidation and characterization of synthetic and natural products. *33*(3), 432-455.
- Depciuch, J., Sowa-Kućma, M., Nowak, G., Dudek, D., Siwek, M., Styczeń, K., Parlińska-Wojtan, M. J. J. o. p., & analysis, b. (2016). Phospholipid-protein balance in affective disorders: Analysis of human blood serum using Raman and FTIR spectroscopy. A pilot study. *131*, 287-296.
- Devi, G. J. J. J. o. P. C. M. T. (2021). Quantitative phytochemical and chromatographic analysis of phenolic compounds in methanolic leaf extract of *Costus pictus* D. Don. 1-10.
- Diarsa, M., & Gupte, A. J. J. o. N. F. (2020). Optimization and Extraction of Natural Dye from *Tagetes Erecta* and Dyeing of Cotton and Silk Fabric Using Banana (*Musa Sp.*) Pseudo Stem Sap. 1-13.
- Ding, Y., & Freeman, H. S. J. C. T. (2017). Mordant dye application on cotton: optimisation and combination with natural dyes. *133*(5), 369-375.
- Ding, Y., Zhendong, W., Chuanxiong, Z., Ruobai, X., & Wenliang, X. J. T. R. J. (2021). A study on the applicability of pigment digital printing on cotton fabrics. 0040517521997926.
- Dou, J., Heinonen, J., Vuorinen, T., Xu, C., Sainio, T. J. S., & Technology, P. (2021). Chromatographic recovery and purification of natural phytochemicals from underappreciated willow bark water extracts. *261*, 118247.
- Dreesen, L., Humbert, C., Hollander, P., Mani, A. A., Ataka, K., Thiry, P. A., & Peremans, A. J. C. p. l. (2001). Study of the water/poly (ethylene glycol) interface by IR-visible sum-frequency generation spectroscopy. *333*(5), 327-331.
- Drivas, I., Blackburn, R. S., & Rayner, C. M. (2011). Natural anthraquinonoid colorants as platform chemicals in the synthesis of sustainable disperse dyes for polyesters. *Dyes and Pigments*, *88*(1), 7-17. doi:10.1016/j.dyepig.2010.04.009

- Drivas, I., Blackburn, R. S., Rayner, C. M. J. D., & Pigments. (2011). Natural anthraquinonoid colorants as platform chemicals in the synthesis of sustainable disperse dyes for polyesters. *88*(1), 7-17.
- Ebrahim, W., & Ebada, S. S. J. C. o. N. C. (2021). Antimicrobial Metabolites from Extremophilic Fungus *Botryotrichum piluliferum* Strain WESH19. *57*(4), 654-658.
- Echeverría, I., López-Caballero, M. E., Gómez-Guillén, M. C., Mauri, A. N., & Montero, M. P. J. I. j. o. f. m. (2018). Active nanocomposite films based on soy proteins-montmorillonite-clove essential oil for the preservation of refrigerated bluefin tuna (*Thunnus thynnus*) fillets. *266*, 142-149.
- Eifler, C., Diekamp, K. J. R. J. o. T., & Apparel. (2013). Consumer acceptance of sustainable fashion in Germany.
- Emam, H. E., Abdelhamid, H. N., Abdelhameed, R. M. J. D., & pigments. (2018). Self-cleaned photoluminescent viscose fabric incorporated lanthanide-organic framework (Ln-MOF). *159*, 491-498.
- Falcão, L., & Araújo, M. E. M. J. J. o. c. h. (2013). Tannins characterization in historic leathers by complementary analytical techniques ATR-FTIR, UV-Vis and chemical tests. *14*(6), 499-508.
- Fengel, D. (1992). Characterization of cellulose by deconvoluting the OH valency range in FTIR spectra.
- Fernandes, A., & Maharani, R. (2022). *The Potential of Production and Characteristic of Oleoresin Tapped from Dipterocarpus verrucosus as Natural Ingredient for Multi Purposes*. Paper presented at the 7th International Conference on Biological Science (ICBS 2021).
- Ferraz, E. R., Grando, M. D., & Oliveira, D. P. (2011). The azo dye Disperse Orange 1 induces DNA damage and cytotoxic effects but does not cause ecotoxic effects in *Daphnia similis* and *Vibrio fischeri*. *J Hazard Mater*, *192*(2), 628-633. doi:10.1016/j.jhazmat.2011.05.063
- Ferreira, F., Pinheiro, I., Gouveia, R., Thim, G., & Lona, L. J. P. c. (2018). Functionalized cellulose nanocrystals as reinforcement in biodegradable polymer nanocomposites. *39*, E9-E29.
- Festucci-Buselli, R. A., Otoni, W. C., & Joshi, C. P. J. B. J. o. P. P. (2007). Structure, organization, and functions of cellulose synthase complexes in higher plants. *19*(1), 1-13.
- Flamini, G., Najar, B., Leonardi, M., Ambryszewska, K. E., Cioni, P. L., Parri, F., Melai, B., & Pistelli, L. J. N. P. R. (2021). Essential oil composition of *Salvia rosmarinus* penn. wild samples collected from six sites and different seasonal periods in Elba Island (Tuscan Archipelago, Italy). 1-7.

- Fröse, A., Schmidtke, K., Sukmann, T., Juhász Junger, I., & Ehrmann, A. (2019). Application of natural dyes on diverse textile materials. *Optik*, *181*, 215-219. doi:10.1016/j.ijleo.2018.12.099
- Gala, S., Sumarno, S., & Mahfud, M. J. J. o. A. E. S. (2020). Comparison of microwave and conventional extraction methods for natural dyes in wood waste of mahogany (Swietenia mahagoni). *18*(4), 618-623.
- Gandhi, G. R., Stalin, A., Balakrishna, K., Ignacimuthu, S., Paulraj, M. G., & Vishal, R. J. B. e. B. A.-G. S. (2013). Insulin sensitization via partial agonism of PPAR γ and glucose uptake through translocation and activation of GLUT4 in PI3K/p-Akt signaling pathway by embelin in type 2 diabetic rats. *1830*(1), 2243-2255.
- Ganesan, P., & Karthik, T. J. T. J. o. T. T. I. (2017). Analysis of colour strength, colour fastness and antimicrobial properties of silk fabric dyed with natural dye from red prickly pear fruit. *108*(7), 1173-1179.
- Gashti, M. P., Rashidian, R., Almasian, A., Zohouri, A. B. J. P., & Technology, R. (2013). A novel method for colouration of cotton using clay nano-adsorbent treatment.
- Gautam, S., & Sharma, A. J. H. J. o. A. R. (2018). Bidens pilosa: a favourable natural colourant for cotton fabric printing. *44*(1&2), 75-79.
- Gautrot, J. E., Hodge, P., Cupertino, D., & Helliwell, M. J. N. J. o. C. (2006). Experimental evidence for carbonyl- π electron cloud interactions. *30*(12), 1801-1807.
- Geng, F., Hu, B., Li, C., Zhao, C., Lafon, O., Trébosc, J., Amoureux, J.-P., Shen, M., & Hu, B. J. J. o. M. C. A. (2020). Anionic redox reactions and structural degradation in a cation-disordered rock-salt Li 1.2 Ti 0.4 Mn 0.4 O 2 cathode material revealed by solid-state NMR and EPR. *8*(32), 16515-16526.
- Ghaheh, F. S., Mortazavi, S. M., Alihosseini, F., Fassihi, A., Nateri, A. S., & Abedi, D. J. J. o. C. P. (2014). Assessment of antibacterial activity of wool fabrics dyed with natural dyes. *72*, 139-145.
- Ghaly, A., Ananthashankar, R., Alhattab, M., & Ramakrishnan, V. J. J. C. E. P. T. (2014). Production, characterization and treatment of textile effluents: a critical review. *5*(1), 1-19.
- Gong, K., Rather, L. J., Zhou, Q., Wang, W., & Li, Q. J. T. J. o. T. T. I. (2020). Natural dyeing of merino wool fibers with Cinnamomum camphora leaves extract with mordants of biological origin: a greener approach of textile coloration. *111*(7), 1038-1046.
- Grancaric, A. M., Colleoni, C., Guido, E., Botteri, L., & Rosace, G. J. P. i. O. C. (2017). Thermal behaviour and flame retardancy of monoethanolamine-doped sol-gel coatings of cotton fabric. *103*, 174-181.

- Grishanov, S. (2011). Structure and properties of textile materials. In *Handbook of Textile and Industrial Dyeing* (10.1533/9780857093974.1.28pp. 28-63).
- Guan, J., Wei, R., Prlj, A., Peng, J., Lin, K. H., Liu, J., Han, H., Corminboeuf, C., Zhao, D., & Yu, Z. J. A. C. I. E. (2020). Direct Observation of Aggregation-Induced Emission Mechanism. *59*(35), 14903-14909.
- Gudala, S., Sharma, A., Rao, V. R., Kumar, A., & Penta, S. J. C. P. (2018). Recent developments in synthesis of embelin heterocyclic derivatives and their biological applications. *72*(5), 1065-1080.
- Guo, X. m., Jiang, C., & Shi, T. S. J. I. c. (2007). Prepared Chiral Nanorods of a Cobalt (II) Porphyrin Dimer and Studied Changes of UV-Vis and CD Spectra with Aggregate Morphologies under Different Temperatures. *46*(12), 4766-4768.
- Gupta, D., & Basak, S. J. J. o. a. p. s. (2010). Surface functionalization of wool using 172 nm UV excimer lamp. *117*(6), 3448-3453.
- Gupta, G., Kazmi, I., Afzal, M., Upadhyay, G., Singh, R., & Habtemariam, S. J. P. (2013). Antidepressant-like activity of Embelin isolated from *Embelia ribes*. *4*(1), 87-95.
- Gupta, G., Kumar, J. M., Garci, A., Nagesh, N., & Therrien, B. J. M. (2014). Exploiting natural products to build metalla-assemblies: The anticancer activity of embelin-derived Rh (III) and Ir (III) metalla-rectangles. *19*(5), 6031-6046.
- Gupta, K., Gupta, P., Singh, P., Singh, S., Agarwal, S. J. N. d. s., & challenges. (2006). Chemistry of natural dyes. 7-34.
- Gupta, V. K. J. C., natural, t. o., dyes, s., & pigments. (2019). Fundamentals of natural dyes and its application on textile substrates. 2019.
- Guyasa, B., Melaku, Y., & Endale, M. J. A. i. p. s. (2018). Antibacterial activity of two flavans from the stem bark of *Embelia schimperi*. *2018*.
- Haddar, W., Ben Ticha, M., Guesmi, A., Khoffi, F., & Durand, B. (2014). A novel approach for a natural dyeing process of cotton fabric with *Hibiscus mutabilis* (Gulzuba): process development and optimization using statistical analysis. *Journal of Cleaner Production*, *68*, 114-120. doi:10.1016/j.jclepro.2013.12.066
- Haji, A., Mehrizi, M. K., Sharifzadeh, J. J. F., & Polymers. (2016). Dyeing of wool with aqueous extract of cotton pods improved by plasma treatment and chitosan: optimization using response surface methodology. *17*(9), 1480-1488.
- Haji, A., & Rahimi, M. J. J. o. N. F. (2020). RSM optimization of wool dyeing with *Berberis thunbergii* DC leaves as a new source of natural dye. 1-14.
- Haji, A. J. C. T. (2020). Application of D-optimal design in the analysis and modelling of dyeing of plasma-treated wool with three natural dyes. *136*(2), 137-146.

- Hameed, I. H., Al-Rubaye, A. F., Kadhim, M. J. J. I. J. o. C. P. R., & Research. (2017). Uses of Nuclear Magnetic Resonance Spectroscopy Technique in Pharmaceutical Analysis: A Review. *8*(2), 79-84.
- Hamidian, H., Tagizadeh, R., Fozooni, S., Abbasalipour, V., Taheri, A., Namjou, M. J. B., & chemistry, m. (2013). Synthesis of novel azo compounds containing 5 (4H)-oxazolone ring as potent tyrosinase inhibitors. *21*(7), 2088-2092.
- Hao, F., Wang, X., & Mohammadnia, M. J. P. A. C. (2021). Preparation and Characterization of a Novel Magnetic Nano Catalyst for Synthesis and Antibacterial Activities of Novel Furan-2 (5 H)-Ones Derivatives. 1-15.
- Harborne, A. (1998). *Phytochemical methods a guide to modern techniques of plant analysis*: springer science & business media.
- Hasan, K. F., Hridam, D., Rahman, M. M., Morshed, M. N., Al Azad, S., Genyang, C. J. A. J. o. P. S., & Engineering. (2016). A review on antibacterial coloration agent's activity, implementation & efficiency to ensure the ecofriendly & green textiles. *4*(1), 39-59.
- Hassan, M. M., & Bhagvandas, M. J. J. o. c. p. (2017). Sustainable low liquor ratio dyeing of wool with acid dyes: Effect of auxiliaries on agglomeration of dye molecules in a dyebath and dyeing uniformity. *152*, 464-473.
- Hassan, M. M. J. R. A. (2020). Enhanced thermal stability, hydrophobicity, UV radiation resistance, and antibacterial properties of wool fabric treated with p-aminobenzenesulphonic acid. *10*(30), 17515-17523.
- Hattori, M., Kusumoto, I. T., Soga, M., & Namba, T. J. J. M. P. S. W.-Y. (1993). Screening of various Ayurvedic medicines for their inhibitory activities on reverse transcriptase and identification of arecatannins and embelin as major inhibitory substances from Areca catechu and Embelia ribes. *10*, 141-148.
- Hayashi, N., Ohnuma, T., Saito, Y., Higuchi, H., & Ninomiya, K. J. T. (2009). Structure and electronic properties of quinone dimers connected with acetylene and diacetylene linkages. *65*(18), 3639-3644.
- Hernandez-Zamora, M., & Martinez-Jeronimo, F. (2019). Exposure to the azo dye Direct blue 15 produces toxic effects on microalgae, cladocerans, and zebrafish embryos. *Ecotoxicology*, *28*(8), 890-902. doi:10.1007/s10646-019-02087-1
- Hore, P. J. (2015). *Nuclear magnetic resonance*: Oxford University Press, USA.
- Hospodarova, V., Singovszka, E., & Stevulova, N. J. A. j. o. a. c. (2018). Characterization of cellulosic fibers by FTIR spectroscopy for their further implementation to building materials. *9*(6), 303-310.

- Hosseinnezhad, M., Khosravi, A., Gharanjig, K., & Moradian, S. J. A. J. o. C. (2017). The comparison of spectra and dyeing properties of new azonaphthalimide with analogues azobenzene dyes on natural and synthetic polymers. *10*, S3284-S3291.
- Hsu, J.-L., Huang, S.-Y., Chow, N.-H., & Chen, S.-H. J. A. c. (2003). Stable-isotope dimethyl labeling for quantitative proteomics. *75*(24), 6843-6852.
- Hsueh, C. C., Wu, C. C., & Chen, B. Y. (2019). Polyphenolic compounds as electron shuttles for sustainable energy utilization. *Biotechnol Biofuels*, *12*, 271. doi:10.1186/s13068-019-1602-9
- Hu, Z., Zhang, L., Zhong, L., Zhou, Y., Xue, J., & Li, Y. J. C. p. (2019). Preparation of an antibacterial chitosan-coated biochar-nanosilver composite for drinking water purification. *219*, 290-297.
- Ibraheem, N. A., Hasan, M. M., Khan, R. Z., Mishra, P. K. J. A. J. o. s., & technology. (2012). Understanding color models: a review. *2*(3), 265-275.
- Ilyas, R. A., Sapuan, S. M., Ibrahim, R., Abrial, H., Ishak, M., Zainudin, E., Asrofi, M., Atikah, M. S. N., Huzaifah, M. R. M., Radzi, A. M. J. J. o. M. R., & Technology. (2019). Sugar palm (*Arenga pinnata* (Wurmb.) Merr) cellulosic fibre hierarchy: a comprehensive approach from macro to nano scale. *8*(3), 2753-2766.
- Irfan, M., Zhang, H., Syed, U., & Hou, A. J. J. o. C. P. (2018). Low liquor dyeing of cotton fabric with reactive dye by an eco-friendly technique. *197*, 1480-1487.
- Jabli, M., Almalki, S. G., & Agougui, H. J. I. j. o. b. m. (2020). An insight into methylene blue adsorption characteristics onto functionalized alginate bio-polymer gel beads with λ -carrageenan-calcium phosphate, carboxymethyl cellulose, and celite 545. *156*, 1091-1103.
- Jacob, J., Peter, G., Thomas, S., Haponiuk, J. T., & Gopi, S. J. I. j. o. b. m. (2019). Chitosan and polyvinyl alcohol nanocomposites with cellulose nanofibers from ginger rhizomes and its antimicrobial activities. *129*, 370-376.
- Jeske, H., Schirp, A., & Cornelius, F. J. T. a. (2012). Development of a thermogravimetric analysis (TGA) method for quantitative analysis of wood flour and polypropylene in wood plastic composites (WPC). *543*, 165-171.
- Jones, W. P., & Kinghorn, A. D. J. N. p. i. (2012). Extraction of plant secondary metabolites. 341-366.
- Joshi, R., Ghanty, T. K., & Mukherjee, T. J. J. o. M. S. (2009). Formation of semiquinone radical in the reaction of embelin (2, 5-dihydroxy-3-undecyl-1, 4-benzoquinone) with reductants as well as oxidants. Characterization by pulse radiolysis and structure investigation by quantum chemical study. *928*(1-3), 46-53.

- Jothi, D. J. A. R. J. (2008). Extraction of natural dyes from African marigold flower (*Tagetes erecta* L.) for textile coloration. *8*(2), 49-53.
- Joy, B., Kumar, S. N., Soumya, M., Radhika, A., Vibin, M., & Abraham, A. J. P. (2014). Embelin (2, 5-dihydroxy-3-undecyl-p-benzoquinone): a bioactive molecule isolated from *Embelia ribes* as an effective photodynamic therapeutic candidate against tumor in vivo. *21*(11), 1292-1297.
- Kabir, S. M. F., Chakraborty, S., Hoque, S. M. A., & Mathur, K. (2019). Sustainability Assessment of Cotton-Based Textile Wet Processing. *Clean Technologies, 1*(1), 232-246. doi:10.3390/cleantechnol1010016
- Kamble, V., Attar, U., Umdale, S., Nimbalkar, M., Ghane, S., & Gaikwad, N. (2020). Phytochemical analysis, antioxidant activities and optimized extraction of embelin from different genotypes of *Embelia ribes* Burm f.: a woody medicinal climber from Western Ghats of India. *Physiol Mol Biol Plants, 26*(9), 1855-1865. doi:10.1007/s12298-020-00859-2
- Kamble, V., & Gaikwad, N. J. A. J. P. C. R. (2016). Fourier Transform infrared spectroscopy spectroscopic studies in *Embelia ribes* burm. F.: a vulnerable medicinal plant. *9*(3), 41-47.
- Kamel, M. M., Abdelghaffar, F., & El-Zawahry, M. J. J. o. N. F. (2011). Eco-friendly dyeing of wool with a mixture of natural dyes. *8*(4), 289-307.
- Kandhasamy, S., Liang, B., Yang, D.-P., & Zeng, Y. J. A. A. B. M. (2021). Antibacterial Vitamin K3 Carnosine Peptide-Laden Silk Fibroin Electrospun Fibers for Improvement of Skin Wound Healing in Diabetic Rats.
- Kane, C. L. J. J. o. D. H. (2014). Synthetic Fluorescents: Day-Glo from Novelty to Norm. *27*(3), 256-277.
- Karabulut, K., Atav, R. J. F., & Polymers. (2020). Dyeing of cotton fabric with natural dyes without mordant usage Part I: determining the most suitable dye plants for dyeing and UV protective functionalization. *21*(8), 1773-1782.
- Kasiri, M. B., & Safapour, S. J. E. c. I. (2014). Natural dyes and antimicrobials for green treatment of textiles. *12*(1), 1-13.
- Kaur, V., Hallan, S. S., Nidhi, A., Mishra, N. J. A. J. o. P., & Pharmacology. (2015). Isolation of embelin from and evaluation of its anti-cancer potential in *Embelia ribes* breast cancer. *1*(1), 33-39.
- Kavya, R., Vivekanandan, O., Radhai, R. J. R. J. o. P., & Technology. (2015). Studies on the anti-fertility efficacy of Abrime and Embrelin, the compounds of plant origin on mouse testis and uterus. *8*(4), 369.

- Kawale, M., & Choudhary, A. J. B.-A. Q. J. o. L. S. (2009). Phytochemical analysis of some medicinal plants from Nagpur (Maharashtra State). *6*(2), 108-109.
- Khan, A. A., Iqbal, N., Adeel, S., Azeem, M., Batool, F., Bhatti, I. A. J. D., & Pigments. (2014). Extraction of natural dye from red calico leaves: Gamma ray assisted improvements in colour strength and fastness properties. *103*, 50-54.
- Khan, S. A., Khan, S. B., Khan, L. U., Farooq, A., Akhtar, K., & Asiri, A. M. (2018). Fourier transform infrared spectroscopy: fundamentals and application in functional groups and nanomaterials characterization. In *Handbook of Materials Characterization* (pp. 317-344): Springer.
- Khandelwal, S., Tailor, Y. K., & Kumar, M. J. J. o. M. L. (2016). Deep eutectic solvents (DESs) as eco-friendly and sustainable solvent/catalyst systems in organic transformations. *215*, 345-386.
- Khattab, T. A., Abdelrahman, M. S., Rehan, M. J. E. S., & Research, P. (2020). Textile dyeing industry: environmental impacts and remediation. *27*(4), 3803-3818.
- Kim, H., & Cho, M. J. C. r. (2013). Infrared probes for studying the structure and dynamics of biomolecules. *113*(8), 5817-5847.
- Kiprono, C., Midiwo, J., Kipkemboi, P., & Ladogana, S. J. B. o. t. C. S. o. E. (2004). Larvicidal benzoquinone from *Embelia schimperi*. *18*(1).
- Kiran, S., Hassan, A., Adeel, S., Qayyum, M. A., Yousaf, M. S., Abdullah, M., & Habib, N. J. I. T. (2020). Green dyeing of microwave treated silk using coconut coir based tannin natural dye. *71*(3), 227-234.
- Kleckner, I. R., Foster, M. P. J. B. e. B. A.-P., & Proteomics. (2011). An introduction to NMR-based approaches for measuring protein dynamics. *1814*(8), 942-968.
- Koklukaya, O., Carosio, F., Grunlan, J. C., Wagberg, L. J. A. a. m., & interfaces. (2015). Flame-retardant paper from wood fibers functionalized via layer-by-layer assembly. *7*(42), 23750-23759.
- Kovačević, Z., Sutlović, A., Matin, A., & Bischof, S. J. M. (2021). Natural dyeing of cellulose and protein fibers with the flower extract of *Spartium junceum* l. plant. *14*(15), 4091.
- Křížová, H. J. R. d. i. f. m. s. C. R., Ed. Kanina. (2015). Natural dyes: Their past, present, future and sustainability. 59-71.
- Kulkarni, S., Bodake, U., Pathade, G. J. U. J. o. E. R., & Technology. (2011). Extraction of Natural Dye from Chili (*Capsicum Annum*) for Textile Coloration. *1*(1).

- Kumar, S. G., & Devi, L. G. J. T. J. o. p. c. A. (2011). Review on modified TiO₂ photocatalysis under UV/visible light: selected results and related mechanisms on interfacial charge carrier transfer dynamics. *115*(46), 13211-13241.
- Lal, B., Mishra, N. J. I. J. o. P. S., & Research. (2013). Importance of *Embelia ribes*: An update. *4*(10), 3823.
- Lamblin, M., Sallustrau, A., Commandeur, C., Cresteil, T., Felpin, F.-X., & Dessolin, J. J. T. (2012). Synthesis and biological evaluation of hydrophilic embelin derivatives. *68*(24), 4655-4663.
- Laraib, S., Sharif, S., Bibi, Y., Nisa, S., Aziz, R., Qayyum, A. J. A. J. f. S., & Engineering. (2021). Phytochemical Analysis and Some Bioactivities of Leaves and Fruits of *Myrsine africana* Linn. *46*(1), 53-63.
- Le Troedec, M., Sedan, D., Peyratout, C., Bonnet, J. P., Smith, A., Guinebretiere, R., Gloaguen, V., Krausz, P. J. C. P. A. A. S., & Manufacturing. (2008). Influence of various chemical treatments on the composition and structure of hemp fibres. *39*(3), 514-522.
- Lee, J., Lee, H., Eom, S., & Kim, J. J. C. T. (2001). UV absorber aftertreatment to improve lightfastness of natural dyes on protein fibres. *117*(3), 134-138.
- Lei, W., Fang, C., Zhou, X., Yin, Q., Pan, S., Yang, R., Liu, D., & Ouyang, Y. J. C. p. (2018). Cellulose nanocrystals obtained from office waste paper and their potential application in PET packing materials. *181*, 376-385.
- Leng, E., Zhang, Y., Peng, Y., Gong, X., Mao, M., Li, X., & Yu, Y. J. F. (2018). In situ structural changes of crystalline and amorphous cellulose during slow pyrolysis at low temperatures. *216*, 313-321.
- Lewis, D. M. J. C. T. (2014). Developments in the chemistry of reactive dyes and their application processes. *130*(6), 382-412.
- Li, Y., Dong, C., Xu, M.-J., & Lin, W.-H. J. J. o. A. N. P. R. (2019). New alkylated benzoquinones from mangrove plant *Aegiceras corniculatum* with anticancer activity.
- Li, Y., Zhao, C., Lu, C., Zhou, S., Tian, G., He, L., Bao, Y., Fauconnier, M.-L., Xiao, H., & Zheng, J. J. F. C. (2021). Simultaneous determination of 14 bioactive citrus flavonoids using thin-layer chromatography combined with surface enhanced Raman spectroscopy. *338*, 128115.
- Liu, R., Zhu, G., & Zhang, G. J. R. A. (2020). N-Substitution of acridone with electron-donating groups: crystal packing, intramolecular charge transfer and tuneable aggregation induced emission. *10*(12), 7092-7098.

- Lozano-Grande, M. A., Gorinstein, S., Espitia-Rangel, E., Dávila-Ortiz, G., & Martínez-Ayala, A. L. J. I. j. o. a. (2018). Plant sources, extraction methods, and uses of squalene. *2018*.
- Lukhele, T. (2012). *Isolation, characterisation and biological activity of some compounds from rapanea melanophloeos (L.) Mez*: University of Johannesburg (South Africa).
- Ma, X., Wei, Y., Wang, S., Zuo, X., & Shen, B. J. T. R. J. (2020). Sustainable ultrasound-assisted ultralow liquor ratio dyeing of cotton fabric with natural turmeric dye. *90*(5-6), 685-694.
- Mabasa, X., Mathomu, L., Madala, N., Musie, E., & Sigidi, M. J. B. R. I. (2021). Molecular Spectroscopic (FTIR and UV-Vis) and Hyphenated Chromatographic (UHPLC-qTOF-MS) Analysis and In Vitro Bioactivities of the Momordica balsamina Leaf Extract. *2021*.
- Machocho, A. K., Kiprono, P. C., Grinberg, S., & Bittner, S. J. P. (2003). Pentacyclic triterpenoids from *Embelia schimperi*. *62*(4), 573-577.
- Mahendran, S., Badami, S., Ravi, S., Thippeswamy, B., & Veerapur, V. J. P. C. J. (2011). Antioxidant, analgesic and anti-inflammatory properties of new ninhydrin adduct of embelin. *45*(9), 547-551.
- Mahendran, S., Badami, S., Ravi, S., Thippeswamy, B. S., & Veerapur, V. P. (2011). Antioxidant, analgesic and anti-inflammatory properties of new ninhydrin adduct of embelin. *Pharmaceutical Chemistry Journal*, *45*(9), 547-551. doi:10.1007/s11094-011-0676-x
- Mahendran, S., Badami, S., Ravi, S., Thippeswamy, B. S., Veerapur, V. P. J. C., & Bulletin, P. (2011). Synthesis and evaluation of analgesic and anti-inflammatory activities of most active free radical scavenging derivatives of Embelin—A Structure–Activity relationship. *59*(8), 913-919.
- Mahendran, S., Thippeswamy, B., Veerapur, V., & Badami, S. J. P. (2011). Anticonvulsant activity of embelin isolated from *Embelia ribes*. *18*(2-3), 186-188.
- Maithili, V., Dhanabal, S., Mahendran, S., & Vadivelan, R. J. I. j. o. p. (2011). Antidiabetic activity of ethanolic extract of tubers of *Dioscorea alata* in alloxan induced diabetic rats. *43*(4), 455.
- Manguro, L. O. A., Ugi, I., & Lemen, P. J. B. o. t. C. S. o. E. (2004). Further flavonol glycosides of *Embelia schimperi* leaves. *18*(1).
- Mansa, R., & Zou, S. J. E. A. (2021). Thermogravimetric analysis of microplastics: A mini review. *5*, 100117.

- Manyim, S., Kiprof, A. K., Mwasiagi, J. I., Achisa, C. M., Odero, M. P. J. R. J. o. T., & Apparel. (2021). Dyeing of cotton fabric with *Euclea divinorum* extract using response surface optimization method.
- Manyim, S., Kiprof, A. K., Mwasiagi, J. I., & Mecha, A. C. (2021). Eco-Friendly Dyeing of Pretreated Cotton Fabric Using a Natural Dye Extract from *Erythrina abyssinica*. *Journal of Natural Fibers*, 10.1080/15440478.2021.1964125, 1-13. doi:10.1080/15440478.2021.1964125
- Mariselvam, R., Ranjitsingh, A., Mosae Selvakumar, P., Krishnamoorthy, R., Alshatwi, A. A. J. F., & Polymers. (2017). Eco friendly natural dyes from *Syzygium cumini* (L)(Jambolan) fruit seed endosperm and to preparation of antimicrobial fabric and their washing properties. *18*(3), 460-464.
- Martineau, C. J. S. s. n. m. r. (2014). NMR crystallography: Applications to inorganic materials. *63*, 1-12.
- Martínez, M. J. A., & Benito, P. B. J. S. i. N. P. C. (2005). Biological activity of quinones. *30*, 303-366.
- Mathew, S., kumar Prasad, A., Benoy, T., Rakesh, P., Hari, M., Libish, T., Radhakrishnan, P., Nampoori, V., & Vallabhan, C. J. J. o. f. (2012). UV-visible photoluminescence of TiO₂ nanoparticles prepared by hydrothermal method. *22*(6), 1563-1569.
- Melo, M. J. J. H. o. n. c. (2009). History of natural dyes in the ancient mediterranean world. *3-20*.
- Merdan, N., Eyupoglu, S., & Duman, M. N. (2017). Ecological and sustainable natural dyes. In *Textiles and Clothing Sustainability* (pp. 1-41): Springer.
- Miah, M. R., Telegin, F. Y., Miah, M. S., Shahid, M. A., Rahman, M. S., Ran, J. J. I. j. o. p., & photobiology. (2017). Comparative analysis of colour strength and fastness properties on extracts natural dye from onion's outer shell and its use in eco-friendly dyeing of silk fabric. *2*(1), 1-8.
- Misra, H., Rajpurohit, Y., & Khairnar, N. J. J. o. b. (2012). Pyrroloquinoline-quinone and its versatile roles in biological processes. *37*(2), 313-325.
- Mizera, K., Ryszkowska, J. J. J. o. E., & Plastics. (2019). Thermal properties of polyurethane elastomers from soybean oil-based polyol with a different isocyanate index. *51*(2), 157-174.
- Mizoguchi, H., Woodward, P. M., Park, C.-H., & Keszler, D. A. J. J. o. t. A. C. S. (2004). Strong near-infrared luminescence in BaSnO₃. *126*(31), 9796-9800.
- Mohajer, S., Taha, R., Azmi, S. Z. J. P., & Technology, R. (2016). Phytochemical screening and potential of natural dye colourant from pomegranate (*Punica granatum* L.).

- Mollica Nardo, V., Cassone, G., Ponterio, R. C., Saija, F., Sponer, J., Tommasini, M., & Trusso, S. J. T. J. o. P. C. A. (2020). Electric-field-induced effects on the dipole moment and vibrational modes of the centrosymmetric indigo molecule. *124*(51), 10856-10869.
- Mondal, J. A., Nihonyanagi, S., Yamaguchi, S., & Tahara, T. J. J. o. t. A. C. S. (2012). Three distinct water structures at a zwitterionic lipid/water interface revealed by heterodyne-detected vibrational sum frequency generation. *134*(18), 7842-7850.
- Mongkholrattanasit, R., Kryštůfek, J., Wiener, J., Viková, M. J. F., & Europe, T. i. E. (2011). Dyeing, fastness, and UV protection properties of silk and wool fabrics dyed with eucalyptus leaf extract by the exhaustion process.
- Mongkholrattanasit, R., Nakpathom, M., Vuthiganond, N. J. S. C., & Pharmacy. (2021). Eco-dyeing with biocolorant from spent coffee ground on low molecular weight chitosan crosslinked cotton. *20*, 100389.
- Moreira, B. O., Barbosa Filho, M. R. D., de Carvalho, A. L., da Silva, D. G., Cruz, M. P., Yatsuda, R., & David, J. M. J. J. o. C. (2020). Application of response surface methodology for optimization of ultrasound-assisted solid-liquid extraction of phenolic compounds from *Cenostigma macrophyllum*. *34*(10), e3290.
- Mozaffari, E., Maleki, B. J. C. T. i. F. T., & Engineering, T. (2018). Alum mineral and the importance for textile dyeing. *3*(4), 2577-2929.
- Musharraf, S. G., Ali, A., Khan, N. T., Yousuf, M., & Choudhary, M. I. J. S. (2013). Tandem mass spectrometry approach for the investigation of the steroidal metabolism: Structure–fragmentation relationship (SFR) in anabolic steroids and their metabolites by ESI-MS/MS analysis. *78*(2), 171-181.
- Naima, R., Oumam, M., Hannache, H., Sesbou, A., Charrier, B., Pizzi, A., Charrier–El Bouhtoury, F. J. I. C., & Products. (2015). Comparison of the impact of different extraction methods on polyphenols yields and tannins extracted from Moroccan *Acacia mollissima* barks. *70*, 245-252.
- Nambela, L., Haule, L. V., & Mgani, Q. J. J. o. C. P. (2020). A review on source, chemistry, green synthesis and application of textile colorants. *246*, 119036.
- Naveed, R., Bhatti, I. A., Adeel, S., Ashar, A., Sohail, I., Khan, M. U. H., Masood, N., Iqbal, M., & Nazir, A. J. J. o. N. F. (2020). Microwave-Assisted extraction and dyeing of cotton fabric with mixed natural dye from pomegranate rind (*punica granatum L.*) and turmeric rhizome (*curcuma longa L.*). 1-8.
- Ndukwe, I., Bello, A., Habila, J., & John, C. J. A. J. o. B. (2007). Phytochemical and antimicrobial screening of the crude petroleum spirit and methanol extracts of the stem bark, leaves and roots of *Ficus thoningii* (blume). *6*(23).

- Ngamwonglumlert, L., Devahastin, S., Chiewchan, N. J. C. r. i. f. s., & nutrition. (2017). Natural colorants: Pigment stability and extraction yield enhancement via utilization of appropriate pretreatment and extraction methods. *57*(15), 3243-3259.
- Norgard, J., & Best, G. L. (2017). The electromagnetic spectrum. In *National Association of Broadcasters Engineering Handbook* (pp. 3-10): Routledge.
- Odero, M. P., Kiprop, A. K., K'Owino, I. O., Arimi, M., Manyim, S. J. R. J. o. T., & Apparel. (2020). Evaluation of dyeing properties of natural dyes extracted from the heartwood of *Prosopis juliflora* on cotton fabric.
- Oh, J. H., & Park, C. H. J. A. M. I. (2020). Colorful Fluorine-Free Superhydrophobic Polyester Fabric Prepared via Disperse Dyeing Process. *7*(10), 2000127.
- Ohno, Y. J. I.-N. B. L. E. D., & Applications. (2017). Color Quality of White LEDs. 457-480.
- Omara, T., Kiprop, A. K., & Kosgei, V. J. (2021). Intraspecific Variation of Phytochemicals, Antioxidant, and Antibacterial Activities of Different Solvent Extracts of *Albizia coriaria* Leaves from Some Agroecological Zones of Uganda. *Evid Based Complement Alternat Med*, 2021, 2335454. doi:10.1155/2021/2335454
- Omorogie, M. O., Naidoo, E. B., Ofomaja, A. E. J. M. E. S., & Environment. (2017). Response surface methodology, central composite design, process methodology and characterization of pyrolyzed KOH pretreated environmental biomass: mathematical modelling and optimization approach. *3*(3), 1171-1186.
- Omosa, L. K., Midiwo, J. O., Mbaveng, A. T., Tankeo, S. B., Seukep, J. A., Voukeng, I. K., Dzatam, J. K., Isemeki, J., Derese, S., & Omolle, R. A. J. S. (2016). Antibacterial activities and structure–activity relationships of a panel of 48 compounds from Kenyan plants against multidrug resistant phenotypes. *5*(1), 1-15.
- Onoji, S. E., Iyuke, S. E., Igbafe, A. I. J. E., & Fuels. (2016). Hevea brasiliensis (rubber seed) oil: extraction, characterization, and kinetics of thermo-oxidative degradation using classical chemical methods. *30*(12), 10555-10567.
- Opanasenko, M., Dhakshinamoorthy, A., Shamzhy, M., Nachtigall, P., Horáček, M., Garcia, H., Čejka, J. J. C. S., & Technology. (2013). Comparison of the catalytic activity of MOFs and zeolites in Knoevenagel condensation. *3*(2), 500-507.
- Opata, M. R., & Dreuw, A. J. T. J. o. P. C. B. (2021). Embelin's versatile photochemistry makes it a potent photosensitizer for photodynamic therapy. *125*(14), 3527-3537.
- Ortiz, D., Salpin, J.-Y., Song, K., & Spezia, R. J. I. J. o. M. S. (2014). Galactose-6-Sulfate collision induced dissociation using QM+ MM chemical dynamics simulations and ESI-MS/MS experiments. *358*, 25-35.

- Otegui, M., Gaspar, M., Maldonado, S., Varetti, E., & Pollero, R. J. N. J. o. B. (1998). Studies on tissues associated to hydroxybenzoquinone secretion in *Myrsine laetevirens* (Myrsinaceae). *18*(4), 447-459.
- Otłowska, O., Ślebioda, M., Kot-Wasik, A., Karczewski, J., & Śliwka-Kaszyńska, M. J. M. (2018). Chromatographic and spectroscopic identification and recognition of natural dyes, uncommon dyestuff components, and mordants: Case study of a 16th century carpet with chintamani motifs. *23*(2), 339.
- Ozougwu, S. U., & Anyakoha, E. U. J. A. J. o. A. R. (2016). Acceptability of cotton fabric treated with dye extracted from Roselle (*Hibiscus sabdariffa*) calyces based on its phytochemical composition and evaluation of organoleptic attributes. *11*(33), 3074-3081.
- Panichayupakaranant, P., Tewtrakul, S., & Yuenyongsawad, S. J. F. C. (2010). Antibacterial, anti-inflammatory and anti-allergic activities of standardised pomegranate rind extract. *123*(2), 400-403.
- Parvinzadeh Gashti, M., Katozian, B., Shaver, M., & Kiumarsi, A. J. C. T. (2014). Clay nanoadsorbent as an environmentally friendly substitute for mordants in the natural dyeing of carpet piles. *130*(1), 54-61.
- Patel, B. (2011). Natural dyes. In *Handbook of textile and industrial dyeing* (pp. 395-424): Elsevier.
- Patel, B., Kanade, P. J. S. C., & Pharmacy. (2021). Iron-tannin complex effect on coloration and functional properties of silk fabric. *22*, 100490.
- Patil, S., & SA, K. J. B. f. (2012). Phytochemical screening, antibacterial and antioxidant activity of *Limonia acidissima* (L). *5*, 131-133.
- Paul, C. K., Gathigia, N. A., Keronei, K., Obala, A., & Ambrose, A. J. J. A. P. A. S. T. (2011). Antimicrobial activity of emblem from *Embelia shimperi* and its Synthetic derivatives. *7*, 25-29.
- Pawar, A., Biranje, S., Patankar, K., Adivarekar, R. V. J. R. J. o. T., & Apparel. (2020). Statistical modelling for optimisation of dyeing of silk with semisynthetic azo dye made by chemical modification of areca nut.
- Pawar, A. B., More, S. P., Adivarekar, R. J. N. p., & bioprospecting. (2018). Dyeing of polyester and nylon with semi-synthetic azo dye by chemical modification of natural source areca nut. *8*(1), 23-29.
- Pawar, A. B., More, S. P., & Adivarekar, R. V. (2018). Dyeing of Polyester and Nylon with Semi-synthetic Azo Dye by Chemical Modification of Natural Source Areca Nut. *Nat Prod Bioprospect*, *8*(1), 23-29. doi:10.1007/s13659-017-0144-8

- Peggie, D. A., Kirby, J., Poulin, J., Genuit, W., Romanuka, J., Wills, D. F., De Simone, A., & Hulme, A. N. J. A. m. (2018). Historical mystery solved: a multi-analytical approach to the identification of a key marker for the historical use of brazilwood (*Caesalpinia* spp.) in paintings and textiles. *10*(6), 617-623.
- Peña, R., Martín, P., Feresin, G. E., Tapia, A., Machin, F., & Estevez-Braun, A. J. J. o. n. p. (2016). Domino synthesis of embelin derivatives with antibacterial activity. *79*(4), 970-977.
- Penas, P. P., Mayer, M. P., Gomes, B. P., Endo, M., Pignatari, A. C., Bauab, K. C., & Pinheiro, E. T. J. J. o. E. (2013). Analysis of genetic lineages and their correlation with virulence genes in *Enterococcus faecalis* clinical isolates from root canal and systemic infections. *39*(7), 858-864.
- Phan, K., Van Den Broeck, E., Van Speybroeck, V., De Clerck, K., Raes, K., De Meester, S. J. D., & Pigments. (2020). The potential of anthocyanins from blueberries as a natural dye for cotton: A combined experimental and theoretical study. *176*, 108180.
- Pisitsak, P., Hutakamol, J., Jeenapak, S., Wanmanee, P., Nuammaiphum, J., & Thongcharoen, R. (2016). Natural dyeing of cotton with *Xylocarpus granatum* bark extract: Dyeing, fastness, and ultraviolet protection properties. *Fibers and Polymers*, *17*(4), 560-568. doi:10.1007/s12221-016-5702-x
- Poojari, R. J. E. o. o. i. d. (2014). Embelin—a drug of antiquity: shifting the paradigm towards modern medicine. *23*(3), 427-444.
- Prabhavathi, R., Devi, A. S., Anitha, D. J. I. J. o. P., & Engineering, T. (2014). Improving the color fastness of the selected natural dyes on cotton (improving the sunlight fastness and wash fastness of the eucalyptus bark dye on cotton). *1*(4), 27-30.
- Prabhu, K., & Bhute, A. S. J. J. N. P. P. R. (2012). Plant based natural dyes and mordants: A Review. *2*(6), 649-664.
- Prabhu, K., Teli, M., Waghmare, N. G. J. F., & Polymers. (2011). Eco-friendly dyeing using natural mordant extracted from *Emblica officinalis* G. Fruit on cotton and silk fabrics with antibacterial activity. *12*(6), 753-759.
- Radhakrishnan, N., Gnanamani, A., Mandal, A. J. B., & medicine. (2011). A potential antibacterial agent Embelin, a natural benzoquinone extracted from *Embelia ribes*. *3*(2), 1-7.
- Radhakrishnan, N., & Gnanamani, A. J. I. J. P. P. S. (2014). 2, 5-dihydroxy-3-undecyl-1, 4-benzoquinone (Embelin)-A second solid gold of India-A Review. *6*(2), 23-30.
- Radhakrishnan, N., Kavitha, V., & Gnanamani, A. J. J. C. P. R. (2013). Studies on synthesis, characterization and biological properties of copper (II) embelin complex. *5*(10), 72-77.

- Radhakrishnan, N., Kavitha, V., Raja, S., Gnanamani, A., & Mandal, A. J. J. A. C. (2011). Embelin-A natural potential cosmetic agent. *29*(2), 99-107.
- Rahman, M. H. (2020). *Production of functional textile filaments from chemically modified cellulose fibers.*
- Ramaraj, R., & Unpaprom, Y. J. B. (2019). Optimization of pretreatment condition for ethanol production from *Cyperus difformis* by response surface methodology. *9*(6), 1-9.
- Ranganath, M., Vipin, H. J. I. J. o. E. T., & Engineering, A. (2014). Optimization of process parameters in turning operation using response surface methodology: a review. *4*(10), 351-360.
- Rather, L. J., Ali, A., Zhou, Q., Ganie, S. A., Gong, K., Haque, Q. M. R., & Li, Q. J. J. o. C. P. (2020). Instrumental characterization of merino wool fibers dyed with *Cinnamomum camphora* waste/fallen leaves extract: An efficient waste management alternative. *273*, 123021.
- Rather, L. J., Shabbir, M., Mohammad, F., Shahid, M., Tang, R., Chen, G. J. I. h. o. t. c., & finishing. (2017). Physico-chemical aspects of wool dyeing: Adsorption, kinetics, and thermodynamics. 143-161.
- Rehman, A., Iqbal, K., Azam, F., Safdar, F., Ashraf, M., Maqsood, H. S., & Basit, A. J. T. J. o. T. T. I. (2021). To enhance the dyeability of cotton fiber with the application of reactive dyes by using chitosan. *112*(8), 1208-1212.
- Ren, Y., Gong, J., Fu, R., Zhang, J., Fang, K., & Liu, X. (2018). Antibacterial dyeing of silk with prodigiosins suspension produced by liquid fermentation. *Journal of Cleaner Production*, *201*, 648-656.
- Repon, M. R., Al Mamun, M. A., & Islam, M. T. J. U. J. o. E. S. (2016). Eco-friendly cotton coloration using banana (*Musa sapientum*) waste: optimization of dyeing temperature. *4*(1), 14-20.
- Repon, M. R., Islam, M. T., Al Mamun, M. A. J. F., & Textiles. (2017). Ecological risk assessment and health safety speculation during color fastness properties enhancement of natural dyed cotton through metallic mordants. *4*(1), 1-17.
- Rondevaldova, J., Leuner, O., Teka, A., Lulekal, E., Havlik, J., Van Damme, P., Kokoska, L. J. E.-B. C., & Medicine, A. (2015). In vitro antistaphylococcal effects of *Embelia schimperii* extracts and their component embelin with oxacillin and tetracycline. *2015*.
- Ross, C. L. J. G. a. i. h., & medicine. (2019). RETRACTED: Energy Medicine: Current Status and Future Perspectives. *8*, 2164956119831221.

- Roy Choudhury, A. K. J. T. P. (2013). Green chemistry and the textile industry. *45*(1), 3-143.
- Rozina, Ahmad, M., Zafar, M., Yousaf, Z., Ullah, S. A., Sultana, S., & Bibi, F. (2022). Identification of novel, non-edible oil seeds via scanning electron microscopy as potential feedstock for green synthesis of biodiesel. *Microsc Res Tech*, *85*(2), 708-720. doi:10.1002/jemt.23942
- Sadeghi-Kiakhani, M., Tehrani-Bagha, A. R., Safapour, S., Eshaghloo-Galugahi, S., & Etezzad, S. M. (2020). Ultrasound-assisted extraction of natural dyes from Hawthorn fruits for dyeing polyamide fabric and study its fastness, antimicrobial, and antioxidant properties. *Environment, Development and Sustainability*, *23*(6), 9163-9180. doi:10.1007/s10668-020-01017-0
- Safapour, S., Sadeghi-Kiakhani, M., Eshaghloo-Galugahi, S. J. F., & Polymers. (2018). Extraction, Dyeing, and antibacterial properties of crataegus elbursensis fruit natural dye on wool yarn. *19*(7), 1428-1434.
- Salama, A. J. I. J. o. B. M. (2020). Cellulose/silk fibroin assisted calcium phosphate growth: Novel biocomposite for dye adsorption. *165*, 1970-1977.
- Salomon, L., Lorenz, P., Ehrmann, B., Spring, O., Stintzing, F. C., & Kammerer, D. R. J. P. (2021). Impact of Environmental Conditions on Growth and the Phenolic Profile of *Achillea atrata* L. *9*(5), 853.
- Samanta, A. K., & Agarwal, P. (2009). Application of natural dyes on textiles.
- Samanta, A. K., & Konar, A. J. N. d. (2011). Dyeing of textiles with natural dyes. *3*(30-56).
- Samanta, K. K., Pandit, P., Samanta, P., & Basak, S. (2019). Water consumption in textile processing and sustainable approaches for its conservation. In *Water in textiles and fashion* (pp. 41-59): Elsevier.
- Samatha, S., Vasudevan, T. J. J. O. S., & RESEARCH, I. (1996). Natural hair dyes. *55*(11), 885-887.
- Santmartí, A., & Lee, K.-Y. (2018). Crystallinity and thermal stability of nanocellulose. In *Nanocellulose and sustainability* (pp. 67-86): CRC Press.
- Saxena, S., & Raja, A. (2014). Natural dyes: sources, chemistry, application and sustainability issues. In *Roadmap to sustainable textiles and clothing* (pp. 37-80): Springer.
- Saxena, S., & Raja, A. S. M. (2014). Natural Dyes: Sources, Chemistry, Application and Sustainability Issues. In *Roadmap to Sustainable Textiles and Clothing* (10.1007/978-981-287-065-0_2pp. 37-80).

- Schneider-Coppolino, M., Gautam, S., & Gates, B. D. (2022). Nanocatalysts for proton exchange fuel cells: design, preparation, and utilization. In *PEM Fuel Cells* (pp. 465-545): Elsevier.
- Schug, K., & McNair, H. M. J. J. o. C. A. (2003). Adduct formation in electrospray ionization mass spectrometry: II. Benzoic acid derivatives. *985*(1-2), 531-539.
- Sekar, M. J. I. J. o. G. P. (2019). Formulation and evaluation of embelin emulgel for topical delivery. *13*(01).
- Shabbir, M., Rather, L. J., Bukhari, M. N., Shahid, M., Khan, M. A., & Mohammad, F. J. J. o. a. r. (2016). An eco-friendly dyeing of woolen yarn by Terminalia chebula extract with evaluations of kinetic and adsorption characteristics. *7*(3), 473-482.
- Shabbir, M., Rather, L. J., Bukhari, M. N., Ul-Islam, S., Shahid, M., Khan, M. A., & Mohammad, F. (2017). Light Fastness and Shade Variability of Tannin Colorant Dyed Wool with the Effect of Mordanting Methods. *Journal of Natural Fibers*, *16*(1), 100-113. doi:10.1080/15440478.2017.1408521
- Shabbir, M., Rather, L. J., Bukhari, M. N., Ul-Islam, S., Shahid, M., Khan, M. A., & Mohammad, F. J. J. o. N. F. (2019). Light fastness and shade variability of tannin colorant dyed wool with the effect of mordanting methods. *16*(1), 100-113.
- Shafiq, F., Siddique, A., Pervez, M., Hassan, M. M., Naddeo, V., Cai, Y., Hou, A., Xie, K., Khan, M. Q., & Kim, I.-S. J. M. (2021). Extraction of Natural Dye from Aerial Parts of Argy Wormwood Based on Optimized Taguchi Approach and Functional Finishing of Cotton Fabric. *14*(19), 5850.
- Shahid, M., & Mohammad, F. J. J. o. c. p. (2013). Perspectives for natural product based agents derived from industrial plants in textile applications—a review. *57*, 2-18.
- Shaikh, A., Dhadde, S. B., Durg, S., Veerapur, V., Badami, S., Thippeswamy, B., & Patil, J. S. J. P. R. (2016). Effect of Embelin Against Lipopolysaccharide-induced Sickness Behaviour in Mice. *30*(5), 815-822.
- Shankar, R., Lavekar, G., Deb, S., Sharma, B., Rawat, M. J. I. J. o. B., & Conservation. (2012). Distribution, conservation and folk uses of Vaibidang (*Embelia ribes* Burm. f.). *4*(13), 525-529.
- Sharma, A., & Jain, R. (2013). Application of natural dyes: an emerging environment-friendly solution to handmade paper industry. In *Biotechnology for Environmental Management and Resource Recovery* (pp. 279-288): Springer.
- Sharma, V., McKone, H. T., & Markow, P. G. J. J. o. C. E. (2011). A global perspective on the history, use, and identification of synthetic food dyes. *88*(1), 24-28.
- Sheikh, J., Jagtap, P. S., Teli, M. J. F., & Polymers. (2016). Ultrasound assisted extraction of natural dyes and natural mordants vis a vis dyeing. *17*(5), 738-743.

- Shen, J. (2019). Enzymatic treatment of wool and silk fibers. In *Advances in textile biotechnology* (pp. 77-105): Elsevier.
- Shi, J., Nawaz, H., Pohorly, J., Mittal, G., Kakuda, Y., & Jiang, Y. J. F. r. i. (2005). Extraction of polyphenolics from plant material for functional foods—Engineering and technology. *21*(1), 139-166.
- Shin, Y., & Yoo, D. J. J. C. C. (2010). Green chemistry in natural dyeing: Application of chitosan for dyeing protein/cellulose blend fabric. *15*(3), 136-140.
- Shokoofehpoor, F., Gilani, A. G., Chaibakhsh, N., Khorshidi, A., Poormohammadi, Z., & Abolghasemi, S. J. J. o. S. C. (2020). Spectral and Aggregative Properties of Acid Blue 113 in Aqueous and Aqueous Solutions of Urea and in Colloids of Silver Nanoparticles. *49*(6), 849-862.
- Shrimali, H., Mandal, U. K., Nivsarkar, M., & Shrivastava, N. J. F. J. o. P. S. (2019). Fabrication and evaluation of a medicated hydrogel film with embelin from *Embelia ribes* for wound healing activity. *5*(1), 1-10.
- Shu, D., Fang, K., Liu, X., Cai, Y., & An, F. J. J. o. N. F. (2020). High dye fixation pad-steam dyeing of cotton fabrics with reactive dyes based on hydrophobic effect. *17*(5), 665-675.
- Shukla, S., Mehta, A., & Bajpai, V. K. J. J. o. B. A. P. f. N. (2013). Phytochemical screening and anthelmintic and antifungal activities of leaf extracts of *Stevia rebaudiana*. *3*(1), 56-63.
- Shuveksh, P. S., Ahmed, K., Padhye, S., Schobert, R., & Biersack, B. (2017). Chemical and Biological Aspects of the Natural 1,4-Benzoquinone Embelin and its (semi-)Synthetic Derivatives. *Curr Med Chem*, *24*(18), 1998-2009. doi:10.2174/0929867324666170116125731
- Shuveksh, P. S., Ahmed, K., Padhye, S., Schobert, R., & Biersack, B. J. C. m. c. (2017). Chemical and biological aspects of the natural 1, 4-benzoquinone embelin and its (semi-) synthetic derivatives. *24*(18), 1998-2009.
- Sibero, M. T., SISWANTO, A. P., PRIBADI, R., SABDONO, A., RADJASA, O. K., TRIANTO, A., FREDERICK, E. H., WIJAYA, A. P., HARYANTI, D., & TRININGSIH, D. W. J. B. J. o. B. D. (2020). The effect of drying treatment to metabolite profile and cytotoxic potential of *Rhizophora apiculata* leaves. *21*(5).
- Sigrist, M., Pinheiro, J., Azevedo Filho, J., Zucchi, M. J. G., & Research, M. (2011). Genetic diversity of turmeric germplasm (*Curcuma longa*; Zingiberaceae) identified by microsatellite markers. *10*(1), 419-428.
- Silva, A., & Pinto, D. J. C. m. c. (2005). Structure elucidation of xanthone derivatives: studies of nuclear magnetic resonance spectroscopy. *12*(21), 2481-2497.

- Silva, P., Franca, V. H., Queiroz, R. S., Lima, F. S., Freeman, H. S., Costa, S. A. D., & Costa, S. M. D. (2022). Copaifera langsdorffii Desf. bark extract: optimisation of dyeing conditions to wool and colour fastness properties. *Nat Prod Res*, 36(14), 3744-3749. doi:10.1080/14786419.2021.1872567
- Silva, P. M. d. S., Fiaschitello, T. R., Queiroz, R. S. d., Freeman, H. S., Costa, S. A. d., Leo, P., Montemor, A. F., & Costa, S. M. d. (2020). Natural dye from Croton urucurana Baill. bark: Extraction, physicochemical characterization, textile dyeing and color fastness properties. *Dyes and Pigments*, 173. doi:10.1016/j.dyepig.2019.107953
- Simpson, A. J., Simpson, M. J., & Soong, R. (2012). Nuclear magnetic resonance spectroscopy and its key role in environmental research. In: ACS Publications.
- Singh, H. B., Bharati, K., Singh, H., Bharati, K. J. H. o. n. d., & India, p. N. D. W. P. (2014). Enumeration of dyes. 33-260.
- Singh, S., Sarkar, B. K., Ramaiah, M., Devgan, M., & Chowdary, Y. A. J. I. J. o. P. (2015). Formulation, evaluation and stability study of herbal cream containing embelin'. 2(3), 136-138.
- Singha, U., Khanb, M. A., & Mohammada, F. (2018). Dyeing of Wool with Anthraquinone based Natural Colorants from Cassia fistula fruit.
- Sinha, K., Aikat, K., Das, P., & Datta, S. (2016). Dyeing of modified cotton fiber with natural Terminalia arjunadye: Optimization of dyeing parameters using response surface methodology. *Environmental Progress & Sustainable Energy*, 35(3), 719-728. doi:10.1002/ep.12284
- Sinha, K., Aikat, K., Das, P., Datta, S. J. E. P., & Energy, S. (2016). Dyeing of modified cotton fiber with natural Terminalia arjuna dye: Optimization of dyeing parameters using response surface methodology. 35(3), 719-728.
- Sinha, K., Chowdhury, S., Saha, P. D., Datta, S. J. I. C., & Products. (2013). Modeling of microwave-assisted extraction of natural dye from seeds of Bixa orellana (Annatto) using response surface methodology (RSM) and artificial neural network (ANN). 41, 165-171.
- Sivasankar, C., Gayathri, S., Bhaskar, J. P., Krishnan, V., & Pandian, S. K. J. M. p. (2017). Evaluation of selected Indian medicinal plants for antagonistic potential against Malassezia spp. and the synergistic effect of embelin in combination with ketoconazole. 110, 66-72.
- Srinivas, K., Mahesh, C., & Jagadeesh, N. J. I. J. P. (2010). Anti-mitotic activity of embelin derivatives. 1(2), 97-102.
- Stadler, A.-M., & Harrowfield, J. J. C. s. r. (2011). Places and chemistry: Strasbourg—a chemical crucible seen through historical personalities. 40(5), 2061-2108.

- Stebbins, J. F. J. S., dynamics,, & Melts, p. o. S. (2018). Dynamics and structure of silicate and oxide melts: nuclear magnetic resonance studies. 191-246.
- Stoyanova, M., Luchev, D., & Paneva-Marinova, D. (2016). *Optimization of Natural Dyes' Non-contact Characterization and Interdisciplinary Application Using Ensemble Classifiers and Genetic Algorithms*. Paper presented at the Proceedings of the Sixth International Conference Digital Presentation and Preservation of Cultural and Scientific Heritage–DiPP2016.
- Sultana, T., Sultana, S., Nur, H. P., & Khan, M. W. J. J. o. C. S. (2020). Studies on Mechanical, Thermal and Morphological Properties of Betel Nut Husk Nano Cellulose Reinforced Biodegradable Polymer Composites. 4(3), 83.
- Sutradhar, T., & Misra, A. J. T. J. o. P. C. A. (2018). Role of electron-donating and electron-withdrawing groups in tuning the optoelectronic properties of difluoroboron–naphthyridine analogues. 122(16), 4111-4120.
- Sutrisna, P. D., Hadi, R., Valentina, J., Priyantini, H. R., Waluyo, P. W., & Ronyastra, I. (2020). *Natural Dyes Extraction Intended for Coloring Process in Fashion Industries*. Paper presented at the IOP Conference Series: Materials Science and Engineering.
- Swamy, H. K., Krishna, V., Shankarmurthy, K., Rahiman, B. A., Mankani, K., Mahadevan, K., Harish, B., & Naika, H. R. J. J. o. e. (2007). Wound healing activity of embelin isolated from the ethanol extract of leaves of *Embelia ribes* Burm. 109(3), 529-534.
- Takeshita, S., Konishi, A., Takebayashi, Y., Yoda, S., & Otake, K. J. B. (2017). Aldehyde approach to hydrophobic modification of chitosan aerogels. 18(7), 2172-2178.
- Tambi, S., Mangal, A., Singh, N., Sheikh, J. J. P. i. C., Colorants, & Coatings. (2021). Cleaner production of dyed and functional polyester using natural dyes vis-a-vis exploration of secondary shades. 14(2), 121-128.
- Tamilselvi, N., Krishnamoorthy, P., Dhamotharan, R., Arumugam, P., Sagadevan, E. J. J. o. C., & Research, P. (2012). Analysis of total phenols, total tannins and screening of phytocomponents in *Indigofera aspalathoides* (Shivanar Vembu) Vahl EX DC. 4(6), 3259-3262.
- Teli, M., Pandit, P. J. F., & Polymers. (2018). Application of *Sterculia foetida* fruit shell waste biomolecules on silk for aesthetic and wellness properties. 19(1), 41-54.
- Thiagarajan, P., & Nalankilli, G. (2013). Improving light fastness of reactive dyed cotton fabric with antioxidant and UV absorbers.
- Thippeswamy, B. S., Mahendran, S., Biradar, M. I., Raj, P., Srivastava, K., Badami, S., & Veerapur, V. P. J. E. j. o. p. (2011). Protective effect of embelin against acetic acid induced ulcerative colitis in rats. 654(1), 100-105.

- Timmel, C. R., Henbest, K. B. J. P. T. o. t. R. S. o. L. S. A. M., Physical, & Sciences, E. (2004). A study of spin chemistry in weak magnetic fields. *362(1825)*, 2573-2589.
- Tissera, N. D., Wijesena, R. N., & de Silva, K. N. J. U. s. (2016). Ultrasound energy to accelerate dye uptake and dye–fiber interaction of reactive dye on knitted cotton fabric at low temperatures. *29*, 270-278.
- Toerien, E. S., & Khumalo, S. J. J. o. C. S. (2010). Natural dyes and dyeing techniques used by craftswomen in the Northern Hhohho region of Swaziland. *38*.
- Tomaszewska, E., Soliwoda, K., Kadziola, K., Tkacz-Szczesna, B., Celichowski, G., Cichomski, M., Szmaja, W., & Grobelny, J. J. J. o. N. (2013). Detection limits of DLS and UV-Vis spectroscopy in characterization of polydisperse nanoparticles colloids. *2013*.
- Trache, D., & Tarchoun, A. F. J. J. o. C. (2019). Differentiation of stabilized nitrocellulose during artificial aging: Spectroscopy methods coupled with principal component analysis. *33(8)*, e3163.
- Tyub, S., Kamili, A. N., Bhat, M. M. J. J. o. N., & Sciences, N. (2016). In vitro propagation of *Althaea rosea*-a valuable medicinal plant of Kashmir Himalaya. *1(5)*, 1-4.
- Uddin, M. G. J. J. o. T. (2014). Effects of different mordants on silk fabric dyed with onion outer skin extracts. *2014*.
- Vankar, P. S. J. R. (2000). Chemistry of natural dyes. *5(10)*, 73-80.
- Vaz, S. (2019). Chemical Analyses for Agriculture. In *Sustainable Agrochemistry* (pp. 147-182): Springer.
- Verma, A. K., Dash, R. R., & Bhunia, P. J. J. o. e. m. (2012). A review on chemical coagulation/flocculation technologies for removal of colour from textile wastewaters. *93(1)*, 154-168.
- Verma, S., Gupta, G. J. I. J. o. R., & Reviews, A. (2017). Natural dyes and its applications: A brief review. *4(4)*, 57-60.
- Vessecchi, R., Emery, F. S., Galembeck, S. E., & Lopes, N. P. J. R. C. i. M. S. (2010). Fragmentation studies and electrospray ionization mass spectrometry of lapachol: protonated, deprotonated and cationized species. *24(14)*, 2101-2108.
- Viault, G., Grée, D., Das, S., Yadav, J. S., & Grée, R. (2011). Synthesis of a focused chemical library based on derivatives of embelin, a natural product with proapoptotic and anticancer properties. In: Wiley Online Library.
- Wan, Y., & Lee, J.-M. J. A. C. (2021). Toward value-added dicarboxylic acids from biomass derivatives via thermocatalytic conversion. *11(5)*, 2524-2560.

- Wang, S., Liu, Q., Luo, Z., Wen, L., Cen, K. J. F. o. E., & China, P. E. i. (2007). Mechanism study on cellulose pyrolysis using thermogravimetric analysis coupled with infrared spectroscopy. *I(4)*, 413-419.
- Wang, W.-Y., Chiou, J.-C., Chen, W.-X., Yu, J.-L., & Kan, C.-W. J. C. (2021). Biosafety evaluation and quantitative determination of poly (hexamethylene biguanide)(PHMB) coated on cellulosic fabrics by Kubelka–Munk equation. *28(10)*, 6651-6661.
- Wang, Y.-w., Yi, Q.-z., Ding, Y., Ji, F., & Wang, N. (2020). Study on the factors influencing the dyeing performance of cotton fabric with vat dyes based on principal component analysis. *The Journal of The Textile Institute*, *112(9)*, 1460-1466. doi:10.1080/00405000.2020.1824432
- Wang, Y., Lee, C.-h., Tang, Y.-l., & Kan, C.-w. J. C. (2016). Dyeing cotton in alkane solvent using polyethylene glycol-based reverse micelle as reactive dye carrier. *23(1)*, 965-980.
- Wang, Z., Hui, C. J. O., & Chemistry, B. (2021). Contemporary advancements in the semi-synthesis of bioactive terpenoids and steroids. *19(17)*, 3791-3812.
- Wang, Z., Kang, K., Wu, J., Hu, Q., Harper, D. P., Du, G., Wang, S., Xu, K. J. J. o. M. R., & Technology. (2021). Comparative effects of electrospinning ways for fabricating green, sustainable, flexible, porous, nanofibrous cellulose/chitosan carbon mats as anode materials for lithium-ion batteries. *11*, 50-61.
- Wani, S. U. D., Gautam, S. P., Qadrie, Z. L., & Gangadharappa, H. J. I. J. o. B. M. (2020). Silk fibroin as a natural polymeric based bio-material for tissue engineering and drug delivery systems-A review. *163*, 2145-2161.
- Whittemore, T. J., Sayre, H. J., Xue, C., White, T. A., Gallucci, J. C., & Turro, C. J. J. o. t. A. C. S. (2017). New Rh₂ (II, II) complexes for solar energy applications: Panchromatic absorption and excited-state reactivity. *139(41)*, 14724-14732.
- Witzel, C., & Gegenfurtner, K. R. J. A. R. o. V. S. (2018). Color perception: Objects, constancy, and categories. *4*, 475-499.
- Wong-Paz, J. E., Guyot, S., Aguilar-Zárate, P., Muñoz-Márquez, D. B., Contreras-Esquivel, J. C., & Aguilar, C. N. J. F. c. (2021). Structural characterization of native and oxidized procyanidins (condensed tannins) from coffee pulp (*Coffea arabica*) using phloroglucinolysis and thioglycolysis-HPLC-ESI-MS. *340*, 127830.
- Wong, J. P.-C., Wijaya, S., Ting, K.-N., Wiart, C., Mustafa, K. A., Shipton, F., Khoo, T.-J. J. E.-B. C., & Medicine, A. (2014). Crude ethanol extract of *Pithecellobium ellipticum* as a potential lipid-lowering treatment for Hypercholesterolaemia. *2014*.
- Xiao, H., Zhao, T. J. F., & Polymers. (2018). One-bath union dyeing of wool/acrylic blend fabric with cationic reactive dyes based on azobenzene. *19(2)*, 331-339.

- Xu, C. L., Zheng, B., Pei, J. H., Shen, S. J., & Wang, J. Z. J. M. M. R. (2016). Embelin induces apoptosis of human gastric carcinoma through inhibition of p38 MAPK and NF- κ B signaling pathways. *14*(1), 307-312.
- Xu, X., Gong, J., Li, Z., Li, Q., Zhang, J., Wang, L., Huang, J. J. A. S. C., & Engineering. (2020). Mordant Free Dyeing and Functionalization of Wool Fabrics with Biocolorants Derived from *Apocynum venetum* L. Bast. *8*(33), 12686-12695.
- Yadav, V., Ali, J., Garg, M. C. J. J. o. H., Toxic., & Waste, R. (2021). Biosorption of methylene blue dye from textile-industry wastewater onto sugarcane bagasse: response surface modeling, isotherms, kinetic and thermodynamic modeling. *25*(1), 04020067.
- Yan, X., Hong, L., Pei, S., Hamilton, A., Sun, H., Yang, R., Liu, A., Yang, L. J. I. C., & Products. (2021). A natural yellow colorant from *Buddleja officinalis* for dyeing hemp fabric. *171*, 113968.
- Yoshioka, S. J. C. D., & Creativity. (2010). History of Japanese Colour: Traditional Natural Dyeing Methods. *5*(4), 1-7.
- Yusuf, M. J. T., & clothing. (2019). Synthetic dyes: a threat to the environment and water ecosystem. 11-26.
- Zain, N. M., Yusop, S. M., & Ahmad, I. J. J. N. F. S. (2014). Preparation and characterization of cellulose and nanocellulose from pomelo (*Citrus grandis*) albedo. *5*(1), 334.
- Zebeaman, M., & Gebeyehu, R. J. I. J. o. P. (2018). Phytochemical Screening and Antioxidant Activity of the fruit of *Embelia Schimperii* V.(family Myrsinaceae). *4*(2), 27-32.
- Zeeshan, U., Barkat, M. Q., & Mahmood, H. K. J. M. S. P. (2018). Phytochemical and antioxidant screening of *Cassia angustifolia*, *Curcuma zedoaria*, *Embelia ribes*, *Piper nigrum*, *Rosa damascena*, *Terminalia bellerica*, *Terminalia chebula*, *Zingiber officinale* and their effect on stomach and liver. *2*(2), 15-20.
- Zhang, N., Tao, P., Lu, Y., & Nie, S. J. C. (2019). Effect of lignin on the thermal stability of cellulose nanofibrils produced from bagasse pulp. *26*(13), 7823-7835.
- Zhang, Y., Tan, Y.-y., Liu, J.-g., Zhi, X.-x., Huangfu, M.-g., Jiang, G.-l., Wu, X., & Zhang, X. J. J. o. P. R. (2019). Molecular design, synthesis and characterization of intrinsically black polyimide films with high thermal stability and good electrical properties. *26*(7), 1-10.
- Zhao, C., Yan, Y., Gao, J., Yang, L., Zhou, J., Li, H., Huang, K., & Wang, D. J. J. o. M. L. (2021). A novel surface-active monomer decorating a self-floating adsorbent with high pH adaptability for anionic dyes: π - π stacking. *321*, 114864.

- Zheng, H., Xu, Y., Zhang, J., Xiong, X., Yan, J., & Zheng, L. J. J. o. C. P. (2017). An ecofriendly dyeing of wool with supercritical carbon dioxide fluid. *143*, 269-277.
- Zhou, H., Huang, Q., Liu, X., Xu, D., Zhang, W., Fu, S., Feng, X., Zhang, Z. J. D., & Pigments. (2021). Phenothiazine and diphenylsulfone-based donor–acceptor π -systems exhibiting remarkable mechanofluorochromism. *184*, 108868.
- Zhou, J., Tan, D. X., & Han, F. S. J. A. C. I. E. (2020). A Divergent Enantioselective Total Synthesis of Post-Iboga Indole Alkaloids. *59*(42), 18731-18740.
- Zhou, Q., Rather, L. J., Ali, A., Wang, W., Zhang, Y., Haque, Q. M. R., Li, Q. J. D., & Pigments. (2020). Environmental friendly bioactive finishing of wool textiles using the tannin-rich extracts of Chinese tallow (*Sapium sebiferum* L.) waste/fallen leaves. *176*, 108230.
- Zhou, W., Apkarian, R., Wang, Z. L., & Joy, D. (2006). Fundamentals of scanning electron microscopy (SEM). In *Scanning microscopy for nanotechnology* (pp. 1-40): Springer.
- Zhou, Y., Tang, R.-C. J. D., & Pigments. (2016). Modification of curcumin with a reactive UV absorber and its dyeing and functional properties for silk. *134*, 203-211.
- Zhu, H., Ke, X., Yang, X., Sarina, S., & Liu, H. J. A. C. I. E. (2010). Reduction of nitroaromatic compounds on supported gold nanoparticles by visible and ultraviolet light. *49*(50), 9657-9661.
- Zia, K. M., Adeel, S., Aslam, H., Khosa, M. K., Zuber, M. J. J. o. I., & Chemistry, E. (2019). Influence of ultrasonic radiation on extraction and green dyeing of mordanted cotton using neem bark extract. *77*, 317-322.
- Zou, Y., Lu, Y., Wei, D. J. J. o. A., & Chemistry, F. (2004). Antioxidant activity of a flavonoid-rich extract of *Hypericum perforatum* L. in vitro. *52*(16), 5032-5039.
- Zubay, P., Ruttner, K., Ladányi, M., Deli, J., Zámboriné, É. N., Szabó, K. J. I. C., & Products. (2021). In the shade—Screening of medicinal and aromatic plants for temperate zone agroforestry cultivation. *170*, 113764.

APPENDICES

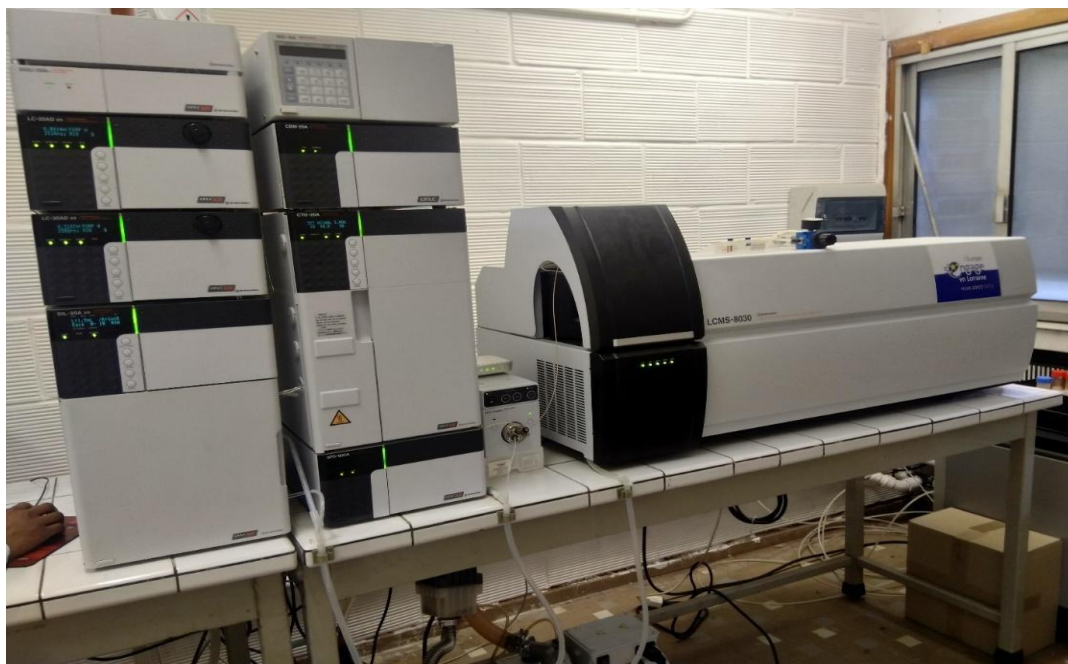
APPENDIX 1: Semi-synthetic experimental set up



APPENDIX 2: ATR-FTIR equipment



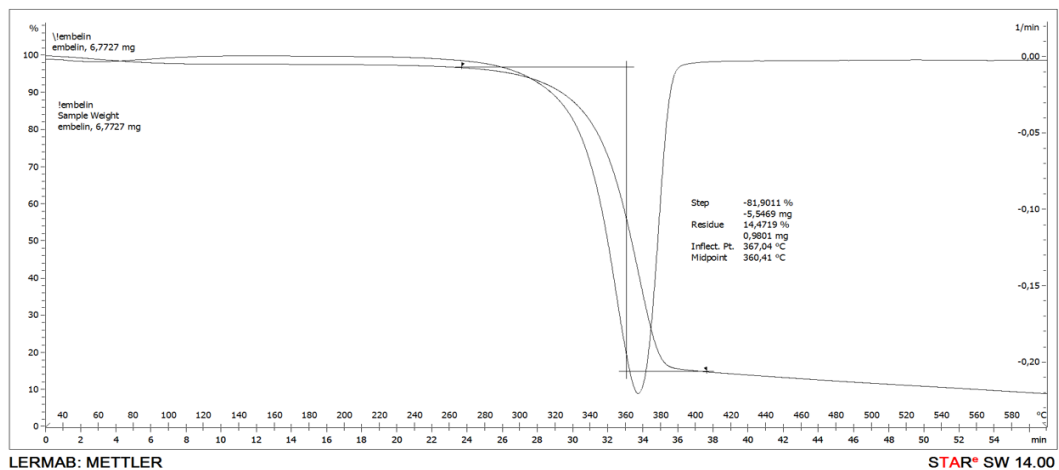
APPENDIX 3: LC/MS equipment



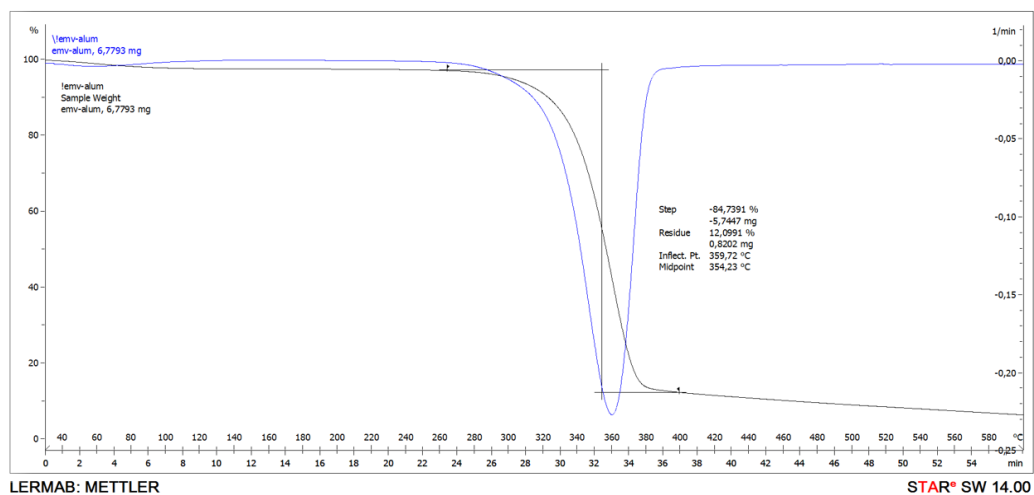
APPENDIX 4: Embelin Ninhydrin Dyes



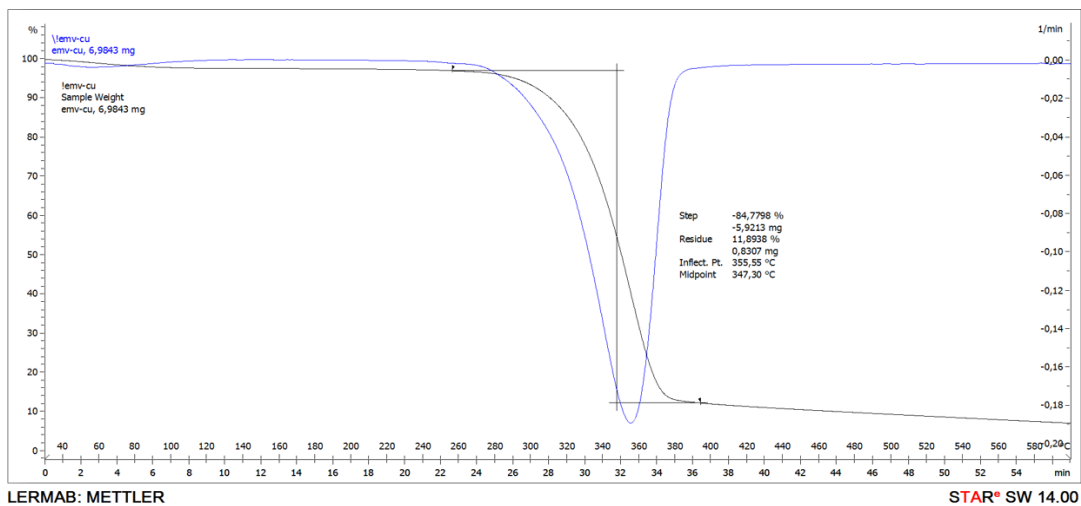
APPENDIX 5: TGA/DSC Embelin



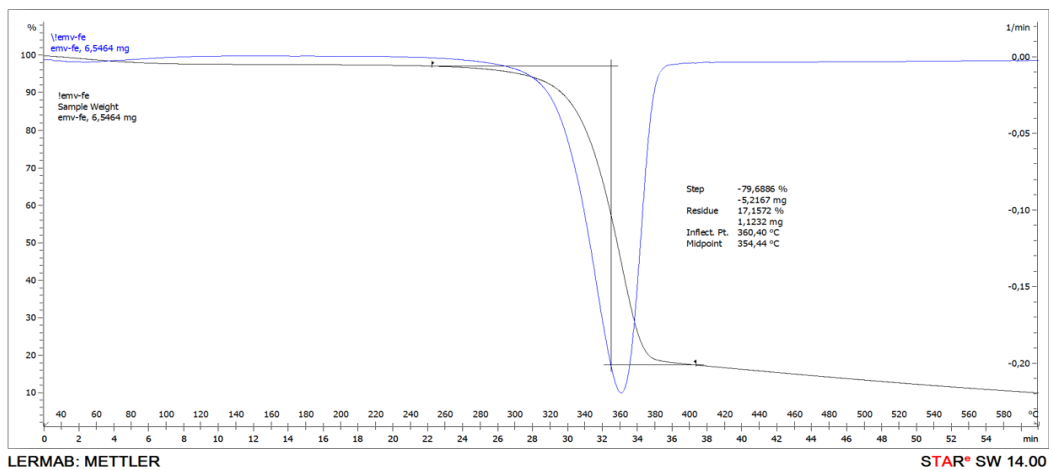
APPENDIX 6: TGA/DSC Emv -alum



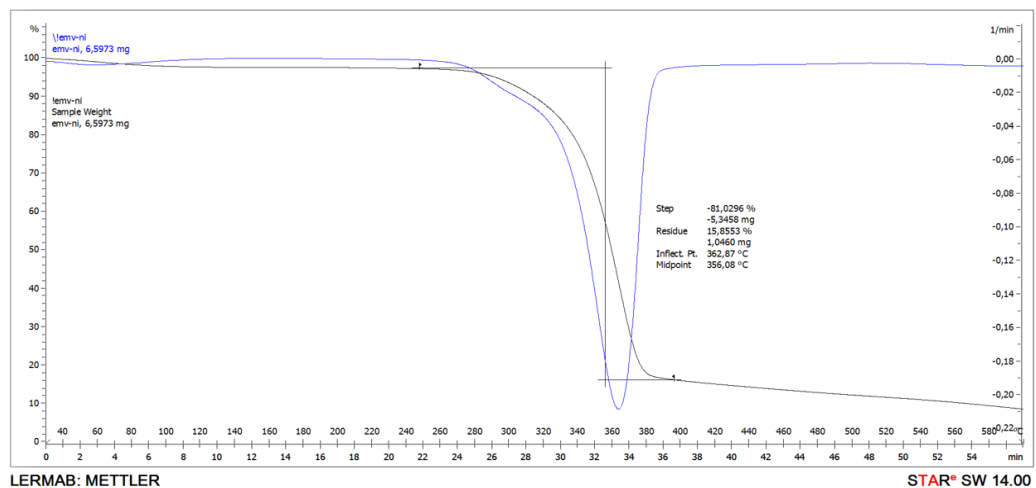
APPENDIX 7: TGA/DSC Emv -cu



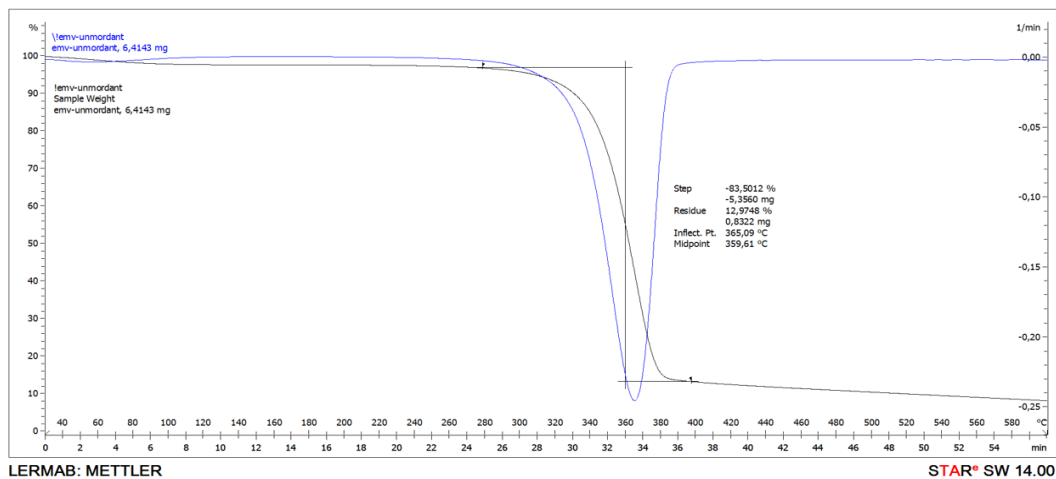
APPENDIX 8: TGA/DSC Emv -Fe



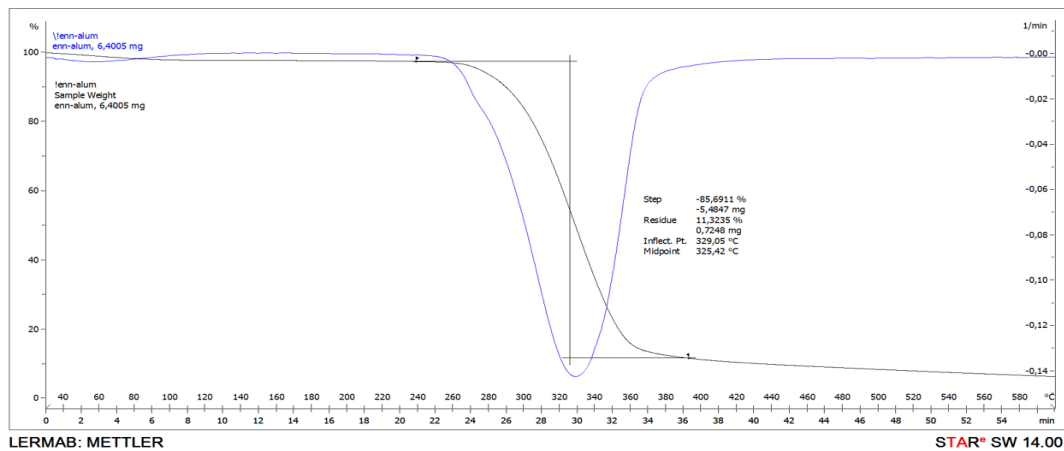
APPENDIX 9 :TGA/DSC Emv -Ni



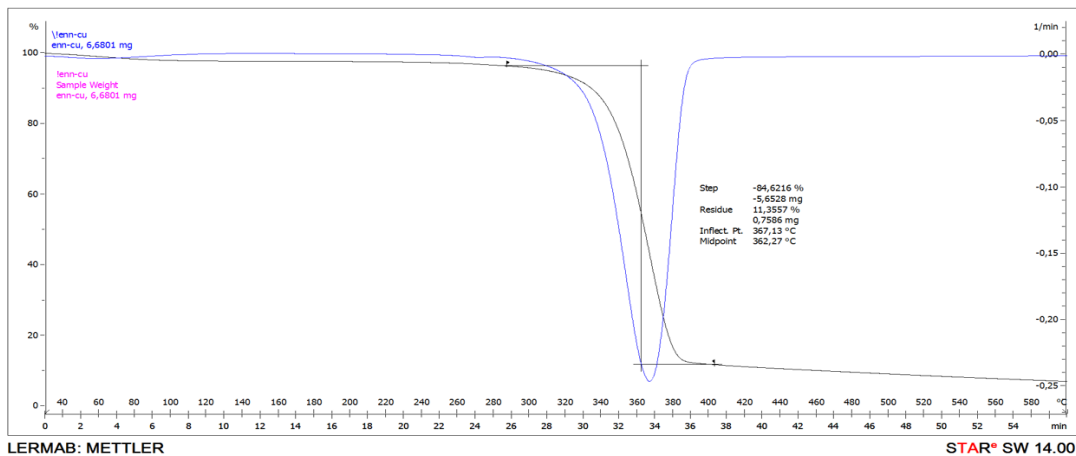
APPENDIX 10: TGA/DSC Emv –no mordant



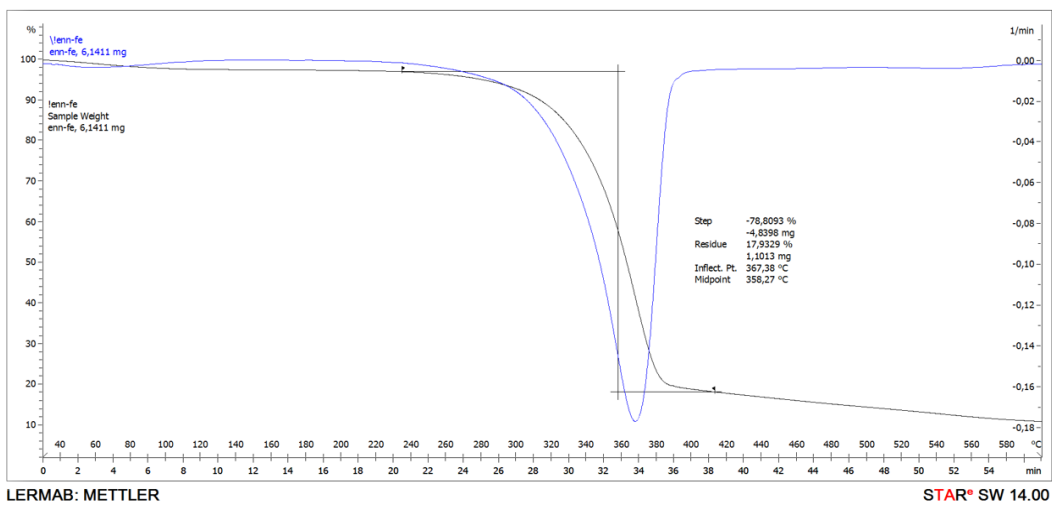
APPENDIX 11: TGA/DSC ENn –Alum



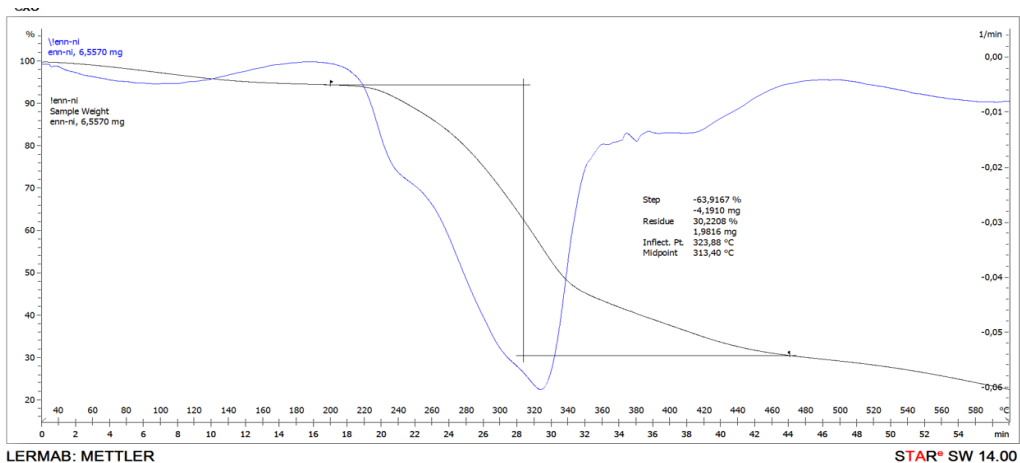
APPENDIX 12: TGA/DSC ENn –Cu

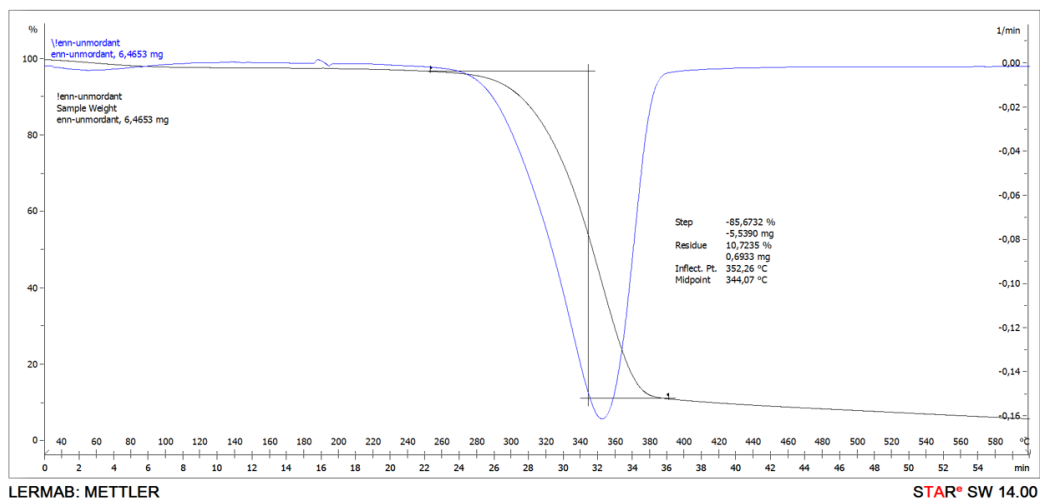


APPENDIX 13: TGA/DSC ENn –Fe



APPENDIX 14: TGA/DSC ENn –Ni



APPENDIX 15: TGA/DSC ENn –unmordant

1.